Adaptive Wireless Transceivers: Turbo-Coded, Turbo-Equalised and Space-Time Coded TDMA, CDMA, MC-CDMA and OFDM Systems

by

©L. Hanzo, C.H. Wong, M.S. Yee
Department of Electronics and Computer Science,
University of Southampton, UK

Contents

Prologue

Motivation of the Book

In recent years the concept of intelligent multi-mode, multimedia transceivers (IMMT) has emerged in the context of wireless systems [1–6]. The range of various existing solutions that have found favour in already operational standard systems was summarised in the excellent overview by Nanda *et al.* [3]. *The aim of these adaptive transceivers is to provide mobile users with the best possible compromise amongst a number of contradicting design factors, such as the power consumption of the hand-held portable station (PS), robustness against transmission errors, spectral efficiency, teletraffic capacity, audio/video quality and so forth [2].*

The fundamental limitation of wireless systems is constituted by their time- and frequency-domain channel fading, as illustrated in Figure 13.39 in terms of the Signal-to-Noise Ratio (SNR) fluctuations experienced by a modem over a dispersive channel. The violent SNR fluctuations observed both versus time and versus frequency suggest that over these channels no fixed-mode transceiver can be expected to provide an attractive performance, complexity and delay trade-off. Motivated by the above mentioned performance limitations of fixed-mode transceivers, IMMTs have attracted considerable research interest in the past decade [1–6]. Some of these research results are collated in this monograph.

In Figure 1 we show the instantaneous channel SNR experienced by the 512-subcarrier OFDM symbols for a single-transmitter, single-receiver scheme and for the space-time block code $\mathbf{G}_2$ [7] using one, two and six receivers over the shortened WATM channel. The average channel SNR is 10 dB. We can see in Figure 1 that the variation of the instantaneous channel SNR for a single transmitter and single receiver is severe. The instantaneous channel SNR may become as low as 4 dB due to deep fades of the channel. On the other hand, we can see that for the space-time block code $\mathbf{G}_2$ using one receiver the variation in the instantaneous channel SNR is slower and less severe. Explicitly, by employing multiple transmit antennas as shown in Figure 1, we have reduced the effect of the channels' deep fades significantly. This is advantageous in the context of adaptive modulation schemes, since higher-order modulation modes can be employed, in order to increase the throughput of the system. However, as we increase the number of receivers, i.e. the diversity order, we observe that the variation of the channel becomes slower. Effectively, by employing higher-order diversity, the fading channels have been converted to AWGN-like channels, as evidenced by the scenario employing the space-time block code $\mathbf{G}_2$ using six receivers. Since adaptive modulation only offers advantages over fading channels, we argue that using adaptive modulation might become unnecessary, as the diversity order is increased. Hence, adaptive modulation can be viewed as a lower-complexity alternative to space-time coding, since only a single transmitter and receiver is required.

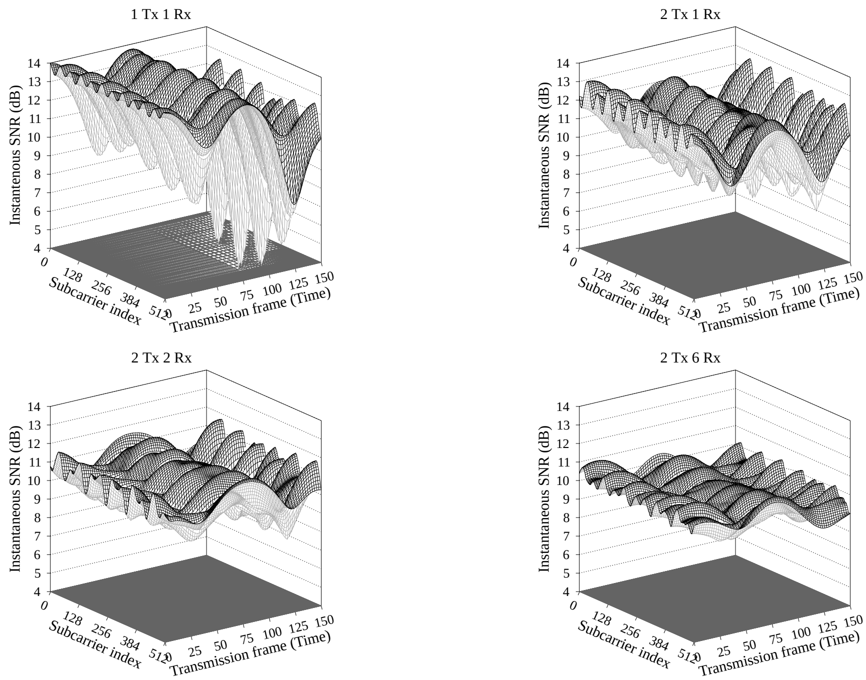

Figure 1: Instantaneous channel SNR versus time and frequency for a 512-subcarrier OFDM modem in the context of a single-transmitter single-receiver as well as for the space-time block code $\mathbf{G}_2$ [7] using one, two and six receivers when communicating over an indoor wireless channel. The average channel SNR is 10 dB. ©IEEE, Liew and Hanzo [8], 2001

Our intention with the book is multifold:

1. Firstly, to pay tribute to all researchers, colleagues and valued friends, who contributed to the field. Hence this book is dedicated to them, since without their quest for better transmission solutions for wireless communications this monograph could not have been conceived. They are too numerous to name here, hence they appear in the author index of the book.

2. Although the potential of adaptive modulation and transmission was recognised some 30 years ago by Cavers [9] and during the nineties the associated research efforts intensified, to date there is no monograph on the topic. Hence it is our hope that the conception of this monograph on the topic will provide an adequate portrayal of the last decade of research and fuel this innovation process.

3. As argued above, adaptive modulation only offers advantages when communicating over fading wireless channels. However, since the space-time coding assisted employment of transmit and receive diversity mitigates the effects of fading, we would like to portray adaptive modulation as a lower-complexity alternative to space-time coding, since only a single transmitter and receiver is required.

4. We expect to stimulate further research by exposing not only the information theoretical limitations of such IMMTs, but also by collating a range of practical problems and design issues for the practitioners. The coherent further efforts of the wireless research community is expected to lead to the solution of the vast range of outstanding problems, ultimately providing us with flexible wireless transceivers exhibiting a performance close to information theoretical limits.

The above mentioned calamities inflicted by the wireless channel can be mitigated by contriving a suite of near-instantaneously adaptive or Burst-by-Burst Adaptive (BbBA) wideband single-carrier [4], multi-carrier or Orthogonal Frequency Division Multiplex [4] (OFDM) as well as Code Division Multiple Access (CDMA) transceivers. The aim of these IMMTs is to communicate over hostile mobile channels at a higher integrity or higher throughput, than conventional fixed-mode transceivers. A number of existing wireless systems already support some grade of adaptivity and future research is likely to promote these principles further by embedding them into the already existing standards. For example, due to their high control channel rate and with the advent of the well-known Orthogonal Variable Spreading Factor (OVSF) codes the thrid-generation UTRA/IMT2000 systems are amenable to not only long-term spreading factor reconfiguration, but also to near-instantaneous reconfiguration on a 10ms transmission burst-duration basis.

With the advent of BbBA QAM, OFDM or CDMA transmissions it becomes possible for mobile stations (MS) to invoke for example in indoor scenarios or in the central propagation cell region - where typically benign channel conditions prevail - a high-throughput modulation mode, such as 4 bit/symbol Quadrature Amplitude Modulation (16QAM). By contrast, a robust, but low-throughput modulation mode, such as 1 bit/symbol Binary Phase Shift Keying (BPSK) can be employed near the edge of the propagation cell, where hostile propagation conditions prevail. The BbBA QAM, OFDM or CDMA mode switching regime is also capable of reconfiguring the transceiver at the rate of the channel's slow- or even fast-fading. This may prevent premature hand-overs and - more importantly - unnecessary powering up, which would inflict an increased interference upon co-channel users, resulting in further potential power increments. This detrimental process could result in all mobiles operating at unnecessarily high power levels.

A specific property of these transceivers is that their bit rate fluctuates, as a function of time. This is not an impediment in the context of data transmission. However, in interactive speech [5] or video [6] communications appropriate source codecs have to be designed, which are capable of promptly reconfiguring themselves according to the near-instantaneous bitrate budget provided by the transceiver.

The expected performance of our BbBA transceivers can be characterised with the aid of a whole plethora of performance indicators. In simple terms, adaptive modems outperform their individual fixed-mode counterparts, since given an average number of transmitted bits per symbol (BPS), their average BER will be lower than that of the fixed-mode modems. From a different perspective, at a given BER their BPS throughput will be always higher. In general, the higher the tolerable BER, the closer the performance to that of the Gaussian channel capacity. Again, this fact underlines the importance of designing programmable-rate, error-resilient source codecs - such as the Advanced Multi-Rate (AMR) speech codec to be employed in UMTS - which do not expect a low BER.

Similarly, when employing the above BbBA or AQAM principles in the frequency domain in the context of OFDM [4] or in conjunction with OVSF spreading codes in CDMA systems, attractive system design trade-offs and a high over-all performance can be attained [6]. However, despite the extensive research in the field by the international community, there is a whole host of problems that remain to be solved and this monograph intends to contribute towards these efforts.

Adaptation Principles

AQAM is suitable for duplex communication between the MS and BS, since the AQAM modes have to be adapted and signalled between them, in order to allow channel quality estimates and signalling to take place. The AQAM mode adaptation is the action of the transmitter in response to time–varying channel conditions. In order to efficiently react to the changes in channel quality, the following steps have to be taken:

- *Channel quality estimation:* In order to appropriately select the transmission parameters to be employed for the next transmission, a reliable estimation of the channel transfer function during the next active transmit timeslot is necessary.

- *Choice of the appropriate parameters for the next transmission:* Based on the prediction of the channel conditions for the next timeslot, the transmitter has to select the appropriate modulation and channel coding modes for the subcarriers.

- *Signalling or blind detection of the employed parameters:* The receiver has to be informed, as to which demodulator parameters to employ for the received packet. This information can either be conveyed within the OFDM symbol itself, at the cost of loss of effective data throughput, or the receiver can attempt to estimate the parameters employed by the remote transmitter by means of blind detection mechanisms [4].

Channel Quality Metrics

The most reliable channel quality estimate is the bit error rate (BER), since it reflects the channel quality, irrespective of the source or the nature of the quality degradation. The BER can be estimated invoking a number of approaches.

Firstly, the BER can be estimated with a certain granularity or accuracy, provided that the system entails a channel decoder or - synonymously - Forward Error Correction (FEC) decoder employing algebraic decoding [10].

Secondly, if the system contains a soft-in-soft-out (SISO) channel decoder, the BER can be estimated with the aid of the Logarithmic Likelihood Ratio (LLR), evaluated either at the input or the output of the channel decoder. A particularly attractive way of invoking LLRs is employing powerful turbo codecs, which provide a reliable indication of the confidence associated with a particular bit decision in the context of LLRs.

Thirdly, in the event that no channel encoder / decoder (codec) is used in the system, the channel quality expressed in terms of the BER can be estimated with the aid of the mean-squared error (MSE) at the output of the channel equaliser or the closely related metric of Pseudo-Signal-to-Noise-Ratio (Pseudo-SNR) [6]. The MSE or pseudo-SNR at the output of the channel equaliser have the important advantage that they are capable of quantifying the severity of the inter-symbol-interference (ISI) and/or Co-channel Interference (CCI) experienced, in other words quantifying the Signal to Interference plus Noise Ratio (SINR).

As an example, let us consider OFDM. In OFDM modems [4] the bit error probability in each subcarrier can be determined by the fluctuations of the channel's instantaneous frequency domain channel transfer function H_n, if no co-channel interference is present. The estimate $\hat{H}_n$ of the channel transfer function can be acquired by means of pilot–tone based channel estimation [4]. For CDMA transceivers similar techniques are applicable, which constitute the topic of this monograph.

The delay between the channel quality estimation and the actual transmission of a burst in relation to the maximal Doppler frequency of the channel is crucial as regards to the adaptive system's performance. If the channel estimate is obsolete at the time of transmission, then poor system performance will result [6].

Transceiver Parameter Adaptation

Different transmission parameters - such as the modulation and coding modes - of the AQAM single- and multi-carrier as well as CDMA transceivers can be adapted to the anticipated channel conditions. For example, adapting the number of modulation levels in response to the anticipated SNR encountered in each OFDM subcarrier can be employed, in order to achieve a wide range of different trade–offs between the received data integrity and throughput. Corrupted subcarriers can be excluded from data transmission and left blank or used for example for Crest–factor reduction. A range of different algorithms for selecting the appropriate modulation modes have to be investigated by future research. **The adaptive channel coding parameters entail code rate, adaptive interleaving and puncturing for convolutional and turbo codes, or varying block lengths for block codes [4].**

Based on the estimated frequency–domain channel transfer function, **spectral pre–distortion at the transmitter of one or both communicating stations can be invoked, in order to partially of fully counteract the frequency–selective fading of the time–dispersive channel**. Unlike frequency–domain equalisation at the receiver — which corrects for the amplitude– and phase–errors inflicted upon the subcarriers by the channel, but which cannot improve the SNR in poor quality OFDM subchannels — spectral pre–distortion at the OFDM transmitter can deliver near–constant signal–to–noise levels for all subcarriers and can be viewed as power control on a subcarrier–by–subcarrier basis.

In addition to improving the system's BER performance in time–dispersive channels, spectral pre–distortion can be employed in order to perform all channel estimation and equalisation functions at only one of the two communicating duplex stations. Low–cost, low power consumption mobile stations can communicate with a base station that performs the channel estimation and frequency–domain equalisation of the uplink, and uses the estimated channel transfer function for pre–distorting the down–link OFDM symbol. This setup would lead to different overall channel quality on the up– and downlink, and the superior pre-equalised downlink channel quality could be exploited by using a computationally less complex channel decoder, having weaker error correction capabilities in the mobile station than in the base station.

If the channel's frequency–domain transfer function is to be fully counteracted by the spectral pre-distortion upon adapting the subcarrier power to the inverse of the channel trans-

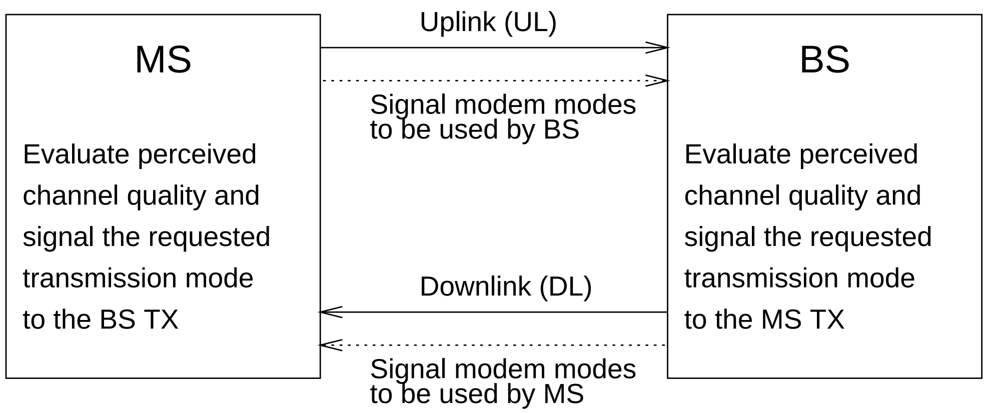

Figure 2: Parameter signalling in BbBA OFDM, CDMA and AQAM modems, IEEE Press-John Wiley, 2000, Hanzo, Webb, Keller [4].

fer function, then the output power of the transmitter can become excessive, if heavily faded subcarriers are present in the system's frequency range. In order to limit the transmitter's maximal output power, hybrid channel pre–distortion and adaptive modulation schemes can be devised, which would de–activate transmission in deeply faded subchannels, while retaining the benefits of pre–distortion in the remaining subcarriers.

BbBA mode signalling plays an important role in adaptive systems and the range of signalling options is summarised in Figure 2 for **closed–loop signalling**. If the channel quality estimation and parameter adaptation have been performed at the transmitter of a particular link, based on open–loop adaptation, then the resulting set of parameters has to be communicated to the receiver in order to successfully demodulate and decode the OFDM symbol. Once the receiver determined the requested parameter set to be used by the remote transmitter, then this information has to be signalled to the remote transmitter in the reverse link. If this signalling information is corrupted, then the receiver is generally unable to correctly decode the OFDM symbol corresponding to the incorrect signalling information, yielding an OFDM symbol error.

Unlike adaptive serial systems, which employ the same set of parameters for all data symbols in a transmission packet [4], adaptive OFDM systems [4] have to react to the frequency selective nature of the channel, by adapting the modem parameters across the subcarriers. The resulting signalling overhead may become significantly higher than that for serial modems, and can be prohibitive for example for subcarrier–by–subcarrier based modulation mode adaptation. In order to overcome these limitations, efficient and reliable signalling techniques have to be employed for practical implementation of adaptive OFDM modems.

If some flexibility in choosing the transmission parameters is sacrificed in an adaptation scheme, like in sub–band adaptive OFDM schemes [4], then the amount of signalling can be reduced. Alternatively, blind parameter detection schemes can be devised, which require little or no signalling information, respectively [4].

In conclusion, fixed mode transceivers are incapable of achieving a good trade-off in terms of performance and complexity. The proposed BbB adaptive system design paradigm is more promising in this respect. A range of problems and solutions were highlighted in conceptual terms with reference to an OFDM-based example, indicating the areas, where substantial future research is required. A specific research topic, which raised substantial research interest recently is invoking efficient channel quality prediction techniques [11]. Before we commence our indepth discourse in the forthcoming chapters, in the next section we provide a brief historical perspective on adaptive modulation.

Milestones in Adaptive Modulation History

Adaptive Single- and Multi-carrier Modulation

Following Cavers' classic contribution [9], BbB-AQAM has been suggested by Webb and Steele [1], stimulating further research in the wireless community for example by Sampei *et al.* [12], showing promising advantages, when compared to fixed modulation in terms of spectral efficiency, BER performance and robustness against channel delay spread. Various systems employing AQAM were also characterised in [4]. The numerical upper bound performance of narrow-band BbB-AQAM over slow Rayleigh flat-fading channels was evaluated by Torrance *et al.* [13], while over wide-band channels by Wong *et al.* [14, 15]. Following these developments, the optimization of the BbB-AQAM switching thresholds was carried employing Powell-optimization using a cost-function, which was based on the combination of the target BER and target Bit Per Symbol (BPS) performance [16]. Adaptive modulation was also studied in conjunction with channel coding and power control techniques by Matsuoka *et al.* [17] as well as Goldsmith and Chua [18, 19].

In the early phase of research more emphasis was dedicated to the system aspects of adaptive modulation in a narrow-band environment. A reliable method of transmitting the modulation control parameters was proposed by Otsuki *et al.* [20], where the parameters were embedded in the transmission frame's mid-amble using Walsh codes. Subsequently, at the receiver the Walsh sequences were decoded using maximum likelihood detection. Another technique of estimating the required modulation mode used was proposed by Torrance *et al.* [21], where the modulation control symbols were represented by unequal error protection 5-PSK symbols. The adaptive modulation philosophy was then extended to wideband multi-path environments by Kamio *et al.* [22] by utilizing a bi-directional Decision Feedback Equaliser (DFE) in a micro- and macro-cellular environment. This equalization technique employed both forward and backward oriented channel estimation based on the pre-amble and post-amble symbols in the transmitted frame. Equalizer tap gain interpolation across the transmitted frame was also utilized, in order to reduce the complexity in conjunction with space diversity [22]. The authors concluded that the cell radius could be enlarged in a macro-cellular system and a higher area-spectral efficiency could be attained for micro-cellular environments by utilizing adaptive modulation. The latency effect, which occurred, when the input data rate was higher than the instantaneous transmission throughput was studied and solutions were formulated using frequency hopping [23] and statistical multiplexing, where the number of slots allocated to a user was adaptively controlled [24].

In reference [25] symbol rate adaptive modulation was applied, where the symbol rate or the number of modulation levels was adapted by using $\frac{1}{8}$-rate 16QAM, $\frac{1}{4}$-rate 16QAM, $\frac{1}{2}$-rate 16QAM as well as full-rate 16QAM and the criterion used to adapt the modem modes was based on the instantaneous received signal to noise ratio and channel delay spread. The slowly varying channel quality of the uplink (UL) and downlink (DL) was rendered similar by utilizing short frame duration Time Division Duplex (TDD) and the maximum normalised delay spread simulated was 0.1. A variable channel coding rate was then introduced by Matsuoka *et al.* in conjunction with adaptive modulation in reference [17], where the transmitted burst incorporated an outer Reed Solomon code and an inner convolutional code in order to achieve high-quality data transmission. The coding rate was varied according to the prevalent channel quality using the same method, as in adaptive modulation in order to achieve a certain target BER performance. A so-called channel margin was introduced in this contribution, which adjusted the switching thresholds in order to incorporate the effects of channel quality estimation errors. As mentioned above, the performance of channel coding in conjunction with adaptive modulation in a narrow-band environment was also characterised by Chua and Goldsmith [18]. In this contribution, trellis and lattice codes were used without channel interleaving, invoking a feedback path between the transmitter and receiver for modem mode control purposes. The effects of the delay in the feedback path on the adaptive modem's performance were studied and this scheme exhibited a higher spectral efficiency, when compared to the non-adaptive trellis coded performance. Pearce, Burr and Tozer [26] as well as Lau and McLeod [27] have also analysed the performance trade-offs associated with employing channel coding and adaptive modulation as efficient fading counter measures.

Subsequent contributions by Suzuki *et al.* [28] incorporated space-diversity and power-adaptation in conjunction with adaptive modulation, for example in order to combat the effects of the multi-path channel environment at a 10Mbits/s transmission rate. The maximum tolerable delay-spread was deemed to be one symbol duration for a target mean BER performance of 0.1%. This was achieved in a Time Division Multiple Access (TDMA) scenario, where the channel estimates were predicted based on the extrapolation of previous channel quality estimates. Variable transmitted power was then applied in combination with adaptive modulation in reference [19], where the transmission rate and power adaptation was optimised in order to achieve an increased spectral efficiency. In this treatise, a slowly varying channel was assumed and the instantaneous received power required in order to achieve a certain upper bound performance was assumed to be known prior to transmission. Power control in conjunction with a pre-distortion type non-linear power amplifier compensator was studied in the context of adaptive modulation in reference [29]. This method was used to mitigate the non-linearity effects associated with the power amplifier, when QAM modulators were used.

Results were also recorded concerning the performance of adaptive modulation in conjunction with different multiple access schemes in a narrow-band channel environment. In a TDMA system, dynamic channel assignment was employed by Ikeda *et al.*, where in addition to assigning a different modulation mode to a different channel quality, priority was always given to those users in reserving time-slots, which benefitted from the best channel quality [30]. The performance was compared to fixed channel assignment systems, where substantial gains were achieved in terms of system capacity. Furthermore, a lower call termination probability was recorded. However, the probability of intra-cell hand-off increased as a result of the associated dynamic channel assignment (DCA) scheme, which constantly searched for a high-quality, high-throughput time-slot for the existing active users. The application of adaptive modulation in packet transmission was introduced by Ue, Sampei and Morinaga [31], where the results showed improved data throughput. Recently, the performance of adaptive modulation was characterised in conjunction with an automatic repeat request (ARQ) system in reference [32], where the transmitted bits were encoded using a cyclic redundant code (CRC) and a convolutional punctured code in order to increase the data throughput.

A recent treatise was published by Sampei, Morinaga and Hamaguchi [33] on laboratory test results concerning the utilization of adaptive modulation in a TDD scenario, where the modem mode switching criterion was based on the signal to noise ratio and on the normalised delay-spread. In these experimental results, the channel quality estimation errors degraded the performance and consequently a channel estimation error margin was devised, in order to mitigate this degradation. Explicitly, the channel estimation error margin was defined as the measure of how much extra protection margin must be added to the switching threshold levels, in order to minimise the effects of the channel estimation errors. The delay-spread also degraded the performance due to the associated irreducible BER, which was not compensated by the receiver. However, the performance of the adaptive scheme in a delay-spread impaired channel environment was better, than that of a fixed modulation scheme. Lastly, the experiment also concluded that the AQAM scheme can be operated for a Doppler frequency of $f_d = 10$Hz with a normalised delay spread of 0.1 or for $f_d = 14$Hz with a normalised delay spread of 0.02, which produced a mean BER of 0.1% at a transmission rate of 1 Mbits/s.

Lastly, the latency and interference aspects of AQAM modems were investigated in [34, 35]. Specifically, the latency associated with storing the information to be transmitted during severely degraded channel conditions was mitigated by frequency hopping or statistical multiplexing. As expected, the latency is increased, when either the mobile speed or the channel SNR are reduced, since both of these result in prolonged low instantaneous SNR intervals. It was demonstrated that as a result of the proposed measures, typically more than 4dB SNR reduction was achieved by the proposed adaptive modems in comparison to the conventional fixed-mode benchmark modems employed. However, the achievable gains depend strongly on the prevalant co-channel interference levels and hence interference cancellation was invoked in [35] on the basis of adjusting the demodulation decision boundaries after estimating the interfering channel's magnitude and phase.

The associated principles can also be invoked in the context of parallel modems. This principle was first proposed by Kalet [36] and was then further developed for example by Czylwik *et al.* [37] as well as by Chow, Cioffi and Bingham [38]. The associated concepts were detailed for example in [4] and will be also augmented in this monograph. Let us now briefly review the recent history of the BbB adaptive concept in the context of CDMA in the next section.

Adaptive Code Division Multiple Access

The techniques described in the context of single- and multi-carrier modulation are conceptually similar to multi-rate transmission [39] in CDMA systems. However, in BbB adaptive CDMA the transmission rate is modified according to the near-instantaneous channel quality, instead of the service required by the mobile user. BbB-adaptive CDMA systems are also useful for employment in arbitrary propagation environments or in hand-over scenarios, such as those encountered, when a mobile user moves from an indoor to an outdoor environment or in a so-called 'birth-death' scenario, where the number of transmitting CDMA users changes frequently [40], thereby changing the interference dramatically. Various methods of multi-rate transmission have been proposed in the research literature. Below we will briefly discuss some of the recent research issues in multi-rate and adaptive CDMA schemes.

Ottosson and Svensson compared various multi-rate systems [39], including multiple spreading factor (SF) based, multi-code and multi-level modulation schemes. According to the multi-code philosophy, the SF is kept constant for all users, but multiple spreading codes transmitted simultaneously are assigned to users requiring higher bit rates. In this case - unless the spreading codes's perfect orthogonality is retained after transmission over the channel - the multiple codes of a particular user interfere with each other. This inevitebly reduces the system's performance.

Multiple data rates can also be supported by a variable SF scheme, where the chip rate is kept constant, but the data rates are varied, thereby effectively changing the SF of the spreading codes assigned to the users; at a fixed chip rate the lower the SF, the higher the supported data rate. Performance comparisons for both of these schemes have been carried out by Ottosson and Svensson [39], as well as by Ramakrishna and Holtzman [41], demonstrating that both schemes achieved a similar performance. Adachi, Ohno, Higashi, Dohi and Okumura proposed the employment of multi-code CDMA in conjunction with pilot symbol-assisted channel estimation, RAKE reception and antenna diversity for providing multi-rate capabilities [42, 43]. The employment of multi-level modulation schemes was also investigated by Ottosson and Svensson [39], where higher-rate users were assigned higher-order modulation modes, transmitting several bits per symbol. However, it was concluded that the performance experienced by users requiring higher rates was significantly worse, than that experienced by the lower-rate users. The use of M-ary orthogonal modulation in providing variable rate transmission was investigated by Schotten, Elders-Boll and Busboom [44]. According to this method, each user was assigned an orthogonal sequence set, where the number of sequences, M, in the set was dependent on the data rate required – the higher the rate required, the larger the sequence set. Each sequence in the set was mapped to a particular combination of $b = (\log_2 M)$ bits to be transmitted. The M-ary sequence was then spread with the aid of a spreading code of a constant SF before transmission. It was found [44] that the performance of the system depended not only on the MAI, but also on the Hamming distance between the sequences in the M-ary sequence set.

Saquib and Yates [45] investigated the employment of the decorrelating detector in conjunction with the multiple-SF scheme and proposed a modified decorrelating detector, which utilized soft decisions and maximal ratio combining, in order to detect the bits of the different-rate users. Multi-rate transmission schemes involving interference cancellation receivers have previously been investigated amongst others by Johansson and Svensson [46, 47], as well as by Juntti [48]. Typically, multiple users transmitting at different bit rates are supported in the same CDMA system invoking multiple codes or different spreading factors. SIC schemes and multi-stage cancellation schemes were used at the receiver for mitigating the MAI [46–48], where the bit rate of the users was dictated by the user requirements. The performance comparison of various multiuser detectors in the context of a multiple-SF transmission scheme was presented for example by Juntti [48], where the detectors compared were the decorrelator, the PIC receiver and the so-called group serial interference cancellation (GSIC) receiver. It was concluded that the GSIC and the decorrelator performed better than the PIC receiver, but all the interference cancellation schemes including the GSIC, exhibited an error floor at high SNRs due to error propagation.

The bit rate of each user can also be adapted according to the near-instantaneous channel quality, in order to mitigate the effects of channel quality fluctuations. Kim [49] analyzed the performance of two different methods of combating the near-instantaneous quality variations of the mobile channel. Specifically, Kim studied the adaptation of the transmitter power or the switching of the information rate, in order to suit the near-instantaneous channel conditions. Using a RAKE receiver [50], it was demonstrated that rate adaptation provided a higher average information rate, than power adaptation for a given average transmit power and a given BER [49]. Abeta, Sampei and Morinaga [51] conducted investigations into an adaptive packet transmission based CDMA scheme, where the transmission rate was modified by varying the channel code rate and the processing gain of the CDMA user, employing the carrier to interference plus noise ratio (CINR) as the switching metric. When the channel quality was favourable, the instantaneous bit rate was increased and conversely, the instantaneous bit rate was reduced when the channel quality dropped. In order to maintain a constant overall bit rate, when a high instantaneous bit rate was employed, the duration of the transmission burst was reduced. Conversely, when the instantaneous bit rate was low, the duration of the burst was extended. This resulted in a decrease in interference power, which translated to an increase in system capacity. Hashimoto, Sampei and Morinaga [52] extended this work also to demonstrate that the proposed system was capable of achieving a higher user capacity with a reduced hand-off margin and lower average transmitter power. In these schemes the conventional RAKE receiver [50] was used for the detection of the data symbols. A variable-rate CDMA scheme – where the transmission rate was modified by varying the channel code rate and, correspondingly, the M-ary modulation constellations – was investigated by Lau and Maric [53]. As the channel code rate was increased, the bit-rate was increased by increasing M correspondingly in the M-ary modulation scheme. Another adaptive system was proposed by Tateesh, Atungsiri and Kondoz [54], where the rates of the speech and channel codecs were varied adaptively [54]. In their adaptive system, the gross transmitted bit rate was kept constant, but the speech codec and channel codec rates were varied according to the channel quality. When the channel quality was low, a lower rate speech codec was used, resulting in increased redundancy and thus a more powerful channel code could be employed. This resulted in an overall coding gain, although the speech quality dropped with decreasing speech rate. A variable rate data transmission scheme was proposed by Okumura and Adachi [55], where the fluctuating transmission rate was mapped to discontinuous transmission, in order to reduce the interference inflicted upon the other users, when there was no transmission. The transmission rate was detected blindly at the receiver with the help of cyclic redundancy check decoding and RAKE receivers were employed for coherent reception, where pilot-symbol-assisted channel estimation was performed.

The information rate can also be varied in accordance with the channel quality, as it will be demonstrated shortly. However, in comparison to conventional power control techniques - which again, may disadvantage other users in an effort to maintain the quality of the links considered - the proposed technique does not disadvantage other users and increases the network capacity [56]. The instantaneous channel quality can be estimated at the receiver and the chosen information rate can then be communicated to the transmitter via explicit signalling in a so-called closed-loop controlled scheme. Conversely, in an open-loop scheme - provided that the downlink and uplink channels exhibit a similar quality - the information rate for the downlink transmission can be chosen according to the channel quality estimate related to the uplink and vice versa. The validity of the above channel reciprocity issues in TDD-CDMA systems have been investigated by Miya *et al.* [57], Kato *et al.* [58] and Jeong *et al.* [59].

Outline of the book

In order to mitigate the impact of dispersive multi-path fading channels, equalization techniques are introduced, which are subsequently incorporated in a wideband adaptive modulation scheme. The performance of various wideband adaptive transmission scheme was then analysed in different environments, resulting in the following outline:

- **Chapter 1**: Square Quadrature Amplitude Modulation (QAM) schemes are introduced and their corresponding performance is analysed over Gaussian and narrow-band Rayleigh fading channels. This is followed by an introduction to equalization techniques with an emphasis on the Minimum Mean Square Error (MMSE) Decision Feedback Equalizer (DFE). The performance of the DFE is then characterised using BPSK, 4QAM, 16QAM and 64QAM modems.

- **Chapter 2**: The recursive Kalman algorithm is formulated and employed in an adaptive channel estimator and adaptive DFE in order to combat the time-variant dispersion of the mobile propagation channel. In this respect, the system parameters of the algorithm are optimised for each application by evaluating the convergence speed of the algorithm. Finally, two receiver structures utilizing the adaptive channel estimator and DFE are compared.

- **Chapter 3**: The concept of AQAM is introduced, where the modulation mode is adapted based on the prevalent channel conditions. Power control is then implemented and analysed in conjunction with AQAM in a narrow-band environment. Subsequently, a wideband AQAM scheme - which incorporates the DFE - is jointly constructed in order to mitigate the effects of the dispersive multi-path fading channel. A numerical upper bound performance is derived for this wideband AQAM scheme, which is subsequently optimised for a certain target BER and transmission throughput performance. Lastly, a comparison is made between the constituent fixed or time-invariant modulation modes and the wideband AQAM scheme in terms of their transmission throughput performance.

- **Chapter 4**: The performance of the wideband channel coded AQAM scheme is presented and analysed. Explicitly, turbo coding techniques are invoked, where each modulation mode was associated with a certain code rate and turbo interleaver size. Consequently, an adaptive code rate scheme is incorporated into the wideband AQAM scheme. The performance of such a scheme is compared to the constituent fixed modulation modes as well as the uncoded AQAM scheme, which was presented in Chapter 3. Furthermore, the concept of turbo equalization is introduced and applied in a wideband AQAM scheme. The iterative nature of the turbo equalizer is also exploited in estimating the channel impulse response (CIR). The chapter is concluded with a comparative study of various joint coding and adaptive modulation schemes, including Trellis Coded Modulation (TCM), turbo TCM (TTCM), Bit Interleaved Coded Modulation (BICM) and its iteratively detected (ID) version, namely BICM-ID.

  In **Chapter 5**: closed form expressions were derived for the average BER, the average BPS throughput and the mode selection probability of various adaptive modulation schemes, which were shown to be dependent on the mode-switching levels as well as on the average SNR experienced. Furthermore, a range of techniques devised for determining the adaptive mode-switching levels are studied comparatively. The optimum switching levels achieving the highest possible BPS throughput while maintaining the average target BER were developed based on the Lagrangian optimisation method. The chapter is concluded with a brief comparison of space-time coding and adaptive modulation in the context of OFDM and MC-CDMA.

- **Chapter 6**: This chapter presents the practical aspects of implementing wideband AQAM schemes, which includes the effects of error propagation inflicted by the DFE and the more detrimental channel quality estimation latency impact of the scheme. The impact of latency is studied under different system delay and normalised Doppler frequencies. The impact of Co-Channel Interference (CCI) on the wideband AQAM scheme is also analysed. In this aspect, joint detection techniques and a more sophisticated switching regime is utilized, in order to mitigate the impact of CCI.

- In **Chapter 7** we cast channel equalisation as a classification problem. We briefly give an overview of neural network and present the design of some neural network based equalisers. In this chapter we opted for studying a neural network structure referred to as the Radial Basis Function (RBF) network in more detail for channel equalisation, since it has an equivalent structure to the so-called optimal Bayesian equalisation solution [60]. The structure and properties of the RBF network is described, followed by the implementation of a RBF network as an equaliser. We will discuss the computational complexity issues of the RBF equaliser with respect to that of conventional linear equalisers and provide some complexity reduction methods. Finally, performance comparisons between the RBF equaliser and the conventional equaliser are given over various channel scenarios.

- **Chapter 8** commences by summarising the concept of adaptive modulation that adapts the modem mode according to the channel quality in order to maintain a certain target bit error rate and an improved bits per symbol throughput performance. The RBF based equaliser is introduced in a wideband Adaptive Quadrature Amplitude Modulation (AQAM) scheme in order to mitigate the effects of the dispersive multipath fading channel. We introduce the short-term Bit Error Rate (BER) as the channel quality measure. Lastly, a comparative study is conducted between the constituent fixed mode, the conventional DFE based AQAM scheme and the RBF based AQAM scheme in terms of their BER and throughput performance.

- In **Chapter 9** we incorporate turbo channel coding in the proposed wideband AQAM scheme. A novel reduced-complexity RBF equaliser utilizing the so-called Jacobian logarithmic relationship [61] is proposed and the turbo-coded performance of the Jacobian RBF equaliser is presented for the various fixed QAM modes. Furthermore, we investigate using various channel quality measures – namely the short-term BER and the average Log-Likelihood Ratio (LLR) magnitude of the data burst generated either by the RBF equaliser or the turbo decoder – in order to control the modem mode-switching regime for our adaptive scheme.

- **Chapter 10** introduces the principles of iterative, joint equalisation and decoding techniques known as turbo equalisation. We present a novel turbo equalisation scheme, which employs a RBF equaliser instead of the conventional trellis-based equaliser. The structure and computational complexity of both the RBF equaliser and trellis-based equaliser are compared and we characterise the performance of these RBF and trellis-based turbo-equalisers. We then propose a reduced-complexity RBF assisted turbo equaliser, which exploits the fact that the RBF equaliser computes its output on a symbol-by-symbol basis and the symbols of the decoded transmission burst, which are sufficiently reliable need not be equalised in the next turbo equalisation iteration. This chapter is concluded with the portayal and characterisation of RBF-based turbo equalised space-time coded schemes.

- In **Chapter 11** the recent history of smart CDMA MUDs is reviewed and the most promising schemes have been comparatively studied, in order to assist in the design of third- and fourth-generation receivers. Future transceivers may become BbB-adaptive, in order to be able to accommodate the associated channel quality fluctuations without disadvantageously affecting the system's capacity. Hence the methods reviewed in this chapter are advantageous, since they often assist in avoiding powering up, which may inflict increased levels of co-channel interference and power consumption. Furthermore, the techniques characterized in the chapter support an increased throughput within a given bandwidth and will contribute towards reducing the constantly increasing demand for more bandwidth. Both successive interference cancellation (SIC) and Parallel Interference Cancellation (PIC) receivers are investigated in the context of AQAM/CDMA schemes, along with joint-detection assisted schemes.

- In **Chapter 12** we provide a brief historical perspective on Orthogonal Frequency Division Multiplex (OFDM) transmissions with reference to the literature of the past 30 years. The advantages and disadvantages of various OFDM techniques are considered briefly and the expected performance is characterized for the sake of illustration in the context of indoor wireless systems. Our discussions will deepen, as we approach the subject of adaptive subcarrier modem mode allocation and turbo channel coding. Our motivation is that of quantifying the performance benefits of employing adaptive channel coded OFDM modems.

- In **Chapter 13** we provide an introduction to the subject of space-time coding combined with adaptive modulation and various channel coding techniques. A performance study is conducted in the context of both fixed-mode and adaptive modulation schemes, when communicating over dispersive wideband channels. We will demonstrate that in conjunction with space-time coding the advantages of employing adaptive modulation erode, since the associated multiple transmitter, multiple receiver assisted diversity scheme efficiently mitigates the channel quality fluctuations of the wireless channel.

Having reviewed the historical developments in the field of AQAM, **in the rest of this monograph we will consider wideband AQAM assisted single- and multi-carrier, as well as CDMA transceivers, communicating over dispersive wideband channels. We will also demonstrate that the potential performance gains attained by AQAM erode, as the diversity order of the systems is increased, although this is achieved at the cost of an increased complexity. We will demonstrate that this is particularly true in conjunction with space time coding assisted transmitter diversity, since Multiple-Input, Multiple-Output (MIMO) systems substantially mitigate the effects of channel quality**

fluctuations. Hence if the added complexity of MIMOs has to be avoided, BbB-adaptive transceivers constitute powerful wideband fading counter-measures. By contrast, there is no need for the employment of BbB-adaptive transceivers, if the higher complexity of MIMOs is affordable, since MIMOs substantially mitigate the effects of channel quality fluctuations, rendering further fading counter-measuers superfluous.

Part I

Near-instantaneously Adaptive Modulation and Filtering Based Equalisation:

C.H. Wong, L. Hanzo, B.J. Choi, S.X. Ng

Chapter 4

Channel-Coded Wideband Adaptive Modulation

In the previous chapter, we introduced the joint Adaptive Quadrature Amplitude Modulation (AQAM) and equalization scheme, where the pseudo-SNR at the output of the DFE was used as the modulation mode switching metric in order to mitigate the effects of a wideband fading channel. In this chapter, the wideband AQAM scheme is extended to incorporate the benefits of channel coding. The general motivation for using channel coding is to exploit the error correction and the error detection capability of the channel codes in order to improve the BER and throughput performance of the wideband AQAM scheme.

As we have shown in Chapter 3, the wideband AQAM scheme was capable of yielding an improved BER and BPS performance, when compared to each individual fixed modulation mode. Since the wideband AQAM scheme improves the BER performance, high coding rate channel codes can be utilized in our coded AQAM scheme. The utilization of these high coding rate channel codes is essential to produce a better coded throughput performance, when compared to the uncoded wideband AQAM scheme, which was discussed in the previous chapter.

Since the wideband AQAM scheme always attempts to invoke the appropriate modulation mode in order to combat the wideband channel effects, the probability of encountering a received transmitted burst with a high instantaneous BER is low, when compared to the constituent fixed modulation modes. This characteristic is advantageous, since due to the less bursty error distribution, the coded wideband AQAM scheme can be implemented without the utilization of high-delay channel interleavers. Consequently we can exploit the error detection capability of the channel codes almost instantaneously at the receiver for every received transmission burst. This is essential, since the error detection capability of the channel codes can provide the receiver with extra intelligence, in order to detect the modulation mode that was utilized. The channel codecs' error detection capability can also be exploited in order to gauge the short term BER of each individual transmitted burst. Hence the short term BER can be used as a modulation mode switching metric, since it can quantify the impact of virtually all channel-induced impairments, such as signal strength variation, ISI, etc. For example, to a certain extent, this metric can incorporate the impact of co-channel interference. In our subsequent discussions the short term BER metric is not exploited, hence the interested reader is referred to the contributions by Yee [61, 127] *et al.* for more details.

In Section 4.1 turbo coding [128] is invoked in conjunction with AQAM and its performance is compared to that of the fixed modulation modes as well as to that of the uncoded AQAM scheme presented in Section 3.3.5. Furthermore, in Section 4.6 channel coding is also exploited for detecting the modulation modes at the receiver. In Section 4.7 it is shown that employing adaptive-rate turbo channel coding in conjunction with adaptive modulation results in a higher effective throughput, than fixed-rate channel coding. Our wideband AQAM scheme is then invoked in the context of turbo equalization in Section 4.10, where channel equalization [129] and channel decoding is implemented jointly and iteratively. The chapter is concluded in Section 4.11 with a system design example cast in the context of a number of powerful wideband joint coding and modulation schemes, namely Trellis Coded Modulation (TCM), Turbo Trellis Coded Modulation (TTCM) and Bit Interleaved Coded Modulation (BICM).

Recent work on combining conventional channel coding with adaptive modulation has been conducted for example by Matsuoka *et al.* [17], where punctured convolutional coding with and without an outer Reed Solomon (RS) code was invoked in a TDD environment. Convolutional coding was also used in conjunction with adaptive modulation by Lau in reference [27], where results were presented in a Frequency Division Multiple Access (FDMA) and Time Division Multiple Access (TDMA) environment, when assuming the presence of a channel feedback path between the receiver and transmitter. Finally, Goldsmith *et al.* [130] demonstrated that in adaptive coded modulation the simulation and theoretical results confirmed a 3dB coding gain at a BER of 10^{-6} for a 4-state trellis code and a coding gain of 4dB was achieved by an 8-state trellis code over Rayleigh-fading channels, while a 128-state code performed within 5dB of the Shannonian capacity limit. Let us now briefly review the concept of turbo coding.

4.1 Turbo Coding

Turbo coding is a form of iterative channel decoding that produces excellent results as demonstrated by Berrou *et al.* [128, 131] in 1993. The concept of turbo coding can be best explained by referring to its encoder and decoder structures. The schematic of the turbo encoder is shown in Figure 4.1. Explicitly, two component encoders are utilized, in order to produce the turbo code, where a so-called random turbo interleaver [128, 132] is placed before the second encoder. The general aim of the turbo encoder is to generate two independent component codes, which encode the same information bits. The role of the turbo interleaver is to ensure that the two encoded bit streams are independent from each other, due to the scrambling of the information bits by the interleaver. The component codes used in the encoder can be either block or convolutional codes. An example of a binary block code, which is amenable to turbo coding is the family of Bose-Chaudhuri-Hocquenghem (BCH) codes [133] that possess multiple error detection and correction capabilities. Explicitly, each BCH code is represented by the notation BCH (n, k, d_{min}), where n, k and d_{min} denote the number of the encoded bits, the number of information bits and the minimum Hamming distance, respectively. The number of parity bits is equal to $n - k$ and the coding rate is $\frac{k}{n}$. The BCH encoder accepts k

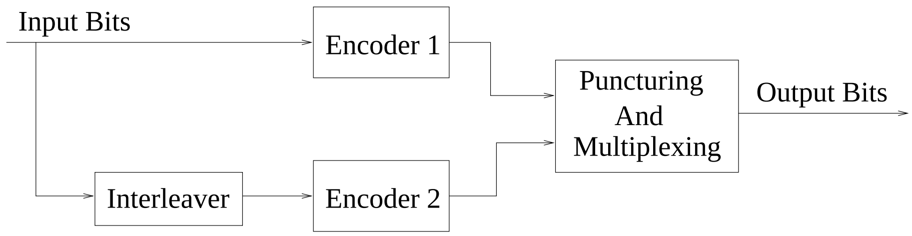

Figure 4.1: Turbo encoder schematic.

information bits and by using a specific polynomial code generator [133], the parity bits are added in order to produce n coded bits. Thus, according to the encoding rules, only certain encoded sequences are legitimate. It is this distinction that enables the decoder to recognize and correct corrupted or illegitimate codewords. We will refrain from discussing the code generation and decoding mechanism, referring the reader to references [10, 133–135]. By referring to Figure 4.1, the generated codewords are punctured and multiplexed, in order to produce the turbo code. However, puncturing of the parity bits is not applied to turbo BCH codes as proposed by Hagenauer [136, 137]. Consequently, for example, a component code of BCH (31, 26, 3) will yield a turbo block code of BCH (36, 26), where the additional five parity bits of the second encoder are included in the output turbo block code, while the systematic information bits produced by the second encoder are discarded.

The other family of constituent turbo encoders that can be utilized is Recursive Systematic Convolutional (RSC) codes, which is shown in Figure 4.2. Here, the constraint length is set to $K = 3$, and the generator polynomials are set in octal terms, to 7 and 5 [133]. Referring to Figure 4.2, a stream of systematic bits, which represents the original information sequence is generated along with the corresponding parity sequence. In forming the convolutional-based turbo code, the systematic bits of the second convolutional encoder are discarded and the two sets of parity sequences are punctured accordingly. The puncturing pattern can be varied in order to produce different code rates.

The iterative decoding structure of the turbo decoder is shown in Figure 4.3. The component decoders require soft inputs and produce soft outputs. Consequently, special decoding algorithms such as the Maximum A Posteriori (MAP) [138] and the Log-MAP [139] algorithms can be invoked, which were proposed by Bahl and Robertson, respectively. These algorithms are highlighted in Appendix A.1 [140]. Essentially, the soft output generated by either decoder determines whether the decoded bit is a binary 1 or 0 as well as the reliability of the output bit decision. Let us now analyse in detail the decoder structure shown in Figure 4.3, where the notations L_{a1} and L_{a2} represent the so-called *a priori* information produced by the first and second decoder, respectively. Similarly, L_p^{D1} and L_p^{D2} denote the so-called *a posteriori* information of the first and second decoders, respectively. Finally, the so-called extrinsic information of the first and second decoders is labelled as L_e^{D1} and L_e^{D2}, respectively.

At the receiver the soft channel outputs are generated, which consist of the systematic and the parity bits, as illustrated in Figure 4.3. The two parity sequences generated by the turbo encoder are utilized by the corresponding decoders. In this respect, the punctured

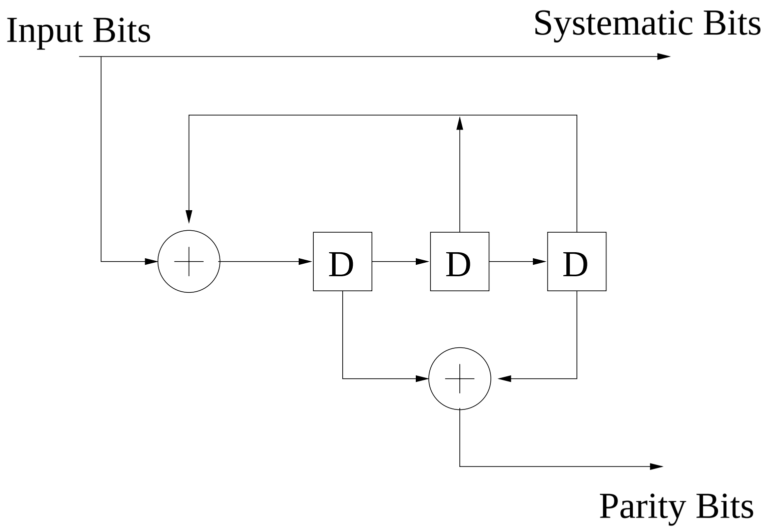

Figure 4.2: Recursive Systematic Convolutional (RSC) encoder.

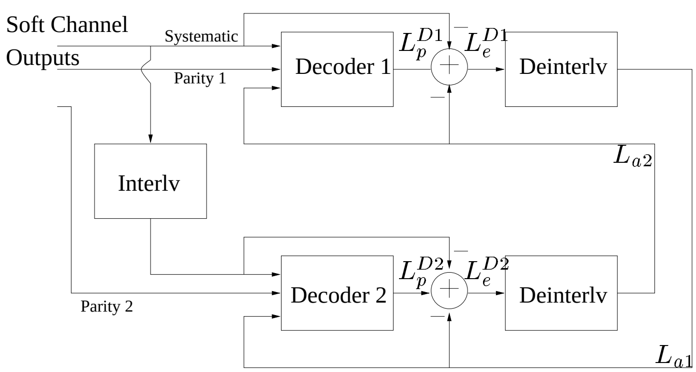

Figure 4.3: Schematic of the turbo decoder.

parity bits are replaced by zeros during the decoding process. In the first iteration, the first component decoder accepts the soft channel outputs and by utilizing the Log-MAP algorithm of Appendix A.1 [140], the decoder produces the *a posteriori* log likelihood ratio (LLR) L_p^{D1}, which is defined as $L(u_n|r)$ in Appendix A.1 [140]. Essentially this LLR represents the log-domain probability that the bit was decoded error freely. The polarity of this LLR can also be used in order to determine whether the decoded bit is a binary 1 or 0. Subsequently, the extrinsic information L_e^{D1}, is generated by subtracting the contribution of the channel outputs, as shown in Figure 4.3. This justifies the terminology 'extrinsic', since it represents the information related to a certain bit carried by sources other than the channel output itself related to this specific bit. Hence the extrinsic information is only influenced by the first decoder, which is then interleaved in order to generate the *a priori* LLR information L_{a1}.

For the sake of presenting the information to the second decoder in the right order, the systematic bits are interleaved in order to form the soft channel outputs as depicted in Figure 4.3. Subsequently, the second decoder utilizes not only the soft channel outputs but also the independent *a priori* LLR values L_{a1}, from the first decoder in order to produce the *a posteriori* LLR L_p^{D2}. This *a posteriori* LLR value is improved at this stage, since it was influenced by the estimates of both decoders. As before, the extrinsic information of the second decoder L_e^{D2}, is generated by subtracting the channel information and the *a priori* information of the first decoder. This essentially removes any contribution generated by the first decoder, when producing the *a priori* information L_{a2}, of the second decoder, which is used in the first decoder for the subsequent iteration. This subtraction process allows us to maintain the independence of the decoding process, which is important for the sake of attaining independent estimates from the two separate decoders for each decoded bit. This process constitutes one turbo decoding iteration and it is repeated, in order to achieve better consecutive estimates of the decoded bits.

After each iteration, the output *a posteriori* LLR is improved, since the decoder can exploit the independent *a priori* information generated by the other decoder. Consequently, as the number of iteration increases, the estimation of the decoded bit improves. The performance of the turbo decoder will vary depending on the size of the turbo interleaver, where a larger interleaver will provide a higher degree of independence of the *a priori* information that is being passed from one decoder to another. This high degree of independence is exploited by both decoders in order to yield an improved decoding performance. The number of iterations also plays an important role, where a higher number of iterations will generally result in a better performance, although at the expense of a higher complexity. However, the gain achieved by each iteration reduces with increasing numbers of iterations, which will be exemplified by Figure 4.4. This is because the two decoders' information becomes more dependent on each other, diminishing the benefits of acquiring two 'opinions' concerning a given received bit. In the next section, the implementation of turbo coding in a wideband AQAM scheme is highlighted.

4.2 System Parameters

The system parameters that were used throughout our associated investigations are listed in Table 4.1. The channel coder parameters, which include the turbo interleaver size and code rate will be varied according to the different system requirements as it will be demonstrated at a later stage.

The generic setup of the turbo coded AQAM scheme consists of the modulation switching mechanism, the turbo coding parameters and the switching thresholds. The modulation mode switching mechanism is identical to that discussed in Section 3.3.2 with the exception that the coding rate and the size of the turbo interleaver is varied according to the modulation mode

Channel Type Normalized Doppler Frequency	COST207 TU(see Figure 3.12) 3.25×10^{-5}
Data Modulation	AQAM (NOTX, BPSK, 4QAM, 16QAM, 64QAM) with perfect channel estimation
Receiver Type	Decision Feedback Equalizer Number of Forward Taps = 35 Number of Backward Taps = 7 Correct Feedback
Turbo Coding Parameters: Number of Iterations Decoding Algorithm	 6 Log-MAP

Table 4.1: Generic system parameters of the turbo coded AQAM scheme.

selected. The modulation mode switching mechanism can be summarized as follows:

$$\text{Modulation Mode} = \begin{cases} NOTX & \text{if } \gamma_{DFE} \leq t_1^c \\ BPSK, I_0, R_0 & \text{if } t_1^c < \gamma_{DFE} \leq t_2^c \\ 4QAM, I_1, R_1 & \text{if } t_2^c < \gamma_{DFE} \leq t_3^c \\ 16QAM, I_2, R_2 & \text{if } t_3^c < \gamma_{DFE} \leq t_4^c \\ 64QAM, I_3, R_3 & \text{if } \gamma_{DFE} > t_4^c, \end{cases} \tag{4.1}$$

where I_n represents the random turbo interleaver size in terms of the number of bits. The coding rate is denoted by R_n and t_n^c represents the coded switching thresholds.

The switching thresholds for the coded AQAM scheme are difficult to numerically optimise in order to achieve a certain target BER due to the non-linear BER versus SNR characteristics of the scheme. However, the switching thresholds for the different turbo coded AQAM schemes are intuitively optimised, in order to achieve target BERs of below 1% and 0.01%, which are termed as the **High-BER** and **Low-BER** schemes, respectively. This coded schemes will be compared to the uncoded AQAM scheme, where the uncoded switching thresholds are set according to Table 3.8 for target BERs of 1% and 0.01%. The burst structures used for the **High-** and **Low-BER** schemes are the non-spread speech and the non-spread data bursts, respectively, which were shown in Figure 3.13.

4.3 Turbo Block Coding Performance of the Fixed QAM Modes

Before we attempt to characterize the Turbo Block Coded AQAM (TBCH-AQAM) scheme, let us study the performance of turbo coding, when applied to the constituent fixed modulation modes. In our experiments the component turbo channel code used was the BCH(31, 26, 3) scheme and a random turbo interleaver [141] of size 9984 bits was chosen. The block channel interleaver size was set to 13824 bits, which corresponded to the channel-coded block-length of the turbo interleaver. The turbo coding performance of the BPSK modulation mode is shown in Figure 4.4, which displayed the BER performance for different number of

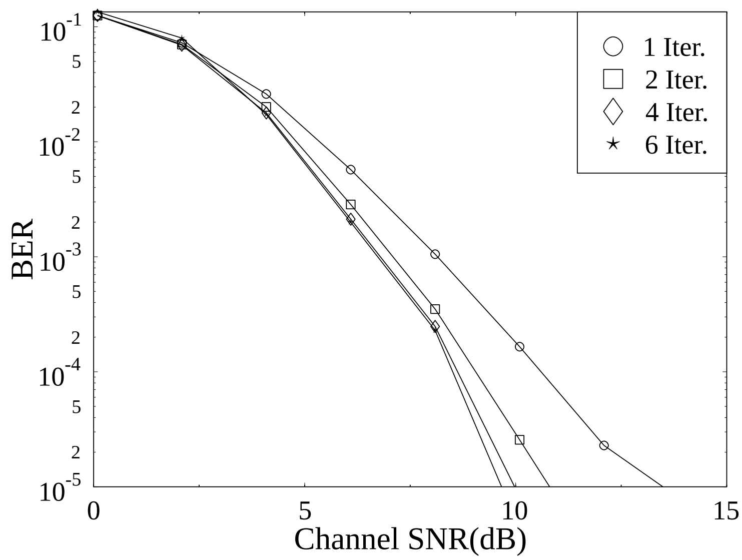

Figure 4.4: Turbo block coded performance of BPSK for different number of iterations with a component code of BCH(31, 26, 3). The system parameters of Table 4.1 and the non-spread speech burst of Figure 3.13 was utilized. The channel interleaver size was set to 13824 bits.

turbo iterations. The performance improved, as the number of turbo iterations was increased, which illustrated the improvement in estimating the decoded bit as a result of the iterative decoding regime. The iteration gain was approximately 2.1dB after six iterations at a BER of 0.01%. Explicitly, the iteration gain measured the difference between the average channel SNR required in order to achieve a particular BER and the corresponding average channel SNR required after n iterations for the same BER. However, the improvements achieved upon each iteration decreased, as the number of iterations increased, as evidenced by Figure 4.4.

The turbo block coded BER performance of the BPSK, 4QAM, 16QAM and 64QAM modes is shown in Figure 4.5 after six iterations using different channel block interleavers, where the uncoded performance is also displayed for comparison. Based on the turbo interleaver size of 9984 bits, the size of the channel interleaver was set to 13824 bits, which corresponded to the channel-coded block-length of the turbo block encoder. In order to assess the impact of the channel interleaver size, a larger channel interleaver of size 4×13824 was also utilized. As expected, in Figure 4.5 the BER performance using the larger channel interleaver was superior, when compared to that using the smaller channel interleaver, although at the cost of an associated higher transmission delay.

Referring again to Figure 4.5, substantial SNR gains were achieved, when comparing

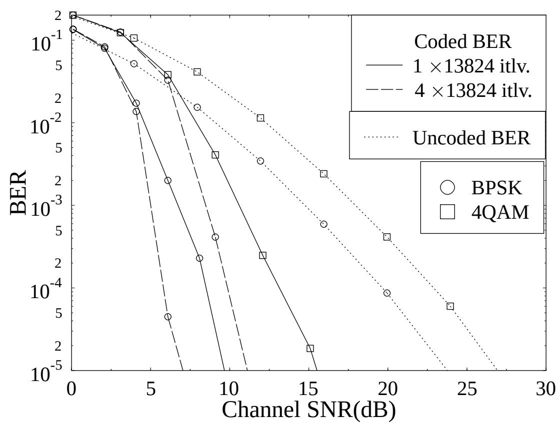

(a) Turbo block coded performance of BPSK and 4QAM.

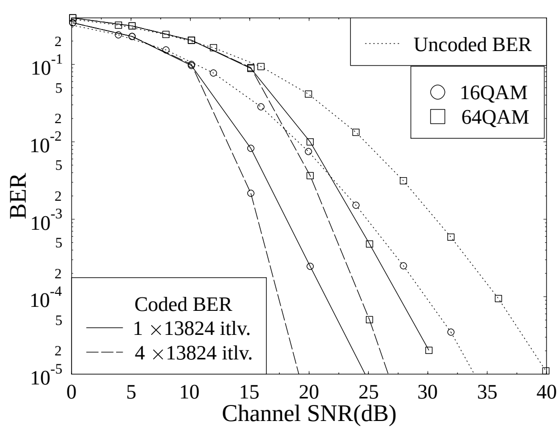

(b) Turbo block coded performance of 16QAM and 64QAM.

Figure 4.5: Turbo block coded performance of each individual modulation modes after six turbo iterations utilizing the system parameters of Table 4.1 and the non-spread speech burst of Figure 3.13. A component code BCH(31, 26, 3) was utilized in conjunction with channel interleavers of size 13824 bits and 4×13824 bits.

the coded and uncoded performance. However the gains achieved at a BER of 0.01% was higher that those achieved at a BER of 1%, as evidenced by Figure 4.5. This observation is important in the context of turbo block coded AQAM scheme, which will be presented in the next section.

4.4 Fixed Coding Rate and Fixed Interleaver Size Turbo Block Coded Adaptive Modulation

In this Fixed Coding Rate and Fixed Interleaver Size Turbo BCH Coded AQAM (**FCFI-TBCH-AQAM**) scheme, we utilized a random turbo interleaver of fixed size and a fixed coding rate for all modulation modes [142]. The turbo interleaver size was set to 9984 and a coding rate of 0.7222 was utilized, which corresponds to a component code of BCH (31, 26, 3). The switching mechanism described by Equation 4.1 was utilized in conjunction with the coded switching thresholds shown in Table 4.2 for the target BERs of 1%, 0.01% and for a near-error-free system.

Target BER	Coded Switching Thresholds (dB)				Burst Type see Figure 3.13
	t_1^c	t_2^c	t_3^c	t_4^c	
$\leq 1\%$	0.1363	2.7258	8.1450	14.1846	Speech
$\leq 0.01\%$	1.2458	3.4579	9.7980	16.7589	Data
Near-Error-Free	2.2458	4.4579	10.7980	17.7589	Data

Table 4.2: The coded switching thresholds, which were experimentally set in order to achieve the target BERs of below 1%, 0.01% and near-error-free for the **FCFI-TBCH-AQAM** scheme described in Section 4.4. The corresponding transmission burst types utilized are shown in Figure 3.13 and the switching mechanism was characterized by Equation 4.1.

The BER and BPS performance of the **FCFI-TBCH-AQAM** scheme is shown in Figure 4.6 for the target BERs of 1% and 0.01%. The uncoded **FCFI-TBCH-AQAM** performance is also depicted for comparison. As expected, the coded BER performance improved significantly, when compared to the uncoded performance, and the target BERs of 1% and 0.01% were achieved. Conversely, the coded BPS was reduced by a factor equal to the coding rate.

The BPS performance of the turbo block coded AQAM scheme was also compared to that of the fixed modulation modes for different channel interleaver sizes, as illustrated by Figure 4.7, where the throughput values were extracted from Figures 4.5 and 4.6. Referring to Figure 4.7(a), where the channel interleaver was set to 13824 bits, the wideband AQAM scheme displayed throughput SNR gains of approximately 1.0dB and 5.0dB for target BERs of 1% and 0.01%, respectively, when considering the corresponding BPS curves. However, by referring to Figure 4.7(b), when the larger channel interleaver size was utilized for the fixed modulation modes, the BPS/SNR gain was minimal for a target BER of 1% while, a BPS/SNR gain of approximately 1.5dB was observed for a target BER of 0.01%. The reduction in the throughput SNR gain achieved by the wideband turbo block coded AQAM scheme was due to the superior performance of the larger channel interleaved fixed modulation modes. However, it is important to note that an associated high transmission delay was incurred.

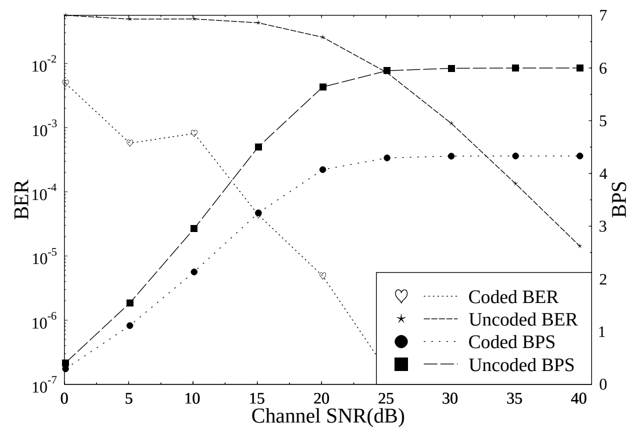

(a) Turbo block coded performance for a target BER of below 1%.

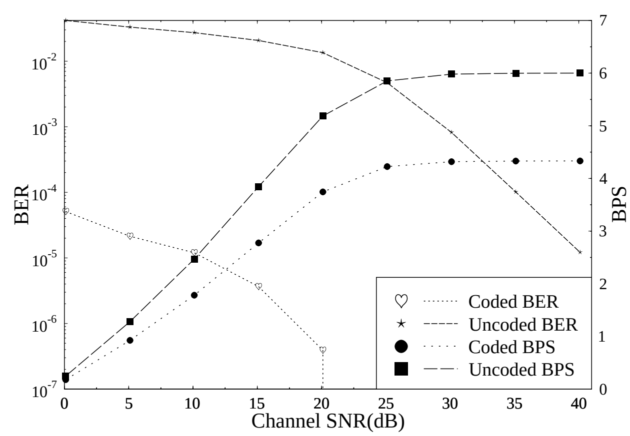

(b) Turbo block coded performance for a target BER of below 0.01%.

Figure 4.6: Turbo block coded and uncoded performance of the **FCFI-TBCH-AQAM** scheme described in Section 4.4, where the generic system parameters of Table 4.1 were utilized. The coded switching regime was characterized by Equation 4.1 with the coding rate and turbo interleaver size set to 0.7222 and 9984 bits, respectively. The coded switching thresholds and transmission burst type were set according to Table 4.2.

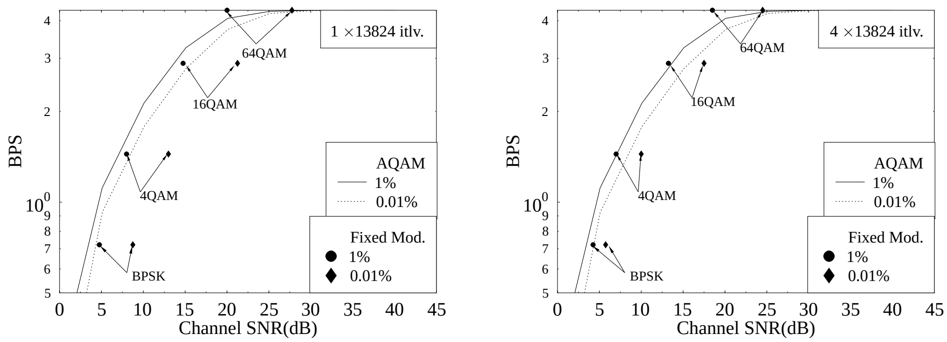

(a) Channel Interleaver of size 1×13824 bits **(b)** Channel Interleaver of size 4×13824 bits

Figure 4.7: Throughput comparison between the **FCFI-TBCH-AQAM** scheme and the constituent fixed modulation modes for target BERs of 1% and 0.01%, which were evaluated from Figures 4.5 and 4.6. Different sized channel interleavers were used for the fixed modulation modes whereas the **FCFI-TBCH-AQAM** scheme employed no channel interleavers.

4.4.1 Comparisons with the Uncoded Adaptive Modulation Scheme

A performance comparison between the **FCFI-TBCH-AQAM** scheme and the uncoded AQAM scheme for the same target BER is presented here. In Section 3.3.5 the uncoded AQAM performance was optimised using the switching thresholds of Table 3.8, in order to achieve target BERs of 1% and 0.01 as evidenced by Figure 3.21(b). These uncoded results were compared to the **FCFI-TBCH-AQAM** scheme in terms of BPS and BER performance. This comparison is exemplified in Figure 4.8.

For the **High-BER** scheme, the coded BER was lower than for the uncoded case, where a high average channel SNR gain of about 20dB was observed across the BER range of 10^{-5} and 10^{-3}. Similarly, in the channel SNR range of 0 to 15dB, the coded BPS performance was better than that of the uncoded AQAM scheme with a maximum SNR gain of 3dB at a channel SNR of 0dB, as evidenced by Figure 4.8(a). However, the BPS performance of the **FCFI-TBCH-AQAM** scheme deteriorated at high average channel SNRs, since its throughput was limited by its coding rate, which converged to a throughput of approximately 4.33 bits per symbol.

For the **Low-BER** scheme of Figure 4.8(b) the same characteristics were observed. However, the BPS gain was higher than that of the **High-BER** scheme. The coded BPS performance was higher, than that of the uncoded scheme for the channel SNR range of 0 to 23dB with a maximum SNR gain of 7dB at a channel SNR of 0dB, as evidenced by the BPS curves of Figure 4.8(b). These SNR gains attained by the **Low-BER** scheme were higher than those of the **High-BER** scheme due to the higher coding gain achieved at a lower target BER. This characteristic was observed also for the fixed modulation modes of Section 4.3, where higher coding gains were recorded for lower BERs due to the steeper decay of the coded

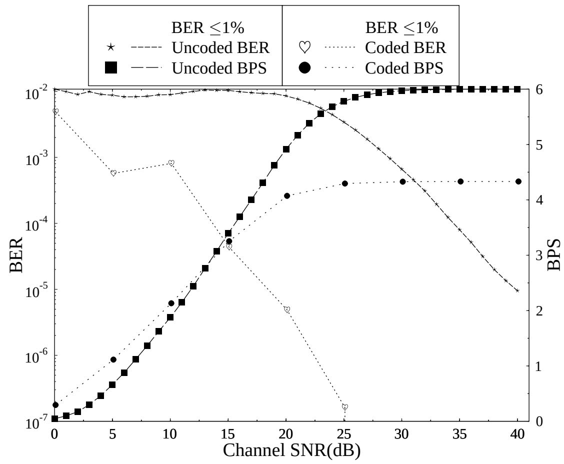

(a) Turbo block coded performance for a target BER of below 1% using the non-spread speech burst of Figure 3.13.

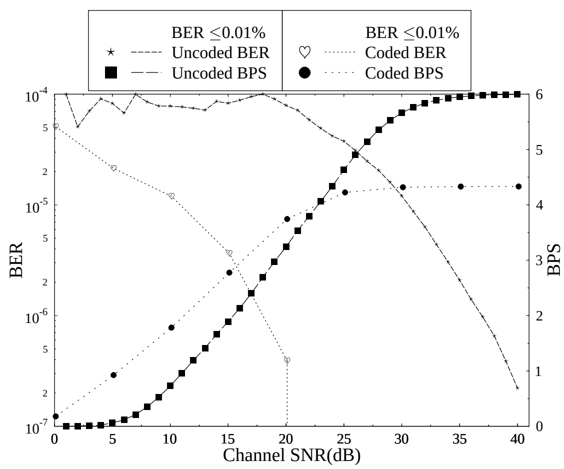

(b) Turbo block coded performance for a target BER of below 0.01% using the non-spread data burst of Figure 3.13.

Figure 4.8: Turbo block coded performance of the **FCFI-TBCH-AQAM** scheme described in Section 4.4, where the generic system parameters of Table 4.1 were utilized. The coded switching regime was characterized by Equation 4.1 with the coding rate and turbo interleaver size set to 0.7222 and 9984 bits, respectively. The coded and uncoded AQAM switching thresholds were set according to Table 4.2 and 3.8, respectively.

BER versus SNR curves. Consequently, for the **Low-BER** scheme, the switching threshold values were lowered by a margin of approximately 7dB, when compared to the **Low-BER** uncoded AQAM scheme. This is evident, when the coded switching thresholds of Table 4.2 are compared to those of the uncoded switching thresholds of Table 3.8. The lowering of the coded switching thresholds resulted in the more frequent utilization of higher-order modulation modes at lower average channel SNRs. Consequently the BPS performance improved, when compared to the uncoded AQAM scheme. By contrast, for the **High-BER** scheme the switching threshold reduction margin was only 3.5dB. The effect of the higher margin for the **Low-BER** scheme was an improved BPS performance, when compared to the **Low-BER** uncoded AQAM scheme.

The switching thresholds for the **FCFI-TBCH-AQAM** scheme were also experimentally determined, which are shown in Table 4.2 in order to achieve a near-error-free communications system. The BER and BPS performance of this near-error-free scheme is shown in Figure 4.9, where the corresponding curves of the **Low-BER** uncoded AQAM scheme were also plotted for comparison. The results characterized a near-error-free system, where the throughput was higher than that of the uncoded AQAM scheme for the channel SNR range of 0 to 22dB. The maximum average channel SNR gain of 6dB was recorded, when considering the associated throughput performance at a channel SNR of 0dB, as evidenced by Figure 4.9.

In summary, we have quantified the average channel SNR gains achieved by the **FCFI-TBCH-AQAM** scheme, when compared to the uncoded AQAM scheme, which was targeted at achieving the same BER performance. We have also noted the associated throughput degradation at high average channel SNRs as a result of the coding rate limitation imposed by the scheme. Subsequently, we revised the coded switching thresholds in order to create a near-error-free **FCFI-TBCH-AQAM** scheme, which also exhibited substantial SNR gains, when compared to the uncoded AQAM scheme. In the next section we shall introduce a range of coded AQAM schemes, which utilizes different interleaver sizes depending on the modulation mode selected. In order to remove the BPS limitation of the rate 0.7222 coded AQAM scheme and to increase its flexibility, it is feasible to introduce a range of further transmission code rates, which will be discussed in Section 4.7.

4.5 Fixed Coding Rate and Variable Interleaver Size Turbo Block Coded Adaptive Modulation

The main motivation in implementing a coded AQAM scheme in conjunction with a variable turbo interleaver size for each modulation mode is to provide the receiver with an error detection capability for each received AQAM data burst without any delay, as well as to vary the coding rate for each modulation mode. In doing so, an intelligent receiver will be capable of blindly detecting the modulation mode without explicit signalling, which will be discussed at a later stage. In order to provide an instantaneous error detection capability at the receiver, the turbo interleaver size must be equal or less than the number of transmitted bits for the transmission burst. This ensures that the received burst can be demodulated and decoded immediately on a burst by burst basis.

This Fixed Coding Rate and Variable Interleaver size Turbo Block Coded AQAM (**FCVI-TBCH-AQAM**) scheme is implemented in conjunction with a fixed coding rate of 0.7222,

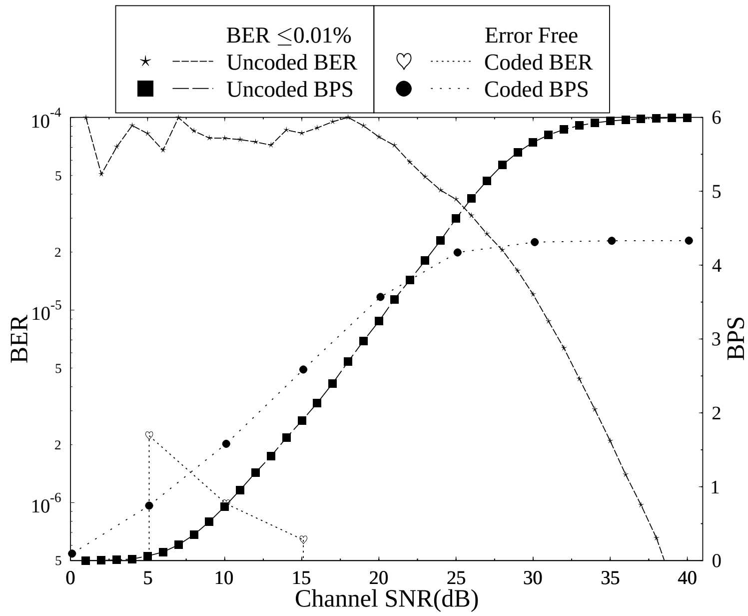

Figure 4.9: Performance of the near-**error-free** of the **FCFI-TBCH-AQAM** scheme of Section 4.4, where the generic system parameters of Table 4.1 were utilized. The coded switching regime was characterized by Equation 4.1 with the coding rate and turbo interleaver size set to 0.7222 and 9984 bits, respectively. The coded switching thresholds and transmission burst type were set according to Table 4.2. The performance was compared to the uncoded AQAM scheme, which was optimised for a target BER of 0.01% according to Table 3.8.

corresponding to the component code of BCH (31, 26, 3) for all modulation modes [143]. The turbo interleaver size is varied according to the modulation mode selected as well as the size of the transmission burst. The general switching regime is summarized in Equation 4.1, where the turbo interleaver size and the switching threshold are listed in Table 4.3 and 4.4, respectively, for the **High-BER**, **Low-BER** and for the near-error-free system. The remaining experimental parameters are listed in Table 4.1.

The BER and BPS performance of the **High-** and **Low-BER FCVI-TBCH-AQAM** scheme is shown in Figure 4.10. The corresponding **High-** and **Low-BER** uncoded AQAM performance curves are also depicted in Figure 4.10 for comparison. The characteristics of the results were similar to those shown in Figure 4.8 of Section 4.4.1 and can be explained similarly. For the **High-BER FCVI-TBCH-AQAM** scheme the throughput was higher than that of the uncoded scheme for the channel SNR range of 0 to 11dB, with a maximum SNR gain of approximately 2.3dB at a channel SNR of 0dB. Similarly, an average channel SNR gain of 8dB was achieved, when comparing the BER performance of the **Low-BER FCVI-TBCH-AQAM** scheme and the uncoded AQAM scheme at an average channel SNR of 20dB.

The throughput performance of **FCVI-TBCH-AQAM** was also compared to that of the

Target BER	Turbo Interleaver Size (Bits)				Burst Type see Figure 3.13
	I_0	I_1	I_2	I_3	
$\leq 1\%$	104	208	416	624	Speech
$\leq 0.01\%$	494	988	1976	2964	Data
Near-Error-Free	494	988	1976	2964	Data

Table 4.3: The turbo interleaver size associated with each modulation mode characterized by Equation 4.1 for the **FCVI-TBCH-AQAM** scheme described in Section 4.5. The target BERs were set to be below 1%, 0.01% and near-error-free, where the corresponding transmission burst types utilized are shown in Figure 3.13.

Target BER	Coded Switching Thresholds (dB)				Burst Type see Figure 3.13
	t_1^c	t_2^c	t_3^c	t_4^c	
$\leq 1\%$	0.6363	3.2258	8.6450	14.6846	Speech
$\leq 0.01\%$	1.9958	4.2079	10.5480	17.5089	Data
Near-Error-Free	3.2458	5.4579	11.7980	18.7589	Data

Table 4.4: The coded switching thresholds, which were experimentally determined in order to achieve the target BERs of below 1%, 0.01% and near-error-free for the **FCVI-TBCH-AQAM** scheme described in Section 4.5. The corresponding transmission burst types utilized are shown in Figure 3.13 and the switching mechanism was characterized by Equation 4.1.

fixed modulation modes shown in Figure 4.5 for target BERs of 1% and 0.01%. For the **Low-BER FCVI-TBCH-AQAM** scheme, a BPS/SNR gain of approximately 1.5dB was achieved, when compared to the fixed modulation modes utilizing the large channel interleavers, as evidenced by Figure 4.11(b). However, by referring to Figure 4.11(a) a more substantial gain of approximately 5.0dB was achieved, when compared to the fixed modulation modes utilizing the smaller channel interleavers. For the **High-BER FCVI-TBCH-AQAM** scheme, minimal gains were achieved, when compared to both the large- and small-channel interleaved fixed modulation modes. It is important to note here that these low gains were achieved despite the larger turbo interleaver and channel interleaver utilized by the fixed modulation modes. This resulted in a high transmission delay for the fixed modulation modes, whereas the **FCVI-TBCH-AQAM** scheme employed low-latency instantaneous burst-by-burst decoding.

In the **Low-BER FCVI-TBCH-AQAM** scheme the SNR gains achieved in the context of the associated BER and BPS performance curves were higher than those of the **High-BER FCVI-TBCH-AQAM** scheme. Explicitly, a higher throughput performance was observed across the average channel SNR range of 0 to 22dB, with the maximum SNR gain of 6dB at an average channel SNR of 0dB. Similarly, a SNR gain of 16dB was achieved at an average channel SNR of 20dB, when the BER performances were compared, as evidenced by Figure 4.8. The higher gains achieved by the **Low-BER** scheme were due to the lower BER requirement, which was justified in Section 4.4.1. The other contributing factor was due to the higher turbo interleaver size that was utilized for the **Low-BER** scheme, which possessed a longer transmission burst structure. Consequently, the turbo block coded bits were more decorrelated, which provided a higher coding gain, as it was argued in Section 4.1.

Lastly, the **FCVI-TBCH-AQAM** scheme was optimised in order to yield a near-error-

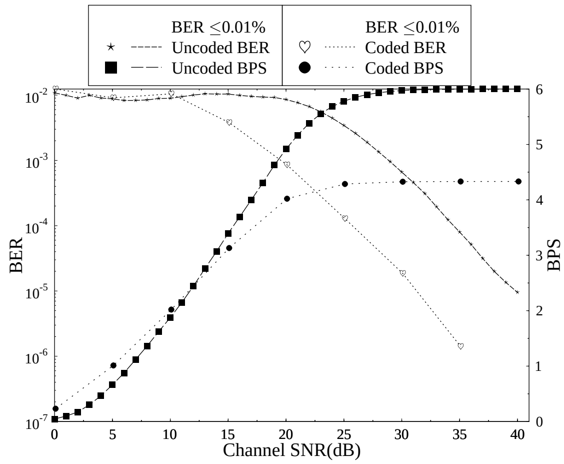

(a) Turbo block coded performance for a target BER of below 1% using the non-spread speech burst of Figure 3.13.

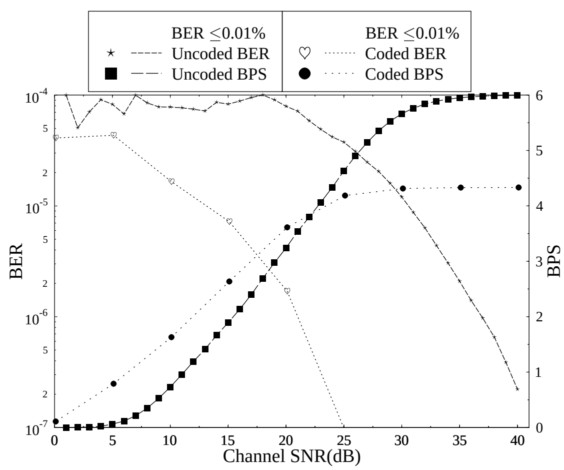

(b) Turbo block coded performance for a target BER of below 0.01% using the non-spread data burst of Figure 3.13.

Figure 4.10: Turbo block coded performance of the **FCVI-TBCH-AQAM** scheme described in Section 4.5, where the generic system parameters of Table 4.1 were utilized. The coded switching regime was characterized by Equation 4.1, where the coding rate was 0.7222 and variable turbo interleaver sizes were listed in Table 4.3, respectively. The coded and uncoded AQAM switching thresholds were set according to Table 4.4 and 3.8, respectively.

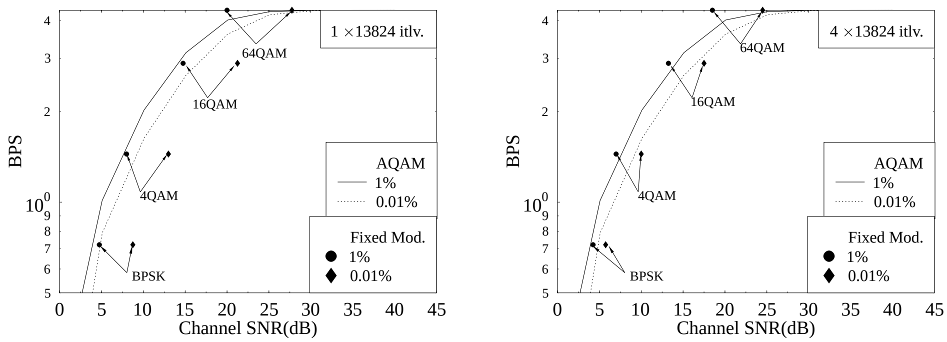

(a) Channel Interleaver of size 1×13824 bits

(b) Channel Interleaver of size 4×13824 bits

Figure 4.11: Throughput comparison between the **FCVI-TBCH-AQAM** scheme and the constituent fixed modulation modes for target BERs of 1% and 0.01%, which were evaluated from Figures 4.5 and 4.6. Different sized channel interleavers were used for the fixed modulation modes whereas the **FCFI-TBCH-AQAM** scheme employed no channel interleavers.

free communication system with the turbo coding parameters and the switching thresholds shown in Tables 4.3 and 4.4, respectively. The corresponding BER and BPS performance is shown in Figure 4.12, where the system was near-error-free. The throughput performance was also better for the average channel SNR range between 0 to 20dB, when compared to that of the uncoded AQAM scheme optimised for a target BER of 0.01%, as evidenced by Figure 4.12.

However, the SNR gains recorded for this variable-sized turbo interleaver scheme were lower than those of the fixed turbo interleaver scheme of Section 4.4 for both target BERs. This gain degradation was due to the reduced turbo interleaver size utilized in the **FCVI-TBCH-AQAM** scheme. Nevertheless, the **FCVI-TBCH-AQAM** scheme can provide a burst by burst error detection capability, which we will exploit in the next section.

4.6 Blind Modulation Detection

In Section 3.3.1 the receiver assumed that the modulation mode of the received packet was known. In reality, some form of signalling is needed in order to convey this information from the transmitter to the receiver [20] [21]. Recently, a blind modulation detection algorithm was proposed by Keller *et al.* in an adaptive OFDM scheme [144]. In this scheme, the mean square phasor error - which is defined as the Euclidean distance between the received equalized data symbols and the nearest legitimate constellation point for a particular AQAM mode - was evaluated. This was repeated for all valid modulation modes utilized in the wideband AQAM scheme. Subsequently, the modulation mode that produced the minimum mean square phasor error was selected. This is an example of a blind detection algorithm,

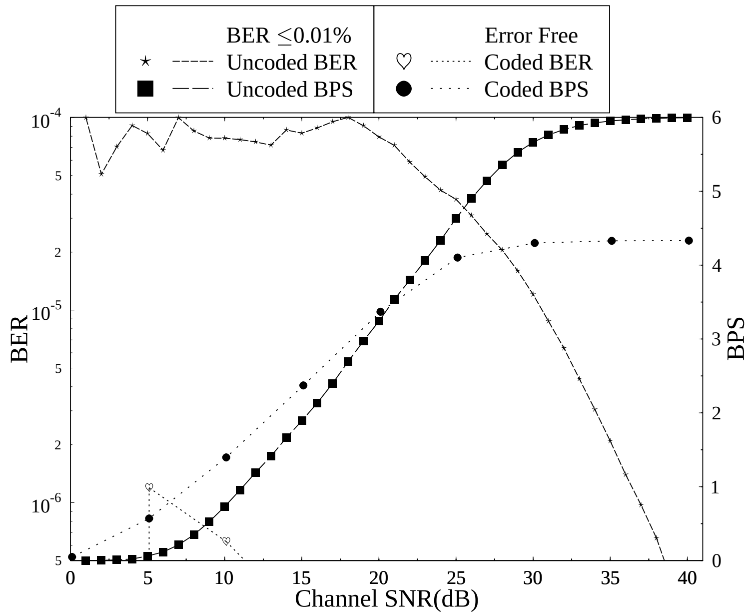

Figure 4.12: The near-**error-free** turbo block coded performance of the **FCVI-TBCH-AQAM** scheme described in Section 4.5. The coded switching regime was characterized by Equation 4.1, where the coding rate was set to 0.7222 and the turbo interleaver sizes were set according to Table 4.3, respectively. The coded switching thresholds and transmission burst type were set according to Table 4.4 and the other generic system parameters were listed Table 4.1. The performance was compared to that of the uncoded AQAM scheme, which was optimised for a target BER of 0.01% according to Table 3.8.

where the receiver is capable of detecting the modulation mode used without any signalling information from the transmitter. The primary motivation for the blind modulation detection algorithm is to reduce the amount of signalling between the receiver and the transmitter, consequently yielding an improved information throughput. This blind MSE modulation detection algorithm can be summarized as follows upon evaluating the accumulated MSE of a transmission burst for all legitimate modem modes :

$$\begin{aligned} e_m &= \frac{\sum_n \mid (R^{eq}_{n,m} - \hat{R}_{n,m}) \mid^2}{n} \\ mod_c &= min(e_m) \quad \text{for } m = \text{BPSK, 4QAM, 16QAM, 64QAM}, \end{aligned} \tag{4.2}$$

where m is the number of possible modulation modes and mod_c is the selected modulation mode based on the minimum average square error of the Euclidean distance e, for all the valid modulation modes. The function $min(e_m)$ is the selection function that selects the minimum of all e_m values, while $R^{eq}_{n,m}$ and $\hat{R}_{n,m}$ is the nth equalized symbol and the corresponding legitimate demapped constellation point of modulation mode m, respectively.

In exploring the performance of this blind MSE modulation detection algorithm, the PDF of all possible mean square phasor errors e_m for the four valid modulation modes is plotted and shown in Figure 4.13. In each of the sub-figures, the actual modulation mode utilized was stated in the respective captions and the PDF of the other valid modulation modes was also displayed. The common trend shown in Figure 4.13 was that the higher-order modulation modes of 64QAM and 16QAM constantly yielded the lowest mean square phasor error, independently of the actual modulation mode that was utilized, which was detrimental as regards to the performance of the blind modulation detection scheme. This characteristic can be explained by noting that the higher-order modulation modes of 64QAM and 16QAM possessed a higher number of legitimate constellation points. Consequently, the probability that the received equalized data symbol situated near a valid constellation point increased, which yielded a lower mean square phasor error. However, when BPSK was utilized, there was sufficient separation between the PDF of the BPSK and 4QAM modes, as evidenced by Figure 4.13(a). Thus this algorithm was capable of detecting the BPSK mode, if BPSK and 4QAM were the only possible valid modulation modes.

Since we have observed the deficiencies in the blind MSE-based algorithm, we will investigate the utilization of channel coding in order to blindly detect the modulation modes in the TBCH-AQAM scheme.

4.6.1 Blind Soft Decision Ratio Modulation Detection Scheme

Before elaborating further on this blind Soft Decision Ratio (SD) based modulation detection algorithm, we will address the concept of transmission blocking in AQAM. Practically, whenever the transmission is disabled, a transmission burst of a known sequence is transmitted, which is used to estimate the channel quality and hence to aid the selection of the next modulation mode. This burst is always BPSK modulated, in order to provide maximum error protection. However, this known sequence must be unique and easily identifiable by the receiver, in order to aid its NOTX mode detection. Consequently, we propose to use binary maximal-length shift register sequences $C^{(a)}$, commonly known as m-sequences, that have the following correlation properties [145]:

$$\begin{aligned} \theta_a(0) &= Q, \\ \theta_a(r) &= -1 \quad \text{for} \quad r \neq 0, \end{aligned} \tag{4.3}$$

where $\theta_a(r) = \sum_{i=0}^{Q-1} C_i^{(a)} C_{r+i}^{(a)}$ and Q is the length of the known m-sequence. Explicitly, at the transmitter, if the NOTX mode is selected, the same m-sequences are concatenated in order to form the transmission burst. Consequently, at the receiver the demodulated burst is correlated with the locally stored known m-sequence and if a maximum amplitude of Q is detected periodically corresponding to the correlation time-shift of zero, then the burst is deemed to be a NOTX mode burst. Having proposed a sequence for the NOTX mode and a technique for detecting it, we will now focus our attention on the detection of the BPSK, 4QAM, 16QAM and 64QAM modes.

Since the variable interleaver-based turbo block coded AQAM scheme employed burst by burst decoding at the receiver, we can exploit the error correction capability of the turbo codec. Consequently, we can utilize the information provided by the channel decoder in terms of its input bit probability and the corresponding output bit probability. In this so-called blind

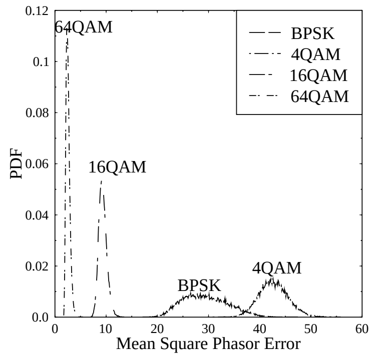

(a) The actual modulation mode was BPSK and the channel SNR was set to 8dB.

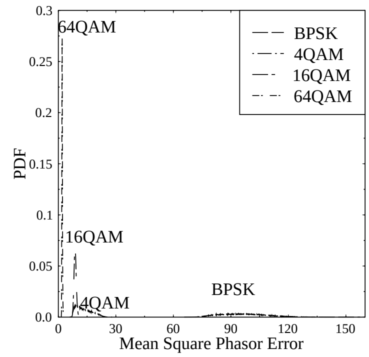

(b) The actual modulation mode was 4QAM and the channel SNR was set to 12dB.

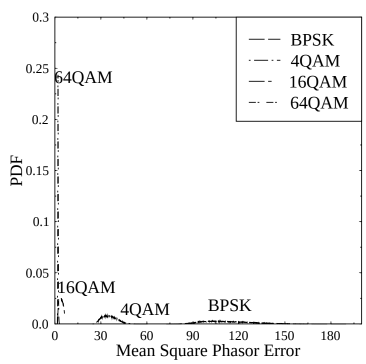

(c) The actual modulation mode was 16QAM and the channel SNR was set to 16dB.

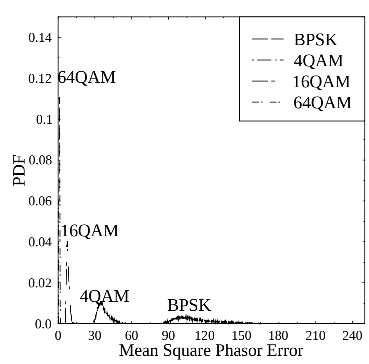

(d) The actual modulation mode was 64QAM and the channel SNR was set to 20dB.

Figure 4.13: The PDF of the mean square phasor error defined in Equation 4.2 for each individual modulation mode and for various channel SNRs.

Soft Decision Ratio (SD) modulation detection scheme, each input bit's probability upon entering the channel decoder is compared against its corresponding output bit probability for each possible modulation modes. The results are then classified into two categories, where one category consists of the number of times the input bit probability is less than the output bit probability and vice-versa for the other category. These two categories are then used to update a Soft Decision counter SD_{ratio}, as follows:

$$\text{SD}^{n,m}_{ratio} = \begin{cases} \text{SD}^{n,m}_{ratio} & \text{if } p^{n,m}_{ipbit} \leq p^{n,m}_{opbit} \\ \text{SD}^{n,m}_{ratio} + 1 & \text{if } p^{n,m}_{ipbit} > p^{n,m}_{opbit}, \end{cases} \tag{4.4}$$
$$\text{for } m = \text{BPSK, 4QAM, 16QAM, 64QAM,}$$

where $p^{n,m}_{ipbit}$ represents the nth input bit probability, which is demodulated using the modulation mode m. Similarly, $p^{n,m}_{opbit}$ denotes the output bit probability of the channel decoder. Subsequently, the average soft decision ratio is calculated for all possible valid modulation modes and the final modulation mode is chosen as follows:

$$\begin{aligned} \text{Average } \text{SD}^{m}_{ratio} &= \frac{\sum_n \text{SD}^{n,m}_{ratio}}{N}, \\ mod_c &= min(\text{Average } \text{SD}^{m}_{ratio}), \\ \text{for } m &= \text{BPSK, 4QAM, 16QAM, 64QAM,} \end{aligned} \tag{4.5}$$

where mod_c denotes the chosen modulation mode and $min(a^m)$ is the selection function that selects the minimum of all a^m values, while N represents the number of coded bits in a transmission burst.

The PDF of the average SD_{ratio} of all the possible modulation modes is shown in Figure 4.14. In each of the sub-figures the actual modulation mode used was stated in the respective captions. Referring to Figure 4.14, there was a clear PDF separation between the actual modulation mode and the other modulation modes, where the SD_{ratio} of the actual modulation mode was centered at the minimum end of the average SD_{ratio} scale. It was this PDF separation that supported the feasibility of the proposed blind SD modulation detection scheme.

This blind modulation detection algorithm was implemented using the simulation parameters of Table 4.1. A conventional binary BCH(31 ,26 ,3) was utilized without channel interleavers for simplicity, although this algorithm can be applied to turbo encoding, since its component code was identical to the above BCH code. The speech-type burst of Figure 3.13 was used and the m-sequence length $Q = 31$. The performance of this algorithm in terms of its modulation Detection Error Rate (DER) is depicted in Figure 4.15(a). The detection algorithm yielded a DER below 10^{-4} at a channel SNR of approximately 24dB. However, a severe DER degradation was observed for channel SNRs between 10 - 20dB. In order to investigate this degradation, the individual Wrong Modulation Error Percentage (WME) was plotted in Figure 4.15(b). This measure recorded the relative frequency of the modulation mode detected by the algorithm, when the detection scheme was in error. As it can be observed in Figure 4.15, whenever the detection algorithm failed, the BPSK mode was frequently chosen compared to the other modulation modes. Referring to Figures 4.14(b) - 4.14(d), we observed that the SD_{ratio} PDF of the BPSK mode had the greatest overlapping region with the PDF of the actual modulation mode at low SD_{ratio} values. This implied

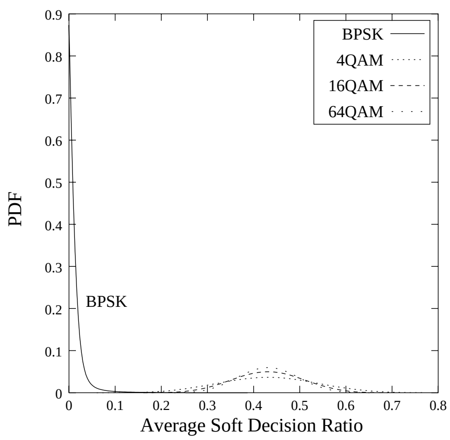

(a) The actual modulation mode was BPSK and the channel SNR was set to 8dB.

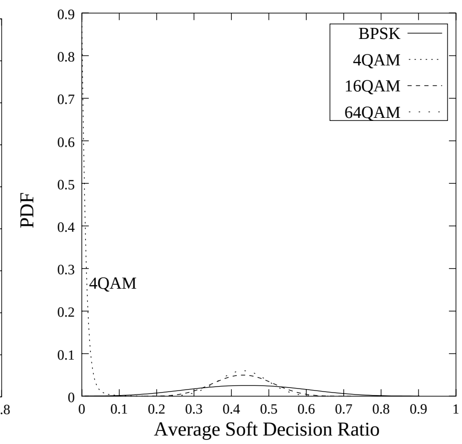

(b) The actual modulation mode was 4QAM and the channel SNR was set to 12dB.

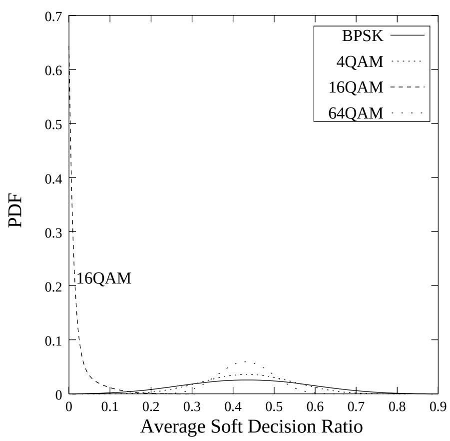

(c) The actual modulation mode was 16QAM and the channel SNR was set to 16dB.

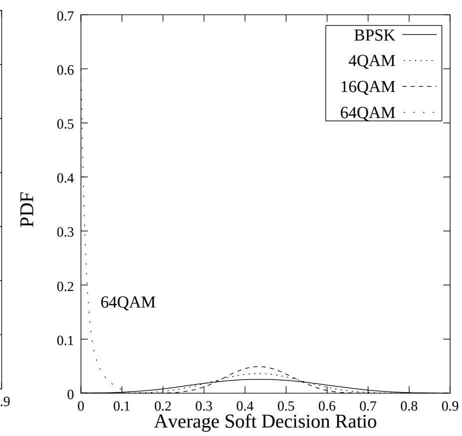

(d) The actual modulation mode was 64QAM and the channel SNR was set to 20dB.

Figure 4.14: The PDF of the average soft decision ratio defined in Equation 4.5 for each individual modulation mode and for various channel SNRs, using a conventional binary BCH(31 ,26 ,3) coding scheme.

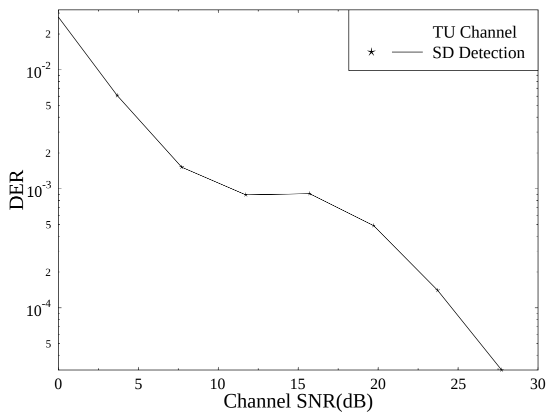

(a) DER performance.

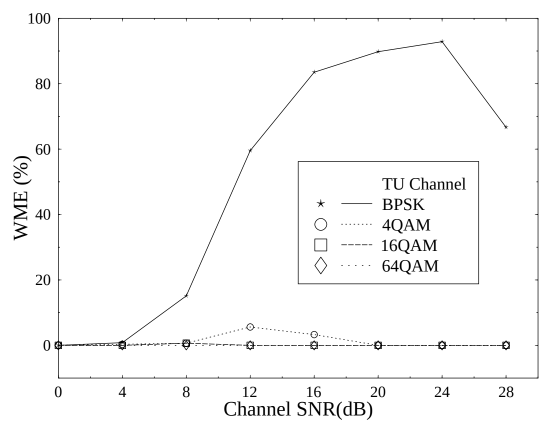

(b) WME performance.

Figure 4.15: The DER and WME performance of the SD algorithm characterized by Equation 4.5. The system parameters of Table 4.1 were utilized and the AQAM switching thresholds were set according to Table 3.8 for the target BER of 1%. The DER and WME measures were defined in Section 4.6.1 and a conventional binary BCH(31, 26, 3) coding scheme was utilized.

that the receiver had a higher probability of selecting BPSK, even though it was the wrong modulation mode.

In order to improve the DER performance, the detection of the BPSK mode has to be more robust. Consequently, here we propose to utilize a hybrid Soft Decision Mean Square Error (SD-MSE) based blind modulation detection algorithm for the coded AQAM scheme.

4.6.2 Hybrid Soft Decision Mean Square Error Modulation Detection Algorithm

In Section 4.6 the concept of utilizing the mean square phasor error at the receiver in order to blindly detect the modulation mode was presented. In Figures 4.13a - 4.13d we have observed that this measure was not sufficiently reliable in order to detect the modulation modes. However, when the BPSK mode was actually utilized, there was a sufficient PDF separation between the mean square phasor error PDF of the BPSK and 4QAM modes, as evidenced by Figure 4.13(a). Consequently we exploited this property in order to detect the BPSK mode. In this hybrid algorithm the BPSK mode is detected by comparing the average square error of the BPSK and 4QAM modes. The other modulation modes - namely 4QAM, 16QAM and 64QAM - were then detected using the SD algorithm of Section 4.6.1. This SD-MSE algorithm can be summarized as follows [143, 146]:

$$mod_c = \begin{cases} \text{BPSK} & \text{if } e_{BPSK} \leq e_{4QAM} \\ min(\text{Average SD}^m_{ratio}) & \text{if } e_{BPSK} > e_{4QAM}, \end{cases} \qquad (4.6)$$
$$\text{for } m = \text{4QAM, 16QAM, 64QAM},$$

where Average SD^m_{ratio} and e_q were defined in Equations 4.5 and 4.2, respectively. The DER performance of this hybrid algorithm is presented in Figure 4.16, where the experimental parameters were identical to those used by the SD algorithm of Section 4.6.1. In Figure 4.16 the performance of the SD detection algorithm is shown as a comparison to that of the SD-MSE algorithm. The hybrid SD-MSE algorithm achieved a DER of 10^{-4} at a channel SNR of approximately 15dB [143, 146]. The improvement of the SD-MSE algorithm was clearly seen in Figure 4.16 where the associated performance was superior to that of the SD-based technique, in the channel SNR range of between 10 - 20dB. Furthermore, the complexity of this SD-MSE algorithm was reduced, since the channel decoder was only used to detect three modes instead of the four modes of the SD algorithm.

In this section we have demonstrated that channel coding can be utilized for detecting the modulation mode at the receiver in a coded AQAM scheme. We have presented three different blind detection algorithms, where the MSE algorithm was deemed unreliable for detecting the four modes. The higher complexity SD and hybrid SD-MSE algorithms were then proposed, where the latter exhibited a better performance in terms of DER.

4.7 Variable Coding Rate Turbo Block Coded Adaptive Modulation

In Sections 4.4 and 4.5 we have characterized a range of turbo block coded AQAM schemes having fixed coding rates for all modulation modes, where a throughput degradation was

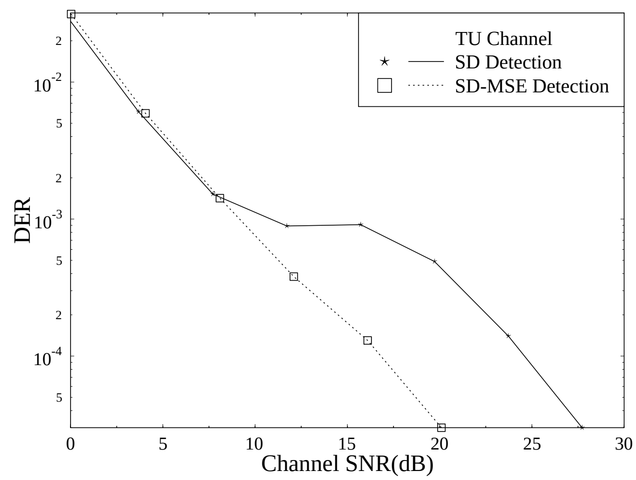

Figure 4.16: The DER performance of the SD-MSE algorithm characterized by Equation 4.6. The system parameters of Table 4.1 were utilized and the AQAM switching thresholds were set according to Table 3.8 for the target BER of 1%. The DER measure was defined in Section 4.6.1 and a conventional binary BCH(31, 26, 3) coding scheme was utilized.

observed at high channel SNRs, when compared to the uncoded AQAM schemes for similar target BERs. However, with the aim of improving the throughput of the turbo block coded AQAM scheme at high average channel SNRs, here we will introduce the concept of variable rate turbo coding AQAM schemes.

Explicitly, we will implement two types of variable code rate schemes. In the first scheme we invoke a switching mechanism that is capable of disabling and enabling the channel encoder for a chosen modulation mode. This scheme will be described in detail in the next section. For the second variable-rate scheme the coding rate is varied by utilizing different BCH component codes for the different modulation modes. Let us now describe the first variable-rate turbo block coded AQAM scheme.

4.7.1 Partial Turbo Block Coded Adaptive Modulation Scheme

In this Partial Turbo Block Coded Adaptive Modulation (**P-TBCH-AQAM**) scheme the option to disable or enable the channel encoder for each individual modulation mode is made available to the transmitter. In order to ensure that the transmitted bits are in their original sequence irrespective of the coding rate, the turbo interleaver size is varied according to the modulation mode selected, as discussed in Section 4.5. The corresponding switching mechanism for this scheme can be summarized as follows:

$$\text{Modulation Mode} = \begin{cases} NOTX & \text{if } \gamma_{DFE} < t_1^c \\ BPSK, I_0, R_0 & \text{if } t_1^c < \gamma_{DFE} \leq t_2^c \\ BPSK, \text{Coding Disabled} & \text{if } t_2^c < \gamma_{DFE} \leq t_3^c \\ 4QAM, I_1, R_1 & \text{if } t_3^c < \gamma_{DFE} \leq t_4^c \\ 4QAM, \text{Coding Disabled} & \text{if } t_4^c < \gamma_{DFE} \leq t_5^c \\ 16QAM, I_2, R_2 & \text{if } t_5^c < \gamma_{DFE} \leq t_6^c \\ 16QAM, \text{Coding Disabled} & \text{if } t_6^c < \gamma_{DFE} \leq t_7^c \\ 64QAM, I_3, R_3 & \text{if } t_7^c < \gamma_{DFE} \leq t_8 \\ 64QAM, \text{Coding Disabled} & \text{if } \gamma_{DFE} > t_8^c, \end{cases} \tag{4.7}$$

where the notations are identical to those in Equation 4.1.

This scheme was simulated with the coding rate set to 0.7222, which corresponded to a turbo component code of BCH (31, 26, 3). The coded switching thresholds were chosen in order to achieve target BERs of 1% and 0.01% as shown in Table 4.6 with the corresponding turbo interleaver size for each modulation mode shown in Table 4.5. The **P-TBCH-AQAM** switching thresholds were set by combining the coded thresholds set in Table 4.4 and the uncoded switching thresholds of Table 3.8. The resulting switching thresholds are shown in Table 4.6, where if any two different switching thresholds associated with their modulation/coding mode exhibited identical values, this implied that the corresponding modulation/coding mode that is selected by these two switching thresholds is discarded. Consequently, in the **High-BER** scheme the un-coded BPSK mode was disabled, whereas for the **Low-BER** scheme the un-coded BPSK, non-coded 4QAM and non-coded 16QAM modes were disabled.

Target BER	Turbo Interleaver Size (Bits)				Burst Type see Figure 3.13
	I_0	I_1	I_2	I_3	
$\leq 1\%$	104	208	416	624	Speech
$\leq 0.01\%$	494	988	1976	2964	Data
Near-Error-Free	494	988	1976	2964	Data

Table 4.5: The turbo interleaver size associated with each modulation mode characterized by Equation 4.7 for the **P-TBCH-AQAM** scheme described in Section 4.7.1. The target BERs were set to be below 1%, 0.01% and near-error-free, where the corresponding transmission burst types utilized are shown in Figure 3.13.

The BER and BPS performance of the **Low-** and **High-BER P-TBCH-AQAM** scheme is shown in Figure 4.17, where the uncoded AQAM performance optimised for similar target BERs is depicted for comparison. For the **High-BER** scheme the BER performance of the **P-TBCH-AQAM** and uncoded AQAM schemes was similar and the target BER of 1% was maintained. In terms of BPS performance, at low to medium channel SNRs the coded scheme performed better, but at higher SNRs, their BPS performances converged to that of 64QAM, since the uncoded 64QAM mode was the dominant transmission mode chosen at high average channel SNRs. The same characteristics can be observed for the **Low-BER P-TBCH-AQAM** scheme, where the channel coding was only disabled, when the 64QAM

Target BER	Coded Switching Thresholds (dB)								Burst Type see Figure 3.13
	t_1^c	t_2^c	t_3^c	t_4^c	t_5^c	t_6^c	t_7^c	t_8^c	
$\leq 1\%$	0.64	3.23	3.23	6.23	8.65	11.65	14.68	17.83	Speech
$\leq 0.01\%$	1.99	4.21	4.21	10.55	10.55	17.51	17.51	23.76	Data

Table 4.6: The coded switching thresholds, which were intuitively optimised in order to achieve the target BERs of below 1% and 0.01% for the **P-TBCH-AQAM** scheme described in Section 4.7.1. The corresponding transmission burst types utilized are shown in Figure 3.13 and the switching mechanism was characterized by Equation 4.7.

mode was selected. The BER performance of the **Low-BER P-TBCH-AQAM** scheme improved at low to medium channel SNRs due to the channel codec's contribution associated with the BPSK, 4QAM and 16QAM modes. However, at channel SNRs of above 20dB the uncoded 64QAM mode became dominant, degrading slightly the BER and converging to the uncoded 64QAM performance. Nevertheless, the target BER of 0.01% was still maintained. The BPS performance of the **Low-BER P-TBCH-AQAM** scheme was similar or superior to that of the **Low-BER** uncoded AQAM scheme, where a maximum SNR gain of approximately 6dB was recorded at an average channel SNR of 0dB, as evidenced by Figure 4.17.

From these results we concluded that - as expected - the **P-TBCH-AQAM** scheme improved the throughput of the system, especially at high channel SNR values, when the channel coding was disabled. However in doing so, the BER performance slightly degraded, although it was still within the target BER limits for which it was optimised. Furthermore, the number of transmission modes was also increased, which increased the amount of signalling between the transmitter and receiver. In the next section, we will introduce another variable rate turbo block coded AQAM scheme, where the coding rate was varied in conjunction with each modulation mode by using different BCH component codes.

4.7.2 Variable Rate Turbo Block Coded Adaptive Modulation Scheme

In this Variable Rate Turbo Block Coded Adaptive Modulation (**VR-TBCH-AQAM**) scheme, a specific BCH code is assigned to each individual modulation mode [142, 146]. The higher-order modulation modes are assigned a higher code rate, in order to improve the effective data throughput at medium to high average channel SNRs and conversely, the lower-order modulation modes will be accompanied by lower code rates, in order to ensure maximum error protection at low average channel SNRs, where these modes have a high selection probability.

The modulation mode switching regime is identical to that of Equation 4.1, where the turbo interleaver size, switching levels and coding rates for all modulation modes are listed in Tables 4.7, 4.8 and 4.9, respectively. The remaining system parameters are listed in Table 4.1.

The turbo interleaver sizes were chosen with the objective of ensuring burst-by-burst turbo decoding at the receiver. Consequently the decoded bits are in the right sequence, irrespective of the different component codes used. However, due to the longer codes used by the 16QAM and 64QAM modes, dummy bits were also included in order to ensure that the number of turbo encoded bits was equal to the transmission burst size. These dummy bits could be used for conveying control or signalling information. Alternatively, these dummy

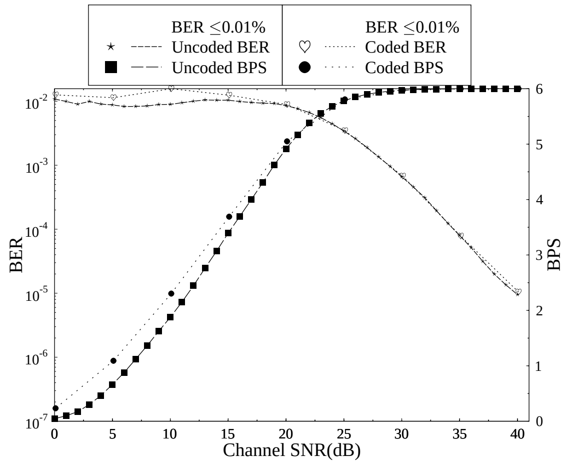

(a) Turbo block coded performance for a target BER of below 1% using the non-spread speech burst of Figure 3.13.

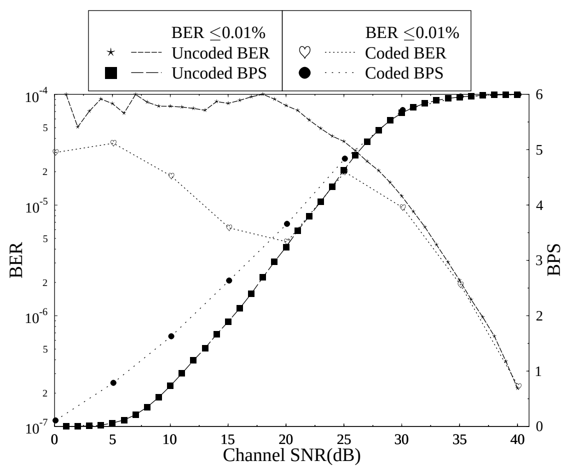

(b) Turbo block coded performance for a target BER of below 0.01% using the non-spread data burst of Figure 3.13.

Figure 4.17: Turbo block coded performance of the **P-TBCH-AQAM** scheme, which was described in Section 4.7.1, where the generic system parameters of Table 4.1 were utilized. The coded switching regime was characterized by Equation 4.7, where the coding rate was 0.7222 and the turbo interleaver sizes were listed in Table 4.5, respectively. The coded and uncoded AQAM switching thresholds were set according to Table 4.6 and 3.8, respectively.

Target BER	Turbo Interleaver Size (Bits)				Burst Type see Figure 3.13
	I_0	I_1	I_2	I_3	
$\leq 1\%$	104	208	456	720	Speech
$\leq 0.01\%$	494	988	2223	3600	Data
Near-Error-Free	494	988	2223	3600	Data

Table 4.7: The turbo interleaver size associated with each modulation mode characterized by Equation 4.1 for the **VR-TBCH-AQAM** scheme described in Section 4.7.2. The target BERs were set to be below 1%, 0.01% and near-error-free, where the corresponding transmission burst types utilized are shown in Figure 3.13.

Target BER	Coded Switching Thresholds (dB)				Burst Type see Figure 3.13
	t_1^c	t_2^c	t_3^c	t_4^c	
$\leq 1\%$	0.6363	3.2258	9.6450	15.6846	Speech
$\leq 0.01\%$	1.9958	4.2079	11.5480	18.5089	Data
Near-Error-Free	3.2458	5.4579	12.7980	19.7589	Data

Table 4.8: The coded switching thresholds, which were experimentally determined in order to achieve target BERs of below 1%, 0.01% and near-error-free for the **VR-TBCH-AQAM** scheme described in Section 4.7.2. The corresponding transmission burst types utilized are shown in Figure 3.13 and the switching mechanism was characterized by Equation 4.1.

	R_0	R_1	R_2	R_3
Turbo Code Rate	0.722	0.722	0.826	0.896
BCH (n, k, d_{min}))	(31, 26, 3)	(31, 26, 3)	(63, 57, 3)	(127, 120, 3)

Table 4.9: The coding rate and the corresponding BCH component code associated with each modulation mode characterized by Equation 4.1 for the **VR-TBCH-AQAM** scheme described in Section 4.7.2.

bits could remain uncoded. In our subsequent discussions concerning this scheme, these dummy bits were not utilized for information transmission.

The corresponding BER and BPS performances are depicted in Figure 4.18. For the **High-BER VR-TBCH-AQAM** scheme, which was targeted at a BER of 1%, the coded BER performance was similar to that of the **High-BER** uncoded AQAM scheme, where a slight SNR gain was observed at average channel SNRs above 25dB. The BPS performance improved for channel SNRs between 0 to 10dB. However, the coded BPS performance degraded at high channel SNRs, when compared to the uncoded AQAM case as a result of the throughput reduction caused by the channel coding scheme. These low SNR gains observed in terms of both the BER and BPS curves were due to the smaller turbo interleaver sizes with respect to the code length as well as due to the higher code rate imposed on the higher-order modulation modes.

The BER performance of the **Low-BER VR-TBCH-AQAM** scheme was similar to that of the **Low-BER** uncoded AQAM scheme for channel SNRs below 15dB. However, at higher average channel SNRs the coded BER performance was superior, where a channel SNR gain of approximately 10dB was recorded across a wide range of BERs. The BPS performance of the **Low-BER VR-TBCH-AQAM** scheme improved for channel SNRs between 0 to 28dB, when compared to the **Low-BER** uncoded AQAM scheme. However, at higher average channel SNRs, the coded throughput was limited by the coding rate and consequently converged to a throughput of approximately 5.3 bits per symbol.

The coded switching thresholds were also re-adjusted experimentally, in order to create a near-error-free system, where the values of the coded switching thresholds are listed in Table 4.8. The BER and BPS performance is shown in Figure 4.19, where the **VR-TBCH-AQAM** scheme was near-error-free. The coded BPS performance, when compared to the **Low-BER** uncoded AQAM, exhibited an SNR gain for channel SNRs between 0 to 25dB. However, the coded BPS curve converged to a throughput of 5.3 bits per symbol at high average channel SNRs due to the limitation imposed by the coding rate of the scheme.

In conjunction with this scheme we have noted a substantial SNR gain for the **Low-BER** and near-error-free **VR-TBCH-AQAM** scheme of Figures 4.18(b) and 4.19. However only a slight SNR gain was observed for the **High-BER** scheme as evidenced by Figure 4.18(a). In the next section, we will analyse the four different turbo block coded AQAM schemes that we have introduced in this treatise and discuss their relative merits and disadvantages.

4.8 Comparisons of the Turbo Block Coded AQAM Schemes

In this section, the relative merits and disadvantages of the various turbo block coded AQAM schemes designed for target BERs of 1%, 0.01% and for near-error-free communication systems are summarized. We compared and contrasted each of these schemes in terms of their BER and BPS performance, considering also their relative complexity and their error detection capabilities. Their coded BER and BPS performances were compared to the uncoded AQAM performance. Comparisons were carried out firstly for similar target BERs in terms of the associated maximum SNR gain observed from the BPS performance curves, secondly, the maximum achievable BPS throughput and thirdly, the gain observed from the BER performance curves were recorded. These measures were termed as the BPS/SNR gain, the maximum BPS and BER/SNR gain, respectively. The BPS/ and BER/SNR gain was measured against the corresponding curves of the uncoded AQAM scheme for similar target BERs, where the optimised switching thresholds are listed in Table 3.8. An additional throughput-related measure was the range of channel SNRs, where the coded BPS was higher than that of the uncoded AQAM scheme for similar target BERs. This measure was termed as the effective BPS gain range.

The relative complexity of the scheme was approximated by each individual channel decoder's complexity. The complexity was measured in terms of the number states generated by the trellis decoding algorithm in order to decode the received bits. The number of trellis states needed for each scheme provided an indication of the amount of floating-point computation needed. The complexity was calculated based on the complexity of the BCH decoder, instead of the total turbo decoding complexity, since the number of turbo decoding iterations was identical for each turbo block coded AQAM scheme. The decoder complexity in terms

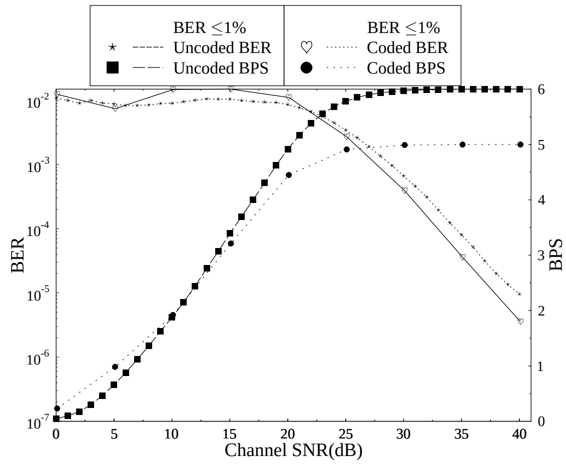

(a) Turbo block coded performance for a target BER of below 1% using the non-spread speech burst of Figure 3.13.

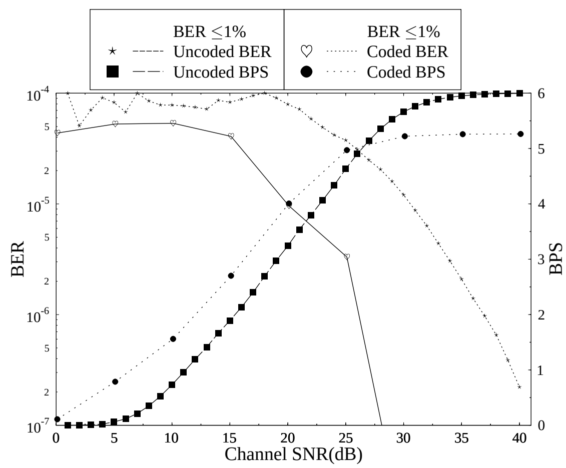

(b) Turbo block coded performance for a target BER of below 0.01% using the non-spread data burst of Figure 3.13.

Figure 4.18: Turbo block coded performance of the **VR-TBCH-AQAM** scheme, which was described in Section 4.7.2, where the generic system parameters of Table 4.1 were utilized. The coded switching regime was characterized by Equation 4.1, where the coding rates and turbo interleaver sizes were listed in Tables 4.9 and 4.7, respectively. The coded and uncoded AQAM switching thresholds were set according to Table 4.8 and 3.8, respectively.

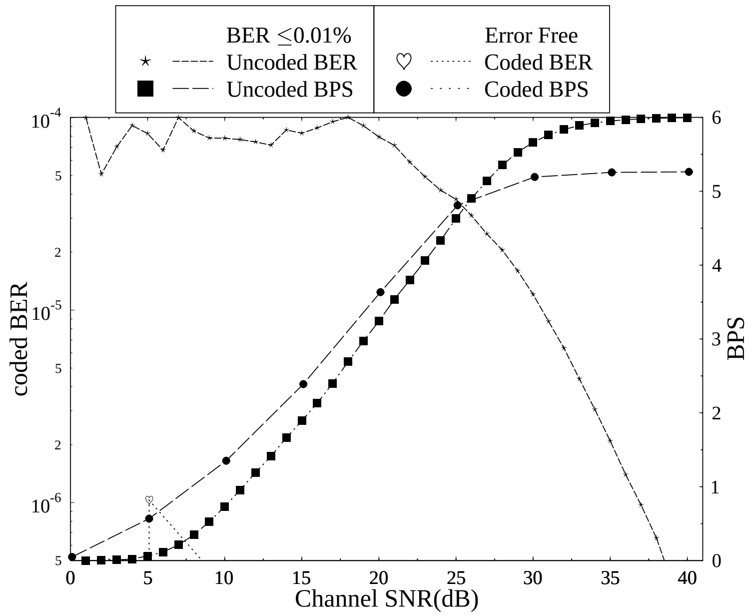

Figure 4.19: The near-**error-free** performance of the **VR-TBCH-AQAM** scheme described in Section 4.7.2. The coded switching regime was characterized by Equation 4.1, where the coding rates and turbo interleaver sizes were set according to Tables 4.9 and 4.7, respectively. The coded switching thresholds and transmission burst types were set according to Table 4.8 while the other generic system parameters were listed in Table 4.1. The performance was also compared to that of the uncoded AQAM scheme, which was optimised for a target BER of 0.01% according to Table 3.8.

of the trellis states was approximated as follows:

$$\begin{aligned} \text{comp}_m &\approx (2k_m - n_m + 3)(2^{n_m - k_m}), \\ average\ \ comp &\approx \frac{\sum_m \text{comp}_m}{4}, \\ \text{for}\ \ m &= \text{BPSK, 4QAM, 16QAM, 64QAM}, \end{aligned} \tag{4.8}$$

where comp_m is the complexity of the decoder associated with modulation mode m. Furthermore n_m and k_m denotes the number of coded bits and uncoded information bits of a certain BCH code associated with the modulation mode m. The term $2^{n_m - k_m}$ represents the total number of trellis states for a particular time instant, although the actual number of states visited in a codeword varies for different time instants, which is quantified by the term $2k_m - n_m + 3$. By assuming that the modulation modes have an equal probability of being selected, the $average\ \ comp$ was the average complexity of the decoder after taking into account the complexity related to each of the four different modes.

The other complexity consideration with regards to these schemes was the number of coded transmission modes that was utilized by each scheme, which incorporated the modulation and coding parameters. The number of modes affected the amount of signalling or modulation detection complexity, where a higher number of modes required a more complex modulation detection scheme. There are four turbo block coded AQAM schemes to be compared, which were described in Sections 4.4, 4.5, 4.7.1 and 4.7.2. Explicitly, their system characteristics and their relative complexity measures are shown in Table 4.10. We will explore their complexity, BPS/SNR and BER/SNR gain comparisons for the **Low-BER** turbo block coded AQAM scheme in the next section.

Turbo Block Coded AQAM Scheme	Interleaver Size	Coding Rate	Total modes	$average\ comp$ see Equation 4.8
FCFI-TBCH-AQAM	Fixed	Fixed	5	768
FCVI-TBCH-AQAM	Varied	Fixed	5	768
P-TBCH-AQAM	Varied	Varied	9	768
VR-TBCH-AQAM	Varied	Varied	5	4960

Table 4.10: Complexity comparisons of the **FCFI-TBCH-AQAM**, **FCVI-TBCH-AQAM**, **P-TBCH-AQAM** and **VR-TBCH-AQAM** schemes, where their characteristics were described in Sections 4.4, 4.5, 4.7.1 and 4.7.2. The channel decoder's complexity was calculated using Equation 4.8.

4.8.1 Comparison of Low-BER Turbo Block Coded AQAM Schemes

In these **Low-BER** Turbo Block Coded AQAM schemes the data burst of Figure 3.13 was utilized and their performance was compared to that of the **Low-BER** uncoded AQAM scheme, which utilized the switching thresholds of Table 3.8. The gain comparisons discussed in Section 4.8 for the different turbo block coded AQAM schemes are tabulated in Table 4.11 and depicted in Figure 4.20.

Turbo Block Coded AQAM Scheme	BPS/SNR gain (dB)	Maximum BPS	Effective BPS gain range(dB)	BER/SNR gain(dB)
FCFI-TBCH-AQAM	7.0	4.3	$0-23$	21.0
FCVI-TBCH-AQAM	6.0	4.3	$0-22$	17.5
P-TBCH-AQAM	6.0	6.0	$0-40$	≈ 0
VR-TBCH-AQAM	6.0	5.3	$0-26$	10.0

Table 4.11: Performance comparisons of the **Low-BER FCFI-TBCH-AQAM**, **FCVI-TBCH-AQAM**, **P-TBCH-AQAM** and **VR-TBCH-AQAM** schemes for a target BER of below 0.01**%**, where their system characteristics were described in Sections 4.4, 4.5, 4.7.1 and 4.7.2. Their performances were compared to the uncoded AQAM performance optimised for a target BER of 0.01% according to Table 3.8. The performance gains of each scheme were extracted from Figure 4.20.

The 0.01% target BER i.e **Low-BER-FCFI-TBCH-AQAM** scheme provided a high

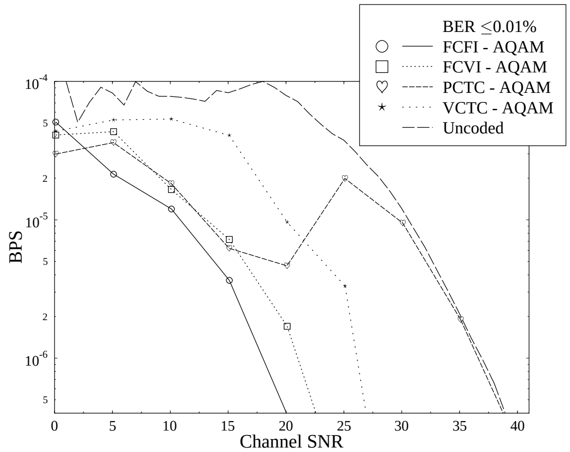

(a) Turbo block coded BER performance for a target BER of below 0.01% using the non-spread data burst of Figure 3.13.

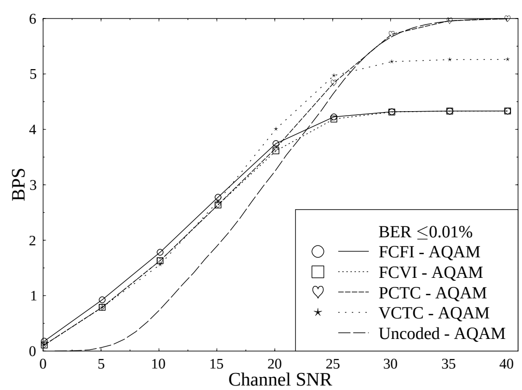

(b) Turbo block coded BPS performance for a target BER of below 0.01% using the non-spread data burst of Figure 3.13.

Figure 4.20: Performance comparisons of the **Low-BER FCFI-TBCH-AQAM**, **FCVI-TBCH-AQAM**, **P-TBCH-AQAM** and **VR-TBCH-AQAM** schemes, where the system characteristics were described in Sections 4.4, 4.5, 4.7.1 and 4.7.2. Their performances were compared to that of the uncoded AQAM scheme optimised for a target BER of 0.01% according to Table 3.8. The performance gains of each scheme were tabulated in Table 4.11.

SNR gain in terms of its BER performance, although a limited throughput of 4.3 bits per symbol was exhibited as evidenced by Table 4.11. The BER/SNR gain of 21dB, which was measured at a channel SNR of 20dB was achieved due to the large turbo interleaver size of 9984 bits and a relatively low code rate, when compared to the other schemes. However, the maximum throughput was limited to 4.3 bits per symbol due to the low coding rate. This scheme also exhibited a better BPS performance, than the uncoded AQAM for the channel SNR range of 0 to 23dB with a maximum SNR gain of 7dB in term of its BPS performance. Furthermore, as a result of the large turbo interleaver size, the burst by burst error detection capability of the receiver in detecting the modulation modes had to be sacrificed.

The 0.01% target BER i.e **Low-BER-FCVI-TBCH-AQAM** scheme yielded a BER/SNR performance gain of 17.5 dB at a channel SNR of 20dB, which was lower than that of the corresponding **FCFI-TBCH-AQAM** scheme of Table 4.11. This was mainly due to the smaller turbo interleaver size used for each modulation mode in the **FCVI-TBCH-AQAM** scheme, which degraded the BER performance of the turbo codec. Consequently, - as seen in Table 4.4 - a more conservative coded switching thresholds was set in order to ensure that the target BER was achieved. This degraded the BPS performance slightly, when compared to the **FCFI-TBCH-AQAM** scheme as it is evidenced by the 6dB maximum BPS/SNR gain and the effective BPS gain range shown in Table 4.11. However, the utilization of the variable turbo interleaver provided the burst-by-burst error detection capability of the receiver. With the exception of the turbo interleavers, both the **FCFI-TBCH-AQAM** and **FCVI-TBCH-AQAM** schemes have the same decoder complexity associated with 768 trellis states and an identical number of switching modes of 5, as evidenced by Table 4.10.

In the **P-TBCH-AQAM** scheme a high coded throughput of 6 bits per symbol was achieved but the BER/SNR gain was approximately zero in Table 4.11, although the target BER was achieved. This highest throughput was achieved as a result of the utilization of un-coded transmission modes, as shown in Equation 4.7. However, when this mode was invoked, the BER performance degraded, resulting in the minimal BER/SNR gain. Nevertheless, the BPS performance improved, when compared to the uncoded AQAM scheme, where an effective BPS gain range was observed for the entire channel SNR range, with a maximum BPS gain of 6dB. The utilization of the variable-sized turbo interleaver was essential, in order to preserve the ordering of bit sequence, when the coding rate was varied. However, due to the un-coded modes, the error detection capability was sacrificed. Furthermore, with the inclusion of the un-coded modes, the number of transmission modes increased to a maximum of 9 modes. Consequently, the adaptive switching regime and the signalling protocol between the transmitter and receiver was more complex.

In the last scheme, the **VR-TBCH-AQAM** scheme provided an average BER.SNR gain of 10dB at an average channel SNR of 20dB and a high average throughput of 5.3 bits per symbol, as a result of the higher coding rate used for this scheme. The utilization of higher coding rates for the higher-order modulation modes degraded the BER performance, when compared to the **FCVI-TBCH-AQAM** scheme, where a constant coding rate was used. However, the throughput performance improved, when compared to the **FCVI-TBCH-AQAM** scheme, where a positive BPS gain was observed for the channel SNR range between 0 to 26dB. The utilization of a variable interleaver size in the **VR-TBCH-AQAM** scheme provided the desirable burst-by-burst error detection capability in order to assist in blind modem mode detection. However, the relative decoder complexity of this scheme increased compared to the other schemes as shown in Table 4.10. This was due to the longer and more complex BCH codes that were used in order to increase the code rate for the higher-order modulation modes.

4.8.2 Comparison of High-BER Turbo Block Coded AQAM Schemes

The speech transmission burst shown in Figure 3.13 was utilized in these turbo block coded AQAM schemes. The associated performances were compared to that of the uncoded **High-BER** AQAM scheme, where the switching thresholds were set according to Table 3.8. The gain comparisons, which were defined in Section 4.8 and were extracted from Figure 4.21 are shown in Table 4.12.

Turbo Block Coded AQAM Scheme	BPS/SNR gain (dB)	Maximum BPS	Effective BPS gain(dB)	BER/SNR gain(dB)
FCFI-TBCH-AQAM	2.5	4.3	$0 - 13$	18.0
FCVI-TBCH-AQAM	2.3	4.3	$0 - 11$	8.5
P-TBCH-AQAM	2.3	6.0	$0 - 40$	≈ 0
VR-TBCH-AQAM	2.3	5.0	$0 - 11$	≈ 0

Table 4.12: Performance comparisons of the **High-BER FCFI-TBCH-AQAM**, **FCVI-TBCH-AQAM**, **P-TBCH-AQAM** and **VR-TBCH-AQAM** schemes for a target BER of below 1**%**, where their characteristics were described in Sections 4.4, 4.5, 4.7.1 and 4.7.2. Their performances were compared to that of the uncoded AQAM scheme optimised for a target BER of 1% according to Table 3.8. The performance gains of each scheme were extracted from Figure 4.21.

Similar analysis to that discussed in Section 4.8.1 can be applied here, where all the **High-BER** turbo block coded AQAM schemes exhibited the same trends as those of the **Low-BER** turbo block coded AQAM schemes. However, the BER and BPS gain was significantly lower than that of the **Low-BER** schemes, as evidenced by Tables 4.12 and 4.11. The reduction in gain was caused by the higher target BER, which yielded a lower coding gain, since the higher steepness of the turbo-coded BER versus SNR curves became more effective for lower target BER schemes. This was also observed for the fixed modulation modes, where a higher coding gain was observed at lower BERs. Consequently, the **High-BER** coded switching thresholds did not reduce significantly, when compared to the switching thresholds of the **High-BER** uncoded AQAM scheme. This meant that a lower BPS/SNR gain was observed for the **High-BER** turbo block coded AQAM schemes, as evidenced by Table 4.12. Furthermore, the shorter speech transmission burst resulted in a smaller interleaver size for the variable interleaver-size turbo block coded AQAM scheme. This further degraded the coded BER and BPS performance, although the target BER of 1% was still achieved.

4.8.3 Near-Error-Free Turbo Block Coded AQAM Schemes

In these schemes, the coded switching thresholds were experimentally determined in order to achieve a near-error-free communication system. The data burst of Figure 3.13 was utilized and the gain comparisons are listed in Table 4.13, which were extracted from Figure 4.22.

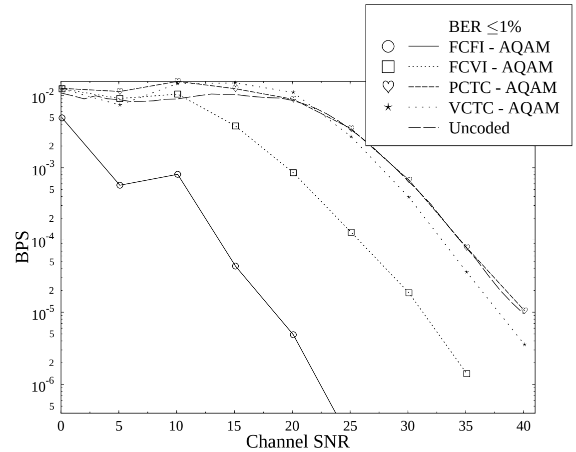

(a) Turbo block coded BER performance for a target BER of below 1% using the non-spread speech burst of Figure 3.13.

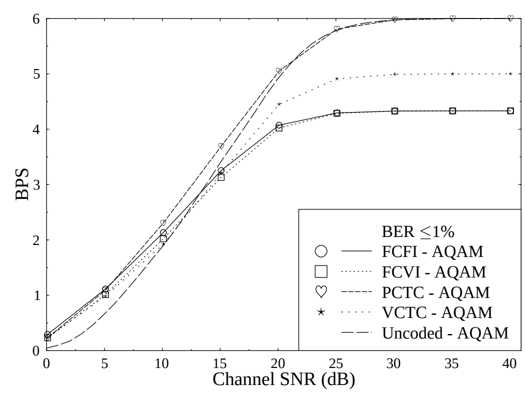

(b) Turbo block coded BER performance for a target BER of below 1% using the non-spread speech burst of Figure 3.13.

Figure 4.21: Performance comparisons of the **High-BER FCFI-TBCH-AQAM**, **FCVI-TBCH-AQAM**, **P-TBCH-AQAM** and **VR-TBCH-AQAM** schemes where the system characteristics were described in Sections 4.4, 4.5, 4.7.1 and 4.7.2. Their performances were compared to that of the uncoded AQAM scheme optimised for a target BER of 1% according to Table 3.8. The performance gains of each scheme were tabulated in Table 4.12.

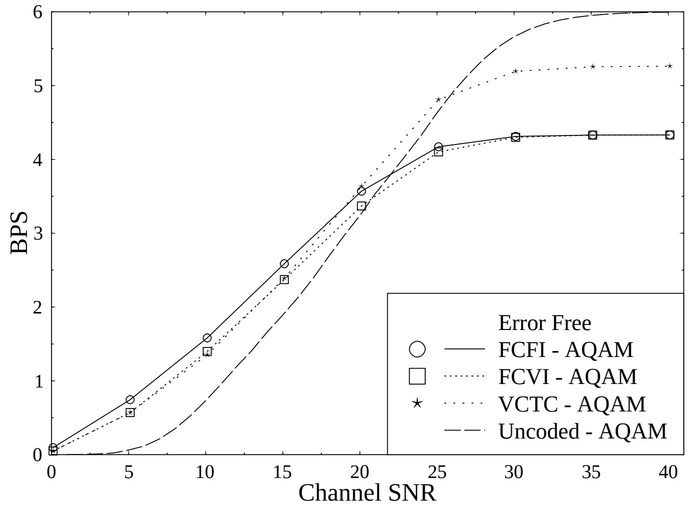

Figure 4.22: Performance comparison of the near-**error-free FCFI-TBCH-AQAM**, **FCVI-TBCH-AQAM** and **VR-TBCH-AQAM** schemes, where the system characteristics were described in Sections 4.4, 4.5 and 4.7.2. Their performances were compared to that of the uncoded AQAM scheme optimised for a target BER of 0.01% according to Table 3.8. The performance gains of each scheme are tabulated in Table 4.12.

No near-error-free **P-TBCH-AQAM** scheme was implemented due to the inclusion of the un-coded modes.

Turbo Block Coded AQAM Scheme	BPS/SNR gain(dB)	Maximum BPS	Effective BPS gain(dB)
FCFI-TBCH-AQAM	6.0	4.3	$0 - 22.5$
FCVI-TBCH-AQAM	5.0	4.3	$0 - 20.0$
VR-TBCH-AQAM	5.0	5.0	$0 - 26.0$

Table 4.13: Performance comparisons of the **FCFI-TBCH-AQAM**, **FCVI-TBCH-AQAM** and **VR-TBCH-AQAM** schemes for a near-**error-free** communication system which were described in Sections 4.4, 4.5 and 4.7.2. Their performances were compared to that of the uncoded AQAM scheme optimised for a target BER of 0.01% according to Table 3.8. The performance gains of each scheme were extracted from Figure 4.22.

The near-error-free turbo block coded AQAM gains for the various schemes exhibited similar trends to those of the **Low-BER** turbo block coded AQAM schemes. Consequently, the analysis presented in Section 4.8.1 can be applied here. In the next section, convolutional codes are utilized as the turbo component codes, in order to reduce the complexity of the turbo block coded AQAM scheme.

4.9 Turbo Convolutional Coded AQAM Schemes

In this section, convolutional codes are utilized as the component code in the turbo codec. Explicitly, a half-rate Recursive Systematic Convolutional (RSC) encoder - which was shown in Figure 4.2 - is used, where $n = 2$, $k = 1$ and the constraint length is set to $K = 3$. This is denoted by CC (2, 1, 3), where the octally represented generator polynomials were set to seven (for the feedback path) and five. The decoding algorithm used in the turbo convolutional scheme was the Log-MAP algorithm described in Appendix A.1 [140]. Let us now present and analyse the performance of the turbo convolutional scheme in the context of fixed modulation modes.

4.9.1 Turbo Convolutional Coded Fixed Modulation Mode Performance

In this section the performance of the turbo convolutional scheme is compared against that of the turbo block coded scheme for different fixed modulation modes and for similar coding rates. The simulation parameters of the turbo block coded scheme are identical to those set in Section 4.3. Similarly, in the turbo convolutional coded scheme, the code rate was set to 0.75 by applying a random puncturing pattern [147]. The sizes of the turbo interleaver and channel interleaver were chosen to be 9990 bits and 13320 bits, respectively, in order to closely match to the parameter set used for the turbo block coded scheme. The remaining simulation parameters are listed in Table 4.1.

The results are shown in Figure 4.23, where the turbo block coded performance is also displayed for comparison. A BER/SNR performance degradation of approximately $1-2$dB was observed at a BER of 1×10^{-4} for the turbo convolutional coded scheme, when compared to that of the turbo block coded scheme [146]. In terms of its complexity, the number of states in the block decoder trellis can be approximated upon following the philosophy of Equation 4.9 :

$$\text{No. of States for Block Codes} = \frac{\text{Encoder Input Block Length}}{k} \times (2k-n+3) \times 2^{n-k}, \tag{4.9}$$

where the encoder's input block length is equal to the turbo interleaver size.

Hence for an encoder input block length of 9984 bits and upon using a component code of BCH (31,26,1), the number of states produced by the block decoder is 294912. Similarly, the total number of states in a convolutional decoder trellis can be approximated by:

$$\text{Number of States for Convolutional Codes} = \text{Encoder Input Block Length} \times 2^{K-1}, \tag{4.10}$$

where K in the constraint length of the encoder.

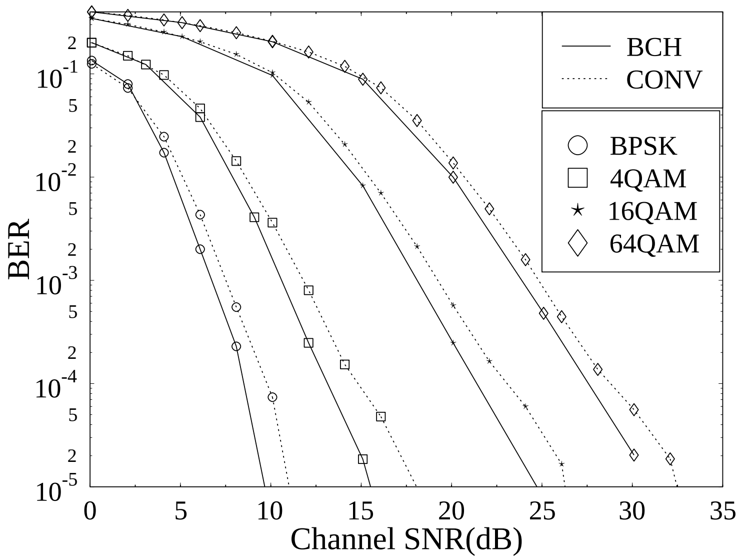

Figure 4.23: The turbo convolutional coded performance of the BPSK, 4QAM, 16QAM and 64QAM modulation modes utilizing the RSC component code CC (2, 1, 3) and the non-spread data burst of Figure 3.13. The other simulation parameters are listed in Table 4.1 and the equivalent turbo block coded performance is also shown for comparison using the BCH(31, 26, 3) component code. The turbo interleaver was of 9990 bits in depth, while the channel interleaver was of size 13320 bits.

Consequently, by applying an encoder input block length of 9990 bits and a RSC component code of CC(2,1,3), the total number of states generated by the convolutional decoder is 39960. This was approximately a factor of seven lower in terms of its complexity, when compared to the block decoder.

4.9.2 Turbo Convolutional Coded AQAM Scheme

In this section, the performance of the turbo convolutional coded scheme is evaluated in the context of a wideband AQAM scheme and compared against the performance of the turbo block coded AQAM schemes. The system parameters are identical to those of the turbo block coded AQAM schemes, which were described in Section 4.3. Essentially, the switching regime of the AQAM scheme is governed by Equation 4.1, where each modulation mode was associated with a certain code rate and turbo interleaver size. In the subsequent experiments the target BER was set to 0.01% and the non-spread data burst of Figure 3.13 was utilized as the transmission burst format. The other simulation parameters are listed in Table 4.1.

As we have seen in conjunction with the turbo block coded AQAM schemes, the performance of the turbo convolutional coded AQAM schemes is analysed by utilizing different turbo interleaver sizes and different code rates for each modulation mode. Explicitly, three different types of the turbo convolutional coded AQAM schemes are studied here:

1. Fixed Coding Rate and Variable Turbo Interleaver Turbo Convolutional Coded AQAM (**FCVI-TCONV-AQAM**) : In this scheme the convolutional coding rate was set to 0.75 and the turbo interleaver size was varied according to Table 4.14 for the different modulation modes, which ensured burst by burst decoding. This scheme was comprehensively described in Section 4.5 in the context of turbo block coded AQAM schemes. In order to provide a fair and pertinent comparison with the turbo block coded AQAM schemes, the switching thresholds were set according to Table 4.15 for achieving a target BER of 0.01%.

2. Partial Turbo Convolutional Coded AQAM (**P-TCONV-AQAM**): This scheme was identical to that described in Section 4.7.1, where the channel encoder could be disabled or enabled for each individual modulation mode. The switching regime was shown in Equation 4.7, where the coding rate was set to 0.75 and the corresponding turbo interleaver size is shown in Table 4.14. Similarly the switching thresholds - which are listed in Table 4.15 - were experimentally chosen, in order to achieve a target BER of 0.01%.

3. Variable Rate Turbo Convolutional Coded AQAM (**VR-TCONV-AQAM**): In this scheme, a specific coding rate was chosen for each modulation mode, which was discussed in Section 4.7.2 in the context of turbo block coded AQAM schemes. The coding rate was varied by utilizing different random puncturing patterns and the resulting code rates are listed in Table 4.14 for each corresponding modulation mode. The codes rates were chosen to be similar to those used for the turbo block coded scheme for comparison purposes. Finally, the switching thresholds for the AQAM scheme are shown in Table 4.15, which were experimentally set, in order to achieve a target BER of 0.01%.

AQAM Scheme	Turbo Interleaver (Bits)				Code Rates			
	I_0	I_1	I_2	I_3	R_0	R_1	R_2	R_3
FCVI-TCONV-AQAM	513	1026	2052	3078	0.75	0.75	0.75	0.75
P-TCONV-AQAM	513	1026	2052	3078	0.75	0.75	0.75	0.75
VR-TCONV-AQAM	513	1026	2280	3694	0.75	0.75	0.83	0.90

Table 4.14: The turbo interleaver size and the corresponding code rates for each modulation mode utilized in the **FCVI-TCONV-AQAM**, **P-TCONV-AQAM** and **VR-TCONV-AQAM** turbo convolutional coded schemes. A RSC code of CC(2, 1, 3) was used and the notations shown accrued from Equations 4.1 and 4.7.

The performance results of these schemes are shown in Figure 4.24, where the equivalent turbo block coded AQAM performance is displayed for comparison. The BER performance of the turbo convolutional coded AQAM schemes and the turbo block coded AQAM schemes were similar and in both cases the target BER of 0.01% was achieved. The characteristics of the results are similar to those of the turbo block coded AQAM schemes, which

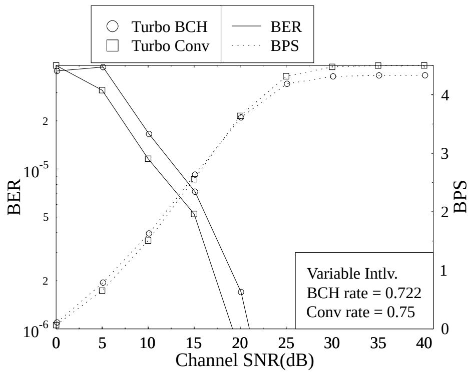

(a) FCVI-TCONV-AQAM

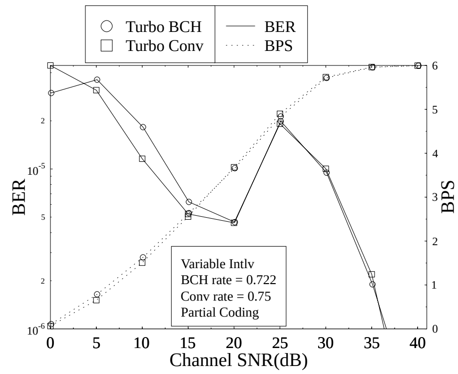

(b) P-TCONV-AQAM

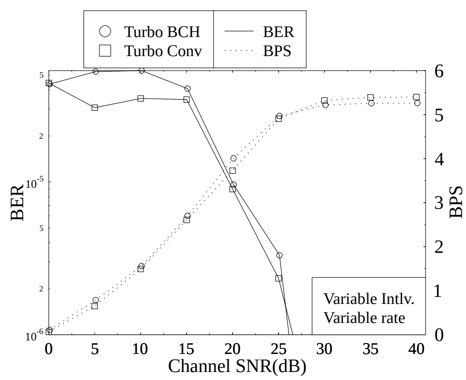

(c) VR-TCONV-AQAM

Figure 4.24: Performance of various turbo convolutional coded AQAM schemes, which utilized the RSC code CC (2, 1, 3) and the non-spread data burst of Figure 3.13. The turbo interleaver size, code rates and switching thresholds are listed in Tables 4.14 and 4.15. The generic simulation parameters are shown in Table 4.1 and the turbo block coded performance with similar parameters is also shown for comparison.

AQAM Scheme	Coded Switching Thresholds (dB)							
	t_1^c	t_2^c	t_3^c	t_4^c	t_5^c	t_6^c	t_7^c	t_8^c
FCVI-TCONV-AQAM	2.99	5.01	11.55	18.01	–	–	–	–
P-TCONV-AQAM	2.99	2.99	5.01	5.01	11.55	11.55	18.01	23.76
VR-TCONV-AQAM	2.99	5.01	12.05	20.01	–	–	–	–

Table 4.15: The switching thresholds for each modulation mode utilized in the **FCVI-TCONV-AQAM**, **P-TCONV-AQAM** and **VR-TCONV-AQAM** turbo convolutional coded schemes. A RSC code of CC(2, 1, 3) was used and the notations shown accrued from Equations 4.1 and 4.7.

were discussed in Sections 4.5, 4.7.1 and 4.7.2 and hence can be interpreted similarly. At low to medium average channel SNRs, a slight SNR gain was achieved by the turbo block coded AQAM schemes in terms of the associated BPS performances, when compared to the BPS curve of the turbo convolutional coded AQAM schemes, as evidenced by Figure 4.24. This was consistent with our expectations, since the switching thresholds of the turbo convolutional coded AQAM schemes were higher than that of the turbo block coded AQAM schemes. Consequently, the higher-order modulation modes were utilized more often at low average channel SNRs in the turbo block coded AQAM schemes. However at high average channel SNRs the maximum throughput of the turbo convolutional coded AQAM schemes were higher due to their slightly higher code rate, when compared to the turbo block coded AQAM schemes. Their associated BER versus channel SNR curves were fairly similar in all these sub-figures of Figure 4.24, although the turbo convolutional code had typically a slightly better BER.

In this section, we have applied a RSC code as the component code in our turbo codec. Subsequently, the turbo codec was applied in the context of fixed modulation modes, where the BER performance degraded by approximately $1 - 2$dB, when compared to the turbo block coded schemes. However, the complexity of the turbo convolutional coded scheme was significantly lower than that of the turbo block coded schemes, as discussed in Section 4.9. Consequently, we applied the turbo convolutional coded scheme in a wideband AQAM scheme, where the performance achieved was comparable to that of the turbo block coded AQAM schemes. In the next section we will explore the recently developed family of iterative equalization and channel decoding techniques, a scheme which is termed as turbo equalization.

4.10 Turbo Equalization

The concept of turbo equalizers is based on a joint iterative channel equalization and decoding technique [129], whereby the channel decoder is utilized in order to improve the performance of the equalization process and vice-versa in an iterative regime. Turbo equalization was pioneered by Douillard, Picart, Jézéquel, Didier, Berrou and Glavieux in 1995 [129]. In this contribution, the implementation of the turbo equalizer was derived by utilizing the previous iterative turbo decoding techniques, which were appropriately modified and incorporated in a so-called serially concatenated system, as shown in Figure 4.25. The detailed schematic of the turbo equalizer is shown in Figure 4.26, which consists of a Soft In/Soft Out (SISO) equalizer and a SISO convolutional decoder. These components are implemented based on the Log-MAP algorithm, which utilizes soft inputs and produces soft outputs. The implementation of the Log-MAP algorithm is similar to that of the turbo decoding scheme, which is described in Appendix A.1 [140]. Furthermore, these components are separated by a channel interleaver and deinterleaver, as shown in Figure 4.26. In our subsequent discussions the notations L^E and L^D represent the output Log Likelihood Ratio (LLR) of the SISO equalizer and that of the SISO decoder, respectively. The subscripts a, p and e denote the *a priori*, *a posteriori* and extrinsic values, respectively.

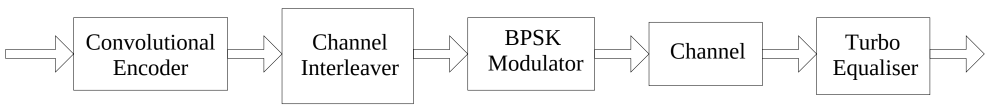

Figure 4.25: Schematic of the serially concatenated convolutional coded BPSK system, which performed the equalization, demodulation and channel decoding iteratively, as proposed by Douillard *et al [129]*.

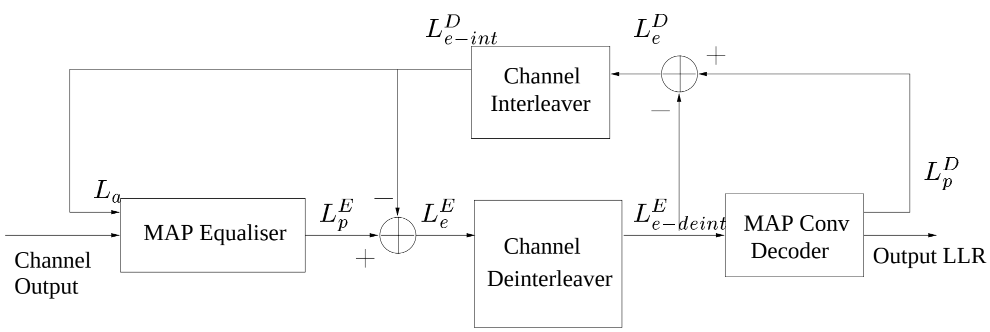

Figure 4.26: Schematic of the turbo equalizer [129] portraying the iterative structure of the equalizer and channel decoder.

Referring to Figure 4.26, the *a posteriori* information L^E_p, for the coded bits was produced by the SISO equalizer upon utilizing the channel outputs and the *a priori* information L_a, which was derived by the SISO decoder in the previous iteration. The extrinsic information of the equalizer L^E_e, was calculated by removing the contribution of the *a priori* information L_a, from the *a posteriori* information L^E_p of the equalizer, as shown in Figure 4.26. This essentially removed the contribution of the SISO decoder due to the previous iteration. The extrinsic information L^E_e, of the equalizer was subsequently deinterleaved, yielding $L_{e-deint}$ and utilized as the input to the SISO channel decoder. Consequently the SISO decoder produced the *a posteriori* information L^D_p, of the coded bits. The extrinsic information L^D_e, produced by the SISO decoder was derived by removing the deinterleaved extrinsic information $L_{e-deint}$, of the SISO equalizer from the SISO decoder's output L^D_p as shown in Figure 4.26. Consequently, the *a priori* information L_a for the next iteration, which was produced after interleaving the extrinsic information L^D_p, of the SISO decoder was independent of any

Transmission Burst type:	Non-Spread Speech Burst of Figure 3.13.
SISO Equalizer:	
Algorithm :	Log-MAP
SISO Decoder:	
Algorithm :	Log-MAP
Code Type :	Recursive Systematic Convolutional Code
Rate :	$\frac{1}{2}$
Constraint Length, K :	5
Octal Generator Polynomials :	$G0 = 35, G1 = 23$
Channel Interleaver size :	4032
Channel Parameters:	
Three Equal Rayleigh-faded Weights	$0.5773 + 0.5773z^{-1} + 0.5773z^{-2}$
Normalised Doppler Frequency:	3.25×10^{-5}

Table 4.16: Generic simulation parameters used in our turbo equalization experiments.

contribution by the SISO equalizer. This process was repeated in an iterative regime, in order to produce a better estimate of the coded bits and consequently a better BER performance.

It is important to note that, unlike in the turbo decoding process, the output of the SISO convolutional decoder consists of both the source and parity LLR values. The technique used to calculate these parity LLR values was derived as an extension of the Log-MAP algorithm, which is described in Appendix A.1.3 [140]. Let us now consider the performance of our turbo-equalized fixed mode modems.

4.10.1 Fixed Modulation Performance With Perfect Channel Estimation

In this section the turbo equalizer is implemented in the context of fixed modulation modes of BPSK, 4QAM and 16QAM. The results are shown in Figure 4.27, where the experimental parameters of Table 4.16 were utilized. In these results the performance of the turbo equalizer in conjunction with one to four iterations was shown for comparison. Referring to Figure 4.27, the BER performance improved upon increasing the number of iterations for all modulation modes. This illustrated the improvement of the estimation of the coded bits as a result of the iterative decoding and equalization process. The maximum iteration gains achieved after 4 iterations were 0.7dB, 1.0dB and 2.0dB for the modulation modes of BPSK, 4QAM and 16QAM, respectively. The iteration gain was defined as the difference between the channel SNR required in order to achieve a certain BER after one iteration and the corresponding channel SNR required after n number of iterations. In Figure 4.27 the law of diminishing returns was observed on the iteration gain, where the gain of subsequent iterations decreased.

The iteration gain was higher for the higher-order modulation mode of 16QAM, when compared to that of the BPSK and 4QAM modulation modes. In this respect, the Euclidean distance between two neighbouring points in the 16QAM constellation was smaller and hence

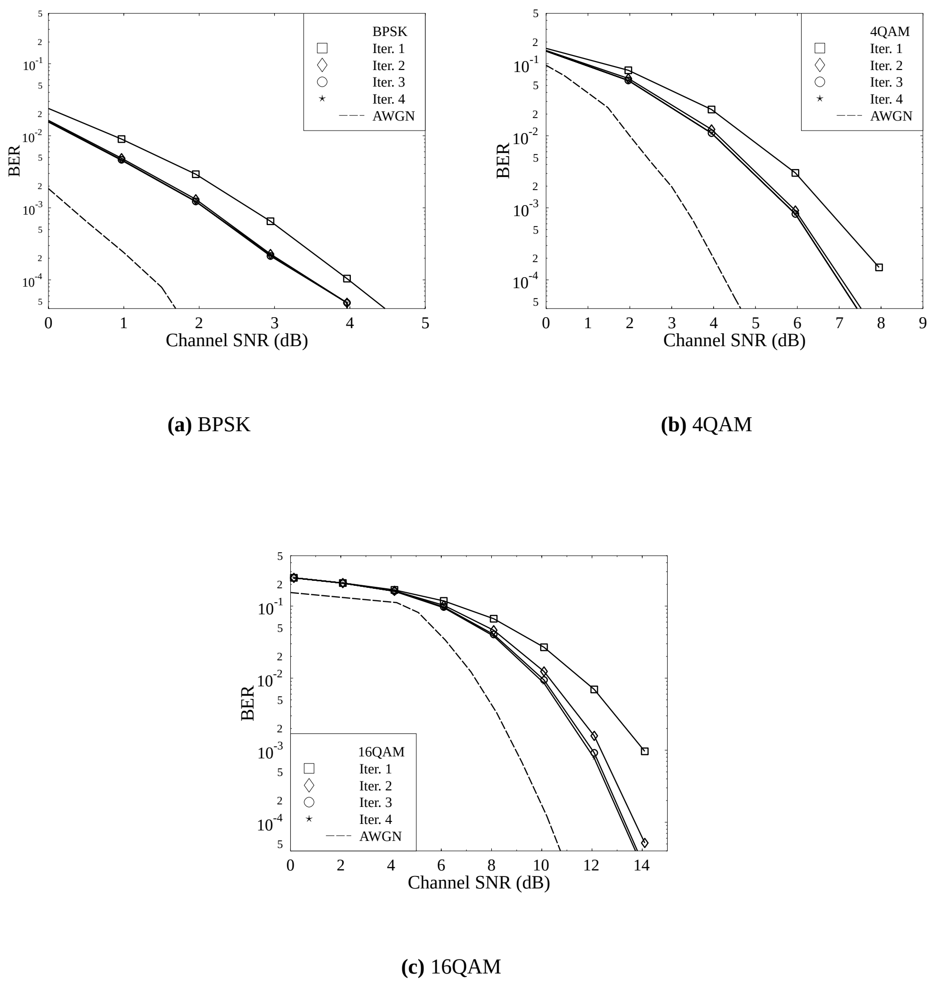

(a) BPSK

(b) 4QAM

(c) 16QAM

Figure 4.27: Performance of the turbo equalizer for one to four iterations in conjunction with different modulation modes and using perfect CIR estimation. The generic simulation parameters are listed in Table 4.16.

it was more gravely affected by ISI and noise. Consequently the BER performance after one iteration incurred higher degradation, when compared to the more robust lower-order modulation modes. However, the impact of ISI was reduced significantly for the subsequent iterations, which resulted in a higher iteration gain for the 16QAM mode. Lastly, a $2-3$dB extra channel SNR was required for maintaining a BER similar to that over the non-dispersive AWGN channel.

4.10.2 Fixed Modulation Performance With Iterative Channel Estimation

In our previous experiments, perfect CIR estimation was utilized, which produced an upper-bound performance for the turbo equalizer. However, in this section, the estimation of the fading CIR is implemented iteratively.

In order to exploit the iterative regime of the turbo equalizer, the CIR was estimated after each iteration, in order to produce a more accurate CIR estimation. In the first iteration, the CIR was estimated by utilizing the mid-amble sequence shown in Figure 3.13 and subsequently the CIR was utilized in the equalization process. However, for the subsequent iterations, the CIR was re-estimated by utilizing the entire transmission frame's symbols derived from the *a posteriori* coded bits of the SISO channel decoder. The *a posteriori* information was transformed from the log domain to modulated symbols using the approach employed by Glavieux *et al.* in Reference [148].

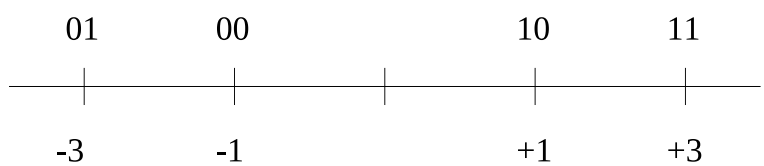

Figure 4.28: The Gray mapping of the 16QAM mode depicting the in-phase or quadrature-phase components and the corresponding bits assignments.

In order to highlight the philosophy of the soft mapper approach, let us consider an example using the in-phase component of the 16QAM modulation mode, where the constellation points employed Gray mapping, as shown in Figure 4.28. In this constellation mapping, the nth 16QAM symbol $d_n = a_n + jb_n$, was associated with four coded data bits represented by $C_{n,i}$, where $i = 1, 2, 3, 4$. Consequently, the first two bits $C_{n,1}$ and $C_{n,2}$, determined the in-phase component of the 16QAM symbol a_n, and similarly, the last two bits $C_{n,3}$ and $C_{n,4}$ determined the quadrature-phase component of the 16QAM symbol b_n. By utilizing the LLR values of each individual bit at the output of the SISO decoder, the average soft in-phase and quadrature-phase component of the symbol, denoted by $\bar{a}_n$ and $\bar{b}_n$ can be calculated as follows [148]:

$$\begin{aligned}\bar{a}_n &= 3 \cdot P\{C_{n,1}=1, C_{n,2}=1\} + 1 \cdot P\{C_{n,1}=1, C_{n,2}=0\} \\ &\quad -1 \cdot P\{C_{n,1}=0, C_{n,2}=0\} - 3 \cdot P\{C_{n,1}=0, C_{n,2}=1\}, \end{aligned} \tag{4.11}$$

$$\begin{aligned}\bar{b}_n &= 3 \cdot P\{C_{n,3} = 1, C_{n,4} = 1\} + 1 \cdot P\{C_{n,3} = 1, C_{n,4} = 0\} \\ &\quad -1 \cdot P\{C_{n,3} = 0, C_{n,4} = 0\} - 3 \cdot P\{C_{n,3} = 0, C_{n,4} = 1\},\end{aligned} \tag{4.12}$$

where $P\{x = 1, y = 1\}$ represented the joint probability that the variable x was a logical one and y was a logical one. The constant factors of 3 and 1 in Equations 4.11 and 4.12 denoted the amplitude imposed by the mapping constellation shown in Figure 4.28. The output LLR $L\{C_{n,i}\}$, of the coded bits was defined as the log of the ratio of the probabilities of the bit taking its two possible values :

$$L\{C_{n,i}\} = ln\left\{\frac{P(C_{n,i} = 1)}{P(C_{n,i} = 0)}\right\}, \qquad for\ i = 1, 2, 3, 4. \tag{4.13}$$

By exploiting the relationship that $P(C_{n,i} = 1) = 1 - P(C_{n,i} = 0)$ and $P(C_{n,i} = 0) = 1 - P(C_{n,i} = 1)$, we can rewrite Equation 4.11 and 4.12 as :

$$\bar{a}_n = \frac{e^{L(C_{n,1})}(3.e^{L(C_{n,2})} + 1) - 1 - 3.e^{L(C_{n,2})}}{(1 + e^{L(C_{n,1})})(1 + e^{L(C_{n,2})})}, \tag{4.14}$$

$$\bar{b}_n = \frac{e^{L(C_{n,3})}(3.e^{L(C_{n,4})} + 1) - 1 - 3.e^{L(C_{n,4})}}{(1 + e^{L(C_{n,3})})(1 + e^{L(C_{n,4})})}. \tag{4.15}$$

Hence, for every iteration $\bar{a}_n$ and $\bar{b}_n$ were calculated, in order to represent the estimated transmitted symbols of the entire frame, which was subsequently used in the CIR estimator. Due to the iterative structure of the CIR estimator, the simple Least Mean Square (LMS) adaptive algorithm [94] was implemented, which obeyed the following equation:

$$\hat{\mathbf{h}}(k+1) = \hat{\mathbf{h}}(k) + \mu\mathbf{u}(k)[r^*(k) - \mathbf{u}^{*T}(k)\hat{\mathbf{h}}(k)], \tag{4.16}$$

where $\hat{\mathbf{h}}(k)$ and $\mathbf{u}(k)$ represented the estimated CIR vector and the training sequence vector at time n, respectively. The channel's output symbol was denoted by $r(k)$ and μ was termed as the step-size of the LMS algorithm. Since this algorithm is widely known and utilized [94], the detailed mechanism of this algorithm is not explored here any further.

The step-size for the initial CIR estimation in the first iteration was set to 0.05 and for subsequent iterations the step-size was reduced to 0.01. In the first iteration the training of the CIR estimator was restricted to the length of the mid-amble sequence. Hence, in this situation, a higher step-size was chosen in order to facilitate fast convergence at the expense of the accuracy of the CIR estimates [94]. However for subsequent iterations the training length was extended to the entire transmitted frame. Consequently the step-size was reduced, in order to improve the accuracy of the CIR estimates [94]. The specific step size values were chosen in order to satisfy the convergence limits specified by Haykin [94].

The performance of the iterative CIR estimator in a turbo equalizer is shown in Figure 4.29 for the modulation modes of BPSK, 4QAM and 16QAM [149]. The simulation parameters used in this experiment are listed in Table 4.16. In each of these figures, the performance of the system employing perfect CIR estimation after four iterations was also depicted for comparison. Referring to Figure 4.29, the performance upon utilizing the iterative CIR estimator approached that of the perfect estimation case. This was a result of the iterative nature

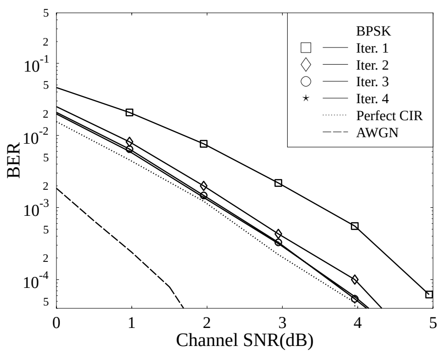

(a) BPSK

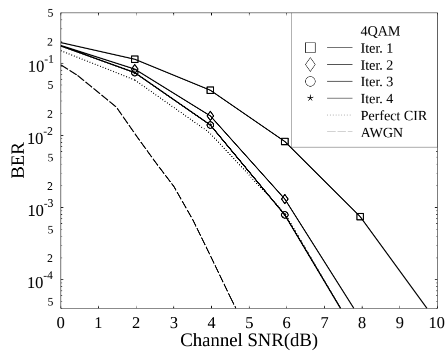

(b) 4QAM

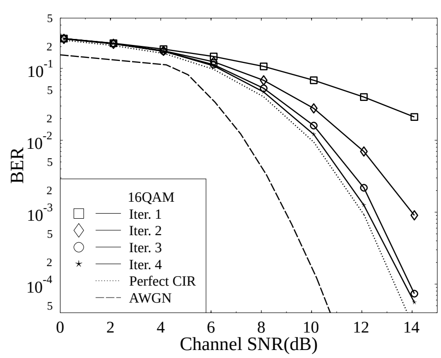

(c) 16QAM

Figure 4.29: Performance of the turbo equalizer for one to four iterations in conjunction with different modulation modes. The iterative LMS CIR estimator described in Section 4.10.2 was utilized and the other simulation parameters are listed in Table 4.16. The performance with perfect CIR estimation is also shown for comparison.

of the turbo equalizer, where the reliability of the decoded information increased for every subsequent iteration. Consequently, the iterative CIR estimator exploited the increased reliability of the decoded symbols, in order to yield an improved channel estimate for the SISO equalizer. This then yielded a more reliable output from the SISO equalizer. Following the above rudimentary introduction to turbo equalization, let us now quantify its performance in a wideband AQAM scenario.

4.10.3 Turbo Equalisation in Wideband Adaptive Modulation

In our previous experiments involving the wideband AQAM scheme, the output SNR of the DFE was used as a measure of the channel quality and subsequently used as a switching metric. However, in implementing the turbo equalizer in the context of wideband AQAM scheme, the SISO equalizer did not provide an SNR estimate in order to ascertain the channel quality on a burst by burst basis. Consequently, we propose to utilize the output SNR of the DFE - which was defined in Equation 3.6 - as the switching metric in an amalgamated wideband AQAM and turbo equalization scheme. In order to justify its utilization, the channel quality, which was quantified in terms of the output SNR of the DFE also had to indicate the performance of the SISO equalizer in terms of the BER. Consequently, we evaluated the correlation between the number of erroneous decisions produced by the SISO equalizer and the output SNR of the DFE on a burst-by-burst basis. This is shown in Figure 4.30, where a 4QAM mode was utilized at a channel SNR of 8dB over a symbol-spaced, equal-weight three-path fading channel. Referring to this figure, the number of error events for the SISO equalizer exhibited a good correlation with the output SNR of the DFE, where the number of error events increased, whenever the output SNR of the DFE decreased and vice versa. Consequently, we can justify the utilization of the output SNR of the DFE as a switching metric in the SISO equalizer [149]. Due to the iterative structure of the turbo equalizer, the switching thresholds were set experimentally, in order to achieve a target BER of approximately 0.01%. Hence the switching thresholds were set as follows : $t_1 = -1.5$dB, $t_2 = 2.5$dB, $t_3 = 6.5$dB and $t_4 = \infty$dB. The iterative LMS-based CIR estimator of Equation 4.16 was also utilized and the simulation parameters were set according to Table 4.16. The BER performance of the joint turbo equalization and AQAM scheme is depicted in Figure 4.31, where the wideband AQAM upper-bound performance employing perfect CIR estimation after four turbo equalization iterations was also shown for comparison [149]. Referring to Figure 4.31, the approximate target BER of 0.01% was achieved and maintained after four iterations. Furthermore, the performance of the wideband AQAM scheme with iterative CIR estimation approached that of the perfect CIR-assisted upper-bound scenario. The BPS performance of the wideband AQAM scheme is shown in Figure 4.32, where the associated performance of the fixed modulation modes of BPSK and 4QAM at a target BER of 0.01% are also depicted for comparison. For a BPS of 0.5, which was equivalent to the throughput of a half-rate coded BPSK mode, a channel SNR gain of 1.7dB was achieved by the wideband AQAM scheme. Similarly an SNR gain of 1.5dB was recorded by the wideband AQAM scheme at a target throughput of one bit per symbol, which was the throughput achieved by a half-rate coded 4QAM mode.

In implementing the turbo equalizer, the complexity incurred in terms of the number of states for the SISO equalizer was equal to m^L, where m was the number of constellation points of the modulation mode and L was the CIR memory length. Hence for higher-order modulation modes such as 64QAM, the complexity incurred was impractical even with a CIR memory length of two symbol-durations. Consequently, throughout our discussions on the turbo equalizer, the 64QAM mode was not utilized. Furthermore, we have restricted the length of the channel memory to two symbol-durations in order to reduce the complexity. Clearly, the complexity issues of this system may render it impractical especially in high delay-spread environments. Let us now review the findings of this chapter.

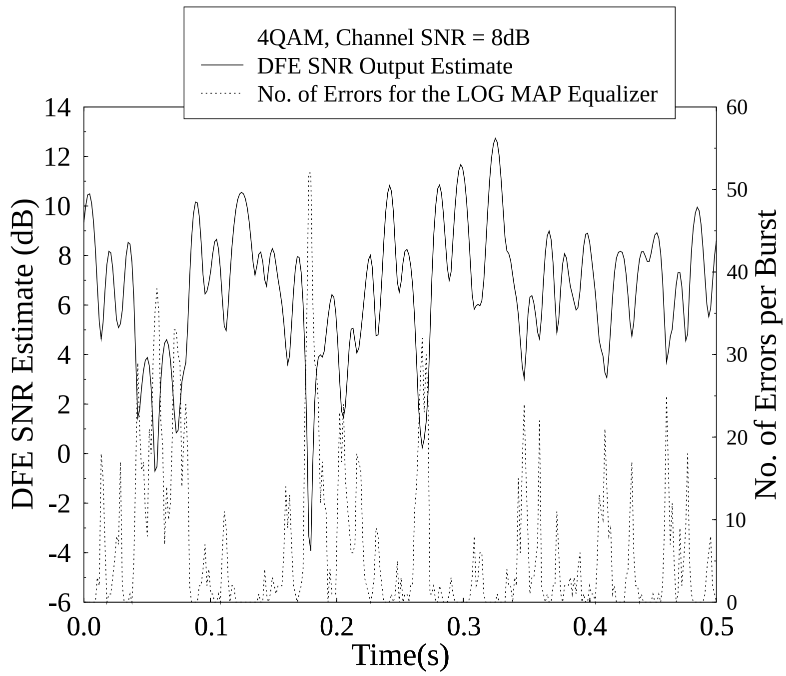

Figure 4.30: Variation of the number of errors per transmission burst produced by the Log-MAP equalizer and the corresponding output SNR estimate of the DFE using the 4QAM mode at a channel SNR of 8dB. The simulation parameters are listed in Table 4.16.

4.11 Burst-by-Burst Adaptive Wideband Coded Modulation

S. X. Ng, C. H. Wong and L. Hanzo

4.11.1 Introduction

Trellis Coded Modulation (TCM) [150], which is based on combining the functions of coding and modulation, is a bandwidth efficient scheme that has been widely recognized as an excellent error control technique suitable for applications in mobile communications [151, 152]. Turbo Trellis Coded Modulation (TTCM) [153] is a more recent channel coding scheme that has a structure similar to that of the family of power efficient binary turbo codes [131], but employs TCM codes as component codes. Rate $2/3$ TTCM was shown in [153] to be $0.5\ dB$ better in Signal-to-Noise Ratio (SNR) terms, than binary turbo codes over AWGN channels using 8-level Phase Shift Keying (8PSK). TTCM was also shown to outperform a similar-complexity TCM scheme in the context of Orthogonal Frequency Division Multiplexing (OFDM) transmission over various dispersive channels [154]. In this latter context,

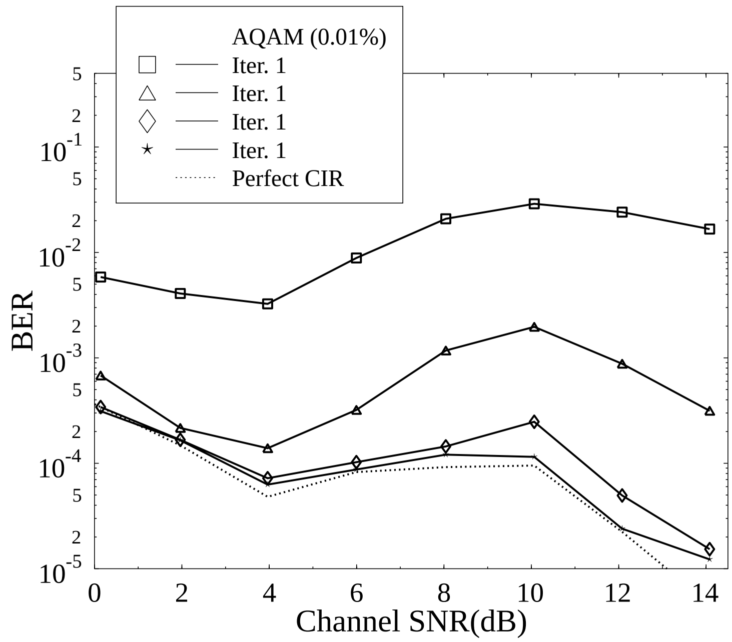

Figure 4.31: Performance of the turbo equalizer for four iterations in conjunction with the wideband AQAM scheme. The iterative LMS CIR estimator described in Section 4.10.2 was utilized and the other simulation parameters are listed in Table 4.16. The performance with perfect CIR estimation is also shown for comparison.

the individual OFDM subcarriers experienced effectively narrowband fading and the TCM as well as TTCM complexity were rendered similar by adjusting the number of turbo iterations and code constraint length. However, the above fixed mode transceiver failed to exploit the time varying nature of the mobile radio channel.

By contrast, in BbB adaptive schemes [1, 15, 17, 19, 34, 130, 143] a higher order modulation mode is employed, when the instantaneous estimated channel quality is high in order to increase the number of Bits Per Symbol (BPS) transmitted and conversely, a more robust lower order modulation mode is employed, when the instantaneous channel quality is low, in order to improve the mean Bit Error Rate (BER) performance. Uncoded adaptive schemes [1, 15, 19, 34] and coded adaptive schemes [17, 130] have been investigated for narrowband fading channels. Finally, a turbo coded wideband adaptive scheme assisted by Decision Feedback Equalizer (DFE) was investigated in [143].

In our practical approach the transmitter A obtains the channel quality estimate generated by receiver B upon receiving the transmission of transmitter B. In other words, the modem mode required by receiver B is superimposed on the transmission burst of transmitter B. Hence a delay of one transmission burst duration is incurred. In the literature, adaptive coding

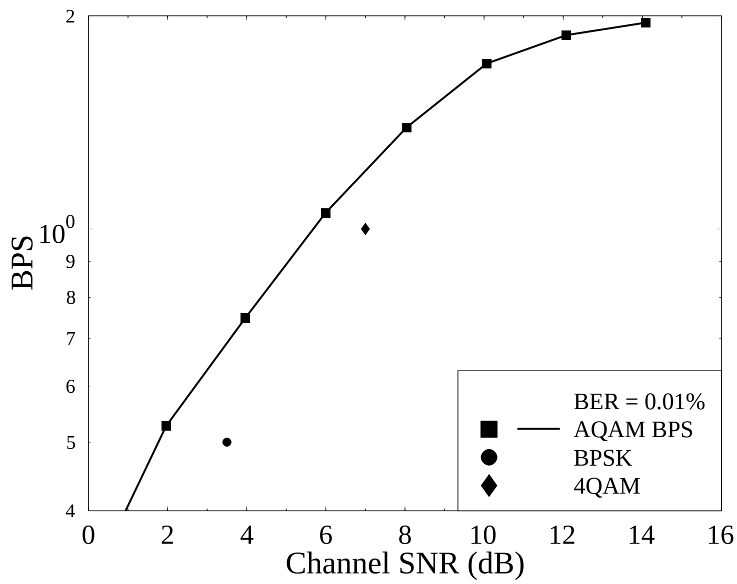

Figure 4.32: Throughput performance of the turbo equalizer for four iterations in conjunction with the wideband AQAM scheme. The iterative LMS CIR estimator described in Section 4.10.2 was utilized and the other simulation parameters are listed in Table 4.16. The throughput of the half-rate coded BPSK and 4QAM modes was also depicted for comparison.

for time-varying channels using outdated fading estimates has been investigated in [155].

Over wideband fading channels the DFE employed will eliminate most of the intersymbol interference (ISI). Consequently, the mean-squared error (mse) at the output of the DFE can be calculated and used as the metric invoked to switch the modulation modes [15]. This ensures that the performance is optimised by employing equalization and BbB adaptive TCM/TTCM jointly, in order to combat the signal power fluctuations and the ISI of the wideband channel.

This section is organized as follows. In Section 4.11.2, the system is outlined. In Section 4.11.3, the performance of fixed-mode TCM and TTCM schemes is evaluated. Section 4.11.4contains the detailed characterisation of the BbB adaptive TCM/TTCM schemes in **System I** and **System II**. In Section 4.11.5, we compare the proposed schemes with other adaptive coded modulation schemes such as Bit-Interleaved Coded Modulation [156]. Finally, we will conclude in Section 4.11.6.

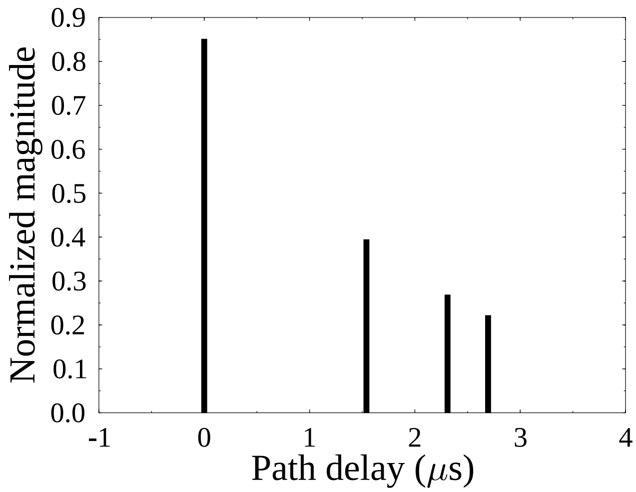

Figure 4.33: The impulse response of a COST 207 Typical Urban (TU) channel [125].

4.11.2 System Overview

The multi-path channel model is characterized by its discretised symbol-spaced COST207 Typical Urban (TU) channel impulse response [125], as shown in Figure 4.33. Each path is faded independently according to a Rayleigh distribution and the corresponding normalised Doppler frequency is 3.25×10^{-5}, the system Baud rate is $2.6\ MBd$, the carrier frequency is $1.9\ GHz$ and the vehicular speed is $30\ mph$. The DFE incorporated 35 feed-forward taps and 7 feedback taps and the transmission burst structure used is shown in Figure 4.34. When considering a Time Division Multiple Access (TDMA)/Time Division Duplex (TDD) system of 16 slots per $4.615\ ms$ TDMA frame, the transmission burst duration is $288\ \mu s$, as specified in the Pan-European FRAMES proposal [126].

The following assumptions are stipulated. Firstly, we assume that the equalizer is capable of estimating the Channel Impulse Response (CIR) perfectly from the equaliser training sequence of Figure 4.34. Secondly, the CIR is time-invariant for the duration of a transmission burst, but varies from burst to burst according to the Doppler frequency, which corresponds to assuming that the CIR is slowly varying. The error propagation of the DFE will degrade the estimated performance, but the effect of error propagation is left for further study.

At the receiver, the CIR is estimated, which is then used to calculate the DFE coefficients [4]. Subsequently, the DFE is used to equalize the ISI-corrupted received signal. In addition, both the CIR estimate and the DFE feed-forward coefficients are utilized to compute the SNR at the output of the DFE. More specifically, by assuming that the residual ISI is near-Gaussian distributed and that the probability of decision feedback errors is negligible, the SNR at the

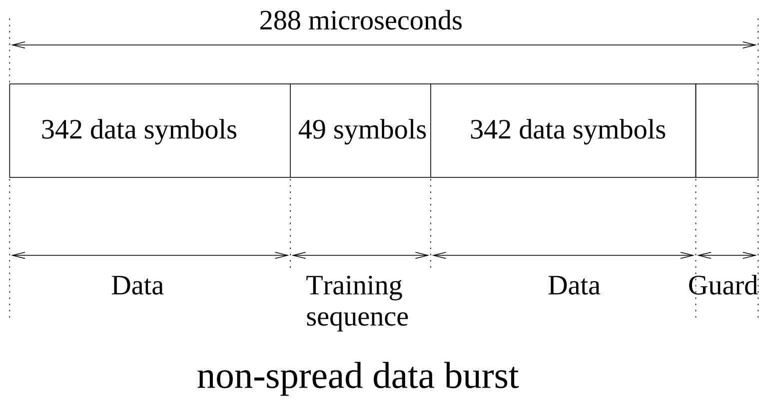

Figure 4.34: Transmission burst structure of the FMA1 non-spread data as specified in the FRAMES proposal [126].

output of the DFE, γ_{dfe}, is calculated as [15]:

$$\begin{aligned}\gamma_{dfe} &= \frac{\text{Wanted Signal Power}}{\text{Residual ISI Power + Effective Noise Power}}. \\ &= \frac{E\left[|s_k \sum_{m=0}^{N_f} C_m h_m|^2\right]}{\sum_{q=-(N_f-1)}^{-1} E\left[|\sum_{m=0}^{N_f-1} C_m h_{m+q} s_{k-q}|^2\right] + N_o \sum_{m=0}^{N_f} |C_m|^2},\end{aligned} \tag{4.17}$$

where C_m and h_m denotes the DFE's feed-forward coefficients and the CIR, respectively. The transmitted signal is represented by s_k and N_o denotes the noise spectral density. Lastly, the number of DFE feed-forward coefficients is denoted by N_f.

The equalizer's SNR, γ_{dfe}, in Equation 4.17, is then compared against a set of adaptive modem mode switching thresholds f_n, and subsequently the appropriate modulation mode is selected [15]. The modem mode required by receiver B is then fed back to transmitter A. The modulation modes that are utilized in this scheme are 4QAM, 8PSK, 16QAM and 64QAM [4].

The simplified block diagram of the BbB adaptive TCM/TTCM **System I** is shown in Figure 4.35, where no channel interleaving is used. Transmitter A extracts the modulation mode required by receiver B from the reverse-link transmission burst in order to adjust the adaptive TCM/TTCM mode suitable for the channel. This incurs one TDMA/TDD frame delay between estimating the actual channel condition at receiver B and the selected modulation mode of transmitter A. Better channel quality prediction can be achieved using the techniques proposed in [11]. We invoke four encoders, each adding one parity bit to each information symbol, yielding the coding rate of $1/2$ in conjunction with the TCM/TTCM mode of 4QAM, $2/3$ for 8PSK, $3/4$ for 16QAM and $5/6$ for 64QAM.

The design of TCM schemes for fading channels relies on the time and space diversity provided by the associated coder [151, 157]. Diversity may be achieved by repetition coding (which reduces the effective data rate), spaced-time coded multiple transmitter/receiver structures [158] (which increases cost and complexity) or by simple interleaving (which induces

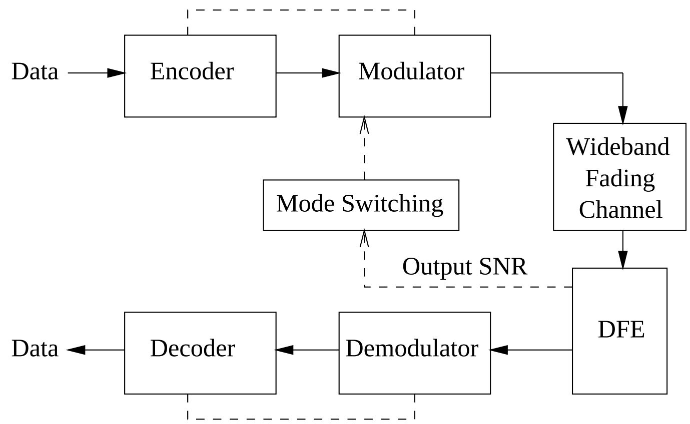

Figure 4.35: **System I** without channel interleaver. The equalizer's output SNR is used to select a suitable modulation mode, which is fed back to the transmitter on a burst-by-burst basis.

latency). In [159] adaptive TCM schemes were designed for narrowband fading channels utilising repetition-based transmissions during deep fades along with ideal channel interleavers and assuming zero delay for the feedback of the channel quality information.

Figure 4.36 shows the block diagram of **System II**, where symbol-based channel interleaving over four transmission bursts is utilised, in order to disperse the bursty symbol errors. Hence, the coded modulation module assembles four bursts using an identical modulation mode, so that they could be interleaved using the symbol-by-symbol random channel interleaver without the need of adding dummy bits. Then, these four-burst TCM/TTCM packets are transmitted to the receiver. Once the receiver has received the 4^{th} burst, the equalizer's output SNR for this most recent burst is used to choose a suitable modulation mode. The selected modulation mode is fed back to the transmitter on the reverse link burst. Upon receiving the modulation mode required by receiver B (after one TDMA frame delay), the coded modulation module assembles four bursts of data from the input buffer for coding and interleaving, which are then stored in the output buffer ready for the next four bursts transmission. Thus the first transmission burst exhibits one TDMA/TDD frame delay and the fourth transmission burst exhibits four frame delay, which is the worst-case scenario.

Soft decision trellis decoding utilizing the Log-Maximum A Posteriori (Log-MAP) algorithm [139] was invoked for TCM/TTCM decoding. The Log-MAP algorithm is a numerically stable version of the MAP algorithm operating in the log-domain, in order to reduce its complexity and to mitigate the numerical problems associated with the MAP algorithm [138]. The TCM scheme invokes Ungerboeck's codes [150], while the TTCM scheme invokes Robertson's codes [153]. A component TCM code memory of 3 was used for the TTCM scheme. The number of turbo iterations for TTCM was fixed to 4 and hence it exhibited a similar decoding complexity to the TCM code of memory 6.

In the next section we present simulation results for our fixed-mode transmissions.

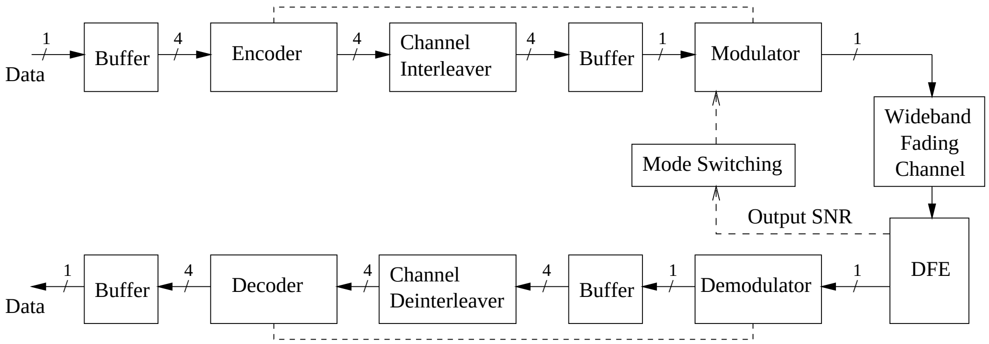

Figure 4.36: System II with channel interleaver length of 4 TDMA/TDD bursts. Data is entered into the input buffer on a burst-by-burst basis and the modulator modulates coded data from the output buffer for transmission on a burst-by-burst basis. The encoder and channel interleaver as well as the decoder and channel deinterleaver operate on a 4-burst basis. The equalizer's output SNR of the 4^{th} burst is used to select a suitable modulation mode and fed back to the transmitter on the reverse link burst.

4.11.3 Performance of the Fixed Modem Modes

Before characterising the proposed wideband BbB adaptive scheme, the BER performance of the fixed modem modes of 4QAM, 8PSK, 16QAM and 64QAM are studied both with and without channel interleavers. These results are shown in Figure 4.37 for TCM, while in Figure 4.38 for TTCM. The random TTCM symbol-interleaver memory was set to 684 symbols, corresponding to the number of data symbols in the transmission burst structure of Figure 4.34, where the corresponding number of bits was the number of data bits per symbol $(BPS) \times 684$. A channel interleaver of 4×684 symbols was utilised, where the number of bits was $(BPS + 1) \times 4 \times 684$ bits, since one parity bit was added to each TCM/TTCM symbol.

As expected, in Figures 4.37 and 4.38 the BER performance of the channel-interleaved scenario was superior compared to that without channel interleaver, although at the cost of an associated higher transmission delay. The SNR-gain difference between the channel interleaved and non-interleaved scenarios was about $5\ dB$ in the TTCM/4QAM mode, but this difference reduced for higher-order modulation modes. Again, this gain was obtained at the cost of a four-burst channel interleaving delay. This SNR-gain difference shows the importance of time diversity in coded modulation schemes.

TTCM has been shown to be more efficient than TCM for transmissions over AWGN channels and narrowband fading channels [153, 154]. Here, we illustrate the advantage of TTCM in comparison to TCM over the dispersive or wideband Gaussian CIR of Figure 4.33 as seen in Figure 4.39. In conclusion, TTCM is superior to TCM in a variety of channels.

Let us now compare the performance of the BbB adaptive TCM/TTCM **system I** and **II**.

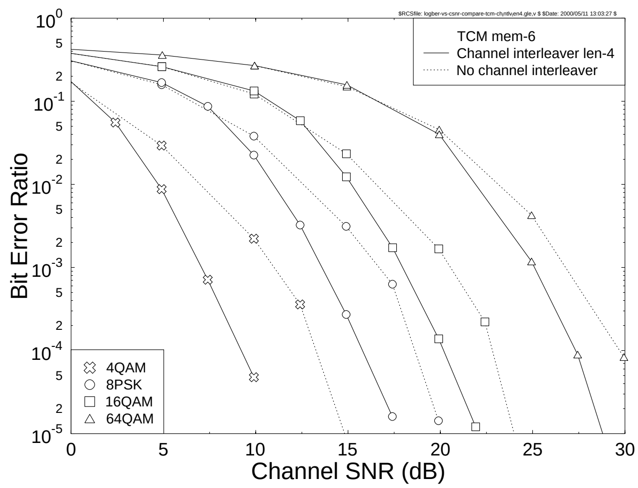

Figure 4.37: TCM performance of each individual modulation mode over the Rayleigh fading COST207 TU channel of Figure 4.33. A TCM code memory of 6 was used, since it had a similar decoding complexity to TTCM in conjunction with 4 iterations using a component TCM code memory of 3.

4.11.4 Performance of System I and System II

The modem mode switching mechanism of the adaptive schemes is characterised by a set of switching thresholds, the corresponding random TTCM symbol-interleavers and the component codes, as follows:

$$\text{Modulation Mode} = \begin{cases} 4QAM, I_0 = 684, R_0 = 1/2 & \text{if } \gamma_{DFE} \leq f_1 \\ 8PSK, I_1 = 1368, R_1 = 2/3 & \text{if } f_1 < \gamma_{DFE} \leq f_2 \\ 16QAM, I_2 = 2052, R_2 = 3/4 & \text{if } f_2 < \gamma_{DFE} \leq f_3 \\ 64QAM, I_3 = 3420, R_3 = 5/6 & \text{if } \gamma_{DFE} > f_3, \end{cases} \tag{4.18}$$

where $f_n, n = 1...3$ are the equalizer's output SNR thresholds, while I_n represents the random TTCM symbol-interleaver size in terms of the number of bits, which is not used for the TCM schemes. The switching thresholds f_n were chosen experimentally, in order to maintain a BER of below 0.01% and these thresholds are listed in Table 4.17.

Let us consider the adaptive TTCM scheme in order to investigate the performance of **System I** and **System II**. The BER and BPS performances of both adaptive TTCM systems using 4 iterations are shown in Figure 4.40, where we observed that the throughput of **System II** was superior to that of **System I**. Furthermore, the overall BER of **System II** was lower than that of **System I**. In order to investigate the switching dynamics of both systems, the mode switching together with the equalizer's output SNR was plotted versus time at an average channel SNR of $25\ dB$ in Figures 4.41 and 4.42. Observe in Table 4.17 that the switching thresholds, f_n of **System II** are lower, than those of **System I**, since the fixed mode based results of **System II** in Figure 4.38 were better. Hence higher-order modulation modes were

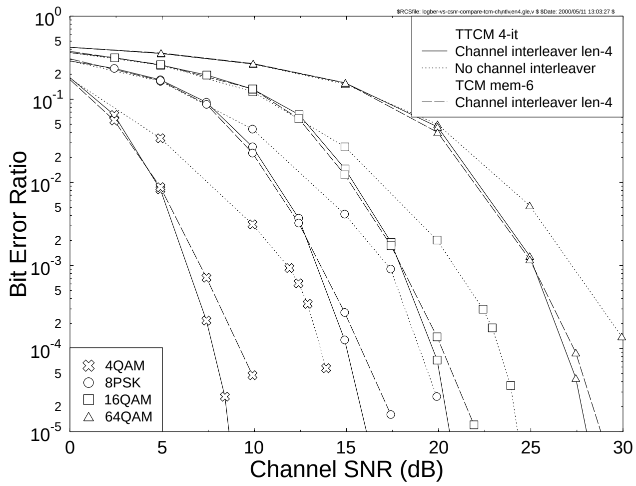

Figure 4.38: TTCM performance of each individual modulation mode over the Rayleigh fading COST207 TU channel of Figure 4.33. A component TCM code memory of 3 was used and the number of turbo iterations was 4. The performance of the TCM code with memory 6 utilising a channel interleaver was also plotted for comparison.

BER < 0.01 % Adaptive System Type		Switching Thresholds f_1	f_2	f_3
TCM, Memory 3	System I	19.56	23.91	30.52
	System II	17.17	21.91	29.61
TCM, Memory 6	System I	19.56	23.88	30.07
	System II	17.14	21.45	29.52
TTCM, 4 iterations	System I	19.69	23.45	30.29
	System II	16.66	21.40	28.47
BICM, Memory 3	System I	19.94	24.06	31.39
BICM-ID, 8 iterations	System II	16.74	21.45	28.97

Table 4.17: The switching thresholds were set experimentally in order to achieve a target BER of below 0.01%. **System I** does not utilise a channel interleaver, while **System II** uses a channel interleaver length of 4 TDMA/TDD bursts.

chosen more frequently, than in **System I**, giving a better BPS throughput. From Figure 4.41 and 4.42, it is clear that **System I** was more flexible in terms of mode switching, while **System II** benefitted from higher diversity gains due to the 4-burst channel interleaver. This diversity gain compensated for the loss of switching flexibility, ultimately providing a better performance in terms of BER and BPS, as seen in Figure 4.40.

In our next endeavour, the adaptive TCM and TTCM schemes of **System I** and **System II** are compared. Figure 4.43 shows the BER and BPS performance of **System I** for adaptive

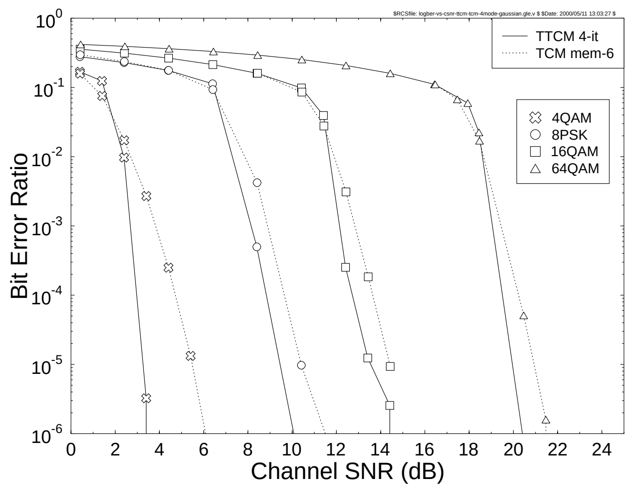

Figure 4.39: TTCM and TCM performance of each individual modulation mode over the unfaded COST207 TU channel of Figure 4.33. The TTCM scheme used component TCM codes of memory 3 and the number of turbo iterations was 4. The performance of the TCM scheme with memory 6 was plotted for comparison with the similar-complexity TTCM scheme.

TTCM using 4 iterations, adaptive TCM of memory 3 (which was the component code of our TTCM scheme) and adaptive TCM of memory 6 (which had a similar decoding complexity to our TTCM scheme). As it can be seen from the fixed mode results of Figures 4.37 and 4.38 in the previous section, TCM and TTCM performed similarly in terms of their BER, when no channel interleaver was used for this slow fading wideband channel. Hence, they exhibited a similar performance in the adaptive schemes of System I, as shown in Figure 4.43. Even the TCM scheme of memory 3 associated with a lower complexity could give a similar BER and BPS performance. This shows that the equalizer plays a dominant role in **System I**, where the coded modulation schemes could not benefit from sufficient diversity due to the lack of interleaving.

When the channel interleaver is introduced in **System II**, the bursty symbol errors are dispersed. Figure 4.44 illustrates the BER and BPS performance of **System II** for adaptive TTCM using 4 iterations, adaptive TCM of memory 3 and adaptive TCM of memory 6. The performance of all these schemes improved in the context of **System II**, as compared to the corresponding schemes in **System I**. The TCM scheme of memory 6 had a lower BER, than TCM of memory 3, and also exhibited a small BPS improvement. As expected, TTCM had the lowest BER and also the highest BPS throughput compared to the other coded modulation schemes.

In summary, we have observed BER and BPS gains for the channel interleaved adaptive coded schemes of **System II** in comparison to the schemes without channel interleaver in **System I**. Adaptive TTCM exhibited a superior performance in comparison to adaptive TCM in **Systems II**.

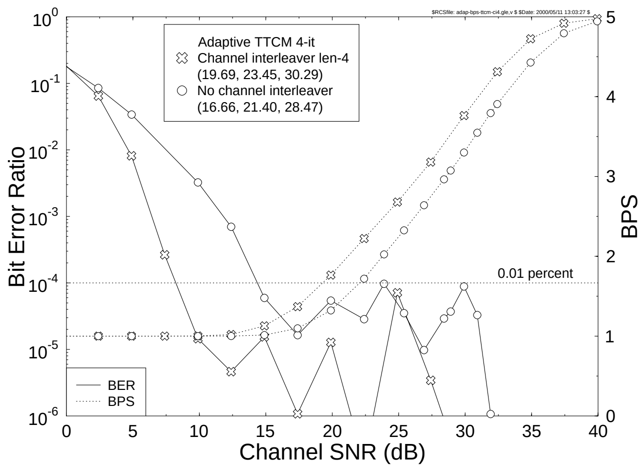

Figure 4.40: BER and BPS performance of adaptive TTCM with 4 turbo iterations in **System I** (without channel interleaver) and in **System II** (with a channel interleaver length of 4 bursts) for a target BER of less than 0.01 %. The legends indicate the associated switching thresholds expressed in dB, as seen in the round brackets.

4.11.5 Performance of Bit-Interleaved Coded Modulation

The above adaptive TCM and TTCM schemes invoked Set-Partitioning (SP) based signal labeling, in order to achieve a higher Euclidean distance between the unprotected bits of the constellation, so that parallel trellis transitions can be associated with the unprotected data bits. This reduced the decoding complexity. In TCM and TTCM random symbol interleavers were utilised for both the turbo interleaver and the channel interleaver.

Another powerful coded modulation scheme utilising bit-based channel interleaving in conjunction with Gray signal labeling is referred to as Bit-Interleaved Coded Modulation (BICM) was proposed in [156, 160]. It combines conventional convolutional codes with several independent bit interleavers, in order to increase the associated diversity order. With bit interleavers, the code diversity order can be increased to the binary Hamming distance of a code, and the number of parallel bit-interleavers equals the number of coded bits in a symbol [160]. The performance of BICM is better, than that of TCM over uncorrelated (or fully interleaved) fading channels but worse than that of TCM in Gaussian channels due to the reduced Euclidean distance imposed by the associated "random modulation" inherent in a bit-interleaved scheme [160].

Recently, iteratively decoded BICM with SP signal labeling, referred to as BICM-ID has also been proposed [161–164]. The philosophy of BICM-ID is to increase the Euclidean distance of the BICM code and to exploit the full advantage of bit interleaving by a simple iterative decoding technique. BICM-ID was shown to be betther than TCM and BICM in both AWGN and uncorrelated Rayleigh fading channels in the references. Rate $2/3$ BICM-ID was shown in [162] to be only about $0.5\ dB$ away from TTCM over AWGN channels using 8PSK.

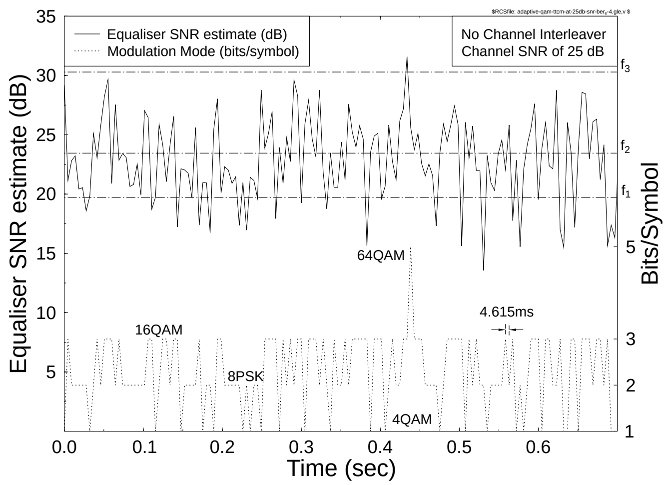

Figure 4.41: Equaliser output SNR estimate and Bits/Symbol versus time plot for adaptive TTCM with 4 turbo iterations in **System I** at an average channel SNR of $25\ dB$, where the modulation mode switching is based upon the equalizer's output SNR, which is compared to the switching thresholds f_n defined in Table 4.17. The duration of one TDMA/TDD frame is 4.615 ms. The TTCM mode can be switched after one frame duration.

In order to further benchmark the performance of our BbB adaptive TCM/TTCM system, an adaptive BICM scheme was constructed using Paaske's convolutional codes [134] for rate $1/2$, $2/3$, $3/4$ and $5/6$, which provides the largest free Hamming distance. The rate $5/6$ code was constructed using a rate $1/2$ code and puncturing, following the approach of [165]. An adaptive BICM-ID scheme was also constructed with soft-decision feedback based iterative decoding method [164].

Figure 4.45 shows the fixed modem modes performance for TCM, TTCM, BICM and BICM-ID in the context of **System II**. For the sake of a fair comparison of the decoding complexity, we used a TCM code memory of 6, TTCM code memory of 3 with 4 turbo iterations, BICM code memory of 6 and a BICM-ID code memory of 3 with 8 decoding iterations. However, BICM-ID had a slightly higher decoding complexity, since the demodulator was invoked in each BICM-ID iteration, whereas in the BICM, TCM and TTCM schemes the demodulator was only visited once in each decoding process. As illustrated in the figure, the BICM scheme performed marginally better than the TCM scheme at a BER below 0.01 %, except in the 64QAM mode. Hence, adaptive BICM is also expected to be better than adaptive TCM in the context of **System II**, when a target BER of less than 0.01 % is desired. This is because when the channel interleaver depth is sufficiently high, the diversity gain of the BICM's bit-interleaver is higher than that of the TCM's symbol-interleaver [156, 160].

Figure 4.46 compares the adaptive BICM and TCM schemes in the context of **System I**, i.e. without channel interleaving, although the BICM scheme invoked an internal bit-interleaver of one burst memory. As it can be seen from the figure, adaptive TCM exhibited a better BPS throughput and BER performance than BICM, due to insufficient channel inter-

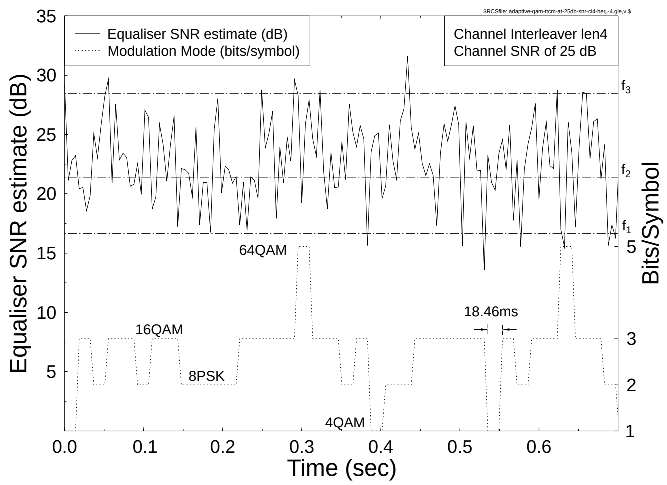

Figure 4.42: Equaliser output SNR estimate and Bits/Symbol versus time plot for adaptive TTCM with 4 turbo iterations in **System II** at an average channel SNR of $25\ dB$, where the modulation mode switching is based upon the equalizer's output SNR which is compared to the switching thresholds f_n defined in Table 4.17. The duration of one TDMA/TDD frame is 4.615 ms. The TTCM mode is maintained for four frame durations, i.e. for 18.46 ms.

leaving depth for BICM scheme in our slow fading wideband channels.

As observe in Figure 4.45, we noticed that BICM-ID had the worst performance at low SNRs in each modulation mode compared to other coded modulation schemes. However, it exhibited a steep slope and therefore at high SNRs it approached the performance of TTCM scheme. The adaptive BICM-ID and TTCM schemes in the context of **System II** were compared in Figure 4.46. The adaptive TTCM exibited a better BPS throughput than adaptive BICM-ID since TTCM had a better performance in fixed modem modes at BER of 0.01 %. However, adaptive BICM-ID exibited a lower BER performance than adaptive TTCM due to the high steepness of BICM-ID in fixed modem modes.

4.11.6 Summary and Conclusions

In this section BbB adaptive TCM and TTCM were proposed for wideband fading channels both with and without channel interleaving and they were characterised in performance terms over the COST 207 TU fading channel. When observing the associated BPS curves, adaptive TTCM exhibited up to $2.5\ dB$ SNR-gain for a channel interleaver length of 4 bursts in comparison to the non-interleaved scenario, as evidenced in Figure 4.40. Upon comparing the BPS curves, adaptive TTCM also exhibited up to $0.7\ dB$ SNR-gain compared to adaptive TCM of the same complexity in the context of **System II** for a target BER of less than 0.01 %, as shown in Figure 4.44. Lastly, adaptive TCM performed better than the adaptive BICM benchmarker in **System I** and the adaptive BICM-ID was marginally worse, than adaptive TTCM in **System II** as discussed in Section 4.11.5. Our future work will consider

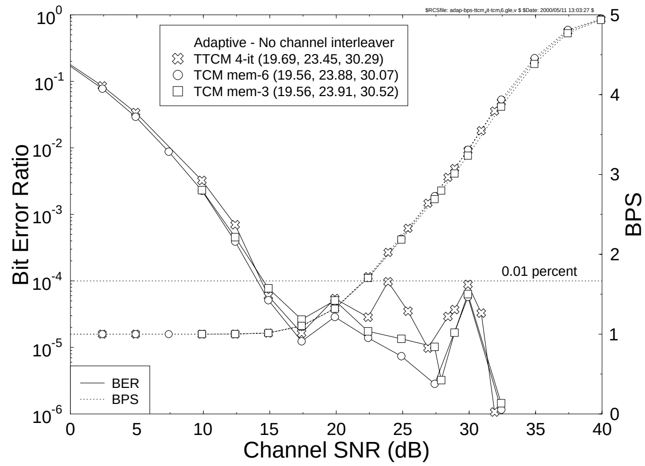

Figure 4.43: BER and BPS performance of adaptive TCM and TTCM without channel interleaving in **System I**, over the Rayleigh fading COST207 TU channel of Figure 4.33. The switching mechanism was characterized by Equation 4.18. The switching thresholds were set experimentally, in order to achieve a BER of below 0.01%, as shown in Table 4.17.

space-time coded BbB adaptive schemes.

4.12 Review and Discussion

In this chapter, we have demonstrated the benefits of turbo channel coding in conjunction with AQAM and channel equalization. In our turbo-coded AQAM schemes we have exploited the error correction capability of turbo coding in order to improve the coded BPS and BER performance, where the gains were recorded in Tables 4.11, 4.12 and 4.13 for different turbo block coded AQAM schemes, which are summarized as follows:

1. **FCFI-TBCH-AQAM** : In this scheme, a fixed turbo interleaver of size 9984 bits and a fixed coding rate of 0.7222 was implemented in conjunction with the switching regime of Equation 4.1.

2. **FCVI-TBCH-AQAM** : The code rate was fixed to 0.7222 and the turbo interleaver was varied according to Table 4.3 for each modulation mode, in order to ensure burst by burst decoding at the receiver.

3. **P-TBCH-AQAM** : Un-coded modes were added to the switching regime described by Equation 4.7, in order to increase the system's throughput. The code rate was set to 0.7222 and the turbo interleaver size was varied according to the size of the transmission burst, as shown in Table 4.5.

4. **VR-TBCH-AQAM** : In this final scheme, the code rate and turbo interleaver size were varied according to Table 4.9 and 4.7, respectively, for each modulation mode.

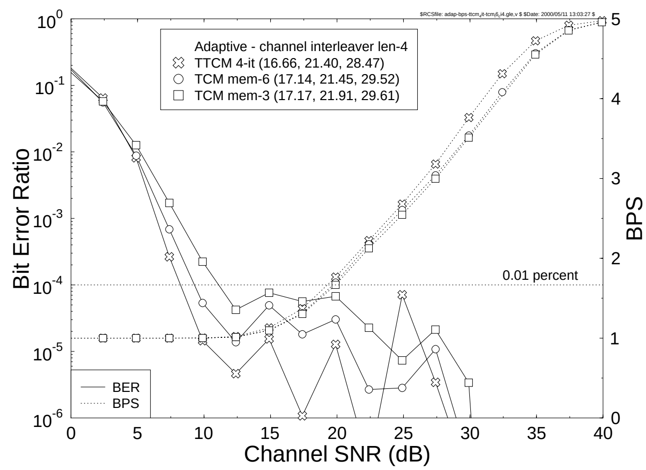

Figure 4.44: BER and BPS performance of adaptive TCM and TTCM using a channel interleaver length of 4 bursts, in **System II** over the Rayleigh fading COST207 TU channel of Figure 4.33. The switching mechanism was characterized by Equation 4.18. The switching thresholds were set experimentally, in order to achieve a BER of below 0.01%, as shown in Table 4.17.

The **FCVI-TBCH-AQAM** scheme demonstrated significant throughput gains, when compared to the individual fixed modulation modes, as evidenced by Figure 4.11. In these comparisons there were minimal SNR gains for the **High-BER** schemes, while the **Low-BER FCVI-TBCH-AQAM** scheme provided SNR gains of 5.0dB and 1.0dB, when compared to the small and large channel interleaved based fixed modulation modes, respectively. As a result of the employment of the channel interleavers, a high transmission delay was incurred by the constituent fixed modulation modes. By contrast, the **FCVI-TBCH-AQAM** scheme employed low-latency burst-by-burst decoding, which might benefit real-time applications, such as video transmission [166, 167].

These four turbo block coded AQAM schemes were also compared and contrasted in terms of their BER/SNR gains, BPS/SNR gains and the relative complexities of the schemes, when compared to the uncoded AQAM scheme having target BERs of 1% and 0.01%. These complexity comparisons were listed in Table 4.10 for all the coded schemes, where the **VR-TBCH-AQAM** scheme exhibited the highest channel decoder complexity as a result of the utilization of more complex BCH codes for this scheme. The complexity of the **P-TBCH-AQAM** scheme also increased due to its higher number of transmission modes. The gains achieved by the **Low-** and **High-BER** coded schemes are listed in Table 4.11 and 4.12, respectively. The gains achieved when the schemes were experimentally optimised for the sake of an creating a near-error-free system was tabulated in Table 4.13. The variation and trends of these gains were linked to the size of the turbo interleaver, the coding rate, the transmission frame size and the targeted BER, as explained in Section 4.8.

In terms of the error correction aspects of these turbo block coded schemes, we have observed the trade-offs involving the BER, BPS throughput, and the complexity of each scheme.

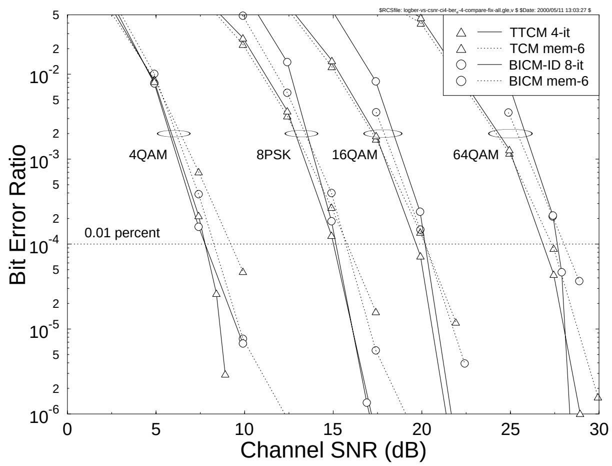

Figure 4.45: BER performance of the fixed modem modes of 4QAM, 8PSK, 16QAM and 64QAM utilising TCM, TTCM, BICM and BICM-ID schemes in the context of **System II**. For the sake of maintaining a similar decoding complexity, we used a TCM code memory of 6, TTCM code memory of 3 with 4 turbo iterations, BICM code memory of 6 and a BICM-ID code memory of 3 with 8 decoding iterations. However, BICM-ID had a slightly higher complexity than the other systems, since the demodulator module was invoked 8 times as compared to only once for its counterparts during each decoding process.

With the exception of the **P-TBCH-AQAM** scheme, the BER/SNR and BPS/SNR gains were evident at low to medium channel SNRs. However, the BPS throughput gain degraded at high channel SNRs due to the associated coding rate limitations. In order to increase the BPS throughput, the **P-TBCH-AQAM** and **VR-TBCH-AQAM** schemes were designed with added complexity. In comparing these two schemes, the **VR-TBCH-AQAM** provided a better BER/SNR versus BPS/SNR gain trade-off in conjunction with a more complex channel decoder. However, it is important to note that all these schemes achieved the targeted BER.

The size of the turbo interleaver was also crucial to the BER and BPS performance, where in the variable turbo interleaver size assisted schemes the gains were significantly lower than those of the **FCFI-TBCH-AQAM** scheme, when a large turbo interleaver size was used. Since the variable turbo interleaver sizes were chosen for supporting burst-by-burst channel decoding, a smaller speech frame shown in Figure 3.13 resulted in a smaller turbo interleaver. The implementation of burst-by-burst decoding also provided near-instantaneous error detection capability at the receiver, which was exploited in blindly detecting the modulation modes.

For the turbo block coded AQAM scheme of Section 4.4, which utilized large fixed-sized turbo interleavers, we have observed that the scheme, which targeted a lower BER displayed a better BER/SNR and BPS/SNR gain, as evidenced by the gains recorded in Tables 4.11 and 4.12. This was as a result of the superior coding gain at lower BERs, which was also observed for the fixed modulation modes of Section 4.3. As a result of the higher coding gain, the coded switching thresholds of the turbo coded AQAM schemes were lowered resulting in higher SNR gains, when compared to the uncoded AQAM schemes for similar target BERs.

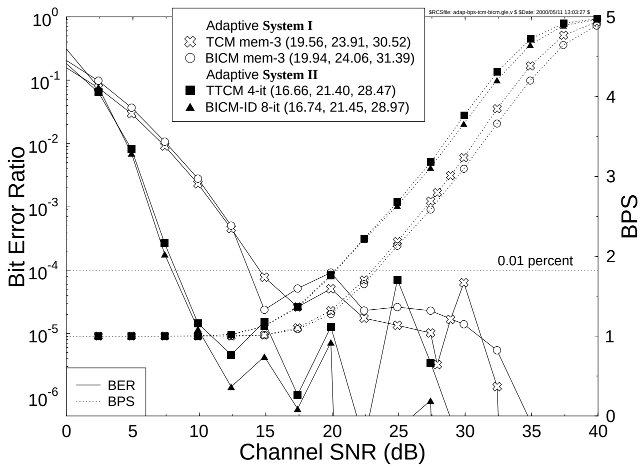

Figure 4.46: BER and BPS performance of the adaptive TCM/BICM **System I**, using memory 3 codes and that of the adaptive TTCM/BICM-ID **System II**, over the Rayleigh fading COST207 TU channel of Figure 4.33. The switching mechanism was characterized by Equation 4.18. The switching thresholds were set experimentally, in order to achieve a BER of below 0.01%, as shown in Table 4.17.

The channel codes were also exploited in order to detect the modulation modes, where the so-called hybrid SD-MSE modulation detection algorithm of Section 4.6.2 was implemented and its performance was shown in Figure 4.16. This hybrid algorithm, which was characterized by Equation 4.6 utilized the MSE algorithm in order to detect the BPSK mode, while the other modes were detected using the SD algorithm of Section 4.6.1. In this respect, a specific transmission frame structure was introduced for the NOTX mode, where a known m-sequence was transmitted in order to estimate the channel quality. Furthermore the unique correlation properties of the m-sequence - described by Equation 4.3 - supported a detection scheme at the receiver as discussed in Section 4.6.1. However, this modulation detection scheme incurred a high complexity as a result of the utilization of the channel decoders for detecting the possible modulation modes.

Convolutional codes were then utilized as the component codes for the turbo codec in Section 4.9. In comparing its performance to that of the turbo block coded schemes, a slight SNR degradation of $1-2$dB was observed for the fixed modulation modes, as evidenced by Figure 4.23. However, the computational complexity incurred by the turbo block coded schemes was higher by a factor of approximately seven when compared to the turbo convolutional schemes. In implementing the turbo convolutional coded AQAM schemes, the performance was similar to that of the turbo block coded AQAM schemes at a reduced complexity.

The concept of iterative channel equalization and decoding, termed as turbo equalization was then introduced in Section 4.10, where gains of approximately $0.7-2.0$dB were observed for the modulation modes of BPSK, 4QAM and 16QAM. Subsequently, an iterative LMS-based CIR estimation technique was proposed, which exploited the iterative nature of this scheme. The CIR estimation based performance approached that of the perfect CIR estimation based performance, as evidenced by Figure 4.29. The turbo equalizer was then implemented in an AQAM scheme, which yielded a gain of approximately $1.0 - 2.0$dB, when compared to the fixed modulation modes.

The application of turbo coding in a wideband AQAM scheme resulted in substantial performance gains, when compared to the fixed modulation modes and to the uncoded wideband AQAM scheme at a certain targeted BER. Furthermore, with the implementation of burst-by-burst decoding at the receiver the error detection capability of the channel codec was exploited, in order to detect the modulation modes as well as to potentially provide channel quality estimates. However, the complexity incurred in these turbo coded AQAM schemes was high due to the iterative regime of the channel decoding process. In the context of turbo equalization the complexity of this scheme increased exponentially, when higher-order modulation modes were used or, when channels exhibiting a long memory were encountered. This severely hindered the implementation of such AQAM schemes.

In this chapter, the performance of the wideband AQAM scheme based on the assumptions listed in Section 3.3.1 was investigated. However, in order to invoke a more practical wideband AQAM scheme, these assumptions are discarded and the resulting performance is analysed in the next chapter. Furthermore, the impact of co-channel interference is also considered, which will form the core of our next chapter.

Part II

Near-instantaneously Adaptive Modulation and Neural Network Based Equalisation:

M.S. Yee, L. Hanzo

Part III

Near-Instantaneously Adaptive CDMA and Space-Time Coded OFDM:

L. Hanzo, T. Keller, E.L. Kuan, T.H. Liew

Chapter 11

Burst-by-Burst Adaptive Multiuser Detection CDMA

E. L. Kuan and L. Hanzo[1]

11.1 Motivation

As argued throughout the previous chapters of the book, mobile propagation channels exhibit time-variant propagation properties [10]. Although apart from simple cordless telephone schemes most mobile radio systems employ power control for mitigating the effects of received power fluctuations, rapid channel quality fluctuations cannot be compensated by practical, finite reaction-time power control schemes. Furthermore, the ubiquitous phenomenon of signal dispersion due to the multiplicity of scaterring and reflecting objects cannot be mitigated by power control. Similarly, other performance limiting factors, such as adjacent- and co-channel intereference as well as multi-user interference vary as a function of time. The ultimate channel quality metric is constituted by the bit error rate experienced, irrespective of the specific impairment encountered. The channel quality variations are typically higher near the fringes of the propagation cell or upon moving from an indoor scenario to an outdoor cell due to the high standard deviation of the shadow- and fast-fading [10] encountered, even in conjunction with agile power control. Furthermore, the bit errors typically occur in bursts due to the time-variant channel quality fluctuations and hence it is plausible that a fixed transceiver mode cannot achieve a high flexibility in such environments.

The design of powerful and flexible transceivers has to be based on finding the best compromise amongst a number of contradicting design factors. Some of these contradicting factors are low power consumption, high robustness against transmission errors amongst various channel conditions, high spectral efficiency, low-delay for the sake of supporting interactive real-time multimedia services, high-capacity networking and so forth [2]. In this chapter we

[1]This chapter is based on Kuan and Hanzo: Burst-by-Burst Adaptive Multiuser Detection CDMA: A Framework for Existing and Future Wireless Standards, submitted to the Proceedings of the IEEE©IEEE, 2001

will address a few of these issues in the context of Direct Sequence Code Division Multiple Access (DS-CDMA) systems. It was argued in [2] that the time-variant optimisation criteria of a flexible multi-media system can only be met by an adaptive scheme, comprising the firmware of a suite of system components and invoking that particular combination of speech codecs, video codecs, embedded un-equal protection channel codecs, voice activity detector (VAD) and transceivers, which fulfills the currently prevalent set of transceiver optimisation requirements.

These requirements lead to the concept of arbitrarily programmable, flexible so-called software radios [313], which is virtually synonymous to the so-called tool-box concept invoked to a degree in a range of existing systems at the time of writing [3]. This concept appears attractive also for third- and future fourth-generation wireless transceivers. A few examples of such optimisation criteria are maximising the teletraffic carried or the robustness against channel errors, while in other cases minimisation of the bandwidth occupancy or the power consumption is of prime concern.

Motivated by these requirements in the context of the CDMA-based third-generation wireless systems [10, 122], the outline of the chapter is as follows. In Section 11.2 we review the current state-of-the-art in multi-user detection with reference to the receiver family-tree of Figure 11.4. Section 11.4 is dedicated to adaptive CDMA schemes, which endeavour to guarantee a better performance than their fixed-mode counterparts. Burst-by-burst (BbB) adaptive adaptive quadrature amplitude modulation (AQAM) based and Variable Spreding Factor (VSF) assisted CDMA system proposals are studied comparatively in Section 11.5. Lastly our conclusions are offered in Section 11.6.

11.2 Multiuser detection

11.2.1 Single-user channel equalisers

11.2.1.1 Zero-forcing principle

The fundamental approach of multiuser equalisers accrues from recognising the fact that the nature of the interference is similar, regardless, whether its source is dispersive multipath propagation or multiuser interference. In other words, the effects of imposing interference on the received signal by a K-path dispersive channel or by a K-user system are similar. Hence below we continue our discourse with a rudimentary overview of single-user equalisers, in order to pave the way for a more detailed discourse on multiuser equalisers.

The concept of zero-forcing (ZF) channel equalizers can be readily followed for example using the approach of [65]. Specifically, the zero-forcing criterion [65] constrains the signal component at the output of the equalizer to be free of intersymbol interference (ISI). More explicitly, this implies that the product of the transfer functions of the dispersive and hence frequency-selective channel and the channel equaliser results in a 'frequency-flat' constant, implying that the concatenated equaliser restores the perfect all-pass channel transfer function. This can be formulated as:

$$G(z) = F(z)B(z) = 1, \tag{11.1}$$

$$F(z) = \frac{1}{B(z)}, \tag{11.2}$$

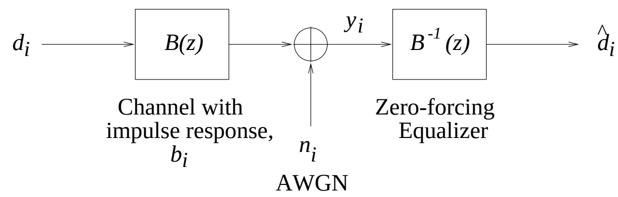

Figure 11.1: Block diagram of a simple transmission scheme using a zero-forcing equalizer.

where $F(z)$ and $B(z)$ are the z-transforms of the ZF-equaliser and that of the dispersive channel, respectively. The impulse response corresponding to the concatenated system hence becomes a Dirac delta, implying that no ISI is inflicted. More explicitly, the zero-forcing equalizer is constituted by the inverse filter of the channel. Figure 11.1 shows the simplified block diagram of the corresponding system.

Upon denoting by $D(z)$ and $N(z)$ the z-transforms of the transmitted signal and the additive noise respectively, the z-transform of the received signal can be represented by $R(z)$, where

$$R(z) = D(z)B(z) + N(z). \tag{11.3}$$

The z-transform of the multiuser equalizer's output will be

$$\begin{aligned} \hat{D}(z) &= F(z)R(z) && (11.4) \\ &= \frac{R(z)}{B(z)} && (11.5) \\ &= D(z) + \frac{N(z)}{B(z)}. && (11.6) \end{aligned}$$

From Equation 11.6, it can be seen that the output signal is free of ISI. However, the noise component is enhanced by the inverse of the transfer function of the channel. This may have a disastrous effect on the output of the equalizer, in terms of noise amplification in the frequency domain at frequencies where the transfer function of the channel was severely attenuated. Hence a disadvantage of the ZF-equaliser is that in an effort to compensate for the effects of the dispersive and consequently frequency-selective channel and the associated ISI it substantially enhances the originally white noise spectrum by frequency-selectively amplifying it. This deficiency can be mitigated by invoking the so-called minimum mean square error linear equalizer, which is capable of jointly minimising the effects of noise and interference, rather than amplifying the effects of noise.

11.2.1.2 Minimum mean square error equalizer

Minimum mean square error (MMSE) equalizers have been considered in depth for example in [65] and a similar approach is followed here. Upon invoking the MMSE criterion [65], the equalizer tap coefficients are calculated in order to minimize the MSE at the output of the multiuser equalizer, where the MSE is defined as :

$$e_k^2 = E[|d_k - \hat{d}_k|^2], \tag{11.7}$$

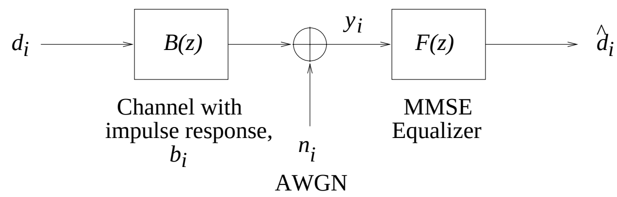

Figure 11.2: Block diagram of a simple transmission scheme employing an MMSE equalizer.

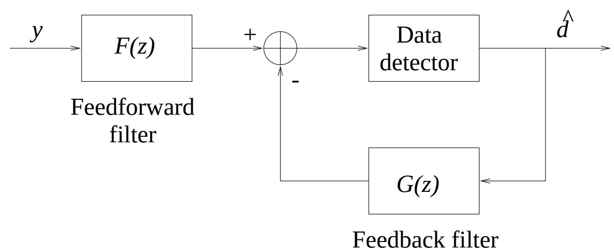

Figure 11.3: Block diagram of a decision feedback equalizer.

where the function $E[x]$ indicates the expected value of x. Figure 11.2 shows the system's schematic using an MMSE equalizer, where $B(z)$ is the channel's transfer function and $F(z)$ is the transfer function of the equalizer. The output of the equalizer is given by :

$$\hat{D}(z) = F(z)B(z)D(z) + F(z)N(z), \tag{11.8}$$

where $D(z)$ is the z-transform of the data bits d_i, $\hat{D}(z)$ is the z-transform of the data estimates $\hat{d}_i$ and $N(z)$ is the z-transform of the noise samples n_i.

11.2.1.3 Decision feedback equalizers

The decision feedback equalizer (DFE) [65] can be separated into two components, a feed-forward filter and a feedback filter. The schematic of a general DFE is depicted in Figure 11.3. The philosophy of the DFE is two-fold. Firstly, it aims for reducing the filter-order of the ZFE, since with the aid of Equation 11.2 and Figure 11.1 it becomes plausible that the inverse filter of the channel, $B^{-1}(z)$, can only be implemented as an Infinite Impulse Response (IIR) filter, requiring a high implementational complexity. Secondly, provided that there are no transmission errors, the output of the hard-decision detector delivers the transmitted data bits, which can provide valuable explicit training data for the DFE. Hence a reduced-length feed-forward filter can be used, which however does not entirely eliminate the ISI. Instead, the feedback filter uses the data estimates at the output of the data detector in order to subtract the ISI from the output of the feed-forward filter, such that the input signal of the data detector has less ISI, than the signal at the output of the feed-forward filter. If it is assumed that the data estimates fed into the feedback filter are correct, then the DFE is superior to the linear equalizers, since the noise enhancement is reduced. One way of explaining this would be to say that if the data estimates are correct, then the noise has been eliminated and there is

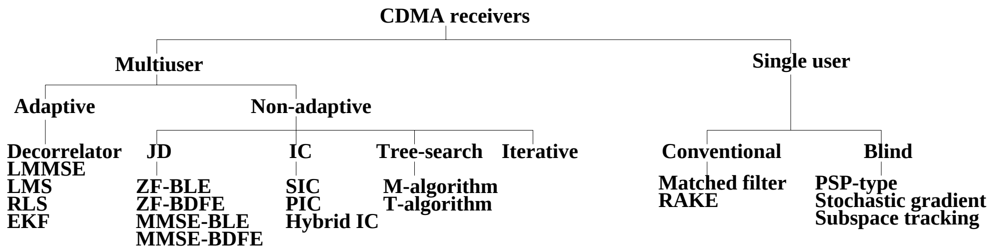

Figure 11.4: Classification of CDMA detectors

no noise enhancement in the feedback loop. However, if the data estimates are incorrect, these errors will propagate through to future decisions and this problem is known as error propagation.

There are two basic DFEs, the ZF-DFE and the MMSE-DFE. Analogous to its linear counterpart, the coefficients of the feedback filter for the ZF-DFE are calculated so that the ISI at the output of the feed-forward filter is eliminated and the input signal of the data detector is free of ISI [50]. Let us now focus our attention on CDMA multiuser detection equalizers.

11.3 Multiuser equaliser concepts

DS-CDMA systems [314, 315] support a multiplicity of users within the same bandwidth by assigning different - typically unique - codes to different users for their communications, in order to be able to distinguish their signals from each other. When the transmitted signal is subjected to hostile wireless propagation environments, the signal of different users interfer with each other and hence CDMA systems are interference-limited due to the multiple access interference (MAI) generated by the users transmitting within the same bandwidth simultaneously. The subject of this chapter is, how the MAI can be mitigated. A whole range of detectors have been proposed in the literature, which will be reviewed with reference to the family-tree of Figure 11.4 during our forthcoming discourse.

The conventional so-called single-user CDMA detectors of Figure 11.4 – such as the matched filter [270,316] and the RAKE combiner [50] – are optimized for detecting the signal of a single desired user. RAKE combiners exploit the inherent multi-path diversity in CDMA, since they essentially consist of matched filters for each resolvable path of the multipath channel. The outputs of these matched filters are then coherently combined according to a diversity combining technique, such as maximal ratio combining, equal gain combining or selection diversity combining [50]. These conventional single-user detectors are inefficient, since the interference is treated as noise and the knowledge of the channel impulse response (CIR) or the spreading sequences of the interferers is not exploited.

In order to mitigate the problem of MAI, Verdú [317] proposed and analyzed the optimum multiuser detector for asynchronous Gaussian multiple access channels. The optimum detector invokes all the possible bit sequences, in order to find the sequence that maximizes the correlation metric given by [215] :

$$\Omega(\mathbf{r},\mathbf{d}) = 2\mathbf{d}^T\mathbf{r} - \mathbf{d}^T\mathbf{R}\mathbf{d}, \tag{11.9}$$

where the elements of the vector $\mathbf{r}$ represent the cross-correlation of the spread, channel-impaired received signal with each of the users' spreading sequence, the vector $\mathbf{d}$ consists of the bits transmitted by all the users during the current signalling instant and the matrix $\mathbf{R}$ is the cross-correlation (CCL) matrix of the spreading sequences. This optimum detector significantly outperforms the conventional single-user detector and – in contrast to single user detectors – it is insensitive to power control errors, which is often termed as being near-far resistant. However, unfortunately its complexity grows exponentially in the order of $O(2^{NK})$, where N is the number of overlapping asynchronous bits considered in the detector's decision window and K is the number of interfering users. In order to reduce the complexity of the receiver and yet to provide an acceptable Bit Error Rate (BER) performance, significant research efforts have been invested in the field of sub-optimal CDMA multiuser receivers [215]. Multiuser detection exploits the base station's knowledge of the spreading sequences and that of the estimated (CIRs) in order to remove the MAI. These multiuser detectors can be categorized in a number of ways, such as linear versus non-linear, adaptive versus non-adaptive algorithms or burst transmission versus continuous transmission regimes. Excellent summaries of some of these sub-optimum detectors can be found in the monographs by Verú [215], Prasad [318], Glisic and Vucetic [319]. Other MAI-mitigating techniques include the employment of adaptive antenna arrays, which mitigate the level of MAI at the receiver by forming a beam in the direction of the wanted user and a null towards the interfering users. Research efforts invested in this area include, amongst others, the investigations carried out by Thompson, Grant and Mulgrew [320,321]; Naguib and Paulraj [322]; Godara [323]; as well as Kohno, Imai, Hatori and Pasupathy [324]. However, the area of adaptive antenna arrays is beyond the scope of this article and the reader is referred to the references cited for further discussions. In the forthcoming section, a brief survey of the sub-optimal multiuser receivers will be presented with reference to Figure 11.4, which constitute an attractive compromise in terms of the achievable performance and the associated complexity.

11.3.1 Linear receivers

Following the seminal work by Verdú [317], numerous sub-optimum multiuser detectors have been proposed for a variety of channels, data modulation schemes and transmission formats [325]. These CDMA detector schemes will be classified with reference to Figure 11.4, which will be referred to throughout our discussions. Lupas and Verdú [326] initially suggested a sub-optimum linear detector for symbol-synchronous transmissions and further developed it for asynchronous transmissions in a Gaussian channel [327]. This linear detector inverted the CCL matrix R seen in Equation 11.9, which was constructed from the CCLs of the spreading codes of the users and this receiver was termed the decorrelating detector. It was shown that this decorrelator exhibited the same degree of near-far resistance, as the optimum multiuser detector. A further sub-optimum multiuser detector investigated was the minimum mean square error (MMSE) detector, where a biased version of the CCL matrix was inverted and invoked, in order to optimize the receiver obeying the MMSE criterion.

Zvonar and Brady [328] proposed a multiuser detector for synchronous CDMA systems designed for a frequency-selective Rayleigh fading channel. Their approach also used a bank of matched filters followed by a so-called whitening filter, but maximal ratio combining was used to combine the resulting signals. The decorrelating detector of [327] was further developed for differentially-encoded coherent multiuser detection in flat fading channels by Zvonar *et al.* [329]. Zvonar also amalgamated the decorrelating detector with diversity combining, in order to achieve performance improvements in frequency selective fading channels [330]. A multiuser detector jointly performing decorrelating CIR estimation and data detection was investigated by Kawahara and Matsumoto [331]. Path-by-path decorrelators were employed for each user in order to obtain the input signals required for CIR estimation and the CIR estimates as well as the outputs of a matched filter bank were fed into a decorrelator for demodulating the data. A variant of this idea was also presented by Hosseinian, Fattouche and Sesay [332], where training sequences and a decorrelating scheme were used for determining the CIR estimate matrix. This matrix was then used in a decorrelating decision feedback scheme for obtaining the data estimates. Juntti, Aazhang and Lilleberg [333] proposed iterative schemes, in order to reduce the complexity. Sung and Chen [334] advocated using a sequential estimator for minimizing the mean square estimation error between the received signal and the signal after detection. The cross-correlations between the users' spreading codes and the estimates of the channel-impaired received signal of each user were needed, in order to obtain estimates of the transmitted data for each user. Duel-Hallen [335] proposed a decorrelating decision-feedback detector for removing the MAI from a synchronous system communicating over a Gaussian channel. The outputs from a bank of filters matched to the spreading codes of the users were passed through a whitening filter. This filter was obtained by decomposing the CCL matrix of the users' spreading codes with the aid of the Cholesky decomposition [223] technique. The results showed that MAI could be removed from each user's signal successively, assuming that there was no error propagation. However, estimates of the received signal strengths of the users were needed, since the users had to be ranked in order of decreasing signal strengths so that the more reliable estimates were obtained first. Duel-Hallen's decorrelating decision feedback detector [335] was improved by Wei and Schlegel [336] with the aid of a sub-optimum variant of the Viterbi algorithm, where the most likely paths were retained in the case of merging paths in the Viterbi algorithm. The decorrelating decision feedback detector [335] was also improved with the assistance of soft-decision convolutional coding by Hafeez and Stark [337]. Soft decisions from a Viterbi channel decoder were fed back into the filter for signal cancellation.

Having reviewed the range of linear receivers, let us now consider the class of joint detection schemes, which can be found in the family-tree of Figure 11.4 in the next section.

11.3.2 Joint detection

11.3.2.1 Joint detection concept

As mentioned before in the context of single-user channel equalisation, the effect of MAI on the desired signal is similar to the impact of multipath propagation-induced Inter-symbol Interference (ISI) on the same signal. Each user in a K-user system suffers from MAI due to the other $(K-1)$ users. This MAI can also be viewed as a single-user signal perturbed by ISI inflicted by $(K-1)$ paths in a multipath channel. Therefore, classic equalization techniques

[50, 79, 94, 270] used to mitigate the effects of ISI can be modified for multiuser detection and these types of multiuser detectors can be classified as joint detection receivers. The joint detection (JD) receivers were developed for burst-based, rather than continuous transmission. The concept of joint detection for the uplink was proposed by Klein and Baier [216] for synchronous burst transmissions, which is visualised with the aid of Figure 11.5.

In Figure 11.5 there are a total of K users in the system, where the information is transmitted in bursts. Each user transmits N data symbols per burst and the data vector for user k is represented as $\mathbf{d}^{(\mathbf{k})}$. Each data symbol is spread with a user-specific spreading sequence, $\mathbf{c}^{(\mathbf{k})}$, which has a length of Q chips. In the uplink, the signal of each user passes through a different mobile channel characterized by its time-varying complex impulse response, $\mathbf{h}^{(\mathbf{k})}$. By sampling at the chip rate of $1/T_c$, the impulse response can be represented by W complex samples. Following the approach of Klein *et al.* [216], the received burst can be represented as $\mathbf{y} = \mathbf{A}\mathbf{d} + \mathbf{n}$, where $\mathbf{y}$ is the received vector and consists of the synchronous sum of the transmitted signals of all the K users, corrupted by a noise sequence, $\mathbf{n}$. The matrix $\mathbf{A}$ is referred to as the system matrix and it defines the system's response, representing the effects of MAI and the mobile channels. Each column in the matrix represents the combined impulse response obtained by convolving the spreading sequence of a user with its channel impulse response, $\mathbf{b}^{(\mathbf{k})} = \mathbf{c}^{(\mathbf{k})} * \mathbf{h}^{(\mathbf{k})}$. This is the impulse response experienced by a transmitted data symbol. Upon neglecting the effects of the noise the joint detection formulation is simply based on inverting the system matrix $\mathbf{A}$, in order to recover the data vector constituted by the superimposed transmitted information of all the K CDMA users. The dimensions of the matrix $\mathbf{A}$ are $(NQ + W - 1) \times KN$ and an example of it can be found in reference [216] by Klein *et al*, where the list of the symbols used is given as :

- K for the total number of users,
- N is the number of data symbols transmitted by each user in one transmission burst,
- Q represents the number of chips in each spreading sequence,
- W denotes the length of the wideband CIR, where W is assumed to be an integer multiple of the number of chip intervals, T_c.
- L indicates the number of multipath components or taps in the wideband CIR.

In order to introduce compact mathematical expressions, matrix notation will be employed. The transmitted data symbol sequence of the k-th user is represented by a vector as :

$$\begin{aligned} &\mathbf{d}^{(k)} = (d_1^{(k)}, d_2^{(k)}, \ldots, d_n^{(k)}, \ldots, d_N^{(k)})^T, \\ &\text{for } k = 1, \ldots, K; \;\; n = 1, \ldots, N, \end{aligned} \tag{11.10}$$

where k is the user index and n is the symbol index. There are N data symbols per transmission burst and each data symbol is generated using an m-ary modulation scheme [50].

The Q-chip spreading sequence vector of the k-th user is expressed as :

$$\begin{aligned} &\mathbf{c}^{(k)} = (c_1^{(k)}, c_2^{(k)}, \ldots, c_q^{(k)}, \ldots, c_Q^{(k)})^T, \\ &\text{for } k = 1, \ldots, K; \;\; q = 1, \ldots, Q. \end{aligned} \tag{11.11}$$

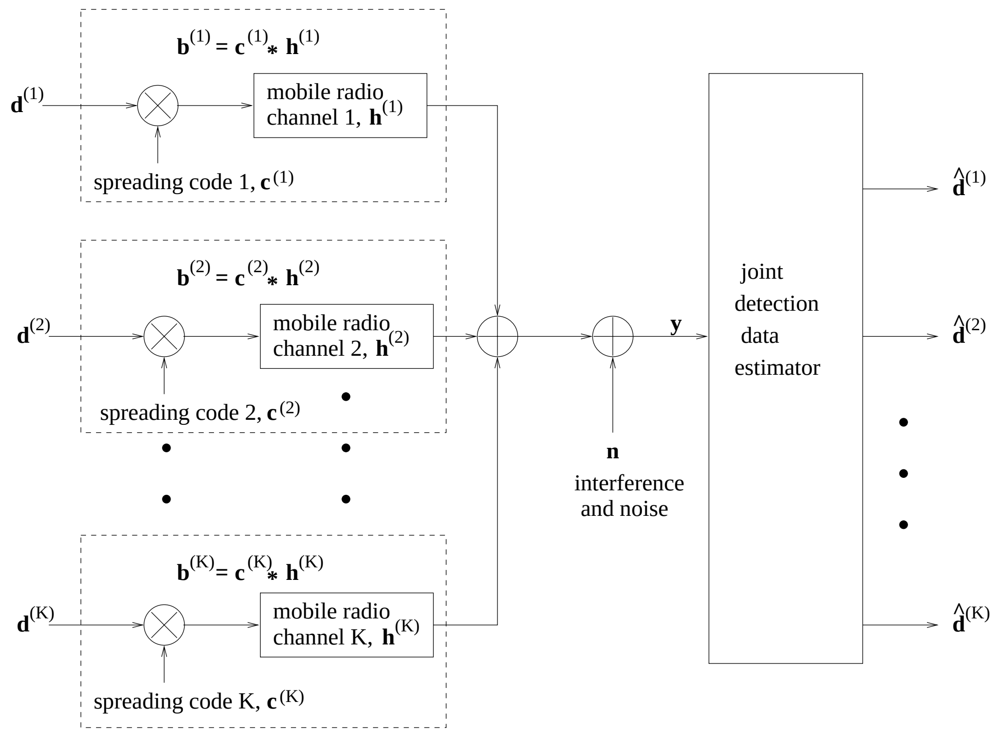

Figure 11.5: System model of a synchronous CDMA system on the up-link using joint detection.

The CIR for the n-th data symbol of the k-th user is represented as :

$$\begin{aligned} &\mathbf{h}_n^{(k)} = (h_n^{(k)}(1), \ldots, h_n^{(k)}(w), \ldots, h_n^{(k)}(W))^T, \\ &\text{for } k = 1, \ldots, K; \; w = 1, \ldots, W, \end{aligned} \tag{11.12}$$

consisting of W complex CIR samples $h_n^{(k)}(w)$ taken at the chip rate of $1/T_c$.

The combined impulse response, $\mathbf{b}_n^{(k)}$, due to the spreading sequence and the CIR is defined by the convolution of $\mathbf{c}^{(k)}$ and $\mathbf{h}_n^{(k)}$, which is represented as :

$$\begin{aligned} \mathbf{b}_n^{(k)} &= (b_n^{(k)}(1), \ldots, b_n^{(k)}(l), \ldots, b_n^{(k)}(Q+W-1))^T \\ &= \mathbf{c}^{(k)} * \mathbf{h}_n^{(k)}, \\ &\quad \text{for } k = 1 \ldots K; \;\; n = 1, \ldots N. \end{aligned} \tag{11.13}$$

In order to represent the ISI due to the N symbols and the dispersive combined impulse responses, the discretised received signal, $\mathbf{r}^{(k)}$, of user k can be expressed as the product of a matrix $\mathbf{A}^{(k)}$ and its data vector $\mathbf{d}^{(k)}$, where :

$$\mathbf{r}^{(k)} = \mathbf{A}^{(k)}\mathbf{d}^{(k)}. \tag{11.14}$$

The i-th element of the received signal vector $\mathbf{r}^{(k)}$ is :

$$r_i^{(k)} = \sum_{n=1}^{N} [\mathbf{A}^{(k)}]_{in} d_n^{(k)}, \text{ for } i = 1, \ldots, NQ + W - 1. \tag{11.15}$$

Again, the matrix $\mathbf{A}^{(k)}$ is the so-called system matrix of the k-th user and it is constructed from the combined impulse responses of Equation 11.13. It represents the effect of the combined impulse responses on each data symbol $d_n^{(k)}$ in the data vector, $\mathbf{d}^{(k)}$. Each column in the matrix $\mathbf{A}$ indexed by n contains the combined impulse response, $\mathbf{b}_n^{(k)}$ that affects the n-th symbol of the data vector. However, since the data symbols are spread by the Q-chip spreading sequences, they are transmitted Q chips apart from each other. Hence the start of the combined impulse response, $\mathbf{b}_n^{(k)}$, for each column is offset by Q rows from the start of $\mathbf{b}_{n-1}^{(k)}$ in the preceding column. Therefore, the element in the $[(n-1)Q + l]$-th row and the n-th column of $\mathbf{A}^{(k)}$ is the l-th element of the combined impulse response, $\mathbf{b}_n^{(k)}$, for $l = 1, \ldots, Q + W - 1$. All other elements in the column are zero-valued.

The pictorial representation of Equation 11.14 is shown in Figure 11.6, where $Q = 4$, $W = 2$ and $N = 3$. As it can be seen from the diagram, in each column of the matrix $\mathbf{A}^{(k)}$ – where a box with an asterisk marks a non-zero element – the vector $\mathbf{b}_n^{(k)}$ starts at an offset of $Q = 4$ rows below its preceding column, except for the first column, which starts at the first row. The total number of elements in the vector $\mathbf{b}_n^{(k)}$ is $(Q + W - 1) = 5$. The total number of columns in the matrix $\mathbf{A}^{(k)}$ equals the number of symbols in the data vector, $\mathbf{d}^{(k)}$, i.e. N. Finally, the received signal vector product, $\mathbf{r}^{(k)}$ in Equation 11.14, has a total of $(NQ + W - 1) = 13$ elements due to the ISI imposed by the multipath channel, as opposed to $NQ = 12$ elements in a narrowband channel.

The joint detection receiver aims for detecting the symbols of all the users jointly by utilizing the information available on the spreading sequences and CIR estimates of all the users. Therefore, as seen in Figure 11.7, the data symbols of all K users can be viewed as the transmitted data sequence of a single user, by concatenating all the data sequences. The overall transmitted sequence can be rewritten as :

$$\begin{aligned} \mathbf{d} &= (\mathbf{d}^{(1)T}, \mathbf{d}^{(2)T}, \ldots, \mathbf{d}^{(K)T})^T & (11.16) \\ &= (d_1, d_2, \ldots, d_{KN})^T, & (11.17) \end{aligned}$$

where $d_j = d_n^{(k)}$ for $j = n + N.(k-1)$, $k = 1, 2, \ldots, K$ and $n = 1, 2, \ldots, N$.

The system matrix for the overall system can be constructed by appending the $\mathbf{A}^{(k)}$ matrix of each of the K users column-wise, whereby :

$$\mathbf{A} = (\mathbf{A}^{(1)}, \mathbf{A}^{(2)}, \ldots, \mathbf{A}^{(k)}, \ldots, \mathbf{A}^{(K)}). \tag{11.18}$$

The construction of matrix $\mathbf{A}$ from the system matrices of the K users is depicted in Figure 11.7. Therefore, the discretised received composite signal can be represented in matrix form as :

$$\begin{aligned} \mathbf{y} &= \mathbf{A}\mathbf{d} + \mathbf{n}, & (11.19) \\ \mathbf{y} &= (y_1, y_2, \ldots, y_{NQ+W-1})^T, & \end{aligned}$$

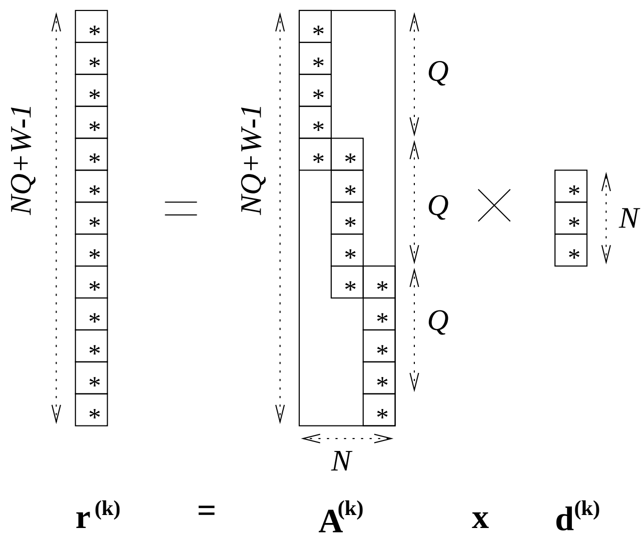

Figure 11.6: Stylized structure of Equation 11.14 representing the received signal vector of a wideband channel, where $Q = 4$, $W = 2$ and $N = 3$. The column vectors in the matrix $\mathbf{A}^{(k)}$ are the combined impulse response vectors, $\mathbf{b}_n^{(k)}$ of Equation 11.13. A box with an asterisk in it represents a non-zero element, and the remaining notation is as follows : K represents the total number of users, N denotes the number of data symbols transmitted by each user, Q represents the number of chips in each spreading sequence, and W indicates the length of the wideband CIR.

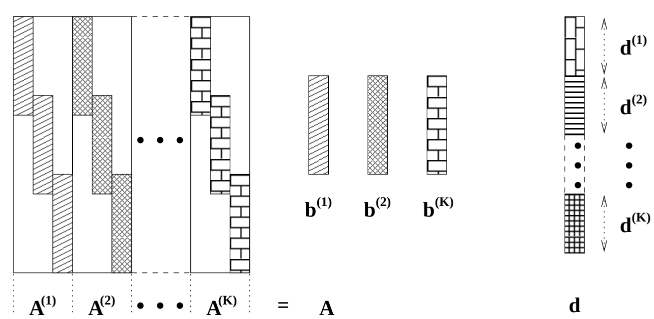

Figure 11.7: The construction of matrix $\mathbf{A}$ from the individual system matrices, $\mathbf{A}^{(k)}$ seen in Figure 11.6, and the data vector $\mathbf{d}$ from the concatenation of data vectors, $\mathbf{d}^{(k)}$, of all K users.

where $\mathbf{n} = (n_1, n_2, \ldots, n_{NQ+W-1})^T$, is the noise sequence, which has a covariance matrix of $\mathbf{R}_n = E[\mathbf{n}.\mathbf{n}^H]$. The composite signal vector $\mathbf{y}$ has $(NQ + W - 1)$ elements for a data burst of length N symbols. Upon multiplying the matrix $\mathbf{A}$ with the vector $\mathbf{d}$ seen in Figure 11.7, we obtain the MAI- and ISI-contaminated received symbols according to Equation 11.19.

Taken as a whole, the system matrix, $\mathbf{A}$, can be constructed from the combined response vectors, $\mathbf{b}_n^{(k)}$ of all the K users, in order to depict the effect of the system's response on the data vector of Equation 11.16. The dimensions of the matrix are $(NQ + W - 1) \times KN$. Figure 11.8 shows an example of the matrix, $\mathbf{A}$, for an N-bit long data burst. For ease of representation, we assumed that the channel length, W, for each user is the same and that it remains constant throughout the data burst. We have also assumed that the channel experiences slow fading and that the fading is almost constant across the data burst. Therefore, the combined response vector for each transmitted symbol of user k is represented by $\mathbf{b}^{(k)}$, where $\mathbf{b}^{(k)} = \mathbf{b}_1^{(k)}\mathbf{b}_2^{(k)} = \ldots = \mathbf{b}_N^{(k)}$. Focusing our attention on Figure 11.8, the elements in the j-th column of the matrix constitute the combined response vector that affects the j-th data symbol in the transmitted data vector $\mathbf{d}$. Therefore, columns $j = 1$ to N of matrix $\mathbf{A}$ correspond to symbols $m = 1$ to N of vector $\mathbf{d}$, which are also the data symbols of user $k = 1$. The next N columns correspond to the next N symbols of data vector $\mathbf{d}$, which are the data symbols of user $k = 2$ and so on.

For user k, each successive response vector, $\mathbf{b}^{(k)}$, is placed at an offset of Q rows from the preceding vector, as shown in Figure 11.8. For example, the combined response vector in column 1 of matrix $\mathbf{A}$ is $\mathbf{b}^{(1)}$ and it starts at row 1 of the matrix because that column corresponds to the first symbol of user $k = 1$. In column 2, the combined response vector is also $\mathbf{b}^{(1)}$, but it is offset from the start of the vector in column 1 by Q rows. This is because the data symbol corresponding to this matrix column is transmitted Q chips later. This is repeated until the columns $j = 1, \ldots, N$ contain the combined response vectors that affect all the data symbols of user $k = 1$. The next column of $j = N + 1$ in the matrix $\mathbf{A}$ contains the combined impulse response vector that affects the data symbol, $d_{N+1} = d_1^{(2)}$, which is the first data symbol of user $k = 2$. In this column, the combined response vector for user $k = 2$, $\mathbf{b}^{(2)}$, is used and the vector starts at row 1 of the matrix because it is the first symbol of this user. The response matrix, $\mathbf{b}^{(2)}$ is then placed into columns $j = N+1, \ldots, 2N$ of the matrix $\mathbf{A}$, with the same offsets for each successive vector, as was carried out for user 1. This process is repeated for all the other users until the system matrix is completely constructed.

The mathematical representation of matrix $\mathbf{A}$ in general can be written as :

$$[\mathbf{A}]_{ij} = \begin{cases} b_n^{(k)}(l) & \text{for } k = 1, \ldots, K; \;\; n = 1, \ldots, N; \\ & l = 1, \ldots, Q + W - 1 \\ 0 & \text{otherwise,} \end{cases} \tag{11.20}$$
$$\text{for } i = 1, \ldots, NQ + W - 1, \quad j = 1, \ldots, KN,$$

where $i = Q(n-1) + l$ and $j = n + N(k-1)$.

Figure 11.9 shows the stylized structure of Equation 11.19 for a specific example. In the figure, a system with $K = 2$ users is depicted. Each user transmits $N = 3$ symbols per transmission burst, and each symbol is spread with a signature sequence of length $Q = 3$ chips. The channel for each user has a dispersion length of $W = 3$ chips. The blocked segments in the figure represent the combination of elements that result in the element y_4, which is obtained from Equation 11.19 by :

$$y_4 = \sum_{i=1}^{KN=6} [\mathbf{A}]_{4,i} d_i + n_4 \tag{11.21}$$
$$= [\mathbf{A}]_{4,1} d_1 + [\mathbf{A}]_{4,2} d_2 + [\mathbf{A}]_{4,4} d_4 + [\mathbf{A}]_{4,5} d_5 + n_4 \tag{11.22}$$

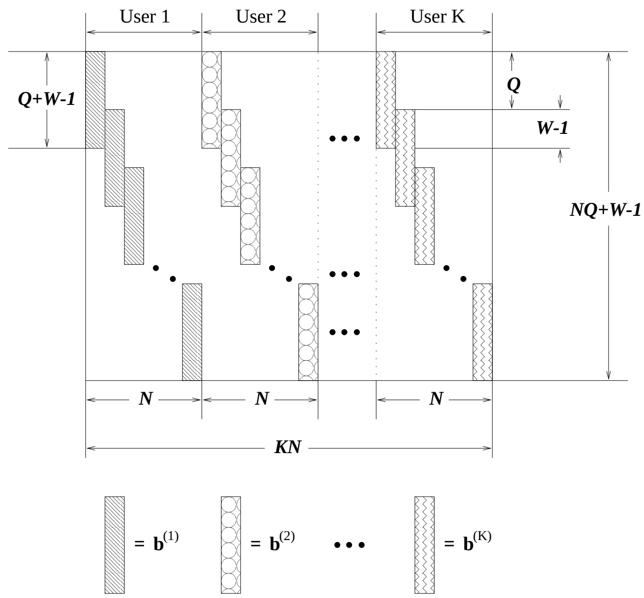

Figure 11.8: Stylized structure of the system matrix $\mathbf{A}$, where $\mathbf{b}^{(1)}$, $\mathbf{b}^{(2)}$ and $\mathbf{b}^{(K)}$ are column vectors representing the combined impulse responses of users 1, 2 and K, respectively in Equation 11.13. The notation is as follows : K represents the total number of users, N denotes the number of data symbols transmitted by each user, Q represents the number of chips in each spreading sequence, and W indicates the length of the wideband CIR.

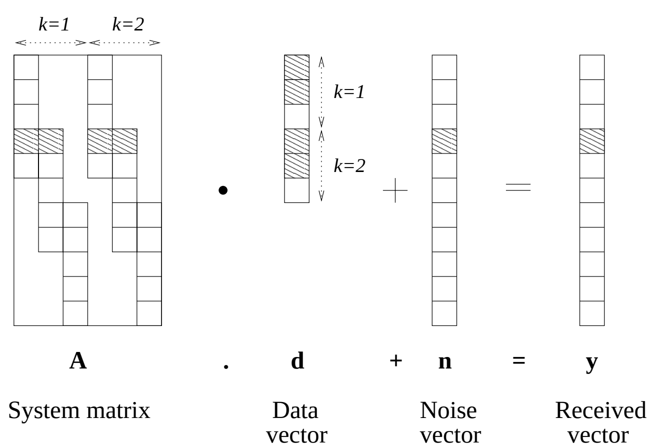

Figure 11.9: Stylized structure of the matrix equation $\mathbf{y} = \mathbf{A}\mathbf{d} + \mathbf{n}$ for a $K = 2$–user system. Each user transmits $N = 3$ symbols per transmission burst, and each symbol is spread with a signature sequence of length $Q = 3$ chips. The channel for each user has a dispersion length of $W = 3$ chips.

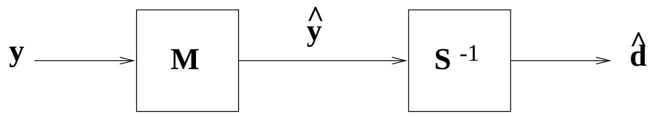

Figure 11.10: Structure of the receiver represented in Equation 11.23

Given the above transmission regime, the basic concept of joint detection is centred around processing the received composite signal vector, $\mathbf{y}$, in order to determine the transmitted data vector, $\mathbf{d}$. This concept is encapsulated in the following set of equations :

$$\hat{\mathbf{y}} = \mathbf{S}\hat{\mathbf{d}} = \mathbf{M}\mathbf{y}, \tag{11.23}$$

where $\mathbf{S}$ is a square matrix with dimensions $(KN \times KN)$ and the matrix $\mathbf{M}$ is a $[KN \times (NQ + W - 1)]$-matrix. These two matrices determine the type of joint detection algorithm, as it will become explicit during our further discourse. The schematic in Figure 11.10 shows the receiver structure represented by this equation.

A range of joint detection schemes designed for uplink communications were proposed by Jung, Blanz, Nasshan, Steil, Baier and Klein, such as the minimum mean-square error block linear equalizer (MMSE-BLE) [198, 209, 217, 218], the zero-forcing block decision feedback equalizer (ZF-BDFE) [209, 218] and the minimum mean-square error block decision feedback equalizer (MMSE-BDFE) [209, 218].

These joint-detection receivers were also combined with coherent receiver antenna diversity (CRAD) techniques [209,217,218,338] and turbo coding [339,340] for performance improvement. Joint detection receivers were proposed also for downlink scenarios by Nasshan, Steil, Klein and Jung [341,342]. CIR estimates were required for the joint detection receivers and CIR estimation algorithms were proposed by Steiner and Jung [343] for employment in conjunction with joint detection. Werner [344] extended the joint detection receiver by combining ZF-BLE and MMSE-BLE techniques with a multistage decision mechanism using soft inputs to a Viterbi decoder.

Having considered the family of JD receivers, which typically exhibit a high complexity, let us now highlight the state-of-the-art in the context of lower complexity interference cancellation schemes in the next section.

11.3.3 Interference cancellation

Interference cancellation (IC) schemes constitute another variant of multiuser detection and they can be broadly divided into three categories, parallel interference cancellation (PIC), successive interference cancellation (SIC) and the hybrids of both, as seen in Figure 11.4. Varanasi and Aazhang [345] proposed a multistage detector for an asynchronous system, where the outputs from a matched filter bank were fed into a detector that performed MAI cancellation using a multistage algorithm. At each stage in the detector, the data estimates $\hat{\mathbf{d}}^{(1)}, \ldots, \hat{\mathbf{d}}^{(K-1)}$ of all the other $(K-1)$ users from the previous stage were used for reconstructing an estimate of the MAI and this estimate was then subtracted from the interfered received signal representing the wanted bit. The computational complexity of this detector was linear with respect to the number of users, K. Figure 11.11 depicts the schematic of

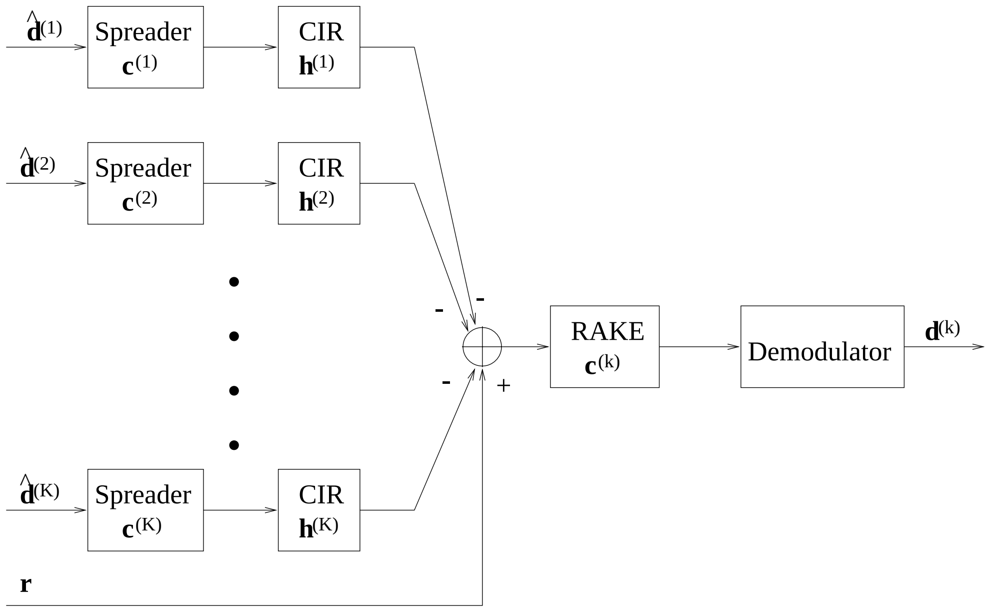

Figure 11.11: Schematic of a single cancellation stage for user k in the parallel interference cancellation (PIC) receiver for K users. The data estimates, $\hat{\mathbf{d}}^{(1)}, \ldots, \hat{\mathbf{d}}^{(K-1)}$ of the other $(K-1)$ users were obtained from the previous cancellation stage and the received signal of each user other than the k-th one is reconstructed and cancelled from the received signal, $\mathbf{r}$.

a single cancellation stage in the PIC receiver. Varanasi further modified the above parallel cancellation scheme, in order to create a parallel group detection scheme for Gaussian channels [346] and later developed it further for frequency-selective slow Rayleigh fading channels [347]. In this scheme, K users were divided into P groups and each group was demodulated in parallel using a group detector. Yoon, Kohno and Imai [348] then extended the applicability of the multistage interference cancellation detector to a multipath, slowly fading channel. At each cancellation stage, hard decisions generated by the previous cancellation stage were used for reconstructing the signal of each user and for cancelling its contribution from the composite signal. The effects of CIR estimation errors on the performance of the cancellation scheme were also considered. A multiuser receiver that integrated MAI rejection and channel decoding was investigated by Giallorenzi and Wilson [349]. The MAI was cancelled via a multistage cancellation scheme and soft-outputs were fed from the Viterbi channel decoder of each user to each stage for improving the performance.

The PIC receiver of Figure 11.11 [345] was also modified for employment in multi-carrier modulation [350] by Sanada and Nakagawa. Specifically, convolutional coding was used in order to obtain improved estimates of the data for each user at the initial stage and these estimates were then utilized for interference cancellation in the following stages. The employment of convolutional coding improved the performance by 1.5 dB. Latva-aho, Juntti and Heikkilä [351] enhanced the performance of the parallel interference cancellation re-

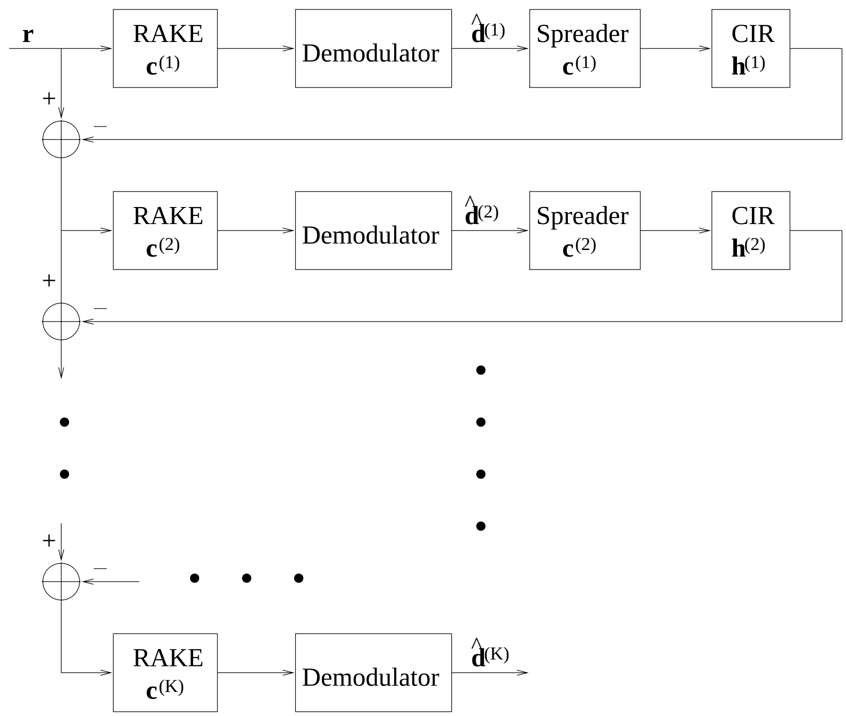

Figure 11.12: Schematic of the successive interference cancellation (SIC) receiver for K users. The users' signals have been ranked, where user 1's signal was received at the highest power, while user K's signal at the lowest power. In the order of ranking, the data estimates of each user are obtained and the received signal of each user is reconstructed and cancelled from the received composite signal, $\mathbf{r}$.

ceiver by feeding back CIR estimates to the signal reconstruction stage of the multistage receiver seen in FIgure 11.11 and proposed an algorithm for mitigating error propagation. Dahlhaus, Jarosch, Fleury and Heddergott [352] combined multistage detection with CIR estimation techniques utilizing the outputs of antenna arrays. The CIR estimates obtained were fed back into the multistage detector in order to refine the data estimates. An advanced parallel cancellation receiver was also proposed by Divsalar, Simon and Raphaeli [353]. At each cancellation stage, only partial cancellation was carried out by weighting the regenerated signals with a less than unity scaling factor. At each consecutive stage, the weights were increased based on the assumption that the estimates became increasingly accurate.

Following the above brief notes on PIC receivers, let us now consider the family of reduced-complexity SIC receivers classified in Figure 11.4. A simple SIC scheme was analyzed by Patel and Holtzman [354]. The received signals were ranked according to their correlation values, which were obtained by utilizing the correlations between the received signal and the spreading codes of the users. The transmitted information of the strongest user was estimated, enabling the transmitted signal to be reconstructed with the aid of the spreader as well as the CIR and subtracted from the received signal, as portrated in Figure 11.12. This was repeated for the next strongest user, where the reconstructed signal of this second user was cancelled from the composite signal remaining after the first cancellation. The interference cancellation was carried out successively for all the other users, until eventually only the signal of the weakest user remained. It was shown that the SIC receiver improved the BER and the system's user capacity over that of the conventional matched filter for the Gaussian, for narrowband Rayleigh and for dispersive Rayleigh channels. Multipath diversity was also exploited by combining the SIC receiver with the RAKE correlator [354]. Again, Figure 11.12 shows the schematic of the SIC receiver. Soong and Krzymien [355] extended the SIC receiver by using reference symbols in order to aid the CIR estimation. The performance of the receiver was investigated in flat and frequency-selective Rayleigh fading channels, as well as in multi-cell scenarios. A soft-decision based adaptive SIC scheme was proposed by Hui and Letaief [356], where soft decisions were used in the cancellation stage and if the decision statistic did not satisfy a certain threshold, no data estimation was carried out for that particular data bit, in order to reduce error propagation.

Hybrid SIC and PIC schemes were proposed by Oon, Li and Steele [357, 358], where SIC was first performed on the received signal, followed by a multistage PIC arrangement. This work was then extended to an adaptive hybrid scheme for flat Rayleigh fading channels [359]. In this scheme, successive cancellation was performed for a fraction of the users, while the remaining users' signals were processed via a parallel cancellation stage. Finally, multistage parallel cancellation was invoked. The number of serial and parallel cancellations performed was varied adaptively according to the BER estimates. Sawahashi, Miki, Andoh and Higuchi [360] proposed a pilot symbol-assisted multistage hybrid successive-parallel cancellation scheme. At each stage, data estimation was carried out successively for all the users, commencing with the user having the strongest signal and ending with the weakest signal. For each user, the interference inflicted by the other users was regenerated using the estimates of the current stage for the stronger users and the estimates of the previous stage for the weaker users. CIR estimates were obtained for each user by employing pilot symbols and a recursive estimation algorithm. Another hybrid successive and parallel interference cancellation receiver was proposed by Sun, Rasmussen, Sugimoto and Lim [361], where the users to be detected were split into a number of groups. Within each group, PIC was performed on the signals of these users belonging to the group. Between the separate groups, SIC was employed. This had the advantage of a reduced delay and improved performance compared to the SIC receiver. A further variant of the hybrid cancellation scheme was constituted by the combination of MMSE detectors with SIC receivers, as proposed by Cho and Lee [362]. Single-user MMSE detectors were used to obtain estimates of the data symbols, which were then fed back into the SIC stages. An adaptive interference cancellation scheme was investigated by Agashe and Woerner [363] for a multicellular scenario, where interference cancellation was performed for both in-cell interferers and out-of-cell interferers. It was shown that cancelling the estimated interference from users having weak signals actually degraded the performance, since the estimates were inaccurate. The adaptive scheme exercised interference cancellation in a discriminating manner, using only the data estimates of users having strong received signals. Therefore signal power estimation was needed and the threshold for signal cancellation was adapted accordingly. Following the above brief discourse on interference cancellation algorithms, let us now focus our attention on the tree-type detection techniques, which were also categorised in Figure 11.4.

11.3.4 Tree-search detection

Several tree-search detection [364–366] receivers have been proposed in the literature, in order to reduce the complexity of the original maximum likelihood detection scheme proposed by Verdú [317]. Specifically, Rasmussen, Lim and Aulin [364] investigated a tree-search detection algorithm, where a recursive, additive metric was developed in order to reduce the search complexity. Reduced tree-search algorithms, such as the well-known M-algorithms [367] and T-algorithms [367] were used by Wei, Rasmussen and Wyrwas [365] in order to reduce the complexity incurred by the optimum multiuser detector. According to the M-algorithm, at every node of the trellis search algorithm, only M surviving paths were retained, depending on certain criteria such as for example the highest-metric M number of paths. Alternatively, all the paths that were within a fixed threshold, T, compared to the highest metric were retained. At the decision node, the path having the highest metric was chosen as the most likely transmitted sequence. Maximal-ratio combining was also used in conjunction with the reduced tree-search algorithms and the combining detectors outperformed the "non-combining" detectors. The T-algorithm was combined with soft-input assisted Viterbi detectors for channel-coded CDMA multiuser detection in the work carried out by Nasiri-Kenari, Sylvester and Rushforth [366]. The recursive tree-search detector generated soft-outputs, which were fed into single-user Viterbi channel decoders, in order to generate the bit estimates.

The so-called multiuser projection based receivers were proposed by Schlegel, Roy, Alexander and Jiang [368] and by Alexander, Rasmussen and Schlegel [369]. These receivers reduced the MAI by projecting the received signal onto a space which was orthogonal to the unwanted MAI, where the wanted signal was separable from the MAI. Having reviewed the two most well-known tree-search type algorithms, we now concentrate on the family of intelligent adaptive detectors in the next section, which can be classified with the aid of Figure 11.4.

11.3.5 Adaptive multiuser detection

In all the multiuser receiver schemes discussed earlier, the required parameters - except for the transmitted data estimates - were assumed to be known at the receiver. In order to remove this constraint while reducing the complexity, adaptive receiver structures have been proposed [370]. An excellent summary of these adaptive receivers has been provided by Woodward and Vucetic [371]. Several adaptive algorithms have been introduced for approximating the performance of the MMSE receivers, such as the Least Mean Squares (LMS) [94] algorithm, the Recursive Least Squares (RLS) algorithm [94] and the Kalman filter [94]. Xie, Short and Rushforth [372] showed that the adaptive MMSE approach could be applied to multiuser receiver structures with a concomitant reduction in complexity. In the adaptive receivers employed for asynchronous transmission by Rapajic and Vucetic [370], training sequences were invoked, in order to obtain the estimates of the parameters required. Lim, Rasmussen and Sugimoto introduced a multiuser receiver for an asynchronous flat-fading channel based on the Kalman filter [373], which compared favourably with the finite impulse response MMSE detector. An adaptive decision feedback based joint detection scheme was investigated by Seite and Tardivel [374], where the least mean squares (LMS) algorithm was used to update the filter coefficients, in order to minimize the mean square error of the data estimates. New adaptive filter architectures for downlink DS-CDMA receivers were suggested by Spangenberg, Cruickshank, McLaughlin, Povey and Grant [40], where an adaptive algorithm was employed in order to estimate the CIR, and this estimated CIR was then used by a channel equalizer. The output of the channel equalizer was finally processed by a fixed multiuser detector in order to provide the data estimates of the desired user.

11.3.6 Blind detection

The novel class of multiuser detectors, referred to as "blind" detectors, does not require explicit knowledge of the spreading codes and CIRs of the multiuser interferers. These detectors do not require the transmission of training sequences or parameter estimates for their operation. Instead, the parameters are estimated "blindly" according to certain criteria, hence the term "blind" detection. RAKE-type blind receivers have been proposed, for example by Povey, Grant and Pringle [375] for fast-fading mobile channels, where decision-directed CIR estimators were used for estimating the multipath components and the output of the RAKE fingers was combined employing various signal combining methods. Liu and Li [376] also proposed a RAKE-type receiver for frequency-selective fading channels. In [376], a weighting factor was utilized for each RAKE finger, which was calculated based on maximizing the signal-to-interference-plus-noise ratio (SINR) at the output of each RAKE finger.

Xie, Rushforth, Short and Moon [377] proposed an approximate Maximum Likelihood Sequence Estimation (MLSE) solution known as the per-survivor processing (PSP) type algorithm, which combined a tree-search algorithm for data detection with the Recursive Least Squares (RLS) adaptive algorithm used for channel amplitude and phase estimation. The PSP algorithm was first proposed by Seshadri [378]; as well as by Raheli, Polydoros and Tzou [379, 380] for blind equalization in single-user ISI-contaminated channels. Xie, Rushforth, Short and Moon extended their own earlier work [377], in order to include the estimation of user-delays along with channel- and data-estimation [381].

Iltis and Mailaender [382] combined the PSP algorithm with the Kalman filter, in order to adaptively estimate the amplitudes and delays of the CDMA users. In other blind detection schemes, Mitra and Poor compared the application of neural networks and LMS filters for obtaining data estimates of the CDMA users [383]. In contrast to other multiuser detectors, which required the knowledge of the spreading codes of all the users, only the spreading code of the desired user was needed for this adaptive receiver [383]. An adaptive decorrelating detector was also developed by Mitra and Poor [384], which was used to determine the spreading code of a new user entering the system.

Blind equalization was combined with multiuser detection for slowly fading channels in the work published by Wang and Poor [385]. Only the spreading sequence of the desired user was needed and a zero-forcing as well as an MMSE detector were developed for data detection. As a further solution, a so-called sub-space approach to blind multiuser detection was also proposed by Wang and Poor [386], where only the spreading sequence and the delay of the desired user were known at the receiver. Based on this knowledge, a blind subspace tracking algorithm was developed for estimating the data of the desired user. Further blind adaptive algorithms were developed by Honig, Madhow and Verdú [387], Mandayam and Aazhang [388], as well as by Ulukus and Yates [389]. In [387], the applicability of two adaptive algorithms to the multiuser detection problem was investigated, namely that of the stochastic gradient algorithm and the least squares algorithm, while in [389] an adaptive detector that converged to the solution provided by the decorrelator was analyzed.

The employment of the Kalman filter for adaptive data, CIR and delay estimation was carried out by Lim and Rasmussen [390]. They demonstrated that the Kalman filter gave a good performance and exhibited a high grade of flexibility. However, the Kalman filter required reliable initial delay estimates in order to initialize the algorithm. Miguez and Castedo [391] modified the well-known constant modulus approach [392, 393] to blind equalization for ISI-contaminated channels in the context of multiuser interference suppression. Fukawa and Suzuki [394] proposed an orthogonalizing matched filtering detector, which consisted of a bank of despreading filters and a signal combiner. One of the despreading filters was matched to the desired spreading sequence, while the other despreading sequences were arbitrarily chosen such that the impulse responses of the filters were linearly independent of each other. The filter outputs were adaptively weighted in the complex domain under the constraint that the average output power of the combiner was minimized. In another design, an iterative scheme used to maximize the so-called log-likelihood function was the basis of the research by Fawer and Aazhang [395]. RAKE correlators were employed for exploiting the multipath diversity and the outputs of the correlators were fed to an iterative scheme for joint CIR estimation and data detection using the Gauss-Seidel [287] algorithm.

11.3.7 Hybrid and novel multiuser receivers

Several hybrid multiuser receiver structures have also been proposed recently [396–399]. Bar-Ness [396] advocated the hybrid multiuser detector that consisted of a decorrelator for detecting asynchronous users, followed by a data combiner maximising the Signal-to-noise Ratio (SNR), an adaptive canceller and another data combiner. The decorrelator matrix was adaptively determined.

A novel multiuser CDMA receiver based on genetic algorithms (GA) was considered by Yen *et al.* [397], where the transmitted symbols and the channel parameters of all the users were jointly estimated. The maximum likelihood receiver of synchronous CDMA systems exhibits a computational complexity that is exponentially increasing with the number of users, since at each signalling instant the corresponding data bit of all users has to be determined. Hence the employment of maximum likelihood detection invoking an exhaustive search is not a practical approach. GAs have been widely used for solving complex optimization problems in engineering, since they typically constitute an attractive compromise in performance versus complexity terms. Using the approach of [397] GAs can be invoked, in order to jointly estimate the users' channel parameters as well as the transmitted bit vector of all the users at the current signalling instant with the aid of a bank of matched filters at the receiver. It was shown in [397] that GA-based multi-user detectors can approach the single-user BER performance at a significantly lower complexity than that of the optimum ML multiuser detector without the employment of training sequences for channel estimation.

The essence of this GA-based technique [397] is that the search-space for the most likely data vector of all the users at a given signalling instant was limited to a certain population of vectors and the candidate vectors were updated at each iteration according to certain probabilistic genetic operations, known as *reproduction*, *crossover* or *mutation*. Commencing with a population of tentative decisions concerning the vector of all the users' received bits at the current signalling instant, the best n data vectors were selected as so-called "parent" vectors according to a certain "fitness" criterion - which can be also considered to be a cost-function - based on the likelihood function [397] in order to generate the so-called "offspring" for the next generation of data vector estimates. The aim is that the off-spring should exhibit a better "fitness" or cost-function contribution, than the "parents", since then the algorithm will converge. The offspring of data vector estimates were generated by employing a so-called uniform "crossover process", where the bits between two parent or candidate data vectors were exchanged according to a random cross-over mask and a certain exchange probability. Finally, the so-called "mutation" was performed, where the value of a bit in the data vector was flipped according to a certain mutation probability. In order to prevent the loss of "high-fitness" parent sequences during the process of evolution of the estimated user data vectors, the "highest-merit" estimated user data vector that was initially excluded from the pool of parent vectors in creating a new generation of candidate data vectors was then used to replace the "lowest-merit" offspring.

Neural network-type multi-user equalizers have also been proposed as CDMA receivers [400,401]. Specifically, Tanner and Cruickshank proposed a non-linear receiver that exploited neural-network structures and employed pattern recognition techniques for data detection [400]. This work [400] was extended to a reduced complexity neural network receiver for the downlink scenario [401]. The advantage of the neural-network based receivers is that they are capable of 'learning' the optimum partitioning rules in the signal constellation space, even, when the received interference-contaminated constellation points linearly non-separable. In this scenario linear receivers would exhibit a residual BER even in the absence of channel noise.

Other novel techniques employed for mitigating the multipath fading effects inflicted upon multiple users include **joint transmitter-receiver optimization** proposed by Jang, Vojčić and Pickholtz [398, 399]. In these schemes, transmitter precoding was carried out, such that the mean squared errors of the signals at all the receivers were minimized. This required the knowledge of the CIRs of all the users and the assumption was made that the channel fading was sufficiently slow, such that CIR prediction could be employed reliably by the transmitter.

Recently, there has been significant interest in **iterative detection** schemes, where channel coding was exploited in conjunction with multiuser detection, in order to obtain a high BER performance. The spreading of the data and the convolutional channel coding was viewed as a serially concatenated code structure, where the CDMA channel was viewed as the inner code and the single user convolutional codes constituted the outer codes. After processing the received signal in a bank of matched filters - often referred to as orthogonalizing whitening matched filter - the matched filter outputs were processed using a so-called **turbo-style iterative decoding (TEQ)** [402] process. In this process, a multiuser decoder was used to produce bit confidence measures, which were used as soft inputs of the single-user channel decoders. These single-user decoders then provided similar confidence metrics, which were fed back to the multiuser detector. This iterative process continued, until no further performance improvement was recorded.

Giallorenzi and Wilson [403] presented the maximum likelihood solution for the asynchronous CDMA channel, where the user data was encoded with the aid of convolutional codes. Near-single-user performance was achieved for the two-user case in conjunction with fixed length spreading codes. The decoder was implemented using the Viterbi channel decoding algorithm, where the number of states increased exponentially with the product of the number of users and the constraint length of the convolutional codes. Later, a suboptimal modification of this technique was proposed [349], where the MAI was cancelled via multistage cancellation and the soft outputs of the Viterbi algorithm were supplied to each stage of the multistage canceller for improving the performance. Following this, several iterative multiuser detection schemes employing channel-coded signals have been presented [404–409]. For example, Alexander, Astenstorfer, Schlegel and Reed [406, 408] proposed the multiuser maximum a-posteriori (MAP) detectors for the decoding of the inner CDMA channel code and invoked single-user MAP decoders for the outer convolutional code. A reduced complexity solution employing the M-algorithm [367] was also suggested, which resulted in a complexity that increased linearly – rather than exponentially, as in [403] – with the number of users [407]. Wang and Poor [409] employed a soft-output multiuser detector for the inner channel code, which combined soft interference cancellation and instantaneous linear MMSE filtering, in order to reduce the complexity. These iterative receiver structures showed considerable promise and near-single-user performance was achieved at high SNRs.

Figure 11.4 portrays the classification of most of the CDMA detectors that have been discussed previously. All the acronyms for the detectors have been defined in the text. Examples of the different classes of detectors are also included. Having considered the family of various CDMA detectors, let us now turn our attention to adaptive rate CDMA schemes.

11.4 Adaptive CDMA Schemes

Mobile radio signals are subject to propagation path loss as well as slow fading and fast fading. Due to the nature of the fading channel, transmission errors occur in bursts, when the channel exhibits deep fades due to shadowing, obstructing vehicles, etc. or when there is a sudden surge of multiple access interference (MAI) or inter-symbol interference (ISI). In mobile communications systems power control techniques are used to mitigate the effects of path loss and slow fading [10]. However, in order to counteract the problem of fast fading and co-channel interference, agile power control algorithms are required [410]. Another technique that can be used to overcome the problems due to the time-variant fluctuations of the channel is Burst-by-Burst (BbB) adaptive transmission [1, 49], where the information rate is varied according to the near-instantaneous quality of the channel, rather than according to user requirements. When the near-instantaneous channel quality is low, a lower information rate is supported, in order to reduce the number of errors. Conversely, when the near-instantaneous channel quality is high, a higher information rate is used, in order to increase the average throughput of the system. More explicitly, this method is similar to multi-rate transmission [39], except that in this case, the transmission rate is modified according to the near-instantaneous channel quality, instead of the service required by the mobile user. BbB-adaptive CDMA systems are also useful for employment in arbitrary propagation environments or in hand-over scenarios, such as those encountered, when a mobile user moves from an indoor to an outdoor environment or in a so-called 'birth-death' scenario, where the number of transmitting CDMA users changes frequently [40], thereby changing the interference dramatically. Various methods of multi-rate transmission have been proposed in the research literature. Next we will briefly discuss some of the current research on multi-rate transmission schemes, before focusing our attention on BbB-adaptive systems.

Ottosson and Svensson compared various multi-rate systems [39], including multiple spreading factor (SF) based, multi-code and multi-level modulation schemes. According to the multi-code philosophy, the SF is kept constant for all users, but multiple spreading codes transmitted simultaneously are assigned to users requiring higher bit rates. In this case - unless the spreading codes's perfect orthogonality is retained after transmission over the channel - the multiple codes of a particular user interfere with each other. This inevitebly reduces the system's performance.

Multiple data rates can also be supported by a variable SF scheme, where the chip rate is kept constant, but the data rates are varied, thereby effectively changing the SF of the spreading codes assigned to the users; at a fixed chip rate the lower the SF, the higher the supported data rate. Performance comparisons for both of these schemes have been carried out by Ottosson and Svensson [39], as well as by Ramakrishna and Holtzman [41], demonstrating that both schemes achieved a similar performance. Adachi, Ohno, Higashi, Dohi and Okumura proposed the employment of multi-code CDMA in conjunction with pilot symbol-assisted channel estimation, RAKE reception and antenna diversity for providing multi-rate capabilities [42, 43]. The employment of multi-level modulation schemes was also investigated by Ottosson and Svensson [39], where higher-rate users were assigned higher-order modulation modes, transmitting several bits per symbol. However, it was concluded that the performance experienced by users requiring higher rates was significantly worse, than that experienced by the lower-rate users. The use of M-ary orthogonal modulation in providing variable rate transmission was investigated by Schotten, Elders-Boll and Busboom [44]. According to this method, each user was assigned an orthogonal sequence set, where the number of sequences, M, in the set was dependent on the data rate required – the higher the rate required, the larger the sequence set. Each sequence in the set was mapped to a particular combination of $b = (\log_2 M)$ bits to be transmitted. The M-ary sequence was then spread with the aid of a spreading code of a constant SF before transmission. It was found [44] that the performance of the system depended not only on the MAI, but also on the Hamming distance between the sequences in the M-ary sequence set.

Saquib and Yates [45] investigated the employment of the decorrelating detector in conjunction with the multiple-SF scheme and proposed a modified decorrelating detector, which utilized soft decisions and maximal ratio combining, in order to detect the bits of the different-rate users. Multi-rate transmission schemes involving interference cancellation receivers have previously been investigated amongst others by Johansson and Svensson [46, 47], as well as by Juntti [48]. Typically, multiple users transmitting at different bit rates are supported in the same CDMA system invoking multiple codes or different spreading factors. SIC schemes and multi-stage cancellation schemes were used at the receiver for mitigating the MAI [46–48], where the bit rate of the users was dictated by the user requirements. The performance comparison of various multiuser detectors in the context of a multiple-SF transmission scheme was presented for example by Juntti [48], where the detectors compared were the decorrelator, the PIC receiver and the so-called group serial interference cancellation (GSIC) receiver. It was concluded that the GSIC and the decorrelator performed better than the PIC receiver, but all the interference cancellation schemes including the GSIC, exhibited an error floor at high SNRs due to error propagation.

The bit rate of each user can also be adapted according to the near-instantaneous channel quality, in order to mitigate the effects of channel quality fluctuations. Kim [49] analyzed the performance of two different methods of combating the near-instantaneous quality variations of the mobile channel. Specifically, Kim studied the adaptation of the transmitter power or the switching of the information rate, in order to suit the near-instantaneous channel conditions. Using a RAKE receiver [50], it was demonstrated that rate adaptation provided a higher average information rate, than power adaptation for a given average transmit power and a given BER [49]. Abeta, Sampei and Morinaga [51] conducted investigations into an adaptive packet transmission based CDMA scheme, where the transmission rate was modified by varying the channel code rate and the processing gain of the CDMA user, employing the carrier to interference plus noise ratio (CINR) as the switching metric. When the channel quality was favourable, the instantaneous bit rate was increased and conversely, the instantaneous bit rate was reduced when the channel quality dropped. In order to maintain a constant overall bit rate, when a high instantaneous bit rate was employed, the duration of the transmission burst was reduced. Conversely, when the instantaneous bit rate was low, the duration of the burst was extended. This resulted in a decrease in interference power, which translated to an increase in system capacity. Hashimoto, Sampei and Morinaga [52] extended this work also to demonstrate that the proposed system was capable of achieving a higher user capacity with a reduced hand-off margin and lower average transmitter power. In these schemes the conventional RAKE receiver [50] was used for the detection of the data symbols. A variable-rate CDMA scheme – where the transmission rate was modified by varying the channel code rate and, correspondingly, the M-ary modulation constellations – was investigated by Lau and Maric [53]. As the channel code rate was increased, the bit-rate was increased by increasing M correspondingly in the M-ary modulation scheme. Another adaptive system was proposed by Tateesh, Atungsiri and Kondoz [54], where the rates of the speech and channel codecs were varied adaptively [54]. In their adaptive system, the gross transmitted bit rate was kept constant, but the speech codec and channel codec rates were varied according to the channel quality. When the channel quality was low, a lower rate speech codec was used, resulting in increased redundancy and thus a more powerful channel code could be employed. This resulted in an overall coding gain, although the speech quality dropped with decreasing speech rate. A variable rate data transmission scheme was proposed by Okumura and Adachi [55], where the fluctuating transmission rate was mapped to discontinuous transmission, in order to reduce the interference inflicted upon the other users, when there was no transmission. The transmission rate was detected blindly at the receiver with the help of cyclic redundancy check decoding and RAKE receivers were employed for coherent reception, where pilot-symbol-assisted channel estimation was performed.

The information rate can also be varied in accordance with the channel quality, as it will be demonstrated shortly. However, in comparison to conventional power control techniques - which again, may disadvantage other users in an effort to maintain the quality of the links considered - the proposed technique does not disadvantage other users and increases the network capacity [56]. The instantaneous channel quality can be estimated at the receiver and the chosen information rate can then be communicated to the transmitter via explicit signalling in a so-called closed-loop controlled scheme. Conversely, in an open-loop scheme - provided that the downlink and uplink channels exhibit a similar quality - the information rate for the downlink transmission can be chosen according to the channel quality estimate related to the uplink and vice versa. The validity of the above channel reciprocity issues in TDD-CDMA systems have been investigated by Miya *et al.* [57], Kato *et al.* [58] and Jeong *et al.* [59].

In the next section two different methods of varying the information rate are considered, namely the Adaptive Quadrature Amplitude Modulated (AQAM) scheme and the Variable Spreading Factor (VSF) scheme. AQAM is an adaptive-rate technique, whereby the data modulation mode is chosen according to some criterion related to the channel quality. On

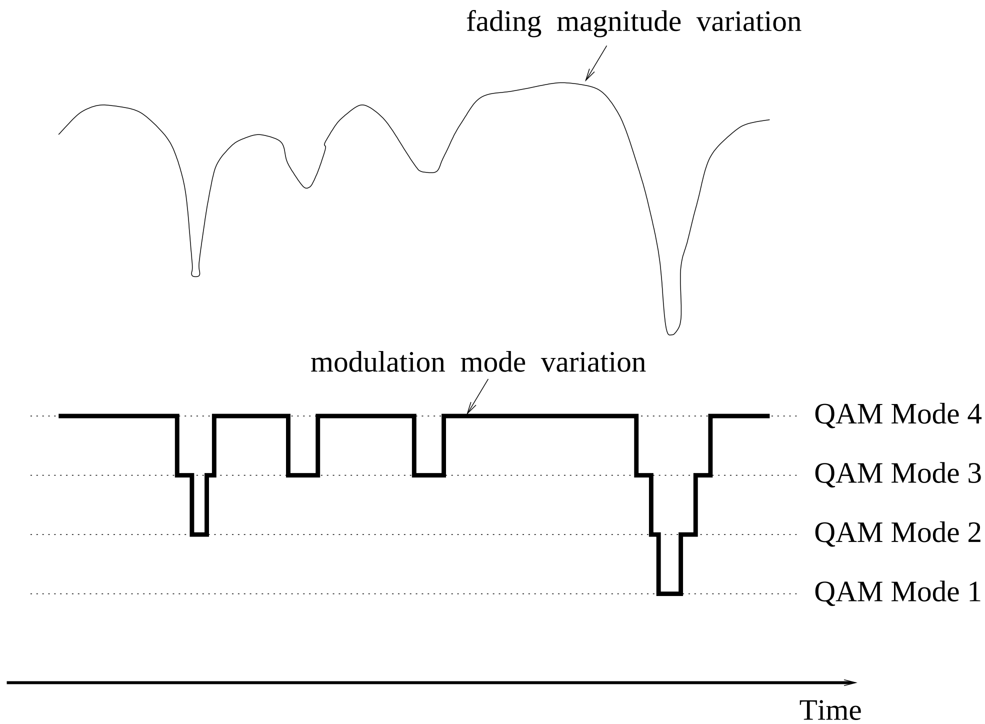

Figure 11.13: Basic concept of a four-mode AQAM transmission in a narrowband channel. The variation of the modulation mode follows the fading variation of the channel over time.

the other hand, in VSF transmission, the information rate is varied by adapting the spreading factor of the CDMA codes used, while keeping the chip rate constant. Further elaborations on these two methods will be given in subsequent sections.

11.5 Burst-by-burst AQAM/CDMA

11.5.1 Burst-by-burst AQAM/CDMA Philosophy

Burst-by-burst AQAM [50] is a technique that attempts to increase the average throughput of the system by switching between modulation modes depending on the instantaneous state or quality of the channel. When the channel quality is favourable, a modulation mode having a high number of constellation points is used to transmit as many bits per symbol as possible, in order to increase the throughput. Conversely, when the channel is hostile, the modulation mode is switched to using a low number of constellation points, in order to reduce the error probability and to maintain a certain adjustable target BER. Figure 11.13 shows the stylized quality variation of the fading channel and the switching of the modulation modes in a four-mode AQAM system, where both the BER and the throughput increase, when switching from Mode 1 to 4.

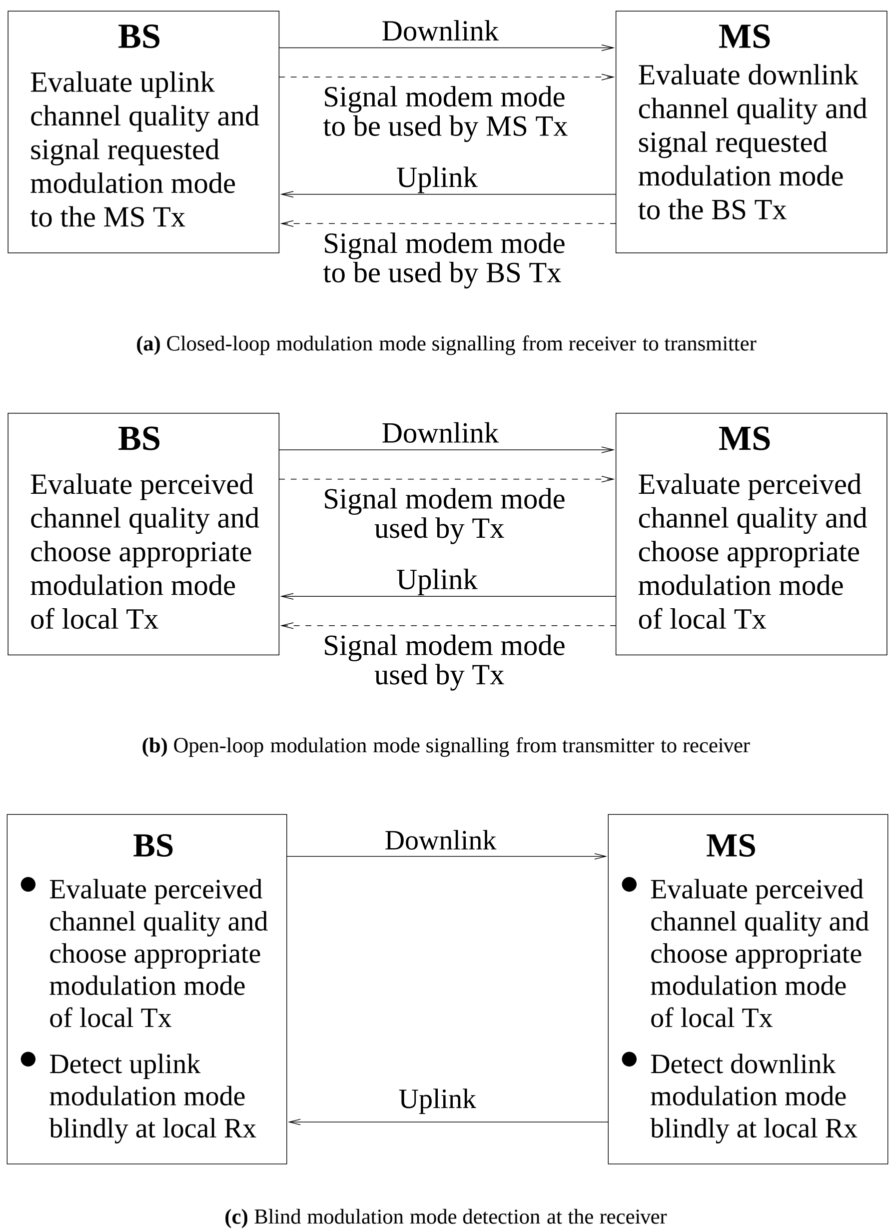

Figure 11.14: Three different methods of modulation mode signalling for the adaptive schemes, where BS represents the Base Station, MS denotes the Mobile Station, the transmitter is represented by Tx and the receiver is denoted by Rx.

In order to determine the best choice of modulation mode in terms of the required trade-off between the BER and the throughput, the near-instantaneous quality of the channel has to be estimated. The near-instantaneous channel quality can be estimated at the receiver and the chosen modulation mode is then communicated using explicit signalling to the transmitter in a closed-loop scheme. In other words, the receiver instructs the remote transmitter as to the choice of the transmitter's required modulation mode, in order to satisfy the receiver's prevalent BER and bits per symbol (BPS) throughput trade-off. This closed-loop scheme is depicted schematically in Figure 11.14(a). By contrast, in the open-loop scheme of Figure 11.14(b), the channel quality estimation can be carried out at the transmitter itself based on the co-located receiver's perception of the channel quality during the last received burst, provided that the uplink and downlink channel quality can be considered similar. Then the transmitter explicitly informs the remote receiver as to the modem mode used in the burst and modulation mode detection would then be performed on this basis at the receiver. This scheme performs most successfully in situations, where the channel fading varies slowly in comparison to the burst transmission rate. Channel quality estimation is inherently less accurate in a fast-fading channel and this lag in the quality estimation renders the choice of modulation mode less appropriate for the channel. Another approach to this issue would be for the receiver to detect the modulation mode used blindly [144, 411], as shown in Figure 11.14(c).

11.5.2 Channel Quality Metrics

As stated earlier, a metric corresponding to the near-instantaneous channel quality is required in order to adapt the AQAM modes. Some examples of these metrics include the carrier-to-interference (C/I) ratio of the channel [12], the SNR of the channel [1,50], the received signal strength indicator's (RSSI) output [121], the mean square error (MSE) at the output of the receiver's channel equalizer and the BER of the system [412]. The most accurate metric is the BER of the system, since this metric corresponds directly to the system's performance, irrespective of the actual source of the channel impairment. However, the BER is dependent on the AQAM mode employed, and cannot be estimated directly for most receivers. For a system that incorporates channel coding, such as turbo coding [128], the so-called log-likelihood ratios (LLR) – which indicate the ratio of the probabilities of the estimated bit taking its two possible values – at the input and output of the turbo decoder can also be employed as the adaptation metric. AQAM systems were first proposed for narrowband channels and the research in this field includes work published by Webb and Steele [1, 50], Sampei, Komaki and Morinaga [12] Goldsmith and Chua [19]; as well as Torrance *et al.* [13]. Webb *et al.* [1, 50] employed Star QAM [50] and the channel quality was determined by measuring the received signal strength and the near-instantaneous BER. Sampei *et al.* [12] switched the modulation modes by estimating the signal to co-channel interference ratio and the expected delay spread of the channel. This work has been extended to wideband channels by Wong *et al.* [15], where the received signal also suffers from ISI in addition to amplitude and phase distortions due to the fading channel. In wideband AQAM systems the channel SNR, the Carrier-to-Interference (C/I) ratio or RSSI metrics cannot be readily estimated or predicted, amongst other factors due to the multipath nature of the channel or as a result of the so-called 'birth-death' processes associated with the sudden appearance or disappearance of communicating users. Additionally, the above simple metrics do not provide accurate measures of

Switching criterion	**Modulation mode**
$\gamma_o(k) < t_1$	V_1
$t_1 \leq \gamma_o(k) < t_2$	V_2
.	.
.	.
.	.
$t_M \leq \gamma_o(k)$	V_M

Table 11.1: The general rules employed for switching the modulation modes in an AQAM system. The choice of modulation modes are denoted by V_m, where the total number of modulation modes is M and $m = 1, 2, \ldots, M$. The modulation modes with the lowest and highest number of constellation points are V_1 and V_M, respectively. The SINR at the output of the multiuser receiver is represented by $\gamma_o(k)$ and the values $(t_1, \cdots, t_M)$ represent the switching thresholds, where $t_1 < t_2 < \cdots < t_M$.

the system performance at the output of the receiver employed, since the effects of the CIR are not considered in the estimation of these metrics. Wong *et al.* [14] proposed a combined adaptive modulation and equalization scheme, where a Kalman-filtered DFE was used to mitigate the effects of ISI inflicted upon the signal. The CIR estimate was used to calculate the Signal to residual ISI plus Noise Ratio (SINR) at the output of the channel equalizer and this SINR value was used to switch the modulation modes. This was a more appropriate switching parameter than the received signal level, since it was a reliable indicator of the performance that could be achieved after equalization.

In AQAM/CDMA systems the SINR – $\gamma_o(k)$, for $k = 1, \ldots, K$ – at the output of the multiuser receiver is estimated for all the K users by employing the estimated CIRs and spreading sequences of all the users [224]. After $\gamma_o(k)$ is calculated, the modulation mode is chosen accordingly and communicated to the transmitter. Let us designate the choice of modulation modes by V_m, where the total number of modulation modes is M and $m = 1, 2, \ldots, M$. The modulation mode having the lowest number of modulation constellation points is V_1 and the one with the highest is V_M. The rules used to switch the modulation modes are tabulated in Table 11.1, where $\gamma_o(k)$ is the SINR of the k-th user at the output of the multiuser receiver and the values $(t_1, \cdots, t_M)$ represent the switching thresholds, where $t_1 < t_2 < \cdots < t_M$.

The schematic of the transmitter is shown in Figure 11.15. The data bits are mapped to their respective symbols according to the modulation mode chosen. The QAM symbols are then spread with the spreading code assigned to the user, modulated on to the carrier and transmitted. At the output of the multiuser receiver, the data estimates are demodulated according to the modulation mode used for transmission. Following the above brief protrayal of the associated AQAM/CDMA philosophy, let us now embark on the comparative performance study of various AQAM/CDMA schemes in the next section.

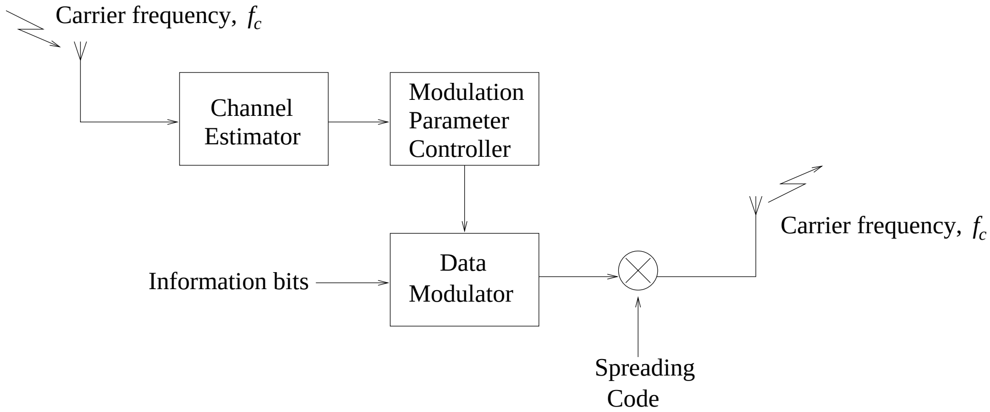

Figure 11.15: The schematic of the transmitter of an AQAM/CDMA system. In this transmitter, a TDD transmission scheme is assumed. Channel estimates are obtained by assuming close correlation between the uplink and downlink channels, which are used to measure the quality of the channel. This quality measure is passed to the modulation parameter controller, which selects the modulation mode according to the thresholds set. The data bits are mapped to QAM symbols according to the chosen modulation mode, spread with the spreading code and modulated on to the carrier.

Parameter	Value
Doppler frequency	80 Hz
Spreading ratio	64
Spreading sequence	Pseudo-random
Chip rate	2.167 MBaud
Burst structure	FMA1 Spread burst 1 [413]
Burst duration	577 μs

Table 11.2: Simulation parameters for the JD, SIC and PIC AQAM-CDMA systems

11.5.3 Comparison of JD, SIC and PIC CDMA receivers for AQAM transmission

In this section a comparative performance study of JD-CDMA, SIC-CDMA and PIC-CDMA systems is provided in the context of AQAM transmissions. The switching criterion employed was the SINR at the output of the respective multiuser receivers. For JD-CDMA, the SINR was estimated by employing the SINR expression given by Klein *et al.* [198], whilst for the SIC and PIC receivers the SINR expression presented by Patel and Holtzman [354] was adopted. For the SIC and PIC receivers, the RAKE receiver was used to provide the initial data estimates required for the subsequent cancellation stages. The rest of the simulation parameters are summarized in Table 11.2. In our investigations the COST 207 [414] channel models developed for the Global System of Mobile Communications known as GSM were employed. Although due to the orthogonal spreading sequences and due to the resultant high

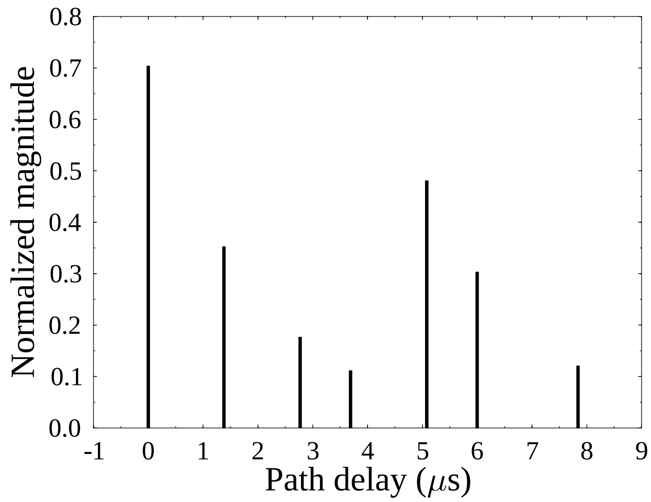

Figure 11.16: Normalized channel impulse response for the COST 207 protect [414] **seven path Bad Urban channel**.

chip-rate the number of resolvable multipath components is higher in our CDMA system than in GSM, nonetheless we used the COST 207 models, since these are widely used in the community. The CIR profile of the COST 207 [414] Bad Urban channel is shown in Figure 11.16.

Figure 11.17 compares the performance of the JD, the SIC receiver and the PIC receiver for a twin-mode, eight-user AQAM-CDMA system, switching between BPSK and 4-QAM. Here, the BER performance of all three receivers was kept as similar as possible and the performance comparison was evaluated on the basis of their BPS throughput. The BPS throughput of the JD was the highest, where approximately 1.9 BPS was achieved at $E_s/N_0 = 14$ dB. The PIC receiver outperformed the SIC receiver in BPS throughput terms, where the BPS throughput of the PIC receiver was approximately 1.55 BPS at $E_s/N_0 = 14$ dB compared to the approximately 1.02 BPS achieved by the SIC receiver. The two IC receivers suffered from MAI and they were unable to match the performance of the JD receiver. The PIC receiver outperformed the SIC receiver, since the received signal powers of all the users were similar on average and hence - as expected - the PIC receiver achieved a higher degree of interference cancellation than the SIC receiver.

The previous performance comparisons between the three multiuser receivers were then extended to triple-mode AQAM systems – switching between BPSK, 4-QAM and 16-QAM – that supported $K = 8$ users, as portrayed in Figure 11.18. For these systems, we can observe from the results that both the PIC and SIC receivers were unable to match the BPS performance of the JD receiver, when the multiuser receivers achieved similar BERs. This was because the increase in the number of users aggravated the MAI, thus degrading the

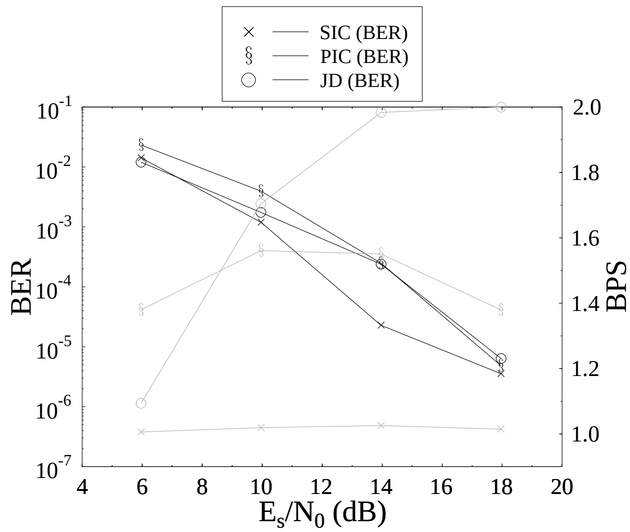

(a) BER comparisons are in bold, BPS comparisons are in grey.

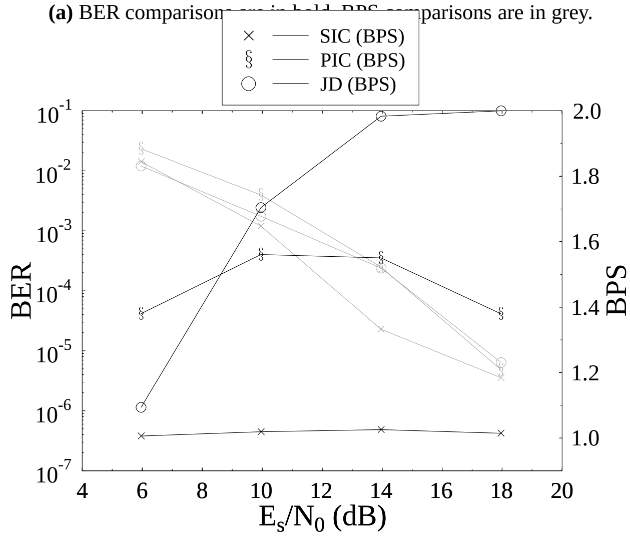

(b) BPS comparisons are in bold, BER comparisons are in grey.

Figure 11.17: Performance comparison of the JD, SIC and PIC CDMA receivers for **twin-mode** (BPSK, 4-QAM) AQAM transmission and $K = 8$ users over the **Bad Urban channel** of Figure 11.16. The rest of the simulation parameters are tabulated in Table 11.2.

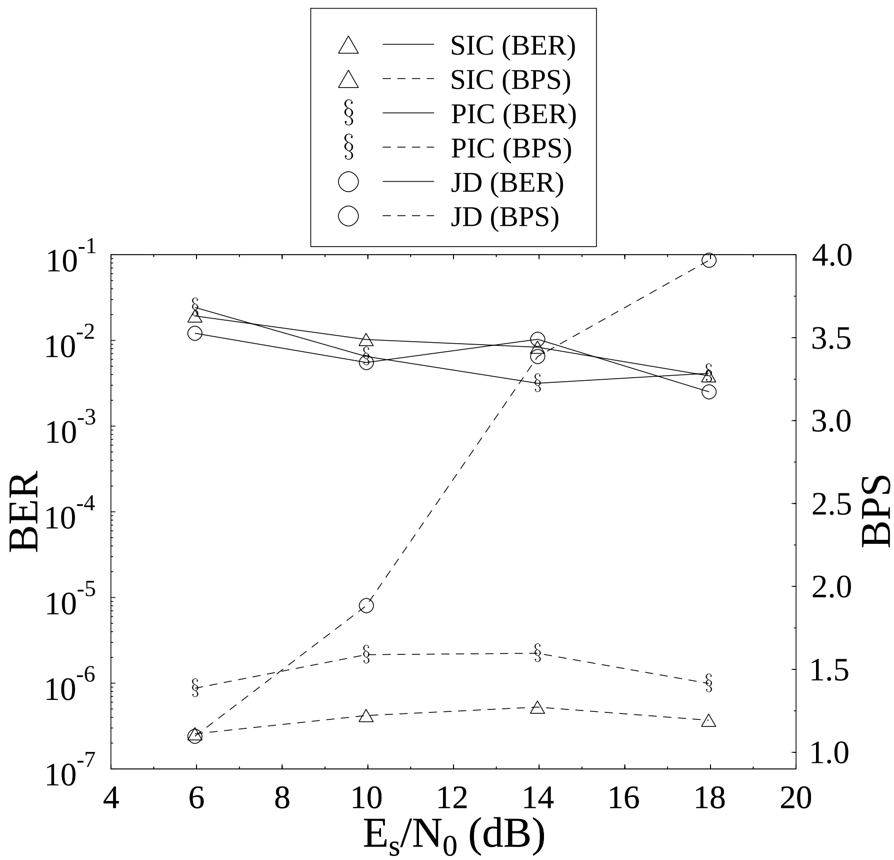

Figure 11.18: BER and BPS performance comparisons for **triple-mode** JD, SIC and PIC AQAM-CDMA schemes supporting $K = 8$ users over the **Bad Urban channel** of Figure 11.16. The modulation mode was chosen to be BPSK, 4-QAM or 16-QAM. The rest of the simulation parameters are tabulated in Table 11.2.

Switching criterion	Spreading code
$\gamma_o(k) < t_1$	$\mathbf{c}_1^{(k)},\ Q_h$
$t_1 \leq \gamma_o(k) < t_2$	$\mathbf{c}_2^{(k)},\ 2^{-1}Q_h$
.	.
.	.
.	.
$t_M \leq \gamma_o(k)$	$\mathbf{c}_M^{(k)},\ 2^{-(M-1)}Q_h$

Table 11.3: The general switching rules for a VSF/CDMA system, where $\gamma_o(k)$ is the SINR of the k-th user at the output of the multiuser receiver. The values of $t_1, \cdots, t_M$ represent the switching thresholds for the different modulation modes, where $t_1 < t_2 < \cdots < t_M$.

ability of the RAKE receivers to provide reliable data estimates for interference cancellation. Here again, the PIC receiver outperformed the SIC receiver in BPS throughput terms.

Let us now provide performance comparisons for the JD, SIC and PIC receivers in the context of VSF-CDMA schemes, rather than AQAM-CDMA.

11.5.4 VSF-CDMA

Multi-rate transmission systems using spreading sequences having different processing gains have been proposed in the literature amongst others by Adachi, Sawahashi and Okawa [415]; Ottosson and Svensson [39]; Ramakrishna and Holtzman [41]; Saquib and Yates [45]; as well as by Johansson and Svensson [46]. In the FRAMES FMA2 Wideband CDMA proposal for UMTS [416], different bit rates are accommodated by supporting variable spreading factor (VSF) [415] and multi-code based operation. In this section, we discuss the employment of VSF codes in adaptive-rate CDMA systems, where the chip rate of the CDMA users is kept constant throughout the transmission, while the bit rate is varied by using spreading codes exhibiting different spreading factors over the course of transmission. For example, by keeping the chip rate constant, the number of bits transmitted in the same period of time upon using a spreading code of length $Q = 16$ is twice the number of bits transmitted upon using a spreading code of length $Q = 32$.

In the VSF-based scheme the rate adaptation is dependent on the channel quality. Generally, when the channel quality is favourable, a code with a low spreading factor is used, in order to increase the throughput. Conversely, when the channel is hostile, a code with a high spreading factor is employed, in order to minimize the number of errors inflicted and to maintain a given target BER performance. Each user in the VSF-CDMA system is assigned M number of legitimate spreading codes having different lengths, $Q_1, Q_2, \ldots, Q_M$. Analogously to the AQAM/CDMA system discussed in Section 11.5, the SINR at the output of the multiuser receiver is estimated and used as the metric for choosing the spreading code to be used for transmission. Generally, when the channel quality is favourable, a code with a low spreading factor will be used, in order to increase the throughput. Conversely, when the channel is hostile, a code with a high spreading factor will be used, in order to minimize the number of errors inflicted. In order to have a system that can accommodate a large number of spreading codes having different SFs, the simplest choice of spreading codes would

Parameter	Value
Doppler frequency	80 Hz
Modulation mode	4-QAM
Spreading sequence	Pseudo-random
Chip rate	2.167 MBaud
Burst structure	FMA1 Spread burst 1 [413]
Burst duration	577 μs

Table 11.4: Simulation parameters for the JD, SIC and PIC VSF-CDMA systems

be those having SFs of $Q = 2^r$, where $r = 1, 2, 3, \cdots$. Let us denote the set of spreading codes assigned to the k-th user by $\{\mathbf{c}_1^{(k)}, \mathbf{c}_2^{(k)}, \cdots, \mathbf{c}_M^{(k)}\}$, where $\mathbf{c}_1^{(k)}$ is the spreading code having the highest spreading factor and the code $\mathbf{c}_M^{(k)}$ has the lowest spreading factor. If the highest spreading factor is denoted by Q_h, then the rules used to choose the spreading code are tabulated in Table 11.3.

11.5.5 Comparison of JD, SIC and PIC CDMA receivers for VSF transmission

In this section, the above JD, PIC and SIC receivers are compared in the context of adaptive VSF/CDMA schemes. The spreading factor used was varied adaptively, opting for $Q_1 = 64$, $Q_2 = 32$ or $Q_3 = 16$, while the rest of the simulation parameters employed are summarized in Table 11.4.

Figure 11.19 portrays the associated BER and throughput comparisons for the adaptive VSF PIC-, SIC- and JD-CDMA schemes using 4-QAM. The minimum and maximum throughput values were approximately 68 kbits/s and 271 kbits/s, respectively, spanning a bit rate range of a factor of four according to $Q_1/Q_3 = 4$. The throughput performance values were normalized to the minimum throughput of 68 kbits/s, thus giving minimum and maximum normalized throughput values of 1 and 4, respectively. We compared the normalized throughput of the JD-CDMA system to that of the PIC and SIC based systems, under the condition of similar BER performances. At low E_s/N_0 values the PIC and SIC receivers outperformed the JD receiver in throughput terms, because the MAI was relatively low in a two-user scenario and the additive noise was the main impairment at low E_s/N_0 values. However, as E_s/N_0 increased, the JD gradually outperformed the two interference cancellation based receivers in both BER and BPS throughput performance terms, achieving a normalized throughput of 3.5 compared to 2.7 and 2 for the PIC and SIC receivers, respectively, at $E_s/N_0 = 16$ dB.

The above triple-mode VSF schemes using 4-QAM were then extended to systems supporting $K = 8$ users. From the results presented in Figure 11.20, it can be seen that the JD consistently outperformed the PIC and SIC receivers in both BER and throughput performance terms. The VSF/IC-CDMA systems were unable to accommodate the variability in the channel conditions and hence their normalized throughput performance remained in the range of 1 to 1.5, compared to the JD, which was capable of achieving a normalized throughput of 2.8 at $E_s/N_0 = 14$ dB.

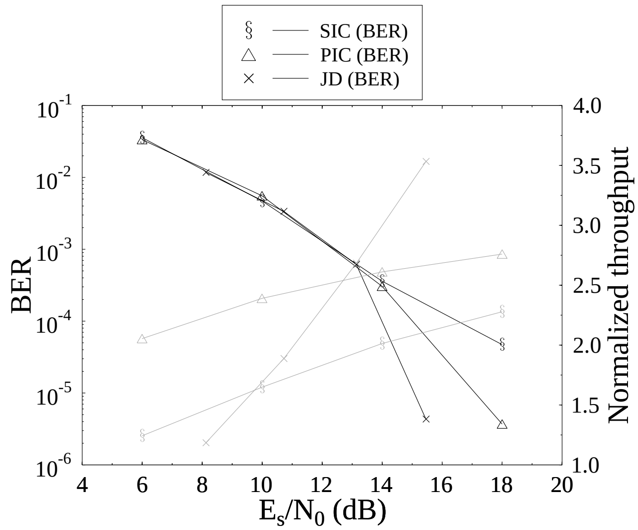

(a) BER comparisons are in bold, throughput comparisons are in grey.

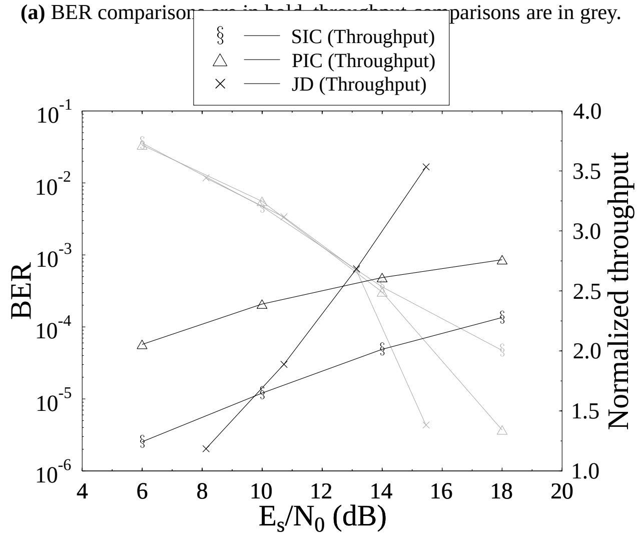

(b) Throughput comparisons are in bold, BER comparisons are in grey.

Figure 11.19: BER and throughput performance comparisons for triple-mode JD, SIC and PIC VSF-CDMA schemes supporting ***K*=2** users over the Bad Urban channel of Figure 11.16. The spreading factor was adaptively varied using $Q_1 = 64$, $Q_2 = 32$ or $Q_3 = 16$; and 4-QAM was used as the data modulation mode. The rest of the simulation parameters are tabulated in Table 11.4.

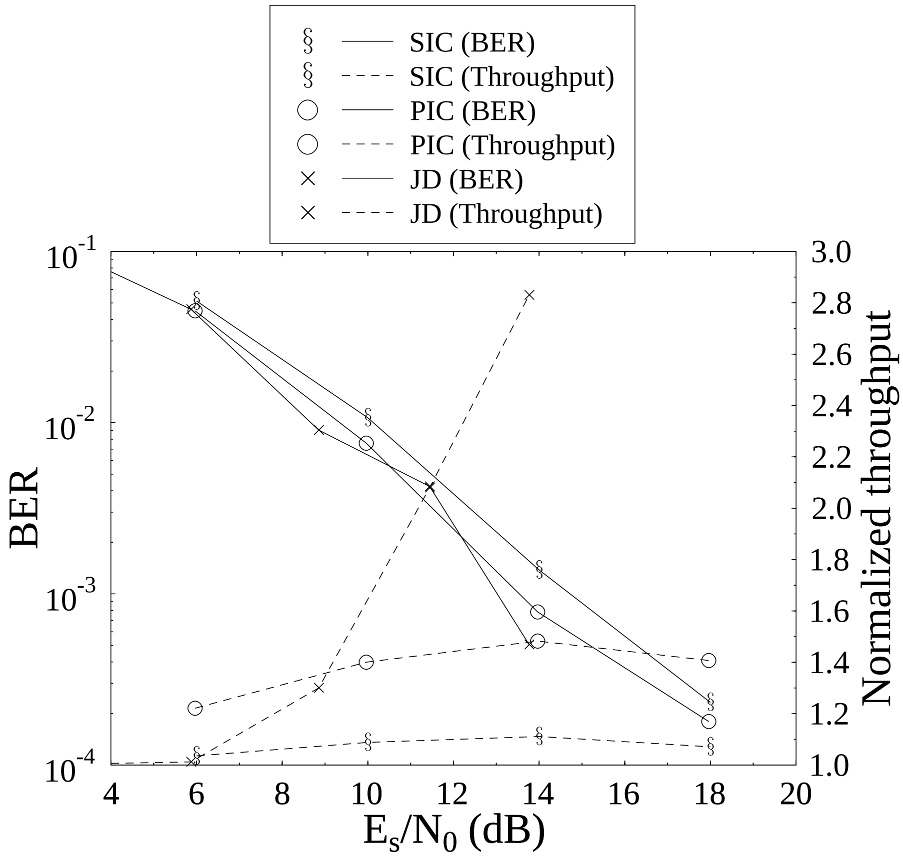

Figure 11.20: BER and throughput performance comparisons for triple-mode JD, SIC and PIC VSF-CDMA schemes supporting ***K*=8** users over the Bad Urban channel of Figure 11.16. The modulation mode was chosen to be 4-QAM. The rest of the simulation parameters are tabulated in Table 11.4.

	JD		**SIC**		**PIC**	
E_s/N_0	BPS	Cmplx	BPS	Cmplx	BPS	Cmplx
10	1.7	2641	1.02	1869	1.55	4605
14	1.98	2641	1.03	1869	1.38	4605

Table 11.5: Performance summary of the eight-user, **twin-mode AQAM-CDMA** results for the JD, SIC and PIC receivers, using a spreading factor of $Q = 64$ and transmitting over the seven-path Bad Urban channel of Figure 11.16. The E_s/N_0 values in the table are the values at which the AQAM-CDMA systems achieved the target BER of 1% or less. The complexity (Cmplx) values are in terms of the number of additions plus multiplications required per detected data symbol.

	JD		SIC		PIC	
E_s/N_0	BPS	Cmplx	BPS	Cmplx	BPS	Cmplx
10	1.88	2641	1.02	1869	1.99	4605
14	3.39	2641	1.03	1869	2	4605

Table 11.6: Performance summary of the eight-user, **triple-mode AQAM-CDMA** results for the JD, SIC and PIC receivers, using a spreading factor of $Q = 64$ and transmitting over the seven-path Bad Urban channel of Figure 11.16. The E_s/N_0 values in the table are the values at which the AQAM systems achieved the target BER of 1% or less. The complexity (Cmplx) values are in terms of the number of additions plus multiplications operations required per detected data symbol.

	JD		SIC		PIC	
E_s/N_0	Tp.	Cmplx	Tp.	Cmplx	Tp.	Cmplx
10	2.07	18298	1.08	1869	1.4	4605
14	2.83	18298	1.11	1869	1.48	4605

Table 11.7: Performance summary of **triple-mode VSF-CDMA** results for the JD, SIC and PIC receivers, where 4-QAM was employed as the modulation mode and transmission was conducted over the Bad Urban channel of Figure 11.16. The number of users in the system was $K = 8$. The E_s/N_0 in the table are the values at which the VSF systems achieved the target BER of 1% or less. The notation "Tp." denotes the throughput values normalized to the throughput of the fixed-rate scheme employing $Q = 64$ and 4-QAM. The complexity (Cmplx) values indicated are valid for the modem mode that incurred the highest complexity for each receiver.

11.6 Review and Discussion

The recent history of smart CDMA MUDs has been reviewed and the most promising schemes have been comparatively studied, in order to assist in the design of third- and fourth-generation receivers. All future transceivers are likely to become BbB-adaptive, in order to be able to accommodate the associated channel quality fluctuations without disadvantageously affecting the system's capacity. Hence the methods reviewed in this chapter are advantageous, since they often assist in avoiding powering up, which may inflict increased levels of co-channel interference and power consumption. Furthermore, the techniques characterized in this chapter support an increased throughput within a given bandwidth and will contribute towards reducing the constantly increasing demand for more bandwidth.

Both SIC and PIC receivers were investigated in the context of AQAM/CDMA schemes, which were outperformed by the JD based twin-mode AQAM/CDMA schemes for a spreading factor of $Q = 64$ and $K = 8$ users. Both IC receivers were unable to provide good performances in the triple-mode AQAM/CDMA arrangement, since the BER curves exhibited error floors. In the VSF/CDMA systems the employment of variable spreading factors of $Q = 32$ and $Q = 16$ enabled the PIC and SIC receivers to provide a reasonable BER and throughput performance, which was nonetheless inferior to that of the JD. When the number of users in the system was increased, the PIC and SIC receivers were unable to exploit the variability in channel conditions in order to provide a higher information throughput, as opposed to the JD scheme, which showed performance gains in both the adaptive-rate AQAM and VSF CDMA schemes. However, the complexity of the IC receivers increased only linearly with the number of CDMA users, K, compared to the joint detector, which exhibited a complexity proportional to $O(K^3)$. Tables 11.5, 11.6 and 11.7 summarize our performance comparisons for all three multiuser detectors in terms of E_s/N_0 required to achieve the target BER of 1% or less, the normalized throughput performance and the associated complexity in terms of the number of operations required per detected symbol. Both the third and future fourth generation standard work may benefit from this study. In conjunction with adaptive beam-steering [56] the order of the receiver performance may change.

Bibliography

[1] W. Webb and R. Steele, “Variable rate QAM for mobile radio,” *IEEE Transactions on Communications*, vol. 43, pp. 2223–2230, July 1995.

[2] L. Hanzo, “Bandwidth-efficient wireless multimedia communications,” *Proceedings of the IEEE*, vol. 86, pp. 1342–1382, July 1998.

[3] S. Nanda, K. Balachandran, and S. Kumar, “Adaptation techniques in wireless packet data services,” *IEEE Communications Magazine*, vol. 38, pp. 54–64, January 2000.

[4] L. Hanzo, W. Webb, and T. Keller, *Single- and Multi-carrier Quadrature Amplitude Modulation*. New York, USA: IEEE Press-John Wiley, April 2000.

[5] L. Hanzo, F. Somerville, and J. Woodard, “Voice compression and communications: Principles and applications for fixed and wireless channels.” 2001 (For detailed contents, please refer to http://www-mobile.ecs.soton.ac.uk.).

[6] L. Hanzo, P. Cherriman, and J. Streit, “Wireless video communications: From second to third generation systems, WLANs and beyond.” IEEE Press, 2001. (For detailed contents please refer to http://www-mobile.ecs.soton.ac.uk.).

[7] S. M. Alamouti, “A simple transmit diversity technique for wireless communications,” *IEEE Journal on Selected Areas in Communications*, vol. 16, pp. 1451–1458, October 1998.

[8] T. Liew and L. Hanzo, “Space-time block coded adaptive modulation aided ofdm,” in *Proceeding of GLOBECOM’2001*, (San Antonio, USA), IEEE, 26-29 November 2001.

[9] J. K. Cavers, “Variable rate transmission for rayleigh fading channels,” *IEEE Transactions on Communications Technology*, vol. COM-20, pp. 15–22, February 1972.

[10] R. Steele and L. Hanzo, eds., *Mobile Radio Communications*. New York, USA: IEEE Press - John Wiley & Sons, 2nd ed., 1999.

[11] A. Duel-Hallen, S. Hu, and H. Hallen, “Long range prediction of fading signals,” *IEEE Signal Processing Magazine*, vol. 17, pp. 62–75, May 2000.

[12] S. Sampei, S. Komaki, and N. Morinaga, “Adaptive modulation/TDMA scheme for large capacity personal multi-media communication systems,” *IEICE Transactions on Communications (Japan)*, vol. E77-B, pp. 1096–1103, September 1994.

[13] J. Torrance and L. Hanzo, “Upper bound performance of adaptive modulation in a slow Rayleigh fading channel,” *Electronics Letters*, vol. 32, pp. 718–719, 11 April 1996.

[14] C. Wong and L. Hanzo, “Upper-bound of a wideband burst-by-burst adaptive modem,” in *Proceedings of VTC’99 (Spring)*, (Houston, TX, USA), pp. 1851–1855, IEEE, 16–20 May 1999.

[15] C. Wong and L. Hanzo, “Upper-bound performance of a wideband burst-by-burst adaptive modem,” *IEEE Transactions on Communications*, vol. 48, pp. 367–369, March 2000.

[16] J. Torrance and L. Hanzo, “Optimisation of switching levels for adaptive modulation in a slow Rayleigh fading channel,” *Electronics Letters*, vol. 32, pp. 1167–1169, 20 June 1996.

[17] H. Matsuoka, S. Sampei, N. Morinaga, and Y. Kamio, "Adaptive modulation system with variable coding rate concatenated code for high quality multi-media communications systems," in *Proceedings of IEEE VTC'96*, vol. 1, (Atlanta, GA, USA), pp. 487–491, IEEE, 28 April–1 May 1996.

[18] A. J. Goldsmith and S. G. Chua, "Adaptive coded modulation for fading channels," in *Proceedings of IEEE International Conference on Communications*, vol. 3, (Montreal, Canada), pp. 1488–1492, 8–12 June 1997.

[19] A. Goldsmith and S. Chua, "Variable-rate variable-power MQAM for fading channels," *IEEE Transactions on Communications*, vol. 45, pp. 1218–1230, October 1997.

[20] S. Otsuki, S. Sampei, and N. Morinaga, "Square QAM adaptive modulation/TDMA/TDD systems using modulation level estimation with Walsh function," *Electronics Letters*, vol. 31, pp. 169–171, February 1995.

[21] J. Torrance and L. Hanzo, "Demodulation level selection in adaptive modulation," *Electronics Letters*, vol. 32, pp. 1751–1752, 12 September 1996.

[22] S. Sampei, N. Morinaga, and Y. Kamio, "Adaptive modulation/TDMA with a BDDFE for 2 mbit/s multi-media wireless communication systems," in *Proceedings of IEEE Vehicular Technology Conference (VTC'95)*, vol. 1, (Chicago, USA), pp. 311–315, IEEE, 15–28 July 1995.

[23] J. Torrance and L. Hanzo, "Latency considerations for adaptive modulation in a slow Rayleigh fading channel," in *Proceedings of IEEE VTC'97*, vol. 2, (Phoenix, AZ, USA), pp. 1204–1209, IEEE, 4–7 May 1997.

[24] J. Torrance and L. Hanzo, "Statistical multiplexing for mitigating latency in adaptive modems," in *Proceedings of IEEE International Symposium on Personal, Indoor and Mobile Radio Communications, PIMRC'97*, (Marina Congress Centre, Helsinki, Finland), pp. 938–942, IEEE, 1–4 September 1997.

[25] T. Ue, S. Sampei, and N. Morinaga, "Symbol rate controlled adaptive modulation/TDMA/TDD for wireless personal communication systems," *IEICE Transactions on Communications*, vol. E78-B, pp. 1117–1124, August 1995.

[26] D. Pearce, A. Burr, and T. Tozer, "Comparison of counter-measures against slow Rayleigh fading for TDMA systems," in *IEE Colloquium on Advanced TDMA Techniques and Applications*, (London, UK), pp. 9/1–9/6, IEE, 28 October 1996. digest 1996/234.

[27] V. Lau and M. Macleod, "Variable rate adaptive trellis coded QAM for high bandwidth efficiency applications in rayleigh fading channels," in *Proceedings of IEEE Vehicular Technology Conference (VTC'98)*, (Ottawa, Canada), pp. 348–352, IEEE, 18–21 May 1998.

[28] T. Suzuki, S. Sampei, and N. Morinaga, "Space and path diversity combining technique for 10 Mbits/s adaptive modulation/TDMA in wireless communications systems," in *Proceedings of IEEE VTC'96*, (Atlanta, GA, USA), pp. 1003–1007, IEEE, 28 April–1 May 1996.

[29] K. Arimochi, S. Sampei, and N. Morinaga, "Adaptive modulation system with discrete power control and predistortion-type non-linear compensation for high spectral efficient and high power efficient wireless communication systems," in *Proceedings of the IEEE International Symposium on Personal, Indoor and Mobile Radio Communications (PIMRC)*, (Helsinki, Finland), pp. 472–477, 1–4 September 1997.

[30] T. Ikeda, S. Sampei, and N. Morinaga, "TDMA-based adaptive modulation with dynamic channel assignment (AMDCA) for high capacity multi-media microcellular systems," in *Proceedings of IEEE Vehicular Technology Conference*, (Phoenix, USA), pp. 1479–1483, May 1997.

[31] T. Ue, S. Sampei, and N. Morinaga, "Adaptive modulation packet radio communication system using NP-CSMA/TDD scheme," in *Proceedings of IEEE VTC'96*, (Atlanta, GA, USA), pp. 416–421, IEEE, 28 April–1 May 1996.

[32] M. Naijoh, S. Sampei, N. Morinaga, and Y. Kamio, "ARQ schemes with adaptive modulation/TDMA/TDD systems for wireless multimedia communication systems," in *Proceedings of the IEEE International Symposium on Personal, Indoor and Mobile Radio Communications (PIMRC)*, (Helsinki, Finland), pp. 709–713, 1–4 September 1997.

[33] S. Sampei, T. Ue, N. Morinaga, and K. Hamaguchi, "Laboratory experimental results of an adaptive modulation TDMA/TDD for wireless multimedia communication systems," in *Proceedings of IEEE International Symposium on Personal, Indoor and Mobile Radio Communications, PIMRC'97*, (Marina Congress Centre, Helsinki, Finland), pp. 467–471, IEEE, 1–4 September 1997.

[34] J. Torrance and L. Hanzo, "Latency and networking aspects of adaptive modems over slow indoors rayleigh fading channels," *IEEE Transactions on Vehicular Technology*, vol. 48, no. 4, pp. 1237–1251, 1998.

[35] J. Torrance, L. Hanzo, and T. Keller, "Interference aspects of adaptive modems over slow Rayleigh fading channels," *IEEE Transactions on Vehicular Technology*, vol. 48, pp. 1527–1545, September 1999.

[36] I. Kalet, "The multitone channel," *IEEE Transactions on Communications*, vol. 37, pp. 119–124, February 1989.

[37] A. Czylwik, "Adaptive OFDM for wideband radio channels," in *Proceeding of IEEE Global Telecommunications Conference, Globecom 96*, (London, UK), pp. 713–718, IEEE, 18–22 November 1996.

[38] P. Chow, J. Cioffi, and J. Bingham, "A practical discrete multitone transceiver loading algorithm for data transmission over spectrally shaped channels," *IEEE Transactions on Communications*, vol. 48, pp. 772–775, 1995.

[39] T. Ottosson and A. Svensson, "On schemes for multirate support in DS-CDMA systems," *Wireless Personal Communications (Kluwer)*, vol. 6, pp. 265–287, March 1998.

[40] S. Spangenberg, D. Cruickshank, S. McLaughlin, G. Povey, and P. Grant, "Advanced multiuser detection techniques for downlink CDMA, version 2.0," tech. rep., Virtual Centre of Excellence in Mobile and Personal Communications Ltd (Mobile VCE), July 1999.

[41] S. Ramakrishna and J. Holtzman, "A comparison between single code and multiple code transmission schemes in a CDMA system," in *Proceedings of IEEE Vehicular Technology Conference (VTC'98)*, (Ottawa, Canada), pp. 791–795, IEEE, 18–21 May 1998.

[42] F. Adachi, K. Ohno, A. Higashi, T. Dohi, and Y. Okumura, "Coherent multicode DS-CDMA mobile Radio Access," *IEICE Transactions on Communications*, vol. E79-B, pp. 1316–1324, September 1996.

[43] T. Dohi, Y. Okumura, A. Higashi, K. Ohno, and F. Adachi, "Experiments on coherent multicode DS-CDMA," *IEICE Transactions on Communications*, vol. E79-B, pp. 1326–1332, September 1996.

[44] H. Schotten, H. Elders-Boll, and A. Busboom, "Adaptive multi-rate multi-code CDMA systems," in *Proceedings of the IEEE Vehicular Technology Conference (VTC)*, (Ottawa, Canada), pp. 782–785, 18–21 May 1998.

[45] M. Saquib and R. Yates, "Decorrelating detectors for a dual rate synchronous DS/CDMAchannel," *Wireless Personal Communications (Kluwer)*, vol. 9, pp. 197–216, May 1999.

[46] A.-L. Johansson and A. Svensson, "Successive interference cancellation schemes in multi-rateDS/CDMA systems," in *Wireless Information Networks (Baltzer)*, pp. 265–279, 1996.

[47] A. Johansson and A. Svensson, "Multistage interference cancellation in multirate DS/CDMA on a mobile radio channel," in *Proceedings of the IEEE Vehicular Technology Conference (VTC)*, (Atlanta, GA, USA), pp. 666–670, 28 April–1 May 1996.

[48] M. Juntti, "Multiuser detector performance comparisons inmultirate CDMA systems," in *Proceedings of the IEEE Vehicular Technology Conference (VTC)*, (Ottawa, Canada), pp. 36–40, 18–21 May 1998.

[49] S. Kim, "Adaptive rate and power DS/CDMA communications in fading channels," *IEEE Communications Letters*, vol. 3, pp. 85–87, April 1999.

[50] L. Hanzo, W. Webb, and T. Keller, *Single- and Multi-Carrier Quadrature Amplitude Modulation: Principles and Applications for Personal Communications, WLANs and Broadcasting*. IEEE Press, 2000.

[51] S. Abeta, S. Sampei, and N. Morinaga, "Channel activation with adaptive coding rate and processing gain control for cellular DS/CDMA systems," in *Proceedings of IEEE VTC'96*, (Atlanta, GA, USA), pp. 1115–1119, IEEE, 28 April–1 May 1996.

[52] M. Hashimoto, S. Sampei, and N. Morinaga, "Forward and reverse link capacity enhancement of DS/CDMA cellular system using channel activation and soft power control techniques," in *Proceedings of the IEEE International Symposium on Personal, Indoor and Mobile Radio Communications (PIMRC)*, (Helsinki, Finland), pp. 246–250, 1–4 September 1997.

[53] V. Lau and S. Maric, "Variable rate adaptive modulation for DS-CDMA," *IEEE Transactions on Communications*, vol. 47, pp. 577–589, April 1999.

[54] S. Tateesh, S. Atungsiri, and A. Kondoz, "Link adaptive multi-rate coding verification system for CDMA mobile communications," in *Proceedings of the IEEE Global Telecommunications Conference (GLOBECOM)*, (London, UK), pp. 1969–1973, 18–22 November 1996.

[55] Y. Okumura and F. Adachi, "Variable-rate data transmission with blind rate detection for coherent DS-CDMA mobile radio," *IEICE Transactions on Communications*, vol. E81B, pp. 1365–1373, July 1998.

[56] J. Blogh, P. Cherriman, and L. Hanzo, "Adaptive beamforming assisted dynamic channel allocation," in *Proceeding of VTC'99 (Spring)*, (Houston, TX, USA), pp. 199–203, IEEE, 16–20 May 1999.

[57] K. Miya, O. Kato, K. Homma, T. Kitade, M. Hayashi, and T. Ue, "Wideband CDMA systems in TDD-mode operation for IMT-2000," *IEICE Transactions on Communications*, vol. E81-B, pp. 1317–1326, July 1998.

[58] O. Kato, K. Miya, K. Homma, T. Kitade, M. Hayashi, and M. Watanabe, "Experimental performance results of coherent wideband DS-CDMA with TDD scheme," *IEICE Transactions on Communications.*, vol. E81-B, pp. 1337–1344, July 1998.

[59] I. Jeong and M. Nakagawa, "A novel transmission diversity system in TDD-CDMA," *IEICE Transactions on Communications*, vol. E81-B, pp. 1409–1416, July 1998.

[60] S. Chen, B. Mulgrew, and P. M. Grant, "A clustering technique for digital communications channel equalization using radial basis function networks," *IEEE Transactions on Neural Networks*, vol. 4, pp. 570–579, July 1993.

[61] M. Yee, T. Liew, and L. Hanzo, "Radial basis function decision feedback equalisation assisted block turbo burst-by-burst adaptive modems," in *Proceedings of VTC '99 Fall*, (Amsterdam, Holland), pp. 1600–1604, 19-22 September 1999.

[62] R. Kalman and R. Bucy, "New results in linear filtering and prediction theory," *Transactions ASME. Journal Basic Engineering*, vol. 83-D, pp. 85–108, 1961.

[63] J. G. Proakis, *Digital Communications*. Mc-Graw Hill International Editions, 3rd ed., 1995.

[64] T. Rappaport, *Wireless Communications Principles and Practice*. Englewood Cliffs, NJ, USA: Prentice-Hall, 1996.

[65] E. Lee and D. Messerschmitt, *Digital Communication*. Dordrecht: Kluwer Academic Publishers, 1988.

[66] I. S. Gradshteyn and I. M. Ryzhik, *Table of Integrals, Series and Products*. New York, USA: Academic Press, 1980.

[67] D. Tufts, "Nyquist's problem - the joint optimisation of the transmitter and receiver in pulse amplitude modulation," *Proceedings of the IEEE*, vol. 53, pp. 248–260, March 1965.

[68] J. Smith, "The joint optimization of transmitted signal and receiving filter for data transmission filters," *Bell Systems Technical Journal*, vol. 44, pp. 2363–2392, December 1965.

[69] E. Hänsler, "Some properties of transmission systems with minimum mean square error," *IEEE Transactions on Communications Technology (Corresp)*, vol. COM-19, pp. 576–579, August 1971.

[70] T. Ericson, "Structure of optimum receiving filters in data transmission systems," *IEEE Transactions on Information Theory (Corresp)*, vol. IT-17, pp. 352–353, May 1971.

[71] G. Forney Jr, "Maximum likelihood sequence estimation of digital sequences in the presence of intersymbol interference," *IEEE Transactions on Information Theory*, vol. IT-18, pp. 363–378, May 1972.

[72] M. Austin, "Decision feedback equalization for fading dispersive channels," Tech. Rep. 461, M.I.T Research Lab. Electron, August 1971.

[73] P. Monsen, "Feedback equalization for fading dispersive channels," *IEEE Transactions on Information Theory*, vol. IT-17, pp. 1144–1153, January 1971.

[74] J. Salz, "Optimum mean square decision feedback equalization," *Bell Systems Techncial Journal*, vol. 52, pp. 1341–1373, October 1973.

[75] D. Falconer and G. Foschini, "Theory of mmse qam system employing decision feedback equalization," *Bell Systems Technical Journal*, vol. 52, pp. 1821–1849, November 1973.

[76] R. Price, "Non-linearly feedback equalized pam versus capacity for noisy filter channels," in *Rec. Int. Conf. Communication*, pp. 12–17, 1972.

[77] R. Lucky, "A survey of the communication theory literature : 1968–1973," *IEEE Transactions on Information Theory*, vol. IT-19, pp. 725–739, July 1973.

[78] C. Belfiore and J. Park Jr, "Decision feedback equalization," *Proceedings of the IEEE*, vol. 67, pp. 1143–1156, August 1979.

[79] S. Qureshi, "Adaptive equalization," in *Advanced Digital Communications Systems and Signal Processing Techniques* (K.Feher, ed.), pp. 640–713, Englewood Cliffs NJ, USA: Prentice-Hall, 1987.

[80] J. Cheung, *Adaptive Equalisers for Wideband TDMA Mobile Radio*. PhD thesis, Department of Electronics and Computer Science, University of Southampton, UK, 1991.

[81] J. Cheung and R. Steele, "Soft-decision feedback equalizer for continuous-phase modulated signals in wide-band mobile radio channels," *IEEE Transactions on Communications*, vol. 42, pp. 1628–1638, February/March/April 1994.

[82] J. Wu, A. Aghvami, and J. Pearson, "A reduced state soft decision feedback viterbi equaliser for mobile radio communications," in *Proceedings of IEEE International Symposium on Personal, Indoor and Mobile Radio Communications*, (Stockholm, Sweden), pp. 234–242, June 1994.

[83] J. Wu and A. Aghvami, "A new adaptive equalizer with channel estimator for mobile radio communications," *IEEE Transactions on Vehicular Technology*, vol. 45, pp. 467–474, August 1996.

[84] Y. Gu and T. Le-Ngoc, "Adaptive combined DFE/MLSE techniques for ISI channels," *IEEE Transactions on Communications*, vol. 44, pp. 847–857, July 1996.

[85] D. Duttweiler, J. Mazo, and D. Messerschmitt, "An upper bound on the error probability on decision feedback equalization," *IEEE Transactions on Information Theory*, vol. IT-20, pp. 490–497, July 1974.

[86] J. Smee and N. Beaulieu, "Error-rate evaluating of linear equalization and decision feedback equalization with error rate performance," *IEEE Transactions On Communications*, vol. 46, pp. 656–665, May 1998.

[87] S. Altekar and N. Beaulieu, "Upper bounds to the error probability of decision feedback equalization," *IEEE Transactions on Communications*, vol. 39, pp. 145–157, January 1993.

[88] M. Tomlinson, "New automatic equalizer employing modulo arithmetic," *IEE Electronics Letters*, vol. 7, pp. 138–139, March 1971.

[89] H. Harashima and H. Miyakawa, "Matched transmission technique for channels with intersymbol interference," *IEEE Transactions on Communications*, vol. COM-20, pp. 774–780, August 1972.

[90] M. Russell and J. Bergmans, "A technique to reduce error propagation in M-ary decision feedback equalization," *IEEE Transactions on Communications*, vol. 43, pp. 2878–2881, December 1995.

[91] M. Chiani, "Introducing erasures in decision feedback equalization to reduce error propagation," *IEEE Transactions on Communications*, vol. 45, pp. 757–760, July 1997.

[92] J. Proakis and D. Manolakis, *Digital Signal Processing — Principles, Algorithms and Applications*. Macmillan, 1992.

[93] D. Mix, *Random Signal Processing*. Englewood Cliffs NJ, USA: Prentice-Hall, 1995.

[94] S. Haykin, *Adaptive Filter Theory*. Englewood Cliffs, NJ, USA: Prentice-Hall, 1996.

[95] B. Widrow and S. Stearns, *Adaptive Signal Processing*. Englewood Cliffs, NJ, USA: Prentice-Hall, 1985.

[96] B. Widrow, "On the statistical on the efficiency of the LMS algorithm with non stationary inputs," *IEEE Transactions on Information Theory*, vol. IT 30, pp. 211–221, March 1984.

[97] B. Widrow, J. McCool, M. Larrimore, and C. Johnson Jr, "Stationary and non-stationary learning characteristics of the LMS adaptive filter," *Proceedings of the IEEE*, vol. 64, pp. 1151–1162, August 1976.

[98] D. Falconer and L. Ljung, "Application of fast kalman estimation to adaptive equalization," *IEEE Transactions on Communications*, vol. COM-26, pp. 1439–1446, October 1978.

[99] D. Godard, "Channel equalization using a kalman filter for fast data transmission," *IBM Journal on Research and Development*, pp. 267–273, May 1974.

[100] A. Clark and R. Harun, "Assessment of kalman-filter channel estimators for an HF radio link," *Proceedings of the IEE*, vol. 133, pp. 513–521, October 1986.

[101] P. Shukla and L. Turner, "Channel estimation-based adaptive dfe for fading multipath radio channels," *IEE Proceedings - I*, vol. 138, pp. 525–543, October 1991.

[102] R. Lucky, "Automatic equalization for digital communication," *Bell Systems Technical Journal*, vol. 44, pp. 547–588, April 1965.

[103] R. Lucky, "Techniques for adaptive equalization of digital communication," *Bell Systems Technical Journal*, vol. 45, pp. 255–286, February 1966.

[104] R. Lawrence and H. Kaufman, "The kalman filter for equalization of a digital communications channel," *IEEE Transactions on Communications*, vol. COM-19, pp. 1137–1141, 1971.

[105] J. Mark, "A note on the modified kalman filter for channel equalization," *Proceedings of the IEEE*, vol. 61, pp. 481–482, 1973.

[106] S. Kleibano, V. Privalkii, and I. Time, "Kalman filter for equalization of digital communications channel," *Automation and Remote Control*, vol. 2, pp. 1097–1102, 1974.

[107] A. Luvinson and G. Pirani, "Design and performance of an adaptive receiver for synchronous data transmission," *IEEE Transactions on AES*, vol. AES-15x, pp. 635–648, 1979.

[108] M. Kumar, M. Yurtseven, and A. Rahrooh, "Design and performance analysis of an adaptive fir kalman equalizer," *Journal of the Franklin Institute*, vol. 330, no. 5, pp. 929–938, 1993.

[109] T. Lee and D. Cunningham, "Kalman filter equalization for QPSK communications," *IEEE Transactions on Communications*, vol. COM-24, pp. 361–364, 1976.

[110] E. D. Messe and G. Corsini, "Adaptive kalman filter equalizer," *IEE Electronicss Letters*, vol. 16, no. 8, pp. 547–549, 1980.

[111] F. Hsu, "Square root kalman filtering for high speed data received over fading dispersive hf channels," *IEEE Transactions on Information Theory*, vol. IT-28, pp. 753–763, 1982.

[112] G. Richards, "Implementation of kalman filters for process identification," *GEC Journal Research*, vol. 1, pp. 100–107, 1983.

[113] M. Mueller, "Least squares algorithms for adaptive equalizers," *Bell Systems Technical Journal*, vol. 60, pp. 1905–1925, October 1981.

[114] A. Sayed and T. Kailath, "A state-space approach to adaptive rls filtering," *IEEE Signal Processing Magazine*, vol. 11, pp. 571–577, July 1994.

[115] S. Bozic, *Digital and Kalman Filtering*. Edward Arnold, 1994.

[116] A. Milewski, "Periodic sequences with optimal properties for channel estimation and fast start-up equalization," *IBM Journal Research and Development*, vol. 54, pp. 425–528, September 1983.

[117] L. Scharf, *Statistical signal processing : Detection, estimation and time signal analysis*. Addison-Wesley Publishing Company, Inc., 1991.

[118] R. Brown and P. Hwang, *Introduction to Random Signals and Applied Kalman Filtering*. New York, USA: John Wiley and Sons, 1997.

[119] W. Press, S. Teukolsky, W. Vetterling, and B. Flannery, "Minimization or maximization of functions," in *Numerical Recipes in C*, ch. 10, pp. 394–455, Cambridge: Cambridge University Press, 1992.

[120] K. Narayanan and L. Cimini, "Equalizer adaptation algorithms for high speed wireless communications," in *Proceedings of IEEE VTC'96*, (Atlanta, GA, USA), pp. 681–685, IEEE, 28 April–1 May 1996.

[121] J. Torrance, *Adaptive Full Response Digital Modulation for Wireless Communications Systems*. PhD thesis, Department of Electronics and Computer Science, University of Southampton, UK, 1997.

[122] T. Ojanperä and R. Prasad, *Wideband CDMA for Third Generation Mobile Communications*. London, UK: Artech House, 1998.

[123] J. Hayes, "Adaptive feedback communications," *IEEE Communication Technology*, vol. 16, pp. 29–34, February 1968.

[124] P. Monsen, "Theoretical and measured performance of a dfe modem on a fading multipath channel," *IEEE Transactions on Communications*, vol. COM-25, pp. 1144–1153, October 1977.

[125] "COST 207: Digital land mobile radio communications, final report." Office for Official Publications of the European Communities, 1989. Luxembourg.

[126] A. Klein, R. Pirhonen, J. Skoeld, and R. Suoranta, "FRAMES multiple access mode 1 — wideband TDMA with and without spreading," in *Proceedings of the IEEE International Symposium on Personal, Indoor and Mobile Radio Communications (PIMRC)*, vol. 1, (Helsinki, Finland), pp. 37–41, 1–4 September 1997.

[127] M. Yee and L. Hanzo, "Radial Basis Function decision feedback equaliser assisted burst-by-burst adaptive modulation," in *Proceedings of IEEE Global Telecommunications Conference (GLOBECOM)*, (Rio de Janeiro, Brazil), 5–9 December 1999.

[128] C. Berrou and A. Glavieux, "Near optimum error correcting coding and decoding: Turbo codes," *IEEE Transactions on Communications*, vol. 44, pp. 1261–1271, October 1996.

[129] C. Douillard, A. Picart, M. Jézéquel, P. Didier, C. Berrou, and A. Glavieux, “Iterative correction of intersymbol interference: Turbo-equalization,” *European Transactions on Communications*, vol. 6, pp. 507–511, 1995.

[130] A. Goldsmith and S. Chua, “Adaptive coded modulation for fading channels,” *IEEE Transactions on Communications*, vol. 46, pp. 595–602, May 1998.

[131] C. Berrou, A. Glavieux, and P. Thitimajshima, “Near shannon limit error-correcting coding and decoding: Turbo codes,” in *Proceedings of the International Conference on Communications*, (Geneva, Switzerland), pp. 1064–1070, May 1993.

[132] P. Robertson, “Illuminating the structure of code and decoder of parallel concatenated recursive systematic (turbo) codes,” *IEEE Globecom*, pp. 1298–1303, 1994.

[133] B. Sklar, *Digital Communications—Fundamentals and Applications*. Englewood Cliffs, NJ, USA: Prentice-Hall, 1988.

[134] S. Lin and D. Constello Jr., *Error Control Coding: Fundamentals and Applications*. Englewood Cliffs, NJ, USA: Prentice-Hall, October 1982. ISBN: 013283796X.

[135] R. Blahut, *Theory and Practice of Error Control Codes*. Reading, MA, USA: Addison-Wesley, 1983. ISBN 0-201-10102-5.

[136] J. Hagenauer, E. Offer, and L. Papke, “Iterative decoding of binary block and convolutional codes,” *IEEE Transactions on Information Theory*, vol. 42, pp. 429–445, March 1996.

[137] R. Pyndiah, “Iterative decoding of product codes: Block turbo codes,” in *Proceedings of the International Symposium on Turbo Codes & Related Topics*, (Brest, France), pp. 71–79, 3–5 September 1997.

[138] L. Bahl, J. Cocke, F. Jelinek, and J. Raviv, “Optimal decoding of linear codes for minimising symbol error rate,” *IEEE Transactions on Information Theory*, vol. 20, pp. 284–287, March 1974.

[139] P. Robertson, E. Villebrun, and P. Hoeher, “A comparison of optimal and sub-optimal MAP decoding algorithms operating in the log domain,” in *Proceedings of the International Conference on Communications*, (Seattle, United States), pp. 1009–1013, June 1995.

[140] B. Yeap, *Turbo Equalisation Algorithms for Full and Partial Response Modulation*. PhD thesis, University of Southampton, UK, 1999.

[141] A. Barbulescu and S. Pietrobon, “Interleaver design for turbo codes,” *IEE Electronics Letters*, pp. 2107–2108, December 1994.

[142] T. Liew, C. Wong, and L. Hanzo, “Block turbo coded burst-by-burst adaptive modems,” in *Proceedings of Microcoll’99, Budapest, Hungary*, pp. 59–62, 21–24 March 1999.

[143] C. Wong, T. Liew, and L. Hanzo, “Turbo coded burst by burst adaptive wideband modulation with blind modem mode detection,” in *Proceeding of ACTS Mobile Communication Summit ’99*, (Sorrento, Italy), pp. 303–308, ACTS, 8–11 June 1999.

[144] T. Keller and L. Hanzo, “Adaptive orthogonal frequency division multiplexing schemes,” in *Proceeding of ACTS Mobile Communication Summit ’98*, (Rhodes, Greece), pp. 794–799, ACTS, 8–11 June 1998.

[145] M. Simon, J. Omura, R. Scholtz, and B. Levitt, *Spread Spectrum Communications Handbook*. New York, USA: McGraw-Hill, 1994.

[146] C. Wong, T. Liew, and L. Hanzo, “Burst-by-burst turbo coded wodeband adaptive modulation,” *Submitted to the IEEE Journal on Selected Areas in Communications*.

[147] U. Wachsmann and J. Huber, “Power and bandwidth efficient digital communications using turbo codes in multilevel codes,” *European Transactions on Telecommunications*, vol. 6, pp. 557–567, September–October 1995.

[148] A. Glavieux, C. Laot, and J. Labat, “Turbo equalization over a frequency selective channel,” in *Proceedings of the International Symposium on Turbo Codes*, (Brest, France), pp. 96–102, 3-5 September 1997.

[149] C. Wong, B. Yeap, and L. Hanzo, “Wideband burst-by-burst adaptive modulation with turbo equalization and iterative channel estimation,” in *Accepted for the Proceedings of the IEEE Vehicular Technology Conference 2000*, 2000.

[150] G. Ungerboeck, “Channel coding with multilevel/phase signals,” *IEEE Transactions on Information Theory*, vol. IT-28, pp. 55–67, January 1982.

[151] D. Divsalar and M. K. Simon, “The design of trellis coded mpsk for fading channel: Performance criteria,” *IEEE Transactions on Communications*, vol. 36, pp. 1004–1012, September 1988.

[152] D. Divsalar and M. K. Simon, “The design of trellis coded MPSK for fading channel: set partitioning for optimum code design,” *IEEE Transactions on Communications*, vol. 36, pp. 1013–1021, September 1988.

[153] P. Robertson and T. Wörz, “Bandwidth efficient turbo trellis-coded modulation using punctured component codes,” *IEEE Journal on Selected Area on Communications*, vol. 16, pp. 206–218, February 1998.

[154] L. Piazzo and L. Hanzo, “TTCM-OFDM over Dispersive Fading Channels,” *IEEE Vehicular Technology Conference*, vol. 1, pp. 66–70, May 2000.

[155] D. Goeckel, “Adaptive coding for fading channels using outdated fading estimates,” *IEEE Transactions on Communications*, vol. 47, pp. 844–855, June 1999.

[156] G. Caire, G. Taricco, and E. Biglieri, “Capacity of bit-interleaved channels,” *Electronics Letters*, pp. 1060–1061, 1996.

[157] J. K. Cavers and P. Ho, “Analysis of the Error Performance of Trellis-Coded Modulations in Rayleigh-Fading Channels,” *IEEE Transactions on Communications*, vol. 40, pp. 74–83, January 1992.

[158] A. Naguib, N. Seshdri, and A. Calderbank, “Increasing data rate over wireless channels,” *IEEE Signal Processing Magazine*, vol. 17, pp. 76–92, May 2000.

[159] S. M. Alamouti and S. Kallel, “Adaptive trellis-coded multiple-phased-shift keying Rayleigh fading channels,” *IEEE Transactions on Communications*, vol. 42, pp. 2305–2341, June 1994.

[160] E. Zehavi, “8-PSK trellis codes for a Rayleigh fading channel,” *IEEE Transactions on Communications*, vol. 40, pp. 873–883, May 1992.

[161] X. Li and J. Ritcey, “Bit-interleaved coded modulation with iterative decoding,” *IEEE Communications Letters*, vol. 1, November 1997.

[162] X. Li and J. Ritcey, “Bit-interleaved coded modulation with iterative decoding — approaching turbo-tcm performance without code concatenation,” in *Proceedings of CISS 1998*, (Princeton University, USA), March 1998.

[163] X. Li and J. Ritcey, “Trellis-coded modulation with bit interleaving and iterative decoding,” *IEEE Journal on Selected Areas in Communications*, vol. 17, April 1999.

[164] X. Li and J. Ritcey, “Bit-interleaved coded modulation with iterative decoding using soft feedback,” *IEE Electronics Letters*, vol. 34, pp. 942–943, May 1998.

[165] J. Hagenauer, “Rate-compatible puncture convolutional codes (RCPC) and their application,” *IEEE Transactions on Communications*, vol. 36, pp. 389–400, April 1988.

[166] C. Wong, P. Cherriman, and L. Hanzo, “Burst-by-burst adaptive wireless video telephony over dispersive channels,” in *Proceeding of Globecom’99*, vol. 1a, (Rio de Janeiro, Brazil), pp. 204–208, IEEE, 5–9 December 1999.

[167] P. Cherriman, C. Wong, and L. Hanzo, “Turbo- and BCH-coded wide-band burst-by-burst adaptive H.263-assisted wireless video telephony,” *IEEE Transactions on Circuits and Systems for Video Technology*, vol. 10, pp. 1355–1363, December 2000.

[168] J. F. Hayes, “Adaptive feedback communications,” *IEEE Transactions on Communication Technology*, vol. 16, no. 1, pp. 29–34, 1968.

[169] W. T. Webb and R. Steele, “Variable rate QAM for mobile radio,” *IEEE Transactions on Communications*, vol. 43, no. 7, pp. 2223–2230, 1995.

[170] R. Steele and W. Webb, “Variable rate QAM for data transmission over Rayleigh fading channels,” in *Proceeedings of Wireless ’91*, (Calgary, Alberta), pp. 1–14, IEEE, 1991.

[171] M. Moher and J. Lodge, “TCMP—a modulation and coding strategy for rician fading channels,” *IEEE Journal on Selected Areas in Communications*, vol. 7, pp. 1347–1355, December 1989.

[172] J. K. Cavers, “An Analysis of Pilot Symbol Assisted Modulation for Rayleigh Fading Channels,” *IEEE Transactions on Vehicular Technology*, vol. 40, pp. 686–693, November 1991.

[173] S. Sampei and T. Sunaga, “Rayleigh fading compensation for QAM in land mobile radio communications,” *IEEE Transactions on Vehicular Technology*, vol. 42, pp. 137–147, May 1993.

[174] W. Lee, "Estimate of channel capacity in Rayleigh fading environment," *IEEE Transactions on Vehicular Technology*, vol. 39, pp. 187–189, August 1990.

[175] A. Goldsmith and P. Varaiya, "Capacity of fading channels with channel side information," *IEEE Transactions on Information Theory*, vol. 43, pp. 1986–1992, November 1997.

[176] M. S. Alouini and A. J. Goldsmith, "Capacity of Rayleigh fading channels under different adaptive transmission and diversity-combining technique," *IEEE Transactions on Vehicular Technology*, vol. 48, pp. 1165–1181, July 1999.

[177] A. Goldsmith and S. Chua, "Variable rate variable power MQAM for fading channels," *IEEE Transactions on Communications*, vol. 45, pp. 1218–1230, October 1997.

[178] M. S. Alouini, X. Tand, and A. J. Goldsmith, "An adaptive modulation scheme for simultaneous voice and data transmission over fading channels," *IEEE Journal on Selected Areas in Communications*, vol. 17, pp. 837–850, May 1999.

[179] D. Yoon, K. Cho, and J. Lee, "Bit error probability of M-ary Quadrature Amplitude Modulation," in *Proc. IEEE VTC 2000-Fall*, vol. 5, pp. 2422–2427, IEEE, September 2000.

[180] E. L. Kuan, C. H. Wong, and L. Hanzo, "Burst-by-burst adaptive joint-detection CDMA," in *Proc. of IEEE VTC'99 Fall*, vol. 2, (Amsterdam, Netherland), pp. 1628–1632, September 1999.

[181] K. J. Hole, H. Holm, and G. E. Oien, "Adaptive multidimensional coded modulation over flat fading channels," *IEEE Journal on Selected Areas in Communications*, vol. 18, pp. 1153–1158, July 2000.

[182] M. Nakagami, "The m-distribution - A general formula of intensity distribution of rapid fading," in *Statistical Methods in Radio Wave Propagation* (W. C. Hoffman, ed.), pp. 3–36, Pergamon Press, 1960.

[183] J. Kreyszig, *Advanced engineering mathematics*. Wiley, 7th edition ed., 1993.

[184] J. Lu, K. B. Letaief, C. I. J. Chuang, and M. L. Lio, "M-PSK and M-QAM BER computation using signal-space concepts," *IEEE Transactions on Communications*, vol. 47, no. 2, pp. 181–184, 1999.

[185] W. H. Press, S. A. Teukolsky, W. T. Vetterling, and B. P. Flannery, *Numerical Recipies in C*. Cambridge University Press, 1992.

[186] T. Keller and L. Hanzo, "Adaptive modulation technique for duplex OFDM transmission," *IEEE Transactions on Vehicular Technology*, vol. 49, pp. 1893–1906, September 2000.

[187] B. J. Choi, M. Münster, L. L. Yang, and L. Hanzo, "Performance of Rake receiver assisted adaptive-modulation based CDMA over frequency selective slow Rayleigh fading channel," *Electronics Letters*, vol. 37, pp. 247–249, February 2001.

[188] G. S. G. Beveridge and R. S. Schechter, *Optimization: Theory and Practice*. McGraw-Hill, 1970.

[189] W. Jakes Jr., ed., *Microwave Mobile Communications*. New York, USA: John Wiley & Sons, 1974.

[190] "COST 207 : Digital land mobile radio communications, final report," tech. rep., Luxembourg, 1989.

[191] R. Price and E. Green Jr., "A communication technique for multipath channels," *Proceedings of the IRE*, vol. 46, pp. 555–570, March 1958.

[192] M. K. Simon and M. S. Alouini, *Digital Communication over Fading Channels: A Unified Approach to Performance Analysis*. John Wiley & Sons, Inc., 2000. ISBN 0471317799.

[193] C. Y. Wong, R. S. Cheng, K. B. Letaief, and R. D. Murch, "Multiuser OFDM with adaptive subcarrier, bit, and power allocation," *IEEE Journal on Selected Areas in Communications*, vol. 17, pp. 1747–1758, October 1999.

[194] T. Keller and L. Hanzo, "Adaptive multicarrier modulation: A convenient framework for time-frequency processing in wireless communications," *Proceedings of the IEEE*, vol. 88, pp. 611–642, May 2000.

[195] J. Bingham, "Multicarrier modulation for data transmission: an idea whose time has come," *IEEE Communications Magazine*, pp. 5–14, May 1990.

[196] N. Yee, J.-P. Linnartz, and G. Fettweis, "Multicarrier CDMA in indoor wireless radio networks," in *PIMRC'93*, pp. 109–113, 1993.

[197] K. Fazel and L. Papke, "On the performance of convolutionally-coded CDMA/OFDM for mobile communication system," in *PIMRC'93*, pp. 468–472, 1993.

[198] A. Klein, G. Kaleh, and P. Baier, “Zero forcing and minimum mean square error equalization for multiuser detection in code division multiple access channels,” *IEEE Transactions on Vehicular Technology*, vol. 45, pp. 276–287, May 1996.

[199] B. J. Choi, T. H. Liew, and L. Hanzo, “Concatenated space-time block coded and turbo coded symbol-by-symbol adaptive OFDM and multi-carrier CDMA systems,” in *Proceedings of IEEE VTC 2001-Spring*, p. P.528, IEEE, May 2001.

[200] B. Vucetic, “An adaptive coding scheme for time-varying channels,” *IEEE Transactions on Communications*, vol. 39, no. 5, pp. 653–663, 1991.

[201] H. Imai and S. Hirakawa, “A new multi-level coding method using error correcting codes,” *IEEE Transactions on Information Theory*, vol. 23, pp. 371–377, May 1977.

[202] S. Chua and A. Goldsmith, “Adaptive coded modulation for fading channels,” *IEEE Transactions on Communications*, vol. 46, pp. 595–602, May 1998.

[203] T. Keller, T. Liew, and L. Hanzo, “Adaptive rate RRNS coded OFDM transmission for mobile communication channels,” in *Proceedings of VTC 2000 Spring*, (Tokyo, Japan), pp. 230–234, 15-18 May 2000.

[204] T. Keller, T. H. Liew, and L. Hanzo, “Adaptive redundant residue number system coded multicarrier modulation,” *IEEE Journal on Selected Areas in Communications*, vol. 18, pp. 1292–2301, November 2000.

[205] T. Liew, C. Wong, and L. Hanzo, “Block turbo coded burst-by-burst adaptive modems,” in *Proceedings of Microcoll’99*, (Budapest, Hungary), pp. 59–62, 21-24 March 1999.

[206] C. Wong, T. Liew, and L. Hanzo, “Turbo coded burst by burst adaptive wideband modulation with blind modem mode detection,” in *ACTS Mobile Communications Summit*, (Sorrento, Italy), pp. 303–308, 8-11 June 1999.

[207] V. Tarokh, N. Seshadri, and A. R. Calderbank, “Space-Time Codes for High Data Rate Wireless Communication: Performance Criterion and Code Construction,” *IEEE Transactions on Information Theory*, vol. 44, pp. 744–765, March 1998.

[208] V. Tarokh, H. Jafarkhani, and A. R. Calderbank, “Space-time block coding for wireless communications: Performance results,” *IEEE Journal on Selected Areas in Communications*, vol. 17, pp. 451–460, March 1999.

[209] P. Jung and J. Blanz, “Joint detection with coherent receiver antenna diversity in CDMA mobile radio systems,” *IEEE Transactions on Vehicular Technology*, vol. 44, pp. 76–88, February 1995.

[210] B.-J. Choi, E.-L. Kuan, and L. Hanzo, “Crest–factor study of MC-CDMA and OFDM,” in *Proceeding of VTC’99 (Fall)*, vol. 1, (Amsterdam, Netherlands), pp. 233–237, IEEE, 19–22 September 1999.

[211] 3GPP, *3rd Generation Patnership Project (3GPP); Technical Specification Group Radio Access Network Physical Channels and Mapping of Transport Channels onto Physical Channels (TDD) (3G TS 25.221 version 3.0.0) (www.3gpp.org)*, October 1999.

[212] W. Lee, *Mobile Cellular Telecommunications: Analog and Digital Systems*. New York, USA: McGraw-Hill, 1995.

[213] W. Webb, “Spectrum efficiency of multilevel modulation schemes in mobile radio communications,” *IEEE Transactions on Communications*, vol. 43, no. 8, pp. 2344–2349, 1995.

[214] C. Lee and R. Steele, “Signal-to-interference calculations for modern TDMA cellular communication systems,” *IEE Proceedings on Communication*, vol. 142, pp. 21–30, February 1995.

[215] S. Verdú, *Multiuser Detection*. Cambridge, UK: Cambridge University Press, 1998.

[216] A. Klein and P. Baier, “Linear unbiased data estimation in mobile radio sytems applying CDMA,” *IEEE Journal on Selected Areas in Communications*, vol. 11, pp. 1058–1066, September 1993.

[217] J. Blanz, A. Klein, M. Nasshan, and A. Steil, “Performance of a cellular hybrid C/TDMA mobile radio system applying joint detection and coherent receiver antenna diversity,” *IEEE Journal on Selected Areas in Communications*, vol. 12, pp. 568–579, May 1994.

[218] P. Jung, J. Blanz, M. Nasshan, and P. Baier, “Simulation of the uplink of the JD-CDMA mobile radio systems with coherent receiver antenna diversity,” *Wireless Personal Communications (Kluwer)*, vol. 1, no. 1, pp. 61–89, 1994.

[219] H. Yoshino, K. Fukawa, and H. Suzuki, "Interference cancelling equalizer (ice) for mobile radio communication," *IEEE Transactions on Vehicular Technology*, vol. 46, pp. 849–61, November 1997.

[220] M. Valenti and B. Woerner, "Combined multiuser reception and channel decoding for TDMA cellular systems," in *Proceedings of IEEE Vehicular Technology Conference*, (Ottawa, Canada), pp. 1915–1919, May 1998.

[221] J. Joung and G. Stuber, "Performance of truncated co-channel interference cancelling MLSE for TDMA systems," in *Proceedings of IEEE Vehicular Technology Conference*, (Ottawa, Canada), pp. 1710–1714, May 1998.

[222] E. Kuan, *Burst-by-burst Adaptive Multiuser Detection CDMATechniques*. PhD thesis, University of Southampton, UK, 1999.

[223] G. Golub and C. van Loan, *Matrix Computations*. North Oxford Academic, 1983.

[224] C. Wong, E. Kuan, and L. Hanzo, "Joint detection based wideband burst-by-burst adaptive modem with co-channel interference," in *Proceedings of the IEEE Vehicular Technology Conference*, (Amsterdam, The Netherlands), pp. 613–617, September 1999.

[225] S. Mak and A. Aghvami, "Detection of trellis-coded modulation on time-dispersive channels," in *Proceeding of IEEE Global Telecommunications Conference, Globecom 96*, (London, UK), pp. 1825–1829, IEEE, 18–22 November 1996.

[226] S. Siu and C. F. N. Cowan, "Performance analysis of the l_p norm back propagation algorithm for adaptive equalisation," *IEE Proceedings*, vol. 140, pp. 43–47, February 1993.

[227] G. J. Gibson, S. Siu, and C. F. N. Cowan, "The application of nonlinear structures to the reconstruction of binary signals," *IEEE Transactions on Signal Processing*, vol. 39, pp. 1877–1884, August 1991.

[228] G. J. Gibson, S. Siu, and C. F. N. Cowan, "Multi-layer perceptron structures applied to adaptive equalizers for data communications," in *ICASSP, IEEE International Conference on Acoustics, Speech and Signal Processing*, vol. 2, (IEEE Service Center, Piscataway, NJ, USA), pp. 1183–1186, IEEE, May 1989.

[229] G. J. Gibson, S. Siu, S. Chen, P. M. Grant, and C. F. N. Cowan, "The application of nonlinear architectures to adaptive channel equalisation," in *IEEE International Conference on Communications*, vol. 2, (IEEE Service Center, Piscataway, NJ, USA), pp. 649–653, IEEE, April 1990.

[230] S. Siu, G. J. Gibson, and C. F. N. Cowan, "Decision feedback equalisation using neural network structures and performance comparison with standard architecture," *IEE Proceedings*, vol. 137, pp. 221–225, August 1990.

[231] S. Chen, G. J. Gibson, and C. F. N. Cowan, "Adaptive channel equalisation using a polynomial-perceptron structure," *IEE Proceedings*, vol. 137, pp. 257–264, October 1990.

[232] C.-H. Chang, S. Siu, and C.-H. Wei, "A polynomial-perceptron based decision feedback equalizer with a robust learning algorithm," *EURASIP Signal Processing*, vol. 47, pp. 145–158, November 1995.

[233] Z.-J. Xiang and G.-G. Bi, "A new lattice polynomial perceptron and its applications to frequency-selective fading channel equalization and ACI suppression," *IEEE Transactions on Communications*, vol. 44, pp. 761–767, July 1996.

[234] Z.-J. Xiang, G.-G. Bi, and T. Le-Ngoc, "Polynomial perceptrons and their applications to fading channel equalization and co-channel interference suppression," *IEEE Transactions on Signal Processing*, vol. 42, pp. 2470–2480, September 1994.

[235] S. Chen, S. McLaughlin, and B. Mulgrew, "Complex-valued radial basis function network, Part II: Application to digital communications channel equalisation," *EURASIP Signal Processing*, vol. 36, pp. 175–188, March 1994.

[236] S. Chen, B. Mulgrew, and S. McLaughlin, "Adaptive Bayesian equalizer with decision feedback," *IEEE Transactions on Signal Processing*, vol. 41, pp. 2918–2927, September 1993.

[237] S. Chen, G. J. Gibson, C. F. N. Cowan, and P. M. Grant, "Reconstruction of binary signals using an adaptive radial basis function equaliser," *EURASIP Signal Processing*, vol. 22, pp. 77–93, January 1991.

[238] B. Mulgrew, "Applying radial basis functions," *IEEE Signal Processing Magazine*, vol. 13, pp. 50–65, March 1996.

[239] C. A. Micchelli, "Interpolation of scatter data: Distance matrices and conditionally positive definite functions," *Constructive Approximation*, vol. 2, pp. 11–22, 1986.

[240] M. J. D. Powell, *Algorithms for Approximation*, ch. Radial Basis Functions for Multivariable Interpolation: a review, pp. 143–167. Oxford: Clarendon Press, 1987.

[241] H. L. V. Trees, *Detection, Estimation and Modulation Theory, Part 1*. New York: John Wiley and Sons, 1968.

[242] E. R. Kandel, *Principles of Neural Science*, ch. Nerve cells and behavior, pp. 13–24. Elsevier, New York, 2nd. ed., 1985.

[243] S. Haykin, *Neural Networks : A Comprehensive Foundation*. Macmillan Publishing Company, 1994.

[244] C. M. Bishop, *Neural Networks for Pattern Recognition*. Oxford University Press, 1995.

[245] D. E. Rumelhart, G. E. Hinton, and R. J. Williams, *Parallel Distributed Processing: Explorations in the Microstructure of Cognition*, ch. Learning internal representations by error propagation, pp. 318–362. Cambridge, Mass. : MIT Press, 1986.

[246] D. E. Rumelhart, G. E. Hinton, and R. J. Williams, "Learning representations by back-propagating errors," *Nature (London)*, vol. 323, pp. 533–536, 1986.

[247] J. B. Gomm and D. L. Yu, "Selecting radial basis function network centers with recursive orthogonal least squares training," *IEEE Transactions on Neural Networks*, vol. 11, pp. 306–314, March 2000.

[248] R. P. Lippmann, "An introduction to computing with neural nets," *IEEE ASSP Magazine*, pp. 4–22, April 1987.

[249] J. C. Sueiro, A. A. Rodriguez, and A. R. F. Vidal, "Recurrent radial basis function networks for optimal symbol-by-symbol equalization," *EURASIP Signal Processing*, vol. 40, pp. 53–63, October 1994.

[250] W. S. Gan, J. J. Soraghan, and T. S. Durrani, "New functional-link based equaliser," *Electronics Letter*, vol. 28, pp. 1643–1645, August 1992.

[251] A. Hussain, J. J. Soraghan, and T. S. Durrani, "A new artificial neural network based adaptive non-linear equalizer for overcoming co-channel interferenc," in *IEEE Global Telecommunications Conference*, pp. 1422–1426, November 1996.

[252] A. Hussain, J. J. Soraghan, and T. S. Durrani, "A new adaptive functional-link neural-network-based DFE for overcoming co-channel interference," *IEEE Transaction on Communications*, vol. 45, pp. 1358–1362, November 1997.

[253] T. Kohonen, O. Simula, A. Visa, and J. Kangas, "Engineering applications of the self-organizing map," *Proceedings of the IEEE*, vol. 84, pp. 1358–1384, October 1996.

[254] S. Bouchired, M. Ibnkahla, D. Roviras, and F. Castanié, "Neural network equalization of satellite mobile communication channels," *ICASSP, IEEE International Conference on Acoustics, Speech and Signal Processing - Proceedings, 1998*, vol. 6, pp. 3377–3379, May 1998.

[255] S. Bouchired, M. Ibnkahla, D. Roviras, and F. Castanié, "Equalization of satellite UMTS channels using neural network devices," in *ICASSP, IEEE International Conference on Acoustics, Speech and Signal Processing - Proceedings, 1999*, vol. 5, (Phoenix, Arizona), pp. 2563–2566, 15-19 March 1999.

[256] S. Bouchired, D. Roviras, and F. Castanié, "Equalization of satellite mobile channels with neural network techniques," *Space Communications*, vol. 15, no. 4, pp. 209–220, 1998-1999.

[257] G. J. Gibson and C. F. N. Cowan, "On the decision regions of multilayer perceptrons," *Proceedings of the IEEE*, vol. 78, pp. 1590–1594, October 1990.

[258] N. E. Cotter, "The Stone-Weierstrass theorem and its application to neural networks," *IEEE Transactions on Neural Networks*, vol. 1, pp. 290–295, December 1990.

[259] T. M. Cover, "Geometrical and statistical properties of systems of linear inequalities with applications in pattern recognition," *IEEE Transactions on Electronic Computers*, vol. 14, pp. 326–334, 1965.

[260] W. A. Light, "Some aspects of radial basis function approximation," *Approximation Theory, Spline Functions and Applications, NATO ASI Series*, vol. 256, pp. 163–190, 1992.

[261] V. A. Morozov, *Regularization Methods for Ill-Posed Problems*. Boca Raton, FL, USA: CRC Press, 1993.

[262] A. N. Tikhonov and V. Y. Arsenin, *Solutions of Ill-posed Problems*. Washington, DC:W. H. Winston, 1977.

[263] T. Poggio and F. Girosi, "Networks for approximation and learning," *Proceedings of the IEEE*, vol. 78, pp. 1481–1497, 1990.

[264] S. Chen, C. F. N. Cowan, and P. M. Grant, "Orthogonal least squares learning algorithm for radial basis function networks," *IEEE Transactions on Neural Networks*, vol. 2, pp. 302–309, March 1991.

[265] S. Chen, E.-S. Chng, and K. Alkadhimi, "Regularised orthogonal least squares algorithm for constructing radial basis function networks," *International Journal of Control*, vol. 64, pp. 829–837, July 1996.

[266] J. MacQueen, "Some methods for classsification and analysis of multivariate observation," in *Proceedings of the 5th Berkeley Symposium on Mathematical Statistics and Probability* (L. M. LeCun and J. Neyman, eds.), vol. 1, (Berkeley), pp. 281–297, University of California Press, 1967.

[267] D. E. Rumelhart and D. Zipser, "Feature discovery by competitive learning," in *Parallel Distributed Processing: Explorations in the Microstructure of Cognition*, vol. 1, Cambridge, MA: Bradford Books, 1986.

[268] D. DeSieno, "Adding a conscience to competitive learning," in *Proceedings 2nd IEEE International Conference on Neural Networks*, vol. 1, pp. 117–124, July 1988.

[269] C. Chinrungrueng and C. H. Sëquin, "Optimal adaptive k-means algorithm with dynamic adjustment of learning rate," *IEEE Transactions on Neural Networks*, vol. 6, pp. 157–169, January 1995.

[270] J. Proakis, *Digital communications*. McGraw-Hill, 1995.

[271] J. C. Sueiro and A. R. F. Vidal, "Recurrent radial basis function networks for optimal blind equalisation," in *Proceedings IEEE Workshop on Neural Networks for Signal Processing*, pp. 562–571, IEEE, June 1993.

[272] S. Chen, S. McLaughlin, B. Mulgrew, and P. M. Grant, "Adaptive Bayesian decision feedback equalizer for dispersive mobile radio channels," *IEEE Transactions on Communications*, vol. 43, pp. 1937–1945, May 1995.

[273] S. N. Crozier, D. D. Falconer, and S. A. Mahmoud, "Least sum of squared errors (LSSE) channel estimation," *IEE Proceedings Part F: Radar and Signal Processing*, vol. 138, pp. 371–378, August 1991.

[274] A. Urie, M. Streeton, and C. Mourot, "An advance TDMA mobile access system for UMTS," in *Proceedings of IEEE International Symposium on Personal, Indoor and Mobile Radio Communications*, (The Hague, The Netherlands), pp. 685–690, 1994.

[275] J. L. Valenzuela and F. Casadevall, "Performance of adaptive Bayesian equalizers in outdoor environment," in *Proceedings of IEEE Vehicular Technology Conference*, vol. 3, pp. 2143–2147, IEEE, May 1997.

[276] E.-S. Chng, H. Yang, and W. Skarbek, "Reduced complexity implementation of Bayesian equaliser using local RBF network for channel equalisation problem," *Electronics Letters*, vol. 32, pp. 17–19, January 1996.

[277] S. K. Patra and B. Mulgrew, "Computational aspects of adaptive radial basis function equalizer design," in *IEEE International Symposium on Circuits and Systems, ISCAS'97*, vol. 1, pp. 521–524, IEEE, Piscataway, NJ, USA, June 1997.

[278] P. Robertson, E. Villebrun, and P. Höher, "A comparison of optimal and sub-optimal map decoding algorithms operating in the log domain," *IEEE International Conference on Communications*, pp. 1009–1013, 1995.

[279] J. Erfanian, S. Pasupathy, and G. Gulak, "Reduced complexity symbol dectectors with parallel structures for ISI channels," *IEEE Transactions on Communications*, vol. 42, pp. 1661–1671, 1994.

[280] S. Chen, B. Mulgrew, E.-S. Chng, and G. J. Gibson, "Space translation properties and the minimum-BER linear-combiner DFE," *IEE Proceedings on Communications*, vol. 145, pp. 316–322, October 1998.

[281] S. Chen, "Importance sampling simulation for evaluation the lower-bound BER of the bayesian DFE." submitted to IEEE Transactions on Communications.

[282] S. Chen, E.-S. Chng, B. Mulgrew, and G. J. Gibson, "Minimum-BER linear-combiner DFE," in *Proceedings of ICC'96*, (Dallas, Texas), pp. 1173–1177, 1996.

[283] S. Chen, S. Gunn, and C. J. Harris, "Decision feedback equalizer design using support vector machines," *IEE Proceedings Vision, Image and Signal Processing*, 2000. Accepted for publication.

[284] S. Chen and C. J. Harris, "Design of the optimal separating hyperplane for the decision feedback equalizer using support vector machine," in *Proceedings of IEEE International Conference on Accoustic, Speech and Signal Processing*, pp. 2701–2704, IEEE, June 5-9 2000.

[285] B. Sklar, "Rayleigh fading channels in mobile digital communication systems, part 1: Characterization," *IEEE Communications Magazine*, vol. 35, pp. 136–146, September 1997.

[286] C. H. Wong, *Wideband Adaptive Full Response Multilevel Transceivers and Equalizers*. PhD thesis, University of Southampton, United Kingdom, November 1999.

[287] W. Press, S. Teukolsky, W. Vetterling, and B. Flannery, *Numerical Recipes in C*. Cambridge: Cambridge University Press, 1992.

[288] R. Iltis, J. Shynk, and K. Giridhar, “Baysian algorithms for blind equalization using parallel adaptive filtering,” *IEEE Transactions on Communications*, vol. 43, pp. 1017–1032, February–April 1994.

[289] J. Rapeli, “UMTS:targets, system concept, and standardization in a global framework,” *IEEE Personal Communications*, vol. 2, pp. 20–28, February 1995.

[290] E. Berruto, M. Gudmundson, R. Menolascino, W. Mohr, and M. Pizarroso, “Research activities on UMTS radio interface, network architectures, and planning,” *IEEE Communications Magazine*, vol. 36, pp. 82–95, February 1998.

[291] T. Ojanperä and R. Prasad, “An overview of air interface multiple access for IMT-2000/UMTS,” *IEEE Communications Magazine*, vol. 36, pp. 82–95, September 1998.

[292] J. Hagenauer and P. Hoeher, “A Viterbi algorithm with soft-decision outputs and its applications,” in *IEEE Globecom*, pp. 1680–1686, 1989.

[293] M. Breiling and L. Hanzo, “Non-iterative optimum super-trellis decoding of turbo codes,” *Electronics Letters*, vol. 33, pp. 848–849, May 1997.

[294] M. Breiling and L. Hanzo, “Optimum non-iterative turbo-decoding,” in *IEEE International Symposium on Personal, Indoor and Mobile Radio Communications, PIMRC, 1997*, vol. 2, pp. 714–718, IEEE, 1997.

[295] P. Robertson, P. Hoeher, and E. Villebrun, “Optimal and sub-optimal maximum a posteriori algorithms suitable for turbo decoding,” *European Transactions on Telecommunications*, vol. 8, pp. 119–125, March/April 1997.

[296] J. Hagenauer, E. E. Offer, and L. Papke, “Iterative decoding of binary block and convolutional codes,” *IEEE Transactions on Information Theory*, pp. 429–437, 1996.

[297] A. Klein, R. Pirhonen, J. Sköld, and R. Suoranta, “FRAMES Multiple Access Mode1 - Wideband TDMA with and without spreading,” in *Proceedings of the IEEE International Symposium on Personal, Indoor and Mobile Radio Communications 1997*, (Helsinki, Finland), pp. 37–41, 1-4 September 1997.

[298] M. Gertsman and J. Lodge, “Symbol-by-symbol MAP demodulation of CPM and PSK signals on Rayleigh flat-fading channels,” *IEEE Transactions on Communications*, vol. 45, pp. 788–799, July 1997.

[299] D. Raphaeli and Y. Zarai, “Combined turbo equalization and turbo decoding,” *IEEE Communications Letters*, vol. 2, pp. 107–109, April 1998.

[300] A. Knickenberg, B. L. Yeap, J. Hamorsky, M. Breiling, and L. Hanzo, “Non-iterative joint channel equalisation and channel decoding,” in *Proceedings of Globecom’99*, (Rio de Janeiro, Brazil), pp. 442–446, 5-9 December 1999.

[301] G. Bauch, H. Khorram, and J. Hagenauer, “Iterative equalization and decoding in mobile communications systems,” in *European Personal Mobile Communications Conference*, (Bonn, Germany), pp. 301–312, 30 September - 2 October 1997.

[302] M. S. Yee and L. Hanzo, “Multi-level radial basis function network based equalisers for Rayleigh channels,” in *Proceedings of IEEE Vehicular Technology Conference*, (Houston, USA), pp. 707–711, IEEE, 16-19 May 1999.

[303] K. Abend, T. J. Harley Jr, B. D. Fritchman, and C. Gumacos, “On optimum receivers for channels having memory,” *IEEE Transactions Information Theory*, vol. IT-14, pp. 818–819, November 1968.

[304] M. S. Yee, T. H. Liew, and L. Hanzo, “Block turbo coded burst-by-burst adaptive radial basis function decision feedback equaliser assisted modems,” in *Proceedings of IEEE Vehicular Technology Conference*, vol. 3, (Amsterdam, Netherlands), pp. 1600–1604, September 1999.

[305] B. L. Yeap, C. H. Wong, and L. Hanzo, “Reduced complexity in-phase/quadrature-phase turbo equalisation,” in *IEEE International Communications Conference*, (Helsinki, Finland), pp. 393–397, 11 - 14 June 2001.

[306] B. L. Yeap, C. H. Wong, and L. Hanzo, “Reduced complexity in-phase/quadrature-phase turbo equalisation.” submitted to IEEE Journal on Selected Areas in Communication, 2000.

[307] L. Hanzo, W. Webb, and T. Keller, *Single- and Multi-carrier Quadrature Amplitude Modulation*. New York: John Wiley-IEEE Press, April 2000.

[308] A. Glavieux, C. Laot, and J. Labat, "Turbo Equalization over a frequency selective channel," in *Proceedings of the International Symposium on Turbo Codes & Related Topics*, (Brest, France), pp. 96–102, 3-5 September 1997.

[309] M. S. Yee, B. L. Yeap, and L. Hanzo, "Radial basis function assisted turbo equalisation," in *Proceedings of IEEE Vehicular Technology Conference*, (Japan, Tokyo), pp. 640–644, IEEE, 15-18 May 2000.

[310] G. Bauch, A. Naguib, and N. Seshadri, "MAP equalization of space-time coded signals over frequency selective channels," in *Proceedings of Wireless Communications and Networking Conference*, (New Orleans, USA), pp. 261–265, September 1999.

[311] B. L. Yeap, T. H. Liew, and L. Hanzo, "Turbo equalization of serially concatenated systematic convolutional codes and systematic space time trellis codes," in *Proceedings of the IEEE Vehicular Technology Conference*, (Rhodes, Greece), pp. 1464–1468, 6 - 9 May 2001.

[312] M. S. Yee, B. L. Yeap, and L. Hanzo, "Radial basis function assisted turbo equalisation," in *Proceedings of the IEEE Vehicular Technology Conference 2000*, (Tokyo, Japan), pp. 640–644, 15-18 May 2000.

[313] "Feature topic: Software radios," *IEEE Communications Magazine*, vol. 33, pp. 24–68, May 1995.

[314] A. Viterbi, *CDMA: Principles of Spread Spectrum Communication*. Reading MA, USA: Addison-Wesley, June 1995. ISBN 0201633744.

[315] L. Miller and J. Lee, *CDMA Systems Engineering Handbook*. London, UK: Artech House, 1998.

[316] A. Whalen, *Detection of signals in noise*. New York, USA: Academic Press, 1971.

[317] S. Verdú, "Minimum probability of error for asynchronous Gaussian multiple-access channel," *IEEE Transactions on Communications*, vol. 32, pp. 85–96, January 1986.

[318] R. Prasad, *Universal Wireless Personal Communications*. London, UK: Artech House Publishers, 1998.

[319] S. Glisic and B. Vucetic, *Spread Spectrum CDMA Systems for Wireless Communications*. London, UK: Artech House, April 1997. ISBN 0890068585.

[320] J. Thompson, P. Grant, and B. Mulgrew, "Smart antenna arrays for CDMA systems," *IEEE Personal Communications Magazine*, vol. 3, pp. 16–25, October 1996.

[321] J. Thompson, P. Grant, and B. Mulgrew, "Performance of antenna array receiver algorithms for CDMA," in *Proceedings of the IEEE Global Telecommunications Conference (GLOBECOM)*, (London, UK), pp. 570–574, 18–22 November 1996.

[322] A. Naguib and A. Paulraj, "Performance of wireless CDMA with m-ary orthogonal modulation and cell site antenna arrays," *IEEE Journal on Selected Areas in Communications*, vol. 14, pp. 1770–1783, December 1996.

[323] L. Godara, "Applications of antenna arrays to mobile communications, part I: Performance improvement, feasibility, and system considerations," *Proceedings of the IEEE*, vol. 85, pp. 1029–1060, July 1997.

[324] R. Kohno, H. Imai, M. Hatori, and S. Pasupathy, "Combination of adaptive array antenna and a canceller of interference for direct-sequence spread-specturn multiple-access system," *IEEE Journal on Selected Areas in Communications*, vol. 8, pp. 675–681, May 1998.

[325] S. Moshavi, "Multi-user detection for DS-CDMA communications," *IEEE Communications Magazine*, vol. 34, pp. 124–136, October 1996.

[326] R. Lupas and S. Verdú, "Linear multiuser detectors for synchronous code divison multiple access channels," *IEEE Transactions on Information Theory*, vol. 35, pp. 123–136, January 1989.

[327] R. Lupas and S. Verdú, "Near-far resistance of multiuser detectors in asynchronous channels," *IEEE Transactions on Communications*, vol. 38, pp. 509–519, April 1990.

[328] Z. Zvonar and D. Brady, "Suboptimal multiuser detector for frequency selective Rayleigh fading synchronous CDMA channels," *IEEE Transactions on Communications*, vol. 43, pp. 154–157, February–April. 1995.

[329] Z. Zvonar and D. Brady, "Differentially coherent multiuser detection in asynchronous CDMA flat Rayleigh fading channels," *IEEE Transactions on Communications*, vol. 43, pp. 1252–1255, February–April 1995.

[330] Z. Zvonar, "Combined multiuser detection and diversity reception for wireless CDMA systems," *IEEE Transactions on Vehicular Technology*, vol. 45, pp. 205–211, February 1996.

[331] T. Kawahara and T. Matsumoto, “Joint decorrelating multiuser detection and channel estimation in asynchronous cdma mobile communications channels,” *IEEE Transactions on Vehicular Technology*, vol. 44, pp. 506–515, August 1995.

[332] M. Hosseinian, M. Fattouche, and A. Sesay, “A multiuser detection scheme with pilot symbol-aided channel estimation for synchronous CDMA systems,” in *Proceedings of the IEEE Vehicular Technology Conference (VTC)*, (Ottawa, Canada), pp. 796–800, 18–21 May 1998.

[333] M. Juntti, B. Aazhang, and J. Lilleberg, “Iterative implementation of linear multiuser detection for dynamic asynchronous CDMA systems,” *IEEE Transactions on Communications*, vol. 46, pp. 503–508, April 1998.

[334] P.-A. Sung and K.-C. Chen, “A linear minimum mean square error multiuser receiver in Rayleigh fading channels,” *IEEE Journal on Selected Areas in Communications*, vol. 14, pp. 1583–1594, October 1996.

[335] A. Duel-Hallen, “Decorrelating decision-feedback multiuser detector for synchronous code-division multiple-access channel,” *IEEE Transactions on Communications*, vol. 41, pp. 285–290, February 1993.

[336] L. Wei and C. Schlegel, “Synchronous DS-SSMA system with improved decorrelating decision-feedback multiuser detection,” *IEEE Transactions on Vehicular Technology*, vol. 43, pp. 767–772, August 1994.

[337] A. Hafeez and W. Stark, “Combined decision-feedback multiuser detection/soft-decision decoding for CDMA channels,” in *Proceedings of the IEEE Vehicular Technology Conference (VTC)*, (Atlanta, GA, USA), pp. 382–386, 28 April–1 May 1996.

[338] A. Steil and J. Blanz, “Spectral efficiency of JD-CDMA mobile radio systems applying coherent receiver antenna diversity,” in *Proceedings of the International Symposium on Spread Spectrum Techniques and Applications (ISSSTA)*, (Mainz, Germany), pp. 313–319, 22–25 September 1996.

[339] P. Jung, M. Nasshan, and J. Blanz, “Application of turbo codes to a CDMA mobile radio system using joint detection and antenna diversity,” in *Proceedings of the IEEE Vehicular Technology Conference (VTC)*, (Stockholm, Sweden), pp. 770–774, 8–10 June 1994.

[340] P. Jung and M. Nasshan, “Results on turbo-codes for speech transmission in a joint detection CDMA mobile radio system with coherent receiver antenna diversity,” *IEEE Transactions on Vehicular Technology*, vol. 46, pp. 862–870, November 1997.

[341] M. Nasshan, A. Steil, A. Klein, and P. Jung, “Downlink cellular radio capacity of a joint detection CDMA mobile radio system,” in *Proceedings of the 45th IEEE Vehicular Technology Conference (VTC)*, (Chicago, USA), pp. 474–478, 25–28 July 1995.

[342] A. Klein, “Data detection algorithms specially designed for the downlink of CDMA mobile radio systems,” in *Proceedings of the IEEE Vehicular Technology Conference (VTC)*, (Phoenix, USA), pp. 203–207, 4–7 May 1997.

[343] B. Steiner and P. Jung, “Optimum and suboptimum channel estimation for the uplink of CDMA mobile radio systems with joint detection,” *European Transactions on Telecommunications*, vol. 5, pp. 39–50, 1994.

[344] M. Werner, “Multistage joint detection with decision feedback for CDMA mobile radio applications,” in *Proceedings of the IEEE International Symposium on Personal, Indoor and Mobile Radio Communications (PIMRC)*, pp. 178–183, 1994.

[345] M. Varanasi and B. Aazhang, “Multistage detection in asynchronous code-division multiple-access communications,” *IEEE Transactions on Communications*, vol. 38, pp. 509–519, April 1990.

[346] M. Varanasi, “Group detection for synchronous Gaussian code-division multiple-access channels,” *IEEE Transactions on Information Theory*, vol. 41, pp. 1083–1096, July 1995.

[347] M. Varanasi, “Parallel group detection for synchronous CDMA communication over frequency-selective Rayleigh fading channels,” *IEEE Transactions on Information Theory*, vol. 42, pp. 116–128, January 1996.

[348] Y. Yoon, R. Kohno, and H. Imai, “A SSMA system with cochannel interference cancellation with multipath fading channels,” *IEEE Journal on Selected Areas in Communications*, vol. 11, pp. 1067–1075, September 1993.

[349] T. Giallorenzi and S. Wilson, “Suboptimum multiuser receivers for convolutionally coded asynchronous DS-CDMA systems,” *IEEE Transactions on Communications*, vol. 44, pp. 1183–1196, September 1996.

[350] Y. Sanada and M. Nakagawa, “A multiuser interference cancellation technique utilizing convolutional codes and multicarrier modulation for wireless indoor communications,” *IEEE Journal on Selected Areas in Communications*, vol. 14, pp. 1500–1509, October 1996.

[351] M. Latva-aho, M. Juntti, and M. Heikkilä, "Parallel interference cancellation receiver for DS-CDMA systems in fading channels," in *Proceedings of the IEEE International Symposium on Personal, Indoor and Mobile Radio Communications (PIMRC)*, (Helsinki, Finland), pp. 559–564, 1–4 September 1997.

[352] D. Dahlhaus, A. Jarosch, B. Fleury, and R. Heddergott, "Joint demodulation in DS/CDMA systems exploiting the space and time diversity of the mobile radio channel," in *Proceedings of the IEEE International Symposium on Personal, Indoor and Mobile Radio Communications (PIMRC)*, (Helsinki, Finland), pp. 47–52, 1–4 September 1997.

[353] D. Divsalar, M. Simon, and D. Raphaeli, "Improved parallel interference cancellation for CDMA," *IEEE Transactions on Communications*, vol. 46, pp. 258–267, February 1998.

[354] P. Patel and J. Holtzman, "Analysis of a simple successive interference cancellation scheme in a DS/CDMA system," *IEEE Journal on Selected Areas in Communications*, vol. 12, pp. 796–807, June 1994.

[355] A. Soong and W. Krzymien, "A novel CDMA multi-user interference cancellation receiver with reference symbol aided estimation of channel parameters," *IEEE Journal on Selected Areas in Communications*, vol. 14, pp. 1536–1547, October 1996.

[356] A. Hui and K. Letaief, "Successive interference cancellation for multiuser asynchronous DS/CDMA detectors in multipath fading links," *IEEE Transactions on Communications*, vol. 46, pp. 384–391, March 1998.

[357] Y. Li and R. Steele, "Serial interference cancellation method for CDMA," *Electronics Letters*, vol. 30, pp. 1581–1583, September 1994.

[358] T. Oon, R. Steele, and Y. Li, "Cancellation frame size for a quasi-single-bit detector in asynchronous CDMA channel," *Electronics Letters*, vol. 33, pp. 258–259, February 1997.

[359] T.-B. Oon, R. Steele, and Y. Li, "Performance of an adaptive successive serial-parallel CDMA cancellation scheme in flat Rayleigh fading channels," in *Proceedings of the IEEE Vehicular Technology Conference (VTC)*, (Phoenix, USA), pp. 193–197, 4–7 May 1997.

[360] M. Sawahashi, Y. Miki, H. Andoh, and K. Higuchi, "Pilot symbol-assisted coherent multistage interference canceller using recursive channel estimation for DS-CDMA mobile radio," *IEICE Transactions on Communications*, vol. E79-B, pp. 1262–1269, September 1996.

[361] S. Sun, L. Rasmussen, H. Sugimoto, and T. Lim, "A hybrid interference canceller in CDMA," in *Proceedings of the IEEE International Symposium on Spread Spectrum Techniques and Applications (ISSSTA)*, (Sun City, South Africa), pp. 150–154, 2–4 September 1998.

[362] Y. Cho and J. Lee, "Analysis of an adaptive SIC for near-far resistant DS-CDMA," *IEEE Transactions on Communications*, vol. 46, pp. 1429–1432, November 1998.

[363] P. Agashe and B. Woerner, "Interference cancellation for a multicellular CDMA environment," *Wireless Personal Communications (Kluwer)*, vol. 3, no. 1–2, pp. 1–14, 1996.

[364] L. Rasmussen, T. Lim, and T. Aulin, "Breadth-first maximum likelihood detection in multiuser CDMA," *IEEE Transactions on Communications*, vol. 45, pp. 1176–1178, October 1997.

[365] L. Wei, L. Rasmussen, and R. Wyrwas, "Near optimum tree-search detection schemes for bit-synchronous multiuser CDMA systems over Gaussian and two-path Rayleigh fading channels," *IEEE Transactions on Communications*, vol. 45, pp. 691–700, June 1997.

[366] M. Nasiri-Kenari, R. Sylvester, and C. Rushforth, "Efficient soft-in-soft-out multiuser detector for synchronous CDMA with error-control coding," *IEEE Transactions on Vehicular Technology*, vol. 47, pp. 947–953, August 1998.

[367] J. Anderson and S. Mohan, "Sequential coding algorithms: a survey and cost analysis," *IEEE Transactions on Communications*, vol. 32, pp. 169–176, February 1984.

[368] C. Schlegel, S. Roy, P. Alexander, and Z.-J. Xiang, "Multiuser projection receivers," *IEEE Journal on Selected Areas in Communications*, vol. 14, pp. 1610–1618, October 1996.

[369] P. Alexander, L. Rasmussen, and C. Schlegel, "A linear receiver for coded multiuser CDMA," *IEEE Transactions on Communications*, vol. 45, pp. 605–610, May 1997.

[370] P. Rapajic and B. Vucetic, "Adaptive receiver structures for asynchornous CDMA systems," *IEEE Journal on Selected Areas in Communications*, vol. 12, pp. 685–697, May 1994.

[371] G. Woodward and B. Vucetic, "Adaptive detection for DS-CDMA," *Proceedings of the IEEE*, vol. 86, pp. 1413–1434, July 1998.

[372] Z. Xie, R. Short, and C. Rushforth, "Family of suboptimum detectors for coherent multiuser communications," *IEEE Journal on Selected Areas in Communications*, vol. 8, pp. 683–690, May 1990.

[373] T. Lim, L. Rasmussen, and H. Sugimoto, "An asynchronous multiuser CDMA detector based on the kalman filter," *IEEE Journal on Selected Areas in Communications*, vol. 16, pp. 1711–1722, December 1998.

[374] P. Seite and J. Tardivel, "Adaptive equalizers for joint detection in an indoor CDMA channel," in *Proceedings of the IEEE Vehicular Technology Conference (VTC)*, (Chicago, USA), pp. 484–488, 25–28 July 1995.

[375] G. Povey, P. Grant, and R. Pringle, "A decision-directed spread-spectrum RAKE receiver for fast-fading mobile channels," *IEEE Transactions on Vehicular Technology*, vol. 45, pp. 491–502, August 1996.

[376] H. Liu and K. Li, "A decorrelating RAKE receiver for CDMA communications over frequency-selective fading channels," *IEEE Transactions on Communications*, vol. 47, pp. 1036–1045, July 1999.

[377] Z. Xie, C. Rushforth, R. Short, and T. Moon, "Joint signal detection and parameter estimation in multiuser communications," *IEEE Transactions on Communications*, vol. 41, pp. 1208–1216, August 1993.

[378] N. Seshadri, "Joint data and channel estimation using blind trellis search techniques," *IEEE Transactions on Communications*, vol. 42, pp. 1000–1011, February/March/April 1994.

[379] A. Polydoros, R. Raheli, and C. Tzou, "Per–survivor processing: a general approach to MLSE in uncertain environments," *IEEE Transactions on Communications*, vol. COM–43, pp. 354–364, February–April 1995.

[380] R. Raheli, G. Marino, and P. Castoldi, "Per-survivor processing and tentative decisions: What is in between?," *IEEE Transactions on Communications*, vol. 44, pp. 127–129, February 1998.

[381] T. Moon, Z. Xie, C. Rushforth, and R. Short, "Parameter estimation in a multi-user communication system," *IEEE Transactions on Communications*, vol. 42, pp. 2553–2560, August 1994.

[382] R. Iltis and L. Mailaender, "Adaptive multiuser detector with joint amplitude and delay estimation," *IEEE Journal on Selected Areas in Communications*, vol. 12, pp. 774–785, June 1994.

[383] U. Mitra and H. Poor, "Adaptive receiver algorithms for near-far resistant CDMA," *IEEE Transactions on Communications*, vol. 43, pp. 1713–1724, February–April 1995.

[384] U. Mitra and H. Poor, "Analysis of an adaptive decorrelating detector for synchronous CDMA," *IEEE Transactions on Communications*, vol. 44, pp. 257–268, February 1996.

[385] X. Wang and H. Poor, "Blind equalization and multiuser detection in dispersive CDMA channels," *IEEE Transactions on Communications*, vol. 46, pp. 91–103, January 1998.

[386] X. Wang and H. Poor, "Blind multiuser detection: a subspace approach," *IEEE Transactions on Information Theory*, vol. 44, pp. 677–690, March 1998.

[387] M. Honig, U. Madhow, and S. Verdú, "Blind adaptive multiuser detection," *IEEE Transactions on Information Theory*, vol. 41, pp. 944–960, July 1995.

[388] N. Mandayam and B. Aazhang, "Gradient estimation for sensitivity analysis and adaptive multiuser interference rejection in code division multiple access systems," *IEEE Transactions on Communications*, vol. 45, pp. 848–858, July 1997.

[389] S. Ulukus and R. Yates, "A blind adaptive decorrelating detector for CDMA systems," *IEEE Journal on Selected Areas in Communications*, vol. 16, no. 8, pp. 1530–1541, 1998.

[390] T. Lim and L. Rasmussen, "Adaptive symbol and parameter estimation in asynchronous multiuser CDMA detectors," *IEEE Transactions on Communications*, vol. 45, pp. 213–220, February 1997.

[391] J. Míguez and L. Castedo, "A linearly constrained constant modulus approach to blind adaptive multiuser interference suppression," *IEEE Communications Letters*, vol. 2, pp. 217–219, August 1998.

[392] D. Godard, "Self–recovering equalization and carrier tracking in two–dimensional data communication systems," *IEEE Transactions on Communications*, vol. COM–28, pp. 1867–1875, November 1980.

[393] K. Wesolowsky, "Analysis and properties of the modified constant modulus algorithm for blind equalization," *European Transactions on Telecommunication*, vol. 3, pp. 225–230, May–June 1992.

[394] K. Fukawa and H. Suzuki, "Orthogonalizing matched filtering (OMF) detector for DS-CDMA mobile communication systems," *IEEE Transactions on Vehicular Technology*, vol. 48, pp. 188–197, January 1999.

[395] U. Fawer and B. Aazhang, "Multiuser receiver for code division multiple access communications over multipath channels," *IEEE Transactions on Communications*, vol. 43, pp. 1556–1565, February–April 1995.

[396] Y. Bar-Ness, "Asynchronous multiuser CDMA detector made simpler: Novel decorrelator, combiner, canceller, combiner (DC^3) structure," *IEEE Transactions on Communications*, vol. 47, pp. 115–122, January 1999.

[397] K. Yen and L. Hanzo, "Hybrid genetic algorithm based multi-user detection schemes for synchronous CDMA systems," in *submitted to the IEEE Vehicular Technology Conference (VTC)*, (Tokyo, Japan), 2000.

[398] W. Jang, B. Vojčić, and R. Pickholtz, "Joint transmitter-receiver optimization in synchronous multiuser communications over multipath channels," *IEEE Transactions on Communications*, vol. 46, pp. 269–278, February 1998.

[399] B. Vojčić and W. Jang, "Transmitter precoding in synchronous multiuser communications," *IEEE Transactions on Communications*, vol. 46, pp. 1346–1355, October 1998.

[400] R. Tanner and D. Cruickshank, "Receivers for nonlinearly separable scenarios in DS-CDMA," *Electronics Letters*, vol. 33, pp. 2103–2105, December 1997.

[401] R. Tanner and D. Cruickshank, "RBF based receivers for DS-CDMA with reduced complexity," in *Proceedings of the IEEE International Symposium on Spread Spectrum Techniques and Applications (ISSSTA)*, (Sun City, South Africa), pp. 647–651, 2–4 September 1998.

[402] C. Berrou, P. Adde, E. Angui, and S. Faudeil, "A low complexity soft-output viterbi decoder architecture," in *Proceedings of the International Conference on Communications*, pp. 737–740, May 1993.

[403] T. Giallorenzi and S. Wilson, "Multiuser ML sequence estimator for convolutionally coded asynchronous DS-CDMA systems," *IEEE Transactions on Communications*, vol. 44, pp. 997–1008, August 1996.

[404] M. Moher, "An iterative multiuser decoder for near-capacity communications," *IEEE Transactions on Communications*, vol. 46, pp. 870–880, July 1998.

[405] M. Moher and P. Guinaud, "An iterative algorithm for asynchronous coded multiuser detection," *IEEE Communications Letters*, vol. 2, pp. 229–231, August 1998.

[406] P. Alexander, A. Grant, and M. Reed, "Iterative detection in code-division multiple-access with error control coding," *European Transactions on Telecommunications*, vol. 9, pp. 419–426, September–October 1998.

[407] P. Alexander, M. Reed, J. Asenstorfer, and C. Schlegel, "Iterative multiuser interference reduction: Turbo CDMA," *IEEE Transactions on Communications*, vol. 47, pp. 1008–1014, July 1999.

[408] M. Reed, C. Schlegel, P. Alexander, and J. Asenstorfer, "Iterative multiuser detection for CDMA with FEC: Near-single-user performance," *IEEE Transactions on Communications*, vol. 46, pp. 1693–1699, December 1998.

[409] X. Wang and H. Poor, "Iterative (turbo) soft interference cancellation and decoding for coded CDMA," *IEEE Transactions on Communications*, vol. 47, pp. 1046–1061, July 1999.

[410] K. Gilhousen, I. Jacobs, R. Padovani, A. Viterbi, L. Weaver Jr., and C. Wheatley III, "On the capacity of a cellular CDMA system," *IEEE Transactions on Vehicular Technology*, vol. 40, pp. 303–312, May 1991.

[411] T. Keller and L. Hanzo, "Blind-detection assisted sub-band adaptive turbo-coded OFDM schemes," in *Proceeding of VTC'99 (Spring)*, (Houston, TX, USA), pp. 489–493, IEEE, 16–20 May 1999.

[412] M. Yee and L. Hanzo, "Multi-level Radial Basis Function network based equalisers for Rayleigh channel," in *Proceeding of VTC'99 (Spring)*, (Houston, TX, USA), pp. 707–711, IEEE, 16–20 May 1999.

[413] T. Ojanperä, A. Klein, and P.-O. Anderson, "FRAMES multiple access for UMTS," *IEE Colloquium (Digest)*, pp. 7/1–7/8, May 1997.

[414] M. Failli, "Digital land mobile radio communications COST 207," tech. rep., European Commission, 1989.

[415] F. Adachi, M. Sawahashi, and K. Okawa, "Tree-structured generation of orthogonal spreading codes with different lengths for forward link of DS-CDMA mobile radio," *Electronics Letters*, vol. 33, pp. 27–28, January 1997.

[416] A. Toskala, J. Castro, E. Dahlman, M. Latva-aho, and T. Ojanperä, "FRAMES FMA2 wideband-CDMA for UMTS," *European Transactions on Telecommunications*, vol. 9, pp. 325–336, July–August 1998.

[417] P. Bello, "Selective fading limitations of the KATHRYN modem and some system design considerations," *IEEE Trabsactions on Communications Technology*, vol. COM–13, pp. 320–333, September 1965.

[418] M. Zimmermann and A. Kirsch, "The AN/GSC-10/KATHRYN/variable rate data modem for HF radio," *IEEE Transactions on Communication Technology*, vol. CCM–15, pp. 197–205, April 1967.

[419] E. Powers and M. Zimmermann, “A digital implementation of a multichannel data modem,” in *Proceedings of the IEEE International Conference on Communications*, (Philadelphia, USA), 1968.

[420] R. W. Chang, “Synthesis of band-limited orthogonal signals for multichannel data transmission,” *Bell Systems Technical Journal*, vol. 46, pp. 1775–1796, December 1966.

[421] R. Chang and R. Gibby, “A theoretical study of performance of an orthogonal multiplexing data transmission scheme,” *IEEE Transactions on Communication Technology*, vol. COM–16, pp. 529–540, August 1968.

[422] B. R. Saltzberg, “Performance of an efficient parallel data transmission system,” *IEEE Transactions on Communication Technology*, pp. 805–813, December 1967.

[423] S. B. Weinstein and P. M. Ebert, “Data transmission by frequency division multiplexing using the discrete fourier transform,” *IEEE Transactions on Communication Technology*, vol. COM–19, pp. 628–634, October 1971.

[424] B. Hirosaki, “An analysis of automatic equalizers for orthogonally multiplexed QAM systems,” *IEEE Transactions on Communications*, vol. COM-28, pp. 73–83, January 1980.

[425] A. Peled and A. Ruiz, “Frequency domain data transmission using reduced computational complexity algorithms,” in *Proceedings of International Conference on Acoustics, Speech, and Signal Processing, ICASSP’80*, vol. 3, (Denver, CO, USA), pp. 964–967, IEEE, 9–11 April 1980.

[426] B. Hirosaki, “An orthogonally multiplexed QAM system using the discrete fourier transform,” *IEEE Transactions on Communications*, vol. COM-29, pp. 983–989, July 1981.

[427] H. Kolb, “Untersuchungen über ein digitales mehrfrequenzverfahren zur datenübertragung,” in *Ausgewählte Arbeiten über Nachrichtensysteme*, no. 50, Universität Erlangen-Nürnberg, 1982.

[428] H. Schüssler, “Ein digitales Mehrfrequenzverfahren zur Datenübertragung,” in *Professoren-Konferenz, Stand und Entwicklungsaussichten der Daten und Telekommunikation*, (Darmstadt, Germany), pp. 179–196, 1983.

[429] K. Preuss, “Ein Parallelverfahren zur schnellen Datenübertragung Im Ortsnetz,” in *Ausgewählte Arbeiten über Nachrichtensysteme*, no. 56, Universität Erlangen-Nürnberg, 1984.

[430] R. Rückriem, “Realisierung und messtechnische Untersuchung an einem digitalen Parallelverfahren zur Datenübertragung im Fernsprechkanal,” in *Ausgewählte Arbeiten über Nachrichtensysteme*, no. 59, Universität Erlangen-Nürnberg, 1985.

[431] L. Cimini, “Analysis and simulation of a digital mobile channel using orthogonal frequency division multiplexing,” *IEEE Transactions on Communications*, vol. 33, pp. 665–675, July 1985.

[432] K. Fazel and G. Fettweis, eds., *Multi-Carrier Spread-Spectrum*. Dordrecht: Kluwer, 1997. ISBN 0-7923-9973-0.

[433] F. Classen and H. Meyr, “Synchronisation algorithms for an OFDM system for mobile communications,” in *Codierung für Quelle, Kanal und Übertragung*, no. 130 in ITG Fachbericht, (Berlin), pp. 105–113, VDE–Verlag, 1994.

[434] F. Classen and H. Meyr, “Frequency synchronisation algorithms for OFDM systems suitable for communication over frequency selective fading channels,” in *Proceedings of IEEE VTC ’94*, (Stockholm, Sweden), pp. 1655–1659, IEEE, 8–10 June 1994.

[435] S. Shepherd, P. van Eetvelt, C. Wyatt-Millington, and S. Barton, “Simple coding scheme to reduce peak factor in QPSK multicarrier modulation,” *Electronics Letters*, vol. 31, pp. 1131–1132, July 1995.

[436] A. E. Jones, T. A. Wilkinson, and S. K. Barton, “Block coding scheme for reduction of peak to mean envelope power ratio of multicarrier transmission schemes,” *Electronics Letters*, vol. 30, pp. 2098–2099, December 1994.

[437] D. Wulich, “Reduction of peak to mean ratio of multicarrier modulation by cyclic coding,” *Electronics Letters*, vol. 32, pp. 432–433, 1996.

[438] S. Müller and J. Huber, “Vergleich von OFDM–Verfahren mit reduzierter Spitzenleistung,” in *2. OFDM–Fachgespräch in Braunschweig*, 1997.

[439] M. Pauli and H.-P. Kuchenbecker, “Neue Aspekte zur Reduzierung der durch Nichtlinearitäten hervorgerufenen Außerbandstrahlung eines OFDM–Signals,” in *2. OFDM–Fachgespräch in Braunschweig*, 1997.

[440] T. May and H. Rohling, “Reduktion von Nachbarkanalstörungen in OFDM–Funkübertragungssystemen,” in *2. OFDM–Fachgespräch in Braunschweig*, 1997.

[441] D. Wulich, “Peak factor in orthogonal multicarrier modulation with variable levels,” *Electronics Letters*, vol. 32, no. 20, pp. 1859–1861, 1996.

[442] H. Schmidt and K. Kammeyer, “Adaptive Subträgerselektion zur Reduktion des Crest faktors bei OFDM,” in *3. OFDM Fachgespräch in Braunschweig*, 1998.

[443] R. Dinis and A. Gusmao, “Performance evaluation of OFDM transmission with conventional and 2-branch combining power amplification schemes,” in *Proceeding of IEEE Global Telecommunications Conference, Globecom 96*, (London, UK), pp. 734–739, IEEE, 18–22 November 1996.

[444] R. Dinis, P. Montezuma, and A. Gusmao, “Performance trade-offs with quasi-linearly amplified OFDM through a 2-branch combining technique,” in *Proceedings of IEEE VTC'96*, (Atlanta, GA, USA), pp. 899–903, IEEE, 28 April–1 May 1996.

[445] R. Dinis, A. Gusmao, and J. Fernandes, “Adaptive transmission techniques for the mobile broadband system,” in *Proceeding of ACTS Mobile Communication Summit '97*, (Aalborg, Denmark), pp. 757–762, ACTS, 7–10 October 1997.

[446] B. Daneshrad, L. Cimini Jr., and M. Carloni, “Clustered-OFDM transmitter implementation,” in *Proceedings of IEEE International Symposium on Personal, Indoor, and Mobile Radio Communications (PIMRC'96)*, (Taipei, Taiwan), pp. 1064–1068, IEEE, 15–18 October 1996.

[447] M. Okada, H. Nishijima, and S. Komaki, “A maximum likelihood decision based nonlinear distortion compensator for multi-carrier modulated signals,” *IEICE Transactions on Communications*, vol. E81B, no. 4, pp. 737–744, 1998.

[448] R. Dinis and A. Gusmao, “Performance evaluation of a multicarrier modulation technique allowing strongly nonlinear amplification,” in *Proceedings of ICC 1998*, pp. 791–796, IEEE, 1998.

[449] T. Pollet, M. van Bladel, and M. Moeneclaey, “BER sensitivity of OFDM systems to carrier frequency offset and wiener phase noise,” *IEEE Transactions on Communications*, vol. 43, pp. 191–193, February/March/April 1995.

[450] H. Nikookar and R. Prasad, “On the sensitivity of multicarrier transmission over multipath channels to phase noise and frequency offset,” in *Proceedings of IEEE International Symposium on Personal, Indoor, and Mobile Radio Communications (PIMRC'96)*, (Taipei, Taiwan), pp. 68–72, IEEE, 15–18 October 1996.

[451] J. Kuronen, V.-P. Kaasila, and A. Mammela, “An all-digital symbol tracking algorithm in an OFDM system by using the cyclic prefix,” in *Proc. ACTS Summit '96*, (Granada, Spain), pp. 340–345, 27–29 November 1996.

[452] M. Kiviranta and A. Mammela, “Coarse frame synchronization structures in OFDM,” in *Proc. ACTS Summit '96*, (Granada, Spain), pp. 464–470, 27–29 November 1996.

[453] Z. Li and A. Mammela, “An all digital frequency synchronization scheme for OFDM systems,” in *Proceedings of the IEEE International Symposium on Personal, Indoor and Mobile Radio Communications (PIMRC)*, (Helsinki, Finland), pp. 327–331, 1–4 September 1997.

[454] W. Warner and C. Leung, “OFDM/FM frame synchronization for mobile radio data communication,” *IEEE Transactions on Vehicular Technology*, vol. 42, pp. 302–313, August 1993.

[455] H. Sari, G. Karam, and I. Jeanclaude, “Transmission techniques for digital terrestrial TV broadcasting,” *IEEE Communications Magazine*, pp. 100–109, February 1995.

[456] P. Moose, “A technique for orthogonal frequency division multiplexing frequency offset correction,” *IEEE Transactions on Communications*, vol. 42, pp. 2908–2914, October 1994.

[457] K. Brüninghaus and H. Rohling, “Verfahren zur Rahmensynchronisation in einem OFDM-System,” in *3. OFDM Fachgespräch in Braunschweig*, 1998.

[458] F. Daffara and O. Adami, “A new frequency detector for orthogonal multicarrier transmission techniques,” in *Proceedings of IEEE Vehicular Technology Conference (VTC'95)*, (Chicago, USA), pp. 804–809, IEEE, 15–28 July 1995.

[459] M. Sandell, J.-J. van de Beek, and P. Börjesson, “Timing and frequency synchronisation in OFDM systems using the cyclic prefix,” in *Proceedings of International Symposium on Synchronisation*, (Essen, Germany), pp. 16–19, 14–15 December 1995.

[460] A. Chouly, A. Brajal, and S. Jourdan, “Orthogonal multicarrier techniques applied to direct sequence spread spectrum CDMA systems,” in *Proceedings of the IEEE Global Telecommunications Conference 1993*, (Houston, TX, USA), pp. 1723–1728, 29 November – 2 December 1993.

[461] G. Fettweis, A. Bahai, and K. Anvari, "On multi-carrier code division multiple access (MC-CDMA) modem design," in *Proceedings of IEEE VTC '94*, (Stockholm, Sweden), pp. 1670–1674, IEEE, 8–10 June 1994.

[462] R. Prasad and S. Hara, "Overview of multicarrier CDMA," *IEEE Communications Magazine*, pp. 126–133, December 1997.

[463] Y. Li and N. Sollenberger, "Interference suppression in OFDM systems using adaptive antenna arrays," in *Proceeding of Globecom'98*, (Sydney, Australia), pp. 213–218, IEEE, 8–12 November 1998.

[464] Y. Li and N. Sollenberger, "Adaptive antenna arrays for OFDM systems with cochannel interference," *IEEE Transactions on Communications*, vol. 47, pp. 217–229, February 1999.

[465] Y. Li, L. Cimini, and N. Sollenberger, "Robust channel estimation for OFDM systems with rapid dispersive fading channels," *IEEE Transactions on Communications*, vol. 46, pp. 902–915, April 1998.

[466] L. Lin, L. Cimini Jr., and J.-I. Chuang, "Turbo codes for OFDM with antenna diversity," in *Proceeding of VTC'99 (Spring)*, (Houston, TX, USA), IEEE, 16–20 May 1999.

[467] C. Kim, S. Choi, and Y. Cho, "Adaptive beamforming for an OFDM sytem," in *Proceeding of VTC'99 (Spring)*, (Houston, TX, USA), IEEE, 16–20 May 1999.

[468] M. Münster, T. Keller, and L. Hanzo, "Co–channel interference suppression assisted adaptive OFDM in interference limited environments," in *Proceeding of VTC'99 (Fall)*, vol. 1, (Amsterdam, Netherlands), pp. 284–288, IEEE, 19–22 September 1999.

[469] F. Mueller-Roemer, "Directions in audio broadcasting," *Journal Audio Engineering Society*, vol. 41, pp. 158–173, March 1993.

[470] G. Plenge, "DAB — a new radio broadcasting system — state of development and ways for its introduction," *Rundfunktech. Mitt.*, vol. 35, no. 2, 1991.

[471] M. Alard and R. Lassalle, "Principles of modulation and channel coding for digital broadcasting for mobile receivers," *EBU Review, Technical No. 224*, pp. 47–69, August 1987.

[472] *Proceedings of 1st International Symposium,DAB*, (Montreux, Switzerland), June 1992.

[473] ETSI, *Digital Audio Broadcasting (DAB)*, 2nd ed., May 1997. ETS 300 401.

[474] ETSI, *Digital Video Broadcasting (DVB)*, 1.1.2 ed., August 1997. EN 300 744.

[475] S. O'Leary and D. Priestly, "Mobile broadcasting of DVB-T signals," *IEEE Transactions on Broadcasting*, vol. 44, pp. 346–352, September 1998.

[476] W.-C. Lee, H.-M. Park, K.-J. Kang, and K.-B. Kim, "Performance analysis of viterbi decoder using channel state information in COFDM system," *IEEE Transactions on Broadcasting*, vol. 44, pp. 488–496, December 1998.

[477] S. O'Leary, "Hierarchical transmission and COFDM systems," *IEEE Transactions on Broadcasting*, vol. 43, pp. 166–174, June 1997.

[478] L. Thibault and M. Le, "Performance evaluation of COFDM for digital audoo broadcasting Part I: parametric study," *IEEE Transactions on Broadcasting*, vol. 43, pp. 64–75, March 1997.

[479] P. Chow, J. Tu, and J. Cioffi, "A discrete multitone transceiver system for HDSL applications," *IEEE journal on selected areas in communications*, vol. 9, pp. 895–908, August 1991.

[480] P. Chow, J. Tu, and J. Cioffi, "Performance evaluation of a multichannel transceiver system for ADSL and VHDSL services," *IEEE journal on selected areas in communications*, vol. 9, pp. 909–919, August 1991.

[481] K. Sistanizadeh, P. Chow, and J. Cioffi, "Multi-tone transmission for asymmetric digital subscriber lines (ADSL)," in *Proceedings of ICC'93*, pp. 756–760, IEEE, 1993.

[482] ANSI, *ANSI/T1E1.4/94-007, Asymmetric Digital Subscriber Line (ADSL) Metallic Interface.*, August 1997.

[483] A. Burr and P. Brown, "Application of OFDM to powerline telecommunications," in *3rd International Symposium On Power-Line Communications*, (Lancaster, UK), 30 March – 1 April 1999.

[484] M. Deinzer and M. Stoger, "Integrated PLC-modem based on OFDM," in *3rd International Symposium On Power-Line Communications*, (Lancaster, UK), 30 March – 1 April 1999.

[485] R. Prasad and H. Harada, "A novel OFDM based wireless ATM system for future broadband multimedia communications," in *Proceeding of ACTS Mobile Communication Summit '97*, (Aalborg, Denmark), pp. 757–762, ACTS, 7–10 October 1997.

[486] C. Ciotti and J. Borowski, “The AC006 MEDIAN project — overview and state–of–the–art,” in *Proc. ACTS Summit ’96*, (Granada, Spain), pp. 362–367, 27–29 November 1996.

[487] J. Borowski, S. Zeisberg, J. Hübner, K. Koora, E. Bogenfeld, and B. Kull, “Performance of OFDM and comparable single carrier system in MEDIAN demonstrator 60GHz channel,” in *Proceeding of ACTS Mobile Communication Summit ’97*, (Aalborg, Denmark), pp. 653–658, ACTS, 7–10 October 1997.

[488] M. D. Benedetto, P. Mandarini, and L. Piazzo, “Effects of a mismatch in the in–phase and in–quadrature paths, and of phase noise, in QDCPSK-OFDM modems,” in *Proceeding of ACTS Mobile Communication Summit ’97*, (Aalborg, Denmark), pp. 769–774, ACTS, 7–10 October 1997.

[489] T. Rautio, M. Pietikainen, J. Niemi, J. Rautio, K. Rautiola, and A. Mammela, “Architecture and implementation of the 150 Mbit/s OFDM modem (invited paper),” in *IEEE Benelux Joint Chapter on Communications and Vehicular Technology, 6th Symposium on Vehicular Technology and Communications*, (Helsinki, Finland), p. 11, 12–13 October 1998.

[490] J. Ala-Laurila and G. Awater, “The magic WAND — wireless ATM network demondtrator system,” in *Proceeding of ACTS Mobile Communication Summit ’97*, (Aalborg, Denmark), pp. 356–362, ACTS, 7–10 October 1997.

[491] J. Aldis, E. Busking, T. Kleijne, R. Kopmeiners, R. van Nee, R. Mann-Pelz, and T. Mark, “Magic into reality, building the WAND modem,” in *Proceeding of ACTS Mobile Communication Summit ’97*, (Aalborg, Denmark), pp. 775–780, ACTS, 7–10 October 1997.

[492] E. Hallmann and H. Rohling, “OFDM-Vorschläge für UMTS,” in *3. OFDM Fachgespräch in Braunschweig*, 1998.

[493] “Universal mobile telecommunications system (UMTS); UMTS terrestrial radio access (UTRA); concept evaluation,” tech. rep., ETSI, 1997. TR 101 146.

[494] ETSI, *CEPT Recommendation TIR 22-06, Harmonized radio frequency bands for HIPERLAN systems*. European Telecommunications Standards Institute, Sophia Antipolis, Cedex, France, January 1998.

[495] ETSI, *ETSI TR 101 683, vO.1.2, Broadband Radio Access networks (BRAN); High Performance Radio Local Area Networks (HIPERLAN) Type 2, System Overview*. European Telecommunications Standards Institute, Sophia Antipolis, Cedex, France, 1999.

[496] N. Prasad and H. Teunissen, “A state-of-the-art of HIPERLAN/2,” in *Proceeding of VTC’99 (Fall)*, (Amsterdam, Netherlands), pp. 2661–2665, IEEE, 19–22 September 1999.

[497] R. van Nee and R. Prasad, *OFDM for wireless multimedia communications*. London: Artech House Publishers, 2000.

[498] K. Fazel, S. Kaiser, P. Robertson, and M. Ruf, “A concept of digital terrestrial television broadcasting,” *Wireless Personal Communications*, vol. 2, pp. 9–27, 1995.

[499] J. Bingham, “Method and apparatus for correcting for clock and carrier frequency offset, and phase jitter in multicarrier modems.” U.S. Patent No. 5206886, 27 April 1993.

[500] T. de Couasnon, R. Monnier, and J. Rault, “OFDM for digital TV broadcasting,” *Signal Processing*, vol. 39, pp. 1–32, 1994.

[501] A. Garcia and M. Calvo, “Phase noise and sub–carrier spacing effects on the performance of an OFDM communications system,” *IEEE Communications Letters*, vol. 2, pp. 11–13, January 1998.

[502] W. Robins, *Phase Noise in signal sources*, vol. 9 of *IEE Telecommunication series*. Peter Peregrinus Ltd., 1982.

[503] T. Keller, “Orthogonal frequency division multiplex techniques for wireless local area networks,” 1996. Internal Report.

[504] S.-G. Chua and A. Goldsmith, “Variable-rate variable-power mQAM for fading channels,” in *Proceedings of IEEE VTC’96*, (Atlanta, GA, USA), pp. 815–819, IEEE, 28 April–1 May 1996.

[505] T. Keller and L. Hanzo, “Sub–band adaptive pre–equalised OFDM transmission,” in *Proceeding of VTC’99 (Fall)*, (Amsterdam, Netherlands), pp. 334–338, IEEE, 19–22 September 1999.

[506] T. Liew and L. Hanzo, “Space-time block codes and concatenated channel codes for wireless communications,” *to appear in the Proceedings of the IEEE*, February 2002.

[507] V. Tarokh, H. Jafarkhani, and A. Calderbank, "Space-time block codes from orthogonal designs," *IEEE Transactions on Information Theory*, vol. 45, pp. 1456–1467, May 1999.

[508] N. Seshadri, V. Tarokh, and A. Calderbank, "Space-time codes for high data rate wireless communications: Code construction," in *Proceedings of IEEE Vehicular Technology Conference '97*, (Phoenix, Arizona), pp. 637–641, 1997.

[509] V. Tarokh, N. Seshadri, and A. Calderbank, "Space-time codes for high data rate wireless communications: Performance criterion and code construction," in *Proc IEEE International Conference on Communications '97*, (Montreal, Canada), pp. 299–303, 1997.

[510] V. Tarokh, A. Naguib, N. Seshadri, and A. Calderbank, "Space-time codes for high data rate wireless communications: Mismatch analysis," in *Proc IEEE International Conference on Communications '97*, (Montreal, Canada), pp. 309–313, 1997.

[511] A. F. Naguib, V. Tarokh, N. Seshadri, and A. R. Calderbank, "A space-time coding modem for high-data-rate wireless communications," *IEEE Journal on Selected Areas in Communications*, vol. 16, pp. 1459–1478, October 1998.

[512] V. Tarokh, A. Naguib, N. Seshadri, and A. R. Calderbank, "Space-time codes for high data rate wireless communication: Performance criteria in the presence of channel estimation errors, mobility, and multile paths," *IEEE Transactions on Communications*, vol. 47, pp. 199–207, February 1999.

[513] R. Horn and C. Johnson, *Matrix Analysis*. New York: Cambridge University Press, 1988.

[514] G. Bauch and N. Al-Dhahir, "Reduced-complexity turbo equalization with multiple transmit and receive antennas over multipath fading channels," in *Proceedings of Information Sciences and Systems*, (Princeton, USA), pp. WP3 13–18, March 2000.

[515] D. Agrawal, V. Tarokh, A. Naguib, and N. Seshadri, "Space-time coded OFDM for high data-rate wireless communication over wideband channels," in *Proceedings of IEEE Vehicular Technology Conference*, (Ottawa, Canada), pp. 2232–2236, May 1998.

[516] Y. Li, N. Seshadri, and S. Ariyavisitakul, "Channel estimation for OFDM systems with transmitter diversity in mobile wireless channels," *IEEE Journal on Selected Areas in Communications*, vol. 17, pp. 461–471, March 1999.

[517] Y. Li, J. Chuang, and N. Sollenberger, "Transmitter diversity for OFDM systems and its impact on high-rate data wireless networks," *IEEE Journal on Selected Areas in Communications*, vol. 17, pp. 1233–1243, July 1999.

[518] W.-J. Choi and J. Cioffi, "Space-time block codes over frequency selective fading channels," in *Proceedings of VTC 1999 Fall*, (Amsterdam, Holland), pp. 2541–2545, 19-22 September 1999.

[519] Z. Liu, G. Giannakis, A. Scaglione, and S. Barbarossa, "Block precoding and transmit-antenna diversity for decoding and equalization of unknown multipath channels," in *Proc 33rd Asilomar Conference Signals, Systems and Computers*, (Pacific Grove, Canada), pp. 1557–1561, 1-4 November 1999.

[520] Z. Liu and G. Giannakis, "Space-time coding with transmit antennas for multiple access regardless of frequency-selective multipath," in *Proc 1st Sensor Array and Multichannel SP Workshop*, (Boston, USA), 15-17 March 2000.

[521] T. Liew, J. Pliquett, B. Yeap, L.-L. Yang, and L. Hanzo, "Comparative study of space time block codes and various concatenated turbo coding schemes," in *PIMRC 2000*, (London, UK), pp. 741–745, 18-21 September 2000.

[522] T. Liew, J. Pliquett, B. Yeap, L.-L. Yang, and L. Hanzo, "Concatenated space time block codes and TCM, turbo TCM, convolutional as well as turbo codes," in *GLOBECOM 2000*, (San Francisco, USA), 27 Nov -1 Dec 2000.

[523] G. Bauch, "Concatenation of space-time block codes and Turbo-TCM," in *Proceedings of IEEE International Conference on Communications*, (Vancouver, Canada), pp. 1202–1206, June 1999.

[524] G. Forney, "The Viterbi algorithm," *Proceedings of the IEEE*, vol. 61, pp. 268–278, March 1973.

[525] J. Torrance and L. Hanzo, "Performance upper bound of adaptive QAM in slow Rayleigh-fading environments," in *Proceedings of IEEE ICCS'96/ISPACS'96*, (Singapore), pp. 1653–1657, IEEE, 25–29 November 1996.

[526] H. Matsuako, S. Sampei, N. Morinaga, and Y. Kamio, "Adaptive modulation systems with variable coding rate concatenated code for high quality multi-media communication systems," in *Proceedings of IEEE Vehicular Technology Conference*, (Atlanta, USA), pp. 487–491, April 1996.

[527] J. Torrance and L. Hanzo, "On the upper bound performance of adaptive QAM in a slow Rayleigh fading," *IEE Electronics Letters*, pp. 169–171, April 1996.

[528] O. Acikel and W. Ryan, "Punctured turbo-codes for BPSK/QPSK channels," *IEEE Transactions on Communications*, vol. 47, pp. 1315–1323, September 1999.

[529] A. Papoulis, *Probability, Random Variables, and Stochastic Processes*. McGraw-Hill, 3 ed., 1991.

[530] J. Woodard, "Turbo coding for Gaussian and fading channels," tech. rep., Southampton University, UK, 1998.

[531] M. Breiling, "Turbo coding simulation results," tech. rep., Universitӑt Karlsruhe, Germany and Southampton University, UK, 1997.

[532] P. Robertson and T. Wórz, "Coded modulation scheme employing turbo codes," *IEE Electronics Letters*, vol. 31, pp. 1546–1547, 31st August 1995.

[533] W. Koch and A. Baier, "Optimum and sub-optimum detection of coded data disturbed by time-varying intersymbol interference," *IEEE Globecom*, pp. 1679–1684, December 1990.

[534] H. Robbins and S. Monroe, "A stochastic approximation method," *Annals of Mathematical Statistics*, vol. 22, pp. 400–407, 1951.

[535] C. Darken and J. Moody, "Towards faster stochastic gradient search," in *Advances in Neural Information Processing System 4* (J. E. Moody, S. J. Hanson, and R. P. Lippmann, eds.), pp. 1009–1016, San Mateo, CA: Morgan Kaufmann, 1992.

[536] W. T. Webb and L. Hanzo, *Modern Quadrature Amplitude Modulation : Principles and Applications for Fixed and Wireless Channels*. London: IEEE Press, and John Wiley & Sons, 1994.

[537] Y. Chow, A. Nix, and J. McGeehan, "Analysis of 16-APSK modulation in AWGN and rayleigh fading channel," *Electronics Letters*, vol. 28, pp. 1608–1610, November 1992.

[538] F. Adachi and M. Sawahashi, "Performance analysis of various 16 level modulation schemes under Rrayleigh fading," *Electronics Letters*, vol. 28, pp. 1579–1581, November 1992.

[539] F. Adachi, "Error rate analysis of differentially encoded and detected 16APSK under rician fading," *IEEE Transactions on Vehicular Technology*, vol. 45, pp. 1–12, February 1996.

[540] Y. C. Chow, A. R. Nix, and J. P. McGeehan, "Diversity improvement for 16-DAPSK in Rayleigh fading channel," *Electronics Letters*, vol. 29, pp. 387–389, February 1993.

[541] Y. C. Chow, A. R. Nix, and J. P. McGeehan, "Error analysis for circular 16-DAPSK in frquency-selective Rayleigh fading channels with diversity reception," *Electronics Letters*, vol. 30, pp. 2006–2007, November 1994.

[542] C. M. Lo and W. H. Lam, "Performance analysis of bandwidth efficient coherent modulation schems with L-fold MRC and SC in Nakagami-m fading channels," in *Proceedings of IEEE PIMRC 2000*, vol. 1, pp. 572–576, September 2000.

[543] S. Benedetto, E. Biglierri, and V. Castellani, *Digital Transmission Theory*. Prentice-Hall, 1987.